

2018

Fundamental Investigations in Organocatalytic Ring-Opening Polymerization: A Trek to New Catalysts

Oleg Kazakov
University of Rhode Island, okazakov@chm.uri.edu

Follow this and additional works at: https://digitalcommons.uri.edu/oa_diss

Recommended Citation

Kazakov, Oleg, "Fundamental Investigations in Organocatalytic Ring-Opening Polymerization: A Trek to New Catalysts" (2018). *Open Access Dissertations*. Paper 761.
https://digitalcommons.uri.edu/oa_diss/761

This Dissertation is brought to you by the University of Rhode Island. It has been accepted for inclusion in Open Access Dissertations by an authorized administrator of DigitalCommons@URI. For more information, please contact digitalcommons-group@uri.edu. For permission to reuse copyrighted content, contact the author directly.

FUNDAMENTAL INVESTIGATIONS IN
ORGANOCATALYTIC RING-OPENING
POLYMERIZATION: A TREK TO NEW CATALYSTS

BY

OLEG I. KAZAKOV

A DISSERTATION SUBMITTED IN PARTIAL FULFILLMENT OF THE
REQUIREMENTS FOR THE DEGREE OF

DOCTOR OF PHILOSOPHY

IN

CHEMISTRY

UNIVERSITY OF RHODE ISLAND

2018

DOCTOR OF PHILOSOPHY DISSERTATION

OF

OLEG KAZAKOV

APPROVED:

Dissertation Committee:

Major Professor Matthew Kiesewetter

Brenton DeBoef

Alvin Bach

Bongsup Cho

Jason Dwyer

Nasser H. Zawia

DEAN OF THE GRADUATE SCHOOL

UNIVERSITY OF RHODE ISLAND

2018

ABSTRACT

Organocatalysis is a powerful tool for polymer synthesis. It has been widely demonstrated that organocatalytic systems enable precise control over polymer microstructure, provide competitively fast reaction rates compared with metal-based catalysts, and effect a broad assortment of polymerization mechanisms. The added value of metal-free polymerizations is that they can be utilized in sensitive applications intolerant to the presence of residual metal-based catalysts.

The initial focus of the present dissertation was placed on mechanistic studies in organocatalytic ring-opening polymerization (ROP) of cyclic esters alongside with subsequent development of new organocatalytic systems for ROP. ROPs of this kind can be mediated by a thiourea-based hydrogen-bond donating catalyst and a strong organic base. The two cocatalysts activate the monomer and initiator for the reaction to commence. The question is: how do the four species interact? The binding between thiourea and bases was investigated – an interaction that had not been previously considered. An array of binding constants between thiourea and various bases was obtained. Importantly, the binding constants proved to correlate with the δ -valerolactone ROP rate depending upon the base used for the polymerization. The theory paved a way to the assessment of weaker bases in ROP.

With the original theory working, a new goal was selected – to investigate the binding between thiourea and *weak* alkylamine bases. A range of binding constants was measured for various thiourea and alkylamine cocatalyst pairs. The correlation between the binding constants and the rate of L-lactide ROP was non-existent. However,

enthalpy and entropy of cocatalyst binding were found to correlate with the L-lactide ROP rate. The more entropically favorable cocatalyst interactions yielded higher rates of L-lactide ROP. Additionally, the enthalpy and entropy of the thiourea-alkylamine binding exhibited enzyme-like compensation behavior similar enzyme-substrate analogues.

Kinetic investigations demonstrated that thiourea-alkylamine mediated ROP of L-lactide exhibited a second-order rate dependence in thiourea. This observation prompted us to assess the effect of two thiourea motifs tethered in one molecule on the ROP rate. The new bis-thiourea catalyst provided exquisite control over ROP, yielded well-defined polymers (narrow polydispersities, predictable molecular weights), was able to polymerize a host of cyclic ester monomers, and brought a significant rate acceleration for polymerizations even at small catalyst loadings, compared with mono-thiourea catalyst.

Seeking active and selective H-bonding catalysts, attention was attracted by the widely available triclocarban, formerly used as an antibacterial soap component. Triclocarban contains a urea functionality that renders the compound a potential H-bond donating catalyst. The examination of triclocarban as a ROP catalyst proved its efficiency for hydrogen-bonding ROP of a broad scope of monomers in different solvents. Having the ROP conditions optimized, extremely active triclocarban-based cocatalyst pairs were discovered. The polymers produced under triclocarban-mediated ROPs display precise macromolecular architecture. Mechanistically, it was proposed that the nature of the catalytic intermediate - neutral hydrogen-bonded or charged imidate - may change depending on the strength of base used in ROP. The quest for

optimization and discovery of potent H-bond donating organic catalysts for ROP, rivaling the metal-based counterparts, continues.

Further, attempts were undertaken in stereoselective organocatalytic ring-opening polymerization (SROP) of lactide. The SROP of lactide is an attractive approach for the generation of polylactides with tunable materials properties. This reaction exemplifies mechanistic control at the molecular level, conferring different bulk properties to the resulting polymer. Conversely, analysis of the bulk material allows for the detailed understanding of the molecular level processes that gave rise to particular material properties. A series of small molecule H-bond mediated catalysts were developed for SROP of *rac*-lactide. Catalytic scaffolds leading to low, moderate, and high stereoselectivity were identified through structure-activity relationships. Future generation catalysts will be made building on these early observations.

ACKNOWLEDGEMENTS

I would like to acknowledge my PhD advisor, Professor Matthew Kiesewetter, for his continuous support, wisdom, teaching, and inspiration throughout my graduate school journey. I would also like to thank my thesis committee members for their support during my PhD degree pursuit.

I want also to express my sincere gratitude to my family for providing me with continuous help during the years of studies at the University of Rhode Island.

Importantly, I want to thank my friends both from Russia and the USA who were by my side during this great yet challenging time.

Root yourself like a plant, grow, and stay cool under pressure.

Thank you.

Oleg

PREFACE

The given thesis employs Manuscript Format.

Chapter 1 presents a literature overview of progress achieved in the field of stereoselective polymerization. A particular emphasis is made on organocatalyzed stereoselective ring-opening polymerization. The chapter is based on the review of various publications pertaining to the topic.

Chapter 2 illuminates the importance of binding between organic hydrogen-bonding cocatalysts in the course of ring-opening polymerization. Specifically, the chapter addresses the binding between a thiourea H-bond donor and various H-bond accepting bases. Binding studies for cocatalysts and kinetic experiments were performed by me, BEMP-catalyzed polymerizations were performed by Partha P. Datta and Meghedi Isajani. The original research article is a result of collaboration between the co-authors (see the publication: Kazakov, O. I.; Datta, P. P.; Isajani, M.; Kieseewetter, E. T.; Kieseewetter, M. K. “Cooperative Hydrogen-Bond Pairing in Organocatalytic Ring-Opening Polymerization” *Macromolecules*, **2014**, *47* (21), 7463–7468).

Chapter 3 offers an explanation of various behavior of structurally similar alkylamine bases utilized as cocatalysts in ring-opening polymerization. The work considers binding interactions between a thiourea catalyst and a slate of weak alkylamine bases. The ramifications of differences in cocatalyst interactions are discussed. All the experiments were performed by me. The original research article resulted from collaboration between the co-authors (see the publication: Kazakov, O. I.;

Kiesewetter, M. K. “Cocatalyst Binding Effects in Organocatalytic Ring-Opening Polymerization of L-Lactide” *Macromolecules*, **2015**, *48* (17), 6121–6126).

Chapter 4 unveils a rate-accelerating hydrogen-bonding catalyst for ring-opening polymerization of l-lactide. The focus of the research project is placed on ring-opening polymerization of l-lactide mediated by a bis-thiourea hydrogen-bonding catalyst. Polymerizations of l-lactide were performed by the very talented Samuel S. Spink. The catalyst synthesis was conducted by Dr. Elizabeth T. Kiesewetter. Low catalyst loading polymerizations and high-temperature NMR spectra acquisitions were performed by me. The original research article is a result of collaboration between the coauthors (see the publication: Spink, S. S.; Kazakov, O. I.; Kiesewetter, E. T.; Kiesewetter, M. K. “Rate Accelerated Organocatalytic Ring-Opening Polymerization of L-Lactide via the Application of a Bis(thiourea) H-bond Donating Cocatalyst” *Macromolecules*, **2015**, *48* (17), 6127–6131).

Chapter 5 describes a commodity product trichloroethane (TCC), for which an alternative application was found in the form of a hydrogen-bonding catalyst for ring-opening polymerization. The project emphasizes the application of TCC as a cocatalyst for polymerization of a set of cyclic ester monomers, and the mechanistic studies into the action of TCC in polymerization were conducted. Polymerizations of δ -valerolactone and were performed by Nayanthara U. Dharmaratne, the majority binding studies were performed by Jinal U. Pothupitiya, ϵ -caprolactone polymerizations were performed by Timothy J. Bannin, high-temperature NMR analysis of polylactide and selected binding studies were performed by me. The original communication is a result of collaboration between the co-authors (see the publication: Dharmaratne, N. U.;

Pothupitiya, J. U.; Bannin, T. J.; Kazakov, O. I.; Kieseewetter, M. K. “Triclocarban: Commercial Antibacterial and Highly Effective H-Bond Donating Catalyst for Ring-Opening Polymerization” *ACS Macro Lett.*, **2017**, 6 (4), 421–425).

Chapter 6 highlights chiral ureas used as catalysts for stereoselective ring-opening polymerization of *rac*-lactide. The project explores the impact of substituents in ureas on the stereoselectivity. The syntheses of H-bonding catalysts and polymerizations of *rac*-lactide were performed by the very talented undergraduate researcher Samuel Spink and me. The chapter is based on the solely experimental and unpublished results.

TABLE OF CONTENTS

ABSTRACT.....	ii
ACKNOWLEDGMENTS.....	v
PREFACE.....	vi
TABLE OF CONTENTS.....	ix
LIST OF TABLES.....	x
LIST OF FIGURES.....	xi
LIST OF SCHEMES.....	xvi
CHAPTER 1.....	1
CHAPTER 2.....	39
CHAPTER 3.....	64
CHAPTER 4.....	104
CHAPTER 5.....	136
CHAPTER 6.....	180

LIST OF TABLES

TABLE	PAGE
Table 1.1. Different physical properties of polylactides depending on their tacticity....	1
Table 2.1. Binding constants and observed rate constants for the bases studied.....	46
Table 2.2. The 1 /BEMP catalyzed ROP of cyclic monomers.....	49
Table 2.3. Thermodynamic Values of Binding between 1 and various bases.....	54
Table 3.1. Thermodynamics of Cocatalyst Binding and Observed Rate Constants for the ROP of L-Lactide.....	68
Table 4.1. HMTETA and Bis(thiourea) cocatalyzed ROP of L-LA.....	107
Table 4.2. Comparison of Alkylamine and (bis)TU Cocatalyzed ROPs of L – Lactide.....	109
Table 4.3. Low Catalyst Loadings in the TU/Alkylamine Catalyzed ROP of L-LA .	111
Table 4.4. Tacticity analysis of poly(lactide)s.....	118
Table 5.1. MTBD and TCC Catalyzed ROP of VL and CL.....	138
Table 5.2. Urea or Thiourea Plus MTBD Cocatalyzed ROP of VL in Acetone.....	141
Table 5.3. Triclocarban Plus BEMP Cocatalyzed ROP of VL and CL	145
Table 5.4. Chain Length Variation for the TCC or di-CC plus MTBD cocatalyzed ROP of VL.....	153
Table 5.5. Solvent Screen of TCC/MTBD cocatalyzed ROP of VL.....	154
Table 5.6. Chain Length Variation for the TCC/MTBD cocatalyzed ROP of VL in acetone- <i>d</i> ₆	154
Table 6.1. ROP of <i>rac</i> -LA catalyzed by chiral TU's	185
Table 6.2. Solvent and base screen for ROP of <i>rac</i> -LA ^a catalyzed by 1	185

Table 6.3. Solvent screen for ROP of <i>rac</i> -LA ^a catalyzed by 8	198
Table 6.4. Base screen for ROP of <i>rac</i> -LA ^a catalyzed by 8	198

LIST OF FIGURES

FIGURE	PAGE
Figure 1.1. Examples of cyclic monomers for ROP.....	5
Figure 1.2. Structures of hydrogen-bonding cocatalysts for bifunctional activation in ROP of cyclic esters.....	8
Figure 1.3. P ₂ - <i>t</i> -Bu, the dimeric phosphazene base.....	12
Figure 1.4. Representative NHC applied for stereocontrolled ROP of <i>rac</i> -LA.....	15
Figure 1.5. Selection of the chiral catalysts screened for kinetic resolution stereoselective ROP of <i>rac</i> -LA	22
Figure 1.6. A selection of catalysts used for screening.....	24
Figure 1.7. A selection of catalysts and initiators employed for the study.....	27
Figure 2.1. For the ROP of VL, observed rate constant (k_{obs}) vs [1] + [DBU].....	42
Figure 2.2. (upper) The bases studied along with the respective binding curves to 1 . (lower) Van't Hoff plots of binding between 1 and various bases.....	55
Figure 2.3. First order evolution of [VL] vs time when [1] = [DBU].....	56
Figure 2.4. First order evolution of [VL] vs time when [1] > [DBU] = 0.05 M.....	57
Figure 2.5. First order evolution of [VL] vs time when [1] = 0.05 M < [DBU]	57
Figure 2.6. For the ROP of VL: (left) observed rate constant vs [1] when [1] > [DBU] = 50 mM; (right) observed rate constant vs [DBU] ⁻¹ when [DBU] > [1] = 50 mM. Conditions: VL (2 M, 100 mg):benzyl alcohol 50:1 in C ₆ D ₆ . Rate = k_{obs} [VL]; where $k_{\text{obs}} = k_{\text{P}}[\mathbf{1} + \text{DBU}][\text{benzyl alcohol}]$	58

Figure 2.7. Mn (GPC) and Mw/Mn vs percent conversion for the 1 /BEMP catalyzed ROP of VL. Reaction conditions: VL (2 M, 100 mg): 1 : BEMP: benzyl alcohol :: 100: 5: 5: 1 in toluene.....	58
Figure 2.8. First order evolution of [VL] vs time for the 1 /BEMP catalyzed ROP of VL. Conditions: VL (2M, 100 mg): 1 : BEMP: benzyl alcohol :: 100: 5: 5: 2 in C6D6.....	59
Figure 3.1. Observed rate constant, k_{obs} , vs concentration in the Me ₆ TREN/ 1 catalyzed ROP of L-LA (1 M, 0.5 mmol) from benzyl alcohol (0.010 mmol) when (left) [1] = 0.05 M and [Me ₆ TREN] > [1]; and (right) [Me ₆ TREN] = 0.05 M and [Me ₆ TREN] < [1].....	70
Figure 3.2. DFT/B3LYP 6-31G* geometry optimized structures of 1 bound to a) PMDETA and b) TACN.....	75
Figure 3.3. First order evolution of [LA] versus time in the 1 /HMTETA catalyzed ROP of LA from benzyl alcohol in CDCl ₃	81
Figure 3.4. First order evolution of [LA] versus time in the 1 /Me ₆ TREN catalyzed ROP of LA from benzyl alcohol in CDCl ₃	81
Figure 3.5. First order evolution of [LA] versus time in the 1 /TMEDA catalyzed ROP of LA from benzyl alcohol in CDCl ₃	82
Figure 3.6. Observed rate constant (k_{obs}) vs concentration plots for the 1 /TMEDA catalyzed ROP of L-LA	83
Figure 3.7. (left) Observed rate constant (k_{obs}) vs [1][Me ₆ TREN], and (right) observed rate constant (k_{obs}) vs [1] ² for the 1 /Me ₆ TREN catalyzed ROP of L-LA	84
Figure 3.8. Binding curves for the association of 1 with alkylamine cocatalysts. The	

curve fitting method was used to extract binding constants, see Experimental Section.

The chemical shift is of the *ortho*-protons of **1**.....84

Figure 3.9. Temperature-dependent binding86

Figure 3.10. **1** + TMEDA86

Figure 3.11. **1** + Me₆TREN87

Figure 3.12. **1** + DABCO88

Figure 3.13. **1** + HMTETA88

Figure 4.1. Alkylamine and thiourea cocatalysts evaluated for the ROP of L-LA107

Figure 4.2. First order evolution of [LA] versus time for the reaction given in the
example ROP experiment118

Figure 4.3. Molecular weight versus conversion plot for the ROP of L-LA from benzyl
alcohol in DCM catalyzed by **2**/HMTETA118

Figure 4.4. GPC traces of the ROP of LA from pyrenebutanol catalyzed by
Me₆TREN/**2** in CH₂Cl₂. The UV trace is shown in blue and the RI trace shown in red
.....119

Figure 4.5. GPC traces showing chain-extension of PLA by sequential addition of LA
to a single reaction mixture119

Figure 4.6. MALDI-TOF of PLA polymerized from benzyl alcohol (BA) by
2/Me₆TREN.....120

Figure 4.7. Activated-TU **2** + LA121

Figure 4.8. Dual monomer activated **2** + LA123

Figure 4.9. Dual monomer activated **2** vacuum.....125

Figure 4.10. Dual monomer activated **2** methylene chloride solvent127

Figure 4.11. Activated-TU 2 vacuum	128
Figure 4.12. Activated-TU 2 methylene chloride solvent	130
Figure 5.1. Base and (thio)urea cocatalysts evaluated for ROP	137
Figure 5.2. First order evolution of VL vs time for the TCC/MTBD catalyzed ring-opening polymerization of VL	155
Figure 5.3. M_n (blue) and M_w/M_n (orange) vs conversion for the TCC/MTBD catalyzed ring-opening polymerization of VL	156
Figure 5.4. GPC traces of the polymers resulting from the chain extension experiment of VL	157
Figure 5.5. First order evolution of CL vs time for the TCC/MTBD catalyzed ring-opening polymerization of CL	158
Figure 5.6. M_n (blue) and M_w/M_n (orange) catalyzed ring-opening polymerization of CL	159
Figure 5.7. Approach to equilibrium evolution of [VL] vs time for the TCC/MTBD catalyzed ring-opening polymerization of VL	160
Figure 5.8. M_n (blue) and M_w/M_n (orange) vs conversion for the TCC/MTBD catalyzed ring-opening polymerization of VL	161
Figure 5.9. GPC traces of the polymers resulting from the chain extension of PVL in acetone	162
Figure 5.10. M_n (blue) and M_w/M_n (orange) vs conversion for the TCC/BEMP catalyzed ring-opening polymerization of VL	163
Figure 5.11. GPC traces of the polymers resulting from the chain extension experiment of VL	164

Figure 5.12. First order evolution of [L-LA] vs time for the TCC/Me ₆ TREN catalyzed ring-opening polymerization	165
Figure 5.13. M _n (blue) and M _w /M _n (orange) vs conversion for the TCC/Me ₆ TREN catalyzed ring-opening polymerization of L-LA	166
Figure 5.14. MALDI-TOF of the PLLA resulting from TCC/Me ₆ TREN cocatalyzed ROP of L-lactide	167
Figure 5.15. Titration binding curve for the CL/ 1-O binding in benzene- <i>d</i> ₆	168
Figure 5.16. Titration binding curve for the CL/ 1-S binding in benzene- <i>d</i> ₆	168
Figure 5.17. Methine region of the methyl-decoupled ¹ H NMR spectrum of PLLA obtained via TCC/Me ₆ TREN cocatalyzed ROP of L-LA.....	169
Figure 5.18. (upper) First order evolution of [VL] vs time for the di-CC/MTBD catalyzed ROP of VL. (lower) The ROP displays a linear evolution of M _n (blue) vs conversion and narrow M _w /M _n (orange).....	170
Figure 5.19. (upper) ¹ H NMR (CD ₃ OD, 400 MHz) spectrum of mono-CC. (lower) ¹³ C NMR (CD ₃ OD, 100 MHz) spectrum of mono-CC	171
Figure 5.20. (upper) ¹ H NMR (CD ₃ OD, 400 MHz) spectrum of di-CC. (lower) ¹³ C NMR (CD ₃ OD, 100 MHz) spectrum of di-CC	172
Figure 5.21. Downfield portion of the ¹ H NMR spectra of TCC plus base ([TCC] = [base] = 5 mM) in acetone- <i>d</i> ₆	173
Figure 6.1. Chiral TU catalysts applied in the study	182
Figure 6.2. Resolution of <i>rac</i> -LA methine protons signal by 1	183
Figure 6.3. Example fitted methine protons signal of <i>Prac</i> LA in homonuclear decoupled ¹ H NMR for P _m calculations.....	189

Figure 6.4. ^1H NMR of catalyst 3 (300 MHz, chloroform- <i>d</i>).....	190
Figure 6.5. ^1H NMR of catalyst 4 (300 MHz, chloroform- <i>d</i>).....	191
Figure 6.6. ^1H NMR of intermediate product Boc-DAP-Leu (300 MHz, chloroform- <i>d</i>).....	194
Figure 6.7. ^1H NMR of intermediate product DAP-Leu (300 MHz, methanol- <i>d</i> ₄).	194
Figure 6.8. ^1H NMR of catalyst 6 (300 MHz, chloroform- <i>d</i>).....	195
Figure 6.9. ^{13}C NMR of catalyst 6 (75 MHz, chloroform- <i>d</i>).....	195
Figure 6.10. ^1H NMR of catalyst 7 (300 MHz, DMSO- <i>d</i> ₆).....	196
Figure 6.11. ^1H NMR of catalyst 8 (300 MHz, chloroform- <i>d</i>).....	197

LIST OF SCHEMES

SCHEME	PAGE
Scheme 1.1. Mechanisms of stereocontrol during the course of polymerization.	3
Scheme 1.2. ROP of an example cyclic ester, VL.....	6
Scheme 1.3. Electrophilic mechanism for ROP.....	7
Scheme 1.4. Nucleophilic mechanism for ROP.....	7
Scheme 1.5. Activation of the initiator and monomer by the cocatalyst pair during the course of ROP.....	7
Scheme 1.6. Postulated mechanism of ROP of LA by the bifunctional TU/A Takemoto catalyst.....	9
Scheme 1.7. Possible distribution patterns of stereocenters in polylactide backbones.....	11

Scheme 1.8. Synthesis of NHCs employed for stereocontrolled ROP of <i>rac</i> -LA.....	16
Scheme 1.9. Proposed chain-end control mechanisms for NHC-mediated stereocontrolled ROP of <i>rac</i> -lactide (top) and <i>meso</i> -lactide (bottom).....	18
Scheme 1.10. Lactide: epimerization and ROP outcomes.....	19
Scheme 1.11. Suggested mechanism of <i>rac</i> -LA epimerization.....	20
Scheme 1.12. Proposed mechanism of LA ROP catalyzed by a chiral (<i>R</i>)- 1a	25
Scheme 1.13. Proposed mechanism of ICD-mediated ROP of LA.....	29
Scheme 1.14. A general synthetic scheme depicting the route towards the catalysts employed in the study.....	31
Scheme 1.15. The proposed mechanism for ROP of LA, mediated by the unnatural densely substituted amino acid H-bonding catalyst.....	34
Scheme 2.1. H-Bonding Mechanism for the ROP of δ -Valerolactone.....	41
Scheme 2.2. Proposed Cocatalyst Binding Mechanism for the ROP of VL.....	44
Scheme 3.1. Common H-Bonding Cocatalysts for the ROP of Lactide.....	65
Scheme 3.2. Proposed mechanism for the Me ₆ TREN/ 1 catalyzed ROP of L-LA.....	73
Scheme 4.1. Second Order Behavior in 1 Inspires Tethered H-Bond Donor 2	106
Scheme 4.2. Proposed Mechanism for the 2 /Me ₆ TREN Catalyzed ROP of L-LA....	113
Scheme 5.1. Proposed Mechanism for TCC/Base Cocatalyzed ROP.....	146

CHAPTER 1

STEREOSELECTIVE ORGANOCATALYTIC RING-OPENING POLYMERIZATION

1.1 Introduction

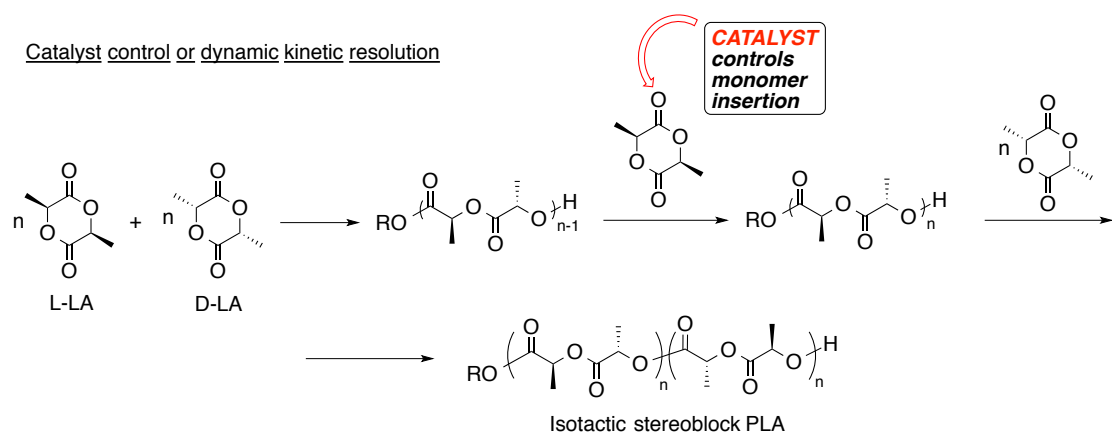
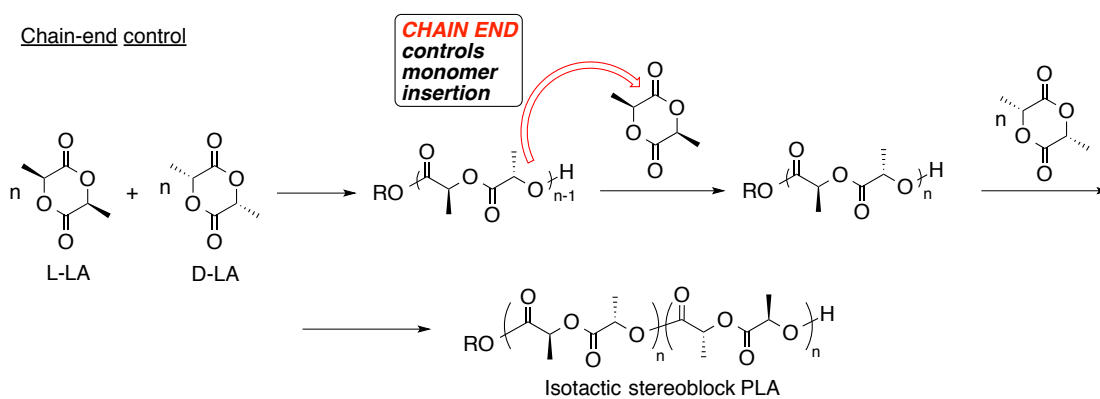
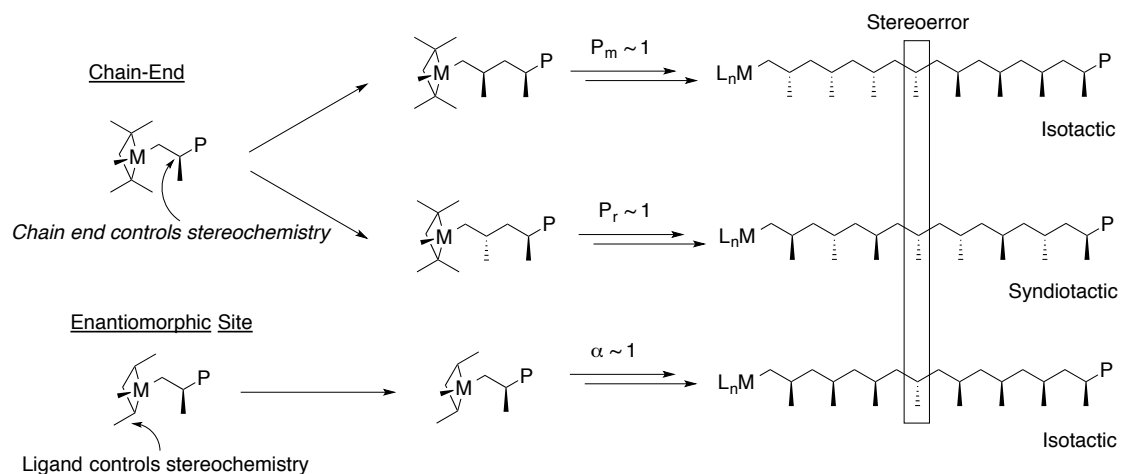
Controlling the stereoselectivity of a polymerization is an important tool of controlling polymer tacticity. Polymer tacticity is a microlevel metric of a polymeric material, that affects its physical properties. Interconnection of macro properties and micro ones is demonstrated by polylactides of different tacticities. Depending on the tacticity of a polylactide (PLA), drastically different melting points (table 1) can be observed for the material.¹

Table 1.1 Different physical properties of polylactides depending on their tacticity.

PLA	Melting point, °C
Atactic	40
Syndiotactic	152
Isotactic (PLLA or PDLA)	180
Isotactic stereoblock	205

Polymer tacticity is often determined during the polymer enchainment via stereocontrol rendered by the catalysts or reagents. One of the first examples of stereocontrolled ROP goes back to the middle of the 20th century when metal-based catalysts for stereocontrolled polymerization of propylene were introduced by the Nobel

Prize laureates Ziegler and Natta (we will refer the reader to widely available literature on this topic). Two major kinds of stereocontrol (scheme 1.1) over the monomer unit addition to a growing polymer chain are known.⁴ First, chain-end control may be implemented. This type of control involves the growing chain end dictating which enantiomer is attached next to the polymer backbone.⁴ Second, catalyst control, constituted by two types, (also known as enantiosite control in case of metal-based routes and dynamic kinetic resolution in the event of organic approaches) may take place. Enantiomorphic site control means that the catalyst determines the relative stereochemistry between two adjacent stereocenters in the growing polymer chain generated from a prochiral monomer (e.g. propylene, scheme 1). On the other hand (scheme 1), in the event of *rac*-lactide (*rac*-LA) we can encounter dynamic kinetic resolution (DKR) control implying that the catalyst “selects” the next chiral center of the monomer added to the growing polymer chain.^{4,5} Tacticity is measured by statistical methods^{4,5} and probabilities of isotactic (P_m) or syndiotactic enchainment (P_r) through chain-end control can be determined. Parameter α can also be determined statistically as a probability of tactic enchainment through enantiomorphic site control. In this chapter we consider various methods that can be implemented to conduct stereoselective polymerization of *rac*-LA using organocatalysis.



Scheme 1.1. Mechanisms of stereocontrol during the course of polymerization. Top pair – formation of a tactic polymer from an achiral monomer.⁴ Bottom pair – formation of a tactic polymer from a chiral monomer.

1.2 Organocatalytic Ring-Opening Polymerization

One underdeveloped tool for stereoselective polymerization is organocatalysis. Organocatalysis facilitates formation of polymers that are utilized in a broad array of products, ranging from commodity packaging materials and microelectronic components, to specialized biomedical devices and drug delivery agents.^{1,2} Utilization of metal-based catalysts in polymerization poses the challenges of catalyst removal upon the polymeric material purification.⁶ This circumstance becomes especially daring in designing polymers for sensitive areas, such as food packaging, microelectronics, and biomedical materials.⁶ To counterbalance the purification difficulty, small molecule organic catalysts were introduced.^{2,6}

The initial research efforts in organocatalytic polymerization yielded the discovery of relatively effective organic polymerization catalysts that could not yet rival the performance of metal-based analogues.⁶ Further research efforts introduced organic catalysts that can operate at small catalyst loadings, furnish high rates of polymerization, and exhibit precise control over macromolecular architectures.¹⁰ A substantial slate of small molecule organocatalysts operate in the range of mole percent to sub-mole percent catalyst loadings with polymerization rates effecting polymer product formation from hours to seconds. A large number of catalytic systems provide exquisite control over polymerization via the polymerization execution in a “living” manner. “Living” polymerization is a chain-growth polymerization that is characterized by a) sequential addition of monomer units in a “one-by-one” mode to the growing polymer chain and b) linear dependence of polymer weight increase on time. The end result of “living” polymerization are polymers characterized by target molecular

weights and narrow polydispersity indices (PDI).^{2,6} PDI is a “polydispersity index” defined as the ratio of weight-average polymer molecular weight (M_w) to number-average molecular weight (M_n) of polymer (eq. 1).

$$\text{PDI} = M_w/M_n \quad (1)$$

Typical monomer substrates for organocatalytic ring-opening polymerization are cyclic species.^{2,6} The set of substrates (figure 1.1) is a representative slate of the monomer pool and the reader can imagine the diversity of polymeric materials that can be generated.

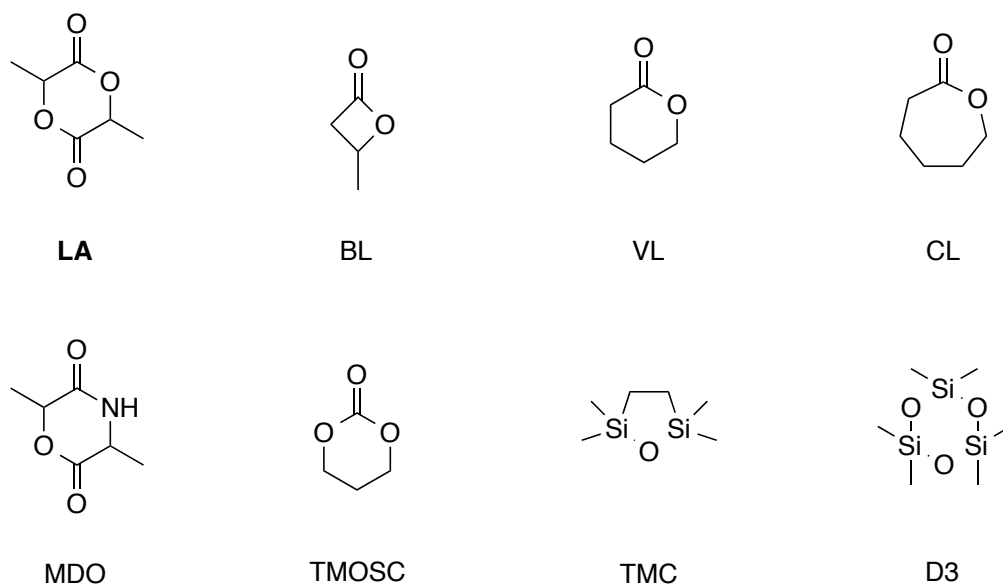
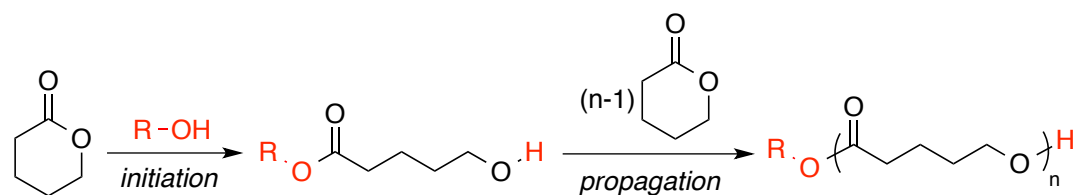


Figure 1.1. Examples of cyclic monomers for ROP.

The monomer ring strain release is the driving force behind the ring opening and subsequent polymerization.^{2,6} The principal scheme for ROP employing VL and benzyl alcohol as the example monomer and initiator, respectively, is demonstrated below

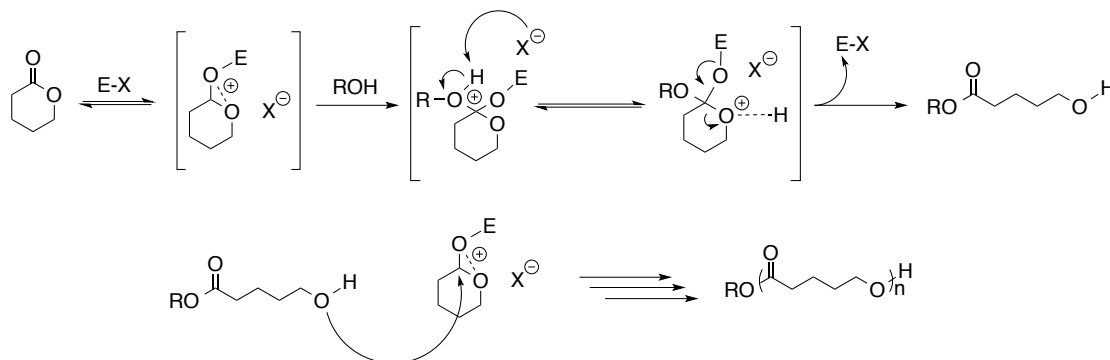
(scheme 1.2). The ratio between the monomer and initiator determines the target chain length of the resultant polymer macromolecule. The polymerization initiation is represented by the nucleophilic attack of the alcohol at the carbonyl carbon of the monomer molecule. This attack leads to the cleavage of the single carbonyl-oxygen bond and formation of a new ester bond and of a hydroxyl in the opened monomer. This hydroxyl is now able to attack the next monomer molecule in a chain-growth manner. That is the propagation stage. Upon the consumption of the monomer, the polymer chain end is terminated with an alcoholic proton. The presence of an alcoholic chain end provides the opportunity of chain-extension upon addition of a fresh batch of monomer.



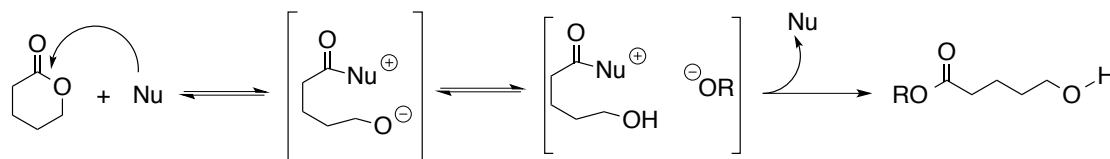
Scheme 1.2. ROP of an example cyclic ester, VL.

Several mechanisms exist for organocatalytic ROP.^{2,3} First, electrophilic monomer activation mechanism (scheme 1.3) was developed that can be mediated by protic acids. Second, nucleophilic monomer activation mechanism (scheme 1.4) was proposed that can be carried out by nucleophilic catalytic species such as N-heterocyclic carbenes and phosphazenes. Third, bifunctional activation mechanism was postulated that employs hydrogen bonding (scheme 1.5). It is a very prominent mechanistic model that will be highlighted in detail later in this work. The different research aims that we

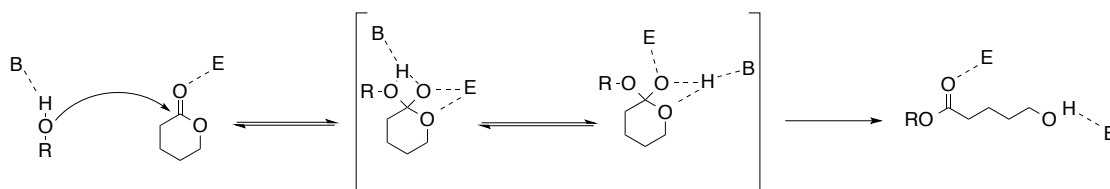
set in the projects described in this thesis are largely based on the hydrogen-bonding mechanistic pathway for organocatalyzed ROP.



Scheme 1.3. Electrophilic mechanism for ROP.



Scheme 1.4. Nucleophilic mechanism for ROP.



Scheme 1.5. Activation of the initiator and monomer by the cocatalyst pair during the course of ROP.

The bifunctional activation mechanism via hydrogen bonding can be carried out by thiourea and amine (TU/A) cocatalyst pairs. According to the theoretical

investigations, TU activates the monomer rendering it a better electrophile, whereas the amine base activates the alcoholic initiator making it a better nucleophile (scheme 1.6).¹⁰ Presumably, the amine base continues to activate the alcoholic chain end of the growing polymer (scheme 1.6) for attacks on the incoming monomer activated by TU. TU/A functionalities can be combined into a unimolecular catalytic species. This fusion is exemplified by Takemoto catalyst (**1**) that possesses a TU/A functionality in one molecule. On the other hand, the TU/A pairing can be represented by two separate molecules. That setting is exemplified by application of cocatalysts **2** and **3** for ROP of LA (figure 2).¹⁰

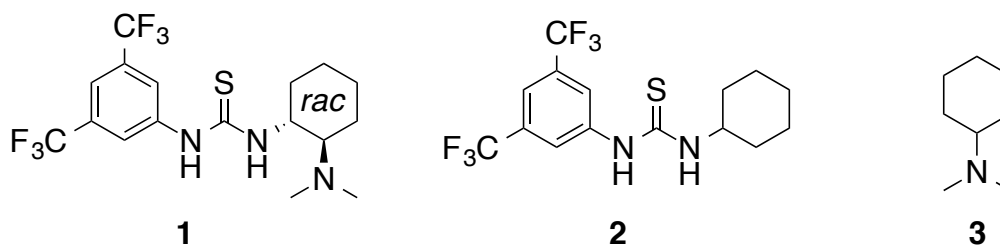
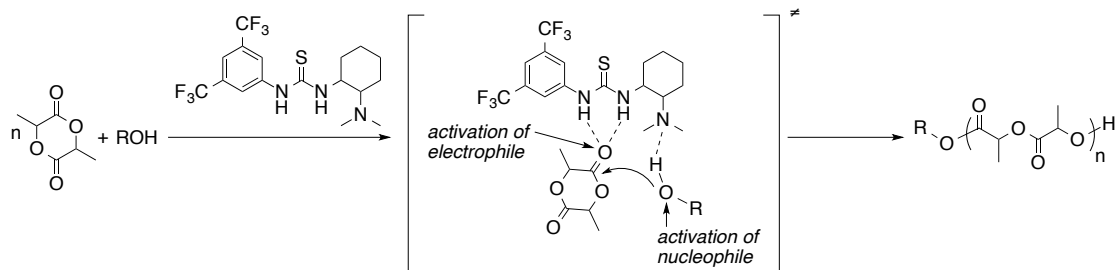


Figure 1.2. Structures of hydrogen-bonding cocatalysts for bifunctional activation in ROP of cyclic esters.¹⁰

ROPs of LA initiated by benzyl alcohol and catalyzed either by **1** or by **2** and **3** are well-controlled and generate polymers with targeted molecular weights and narrow PDIs.¹⁰ Polymerizations can be conducted at mild conditions (room temperature) and in a variety of commodity solvents (dichloromethane, chloroform).¹⁰

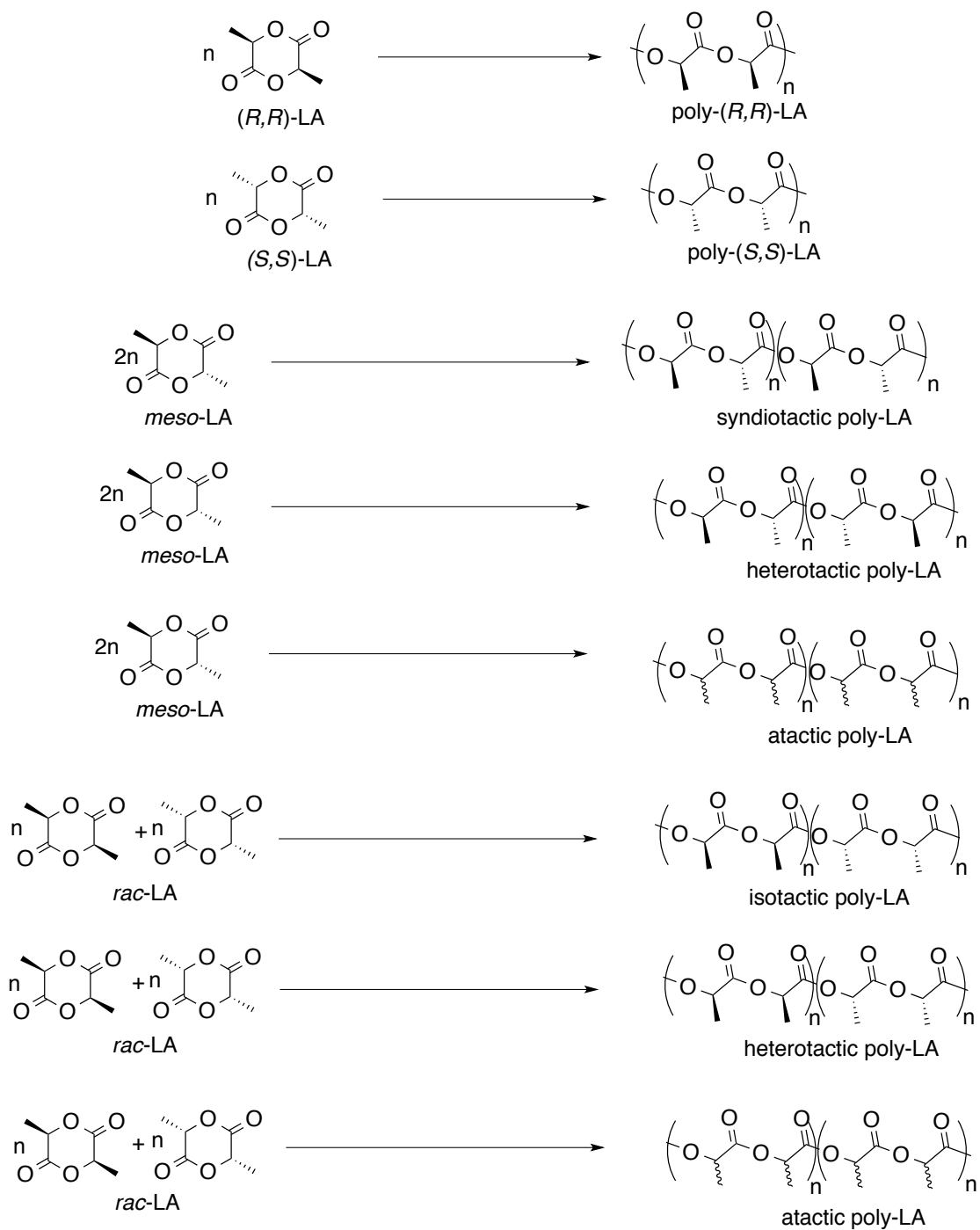


Scheme 1.6. Postulated mechanism of ROP of LA by the bifunctional TU/A Takemoto catalyst.¹⁰

1.3 Lactide in Organocatalytic Ring-Opening Polymerization

A very common monomer for both metal-catalyzed and organocatalytic ring-opening polymerization is lactide (LA).^{7,8} LA attracted substantial attention due to its wide availability as the monomer that can be derived from renewable resources (corn) and biodegradability of the resultant polymers.^{7,8} LA is present in several forms naturally: L-LA, D-LA, *meso*-LA, and as a mixture of stereoisomers, *rac*-LA. This diversity in just a single monomer pool allows for production of polymeric materials with various arrangements of stereocenters in the polymer chain.⁹ Different arrangements of stereocenters in the polymer chain can be both ragtag (no stereocontrol) and highly ordered (upon application of stereosequence control protocols).⁹ Here we provide (scheme 7) the rundown of outcomes for ROP of LA⁴. A pure enantiomer of LA, for instance, L-LA, upon ROP, affords a crystalline isotactic polymer with uniform (S)-stereocenters along the polymer backbone, unless the epimerization is involved in the polymerization process. As a result, a stereoregular poly-L-LA is generated. Upon stereocontrolled ROP of *meso*-LA, a syndiotactic polymer with alternating *R*- and *S*-stereocenters in the chain or a heterotactic polymer with alternating *R*-/*R*- and *S*-/*S*- pairs

of stereocenters can be produced. ROP of *rac*-LA can bring various results. The uncontrolled ROP of *rac*-LA can yield an atactic polymer with randomly placed *R*- and *S*-stereocenters throughout the polymer backbone, furnishing an amorphous material.⁴ The other option is the alternating placement of (*R*-/*R*-) and (*S*-/*S*-) pairs of stereocenters in the polymer backbone, yielding a heterotactic polymer.⁴ Finally, the selective polymerization of one of the stereoisomers in *rac*-LA followed by the polymerization of the other stereoisomer from the racemic mixture, can yield an isotactic stereoblock poly-LA with, in an ideal case, a half polymer chain bearing (*R*)-stereocenters whilst the other half possesses (*S*)-stereocenters.⁴



Scheme 1.7. Possible distribution patterns of stereocenters in polylactide backbones.⁴

1.4 Stereoselective Ring-Opening Polymerization using Phosphazene Bases

Although the field of stereocontrolled ring-opening polymerization is abundant with examples of successful utilization of metal-based catalysts for the goal – control over tacticity - the examples of successful application of small molecule catalysts for SROP are rather sparse.

The successful examples of strong organic bases application in ROP of cyclic esters gave rise to further screening of other bases as candidates for catalysts in ROP. Particularly, phosphazene bases were established to be effective catalysts for ROP.¹¹ The phosphazene bases catalysts are commercially available and possess a wide range of homologues. The steric bulk of certain phosphazene bases is particularly interesting as it may restrict the reacting chiral species mobility, thereby exercising a form of stereocontrol. The absence of chiral motifs in the phosphazene base structure suggested the polymer chain-end control mechanism in the course of ROP. In the work by Hedrick and coworkers, the commercially available phosphazene base (figure 1.3) *t*-Bu-P₂ (^{MeCN}pK_{BH+} = 33.5) was selected as an organocatalyst for ROP of lactide monomers.¹¹

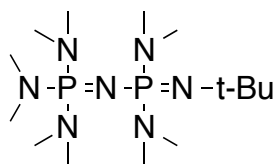


Figure 1.3. P₂-*t*-Bu, the dimeric phosphazene base.

The polymerizations were set up by employing an alcoholic initiator and using toluene as a solvent.¹¹ The polymerization screening with variable conditions produced well-defined polylactides characterized by narrow PDI and controlled molecular

weights indicative of living polymerization.^{2,6} The t-Bu-P₂ catalyst proved to be very efficient in effecting ROP of lactide at small catalyst loadings and furnished fast rates of polymerization.¹¹ Specifically, ROP of L-LA yielded a quantitative polymeric product in only 10 seconds. The conditions for the reaction were: monomer to initiator to catalyst ratio of 100:1:1, initial monomer concentration $[M]_0 = 0.32$ mol/L, degree of polymerization DP = 100. The polymerization exhibited linear evolution of polymer M_n versus the conversion of monomer, the obtained polymer had the molecular weight $M_n = 25800$ g/mol and PDI = 1.23.

The main target of the study was to probe t-Bu-P₂ as a candidate for stereocontrol in ROP of lactide. The temperature screen was applied for this goal. The polymerizations with optimal concentrations of the monomer and catalyst were performed in the range of temperatures from 25 °C to -75 °C.¹¹

Thus, ROP of *rac*-LA with monomer to initiator to catalyst ratio of 100:1:1, $[M]_0 = 0.08$ mol/L, DP = 100, was performed at room temperature. The reaction at 85% conversion furnished a polymer, poly-*rac*-LA (*Prac*LA), with $M_n = 13300$ g/mol and the narrower PDI = 1.06, in 3 minutes.¹¹

The execution of the same polymerization but at the lower temperature of -75 °C at > 99% conversion gave the polymer with $M_n = 27200$ g/mol and slightly broader PDI = 1.11, in 180 minutes.¹¹

Decoupled ¹H NMR of the two *Prac*LAs and statistical analyses of the stereocenters distribution in the two polymers via Markovian models, gave two drastically different isotactic chain propagation probability values: the moderate P_m (room temperature) = 0.72 and excellent P_m (-75 °C) = 0.95.¹¹

The *Prac*LAs synthesized at -75 °C had high degree of crystallinity as demonstrated by glass transition temperature $T_g = 62$ °C and a peak melting point temperature $T_m = 201$ °C which is higher than the one of a similar DP PLLA ($T_m = 163$ °C).¹¹

The polymerization mechanism was suggested to operate via the alcoholic initiator activation due to the increase of the chemical shift of the alkoxy proton from 1.17 ppm in pure alcohol to 7.66 ppm in alcohol with added phosphazene base. The mechanism of stereocontrol was postulated to be of the polymer chain-end kind due to the absence of the chiral moieties in the catalyst structure. Each lactide enantiomer has an equal probability to undergo the first ring-opening event and the open propagating stereocenter of the *i*-th monomer will select the (*i*+1)-st inserted monomer stereocenter to continue the growth of the nascent polymer chain. The lowered temperature provides decreased mobility of the reactive species in solution and allows higher stereoselectivity in the course of ROP of *rac*-LA.¹¹

The research effort by Wade and coworkers built an outstanding case for stereoselective organocatalytic ROP of *rac*-LA. P_2 -*t*-Bu was shown to be a very fast organocatalyst for ROP of *rac*-LA exceeding stereocontrol abilities of a large slate of known organocatalysts and matching stereoselectivity parameters of exquisite metal-based catalytic systems.¹¹

1.5 Stereoselective Ring-Opening Polymerization Using N-Heterocyclic Carbenes

The application of zinc metal in a metal complexes with N-heterocyclic carbenes (NHCs) versus NHCs without a metal counterpart (fig. 1.4) gave rise to the observation of drastically different stereoselectivity patterns in the course of ROP of *rac*-lactide.¹² This observation prompted research efforts in organocatalytic ROP mediated by various substituted NHCs. The project carried out by Dove and coworkers featured the preparation (scheme 1.8) and screening of a number of NHCs (figure 4) that possessed either bulky substituents on the NHC core or bulky substituents alongside with chiral motifs.¹³ The obtained NHCs were synthesized via relatively short pathways allowing flexibility for the catalyst modification to assess possible structure-property relationships.¹³

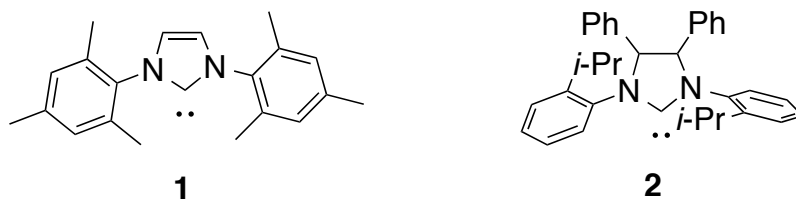
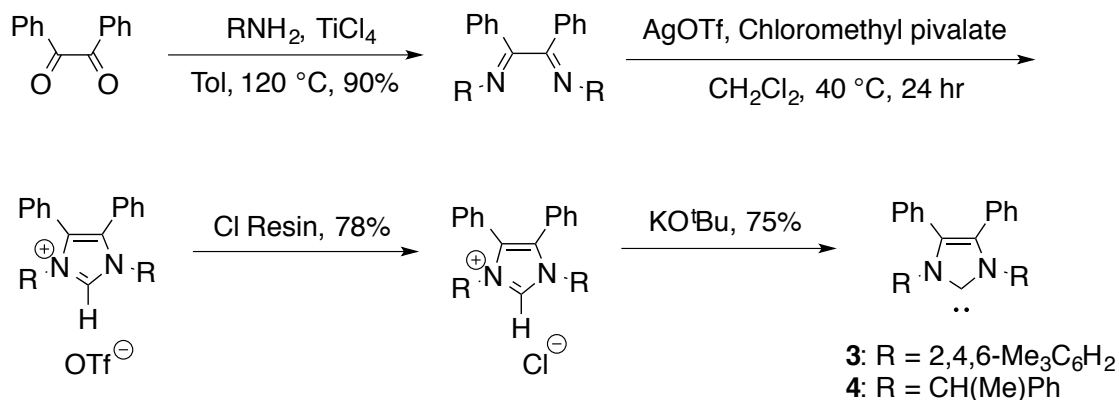


Figure 1.4. Representative NHC applied for stereocontrolled ROP of *rac*-LA.

The NHC catalysts (scheme 8) were applied in a metal-free fashion for ROP of *rac*-lactide and *meso*-lactide. The polymerizations were carried out at various temperatures with the overarching goal in mind to achieve the higher levels of stereoselectivity. It is to be noted that NHCs are significantly fast catalysts which is demonstrated by the representative polymerizations.¹³



Scheme 1.8. Synthesis of NHCs employed for stereocontrolled ROP of *rac*-LA.

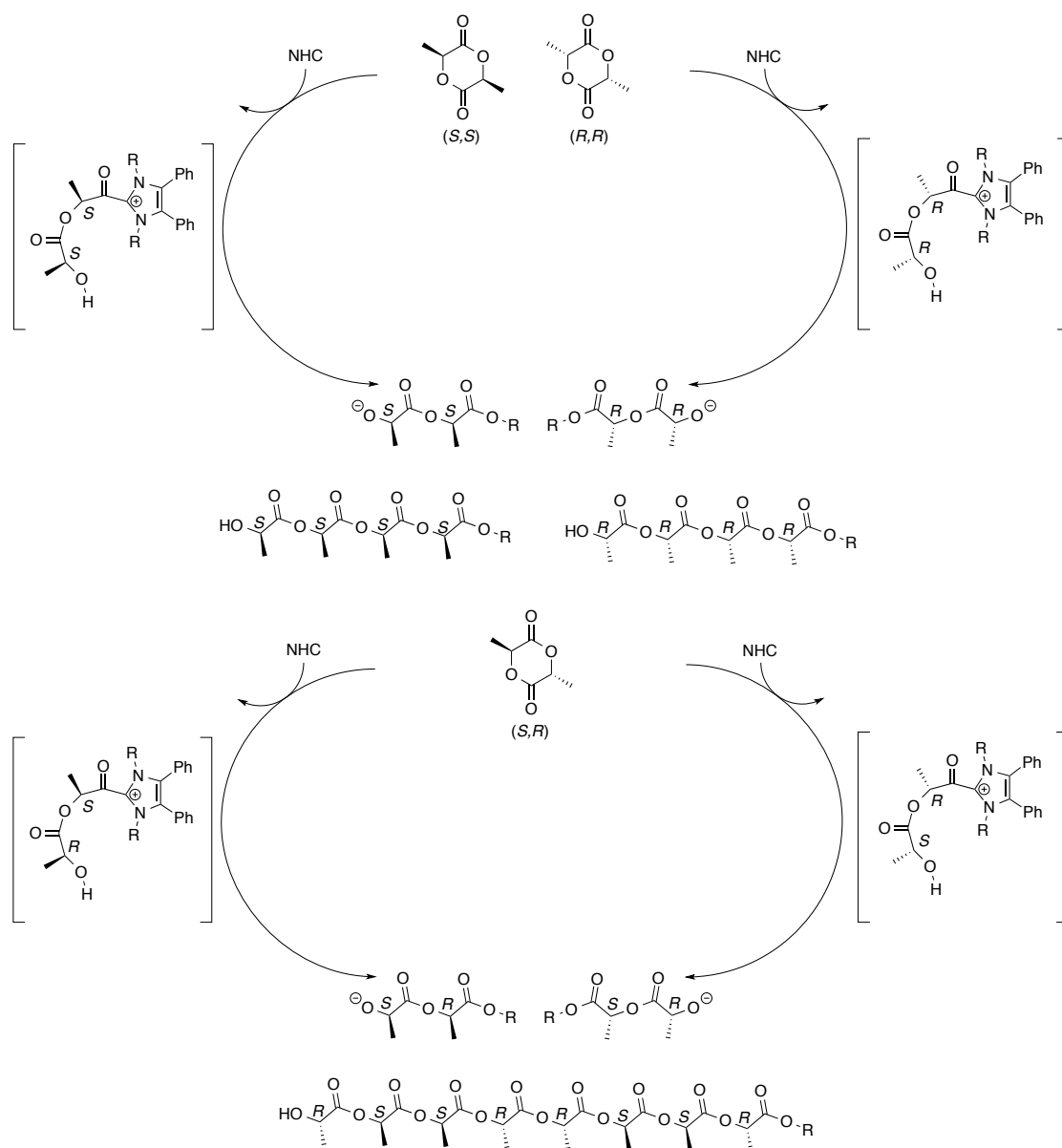
Employing catalyst **3** and starting with monomer to initiator ratio of 100:1, at room temperature, a polymer with a narrow PDI = 1.24 was formed in only 1 minute at 95% conversion. However, the isotactic chain growth propagation probability was fairly low with $P_m = 0.59$.¹³

Next, it was envisioned that stereoselectivity of the ROP might be enhanced upon lowering the reaction environment temperature. The reaction was performed at lower temperatures and a substantial increase in isotactic propagation probabilities was observed as follows: $P_m = 0.72$ at $-15 ^\circ\text{C}$, $P_m = 0.80$ at $-40 ^\circ\text{C}$, $P_m = 0.90$ at $-70 ^\circ\text{C}$, all with catalyst **3**. The steric bulk introduction into the catalyst structure was expressed in a slightly increased P_m value: $P_m = 0.83$ (catalyst **1**) versus $P_m = 0.90$ (catalyst **2**). The polymer synthesized at $-70 ^\circ\text{C}$ underwent a differential scanning calorimetry analysis that revealed the melting point $T_m = 153.3 ^\circ\text{C}$ and $\Delta H_{\text{fus}} = 12.8 \text{ J/g}$.¹³

Polymerizations of *meso*-LA were performed with the same conditions at $25 ^\circ\text{C}$ and $-40 ^\circ\text{C}$ with various NHCs from the ensemble. Catalyst **3** mediated the synthesis of

the polymer with an articulate $P_m = 0.83$ at $-40\text{ }^\circ\text{C}$. The application of the enantiopure catalyst (*R,R*)-4 furnished a heterotactic polymer with $P_m = 0.58$ at $-40\text{ }^\circ\text{C}$.¹³

Mechanistic investigations were undertaken to elucidate the mode of sterecontrol during ROP (scheme 9). The authors postulated that the polymer chain-end control was in operation during ROP of lactides via NHC catalysis. Polymerization of *rac*-LA can yield an isotactic-enriched polymer upon the postulated chain-end control mechanism. The bifurcated ROP of *meso*-LA can yield two products: if the enantiosite control is implemented, a syndiotactic polymer can be produced, whereas the chain-end control mode is expected to furnish a heterotactic polymer. The ROP of *meso*-LA produced heterotactic polymers, which was suggestive of the chain-end control mode of the polymerization. The polymerizations performed with *rac*-LA gave equally isotactic polymers, with significantly increased P_m values at low temperatures for both racemic and pure versions of catalyst 4 – the same polymerization conditions with this catalytic species produced polymers with $P_m = 0.88$ at $-70\text{ }^\circ\text{C}$. Thus, the role of the chiral motifs was non-consequential and the steric bulk of the catalyst determined the polymer tacticity. The mechanistic schemes were devised (scheme 1.9) to summarize the scenarios of stereocontrolled ROP of lactides by means of NHC metal-free catalysts.¹³



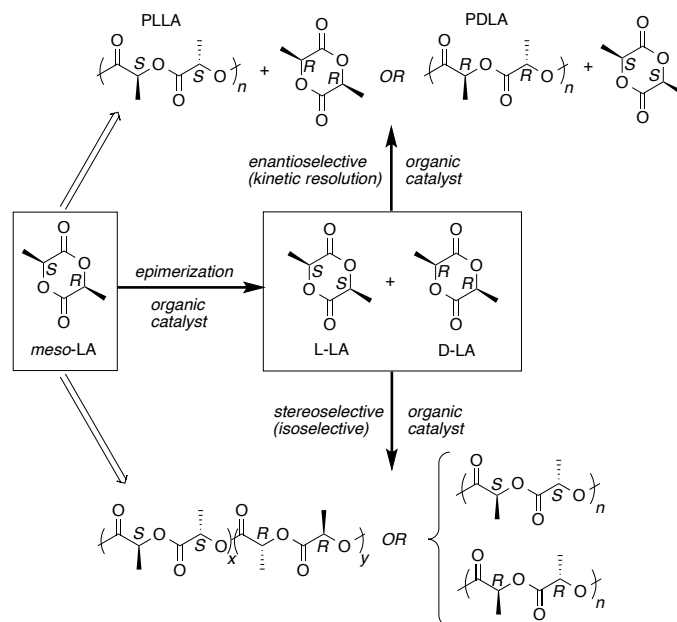
Scheme 1.9. Proposed chain-end control mechanisms for NHC-mediated stereocontrolled ROP of *rac*-lactide (top) and *meso*-lactide (bottom).

1.6 Stereoselective Ring-Opening Polymerization Using Chiral Thioureas

Tremendous progress has been made to date in the field of utilization of thiourea H-bonding catalysts for ROP of cyclic ester monomers.^{2,6} It was possible to achieve highly controlled ROP of a variety of achiral monomers using substituted thioureas and

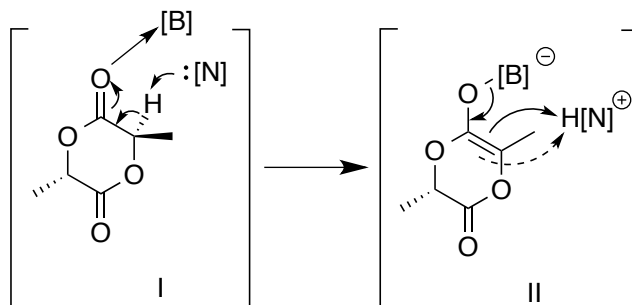
arrange these catalysts in terms of their efficiency to their metal-based counterparts.^{2,6} Thioureas are capable, in particular, of fast and controlled ROP of lactide monomers. However, the examples of achieving isoselective ROP of *rac*-LA using thiourea H-bonding catalysts are almost lacking in the polymer community. Previously, Waymouth and coworkers demonstrated a successful usage of bifunctional Takemoto catalyst for ROP of lactide.¹⁰ The polymerizations produced well-defined polymeric products characterized by controlled molecular weights, narrow PDIs across the range of polymerization experiments and tolerable reaction times.¹⁰

The echoing project undertaken by Chen and coworkers¹⁶ achieved two major goals. First, the task of conversion of *meso*-lactide into *rac*-lactide was set. Second, the development of a stereoselective thiourea-based organocatalyst for ROP of *rac*-lactide was put in the offing¹⁶ (scheme 1010).



Scheme 1.10. Lactide: epimerization and ROP outcomes.

The first objective was approached from the perspective of frustrated Lewis pairs applied for epimerization of lactide (scheme 1.11). Both concepts rest on a solid foundation of previous research as demonstrated by a comprehensive review¹⁴ by Stepan and Erker and a focused project on lactide epimerization¹⁵ by Börner. An effective combination of *meso*-LA epimerization agents, represented by a B/N Lewis pair (scheme 11), was found – DABCO/B(C₆F₅)₃. The established epimerization system exhibited remarkable properties. The optimized epimerization reaction achieved *meso*-to-*rac*-lactide conversion of 95.4% in only 5 minutes with the conditions as follows: 2.88 g scale in *meso*-lactide in 2.0 M solution in toluene with just 0.01 mol. % of the DABCO/B(C₆F₅)₃ epimerization system.¹⁶



Scheme 1.11. Suggested mechanism of *rac*-LA epimerization.

The second objective was fulfilled after the screening of a slate of chiral motifs for stereoselective ROP of *rac*-lactide (fig. 1.5) (figure 5). Amongst the surveyed H-bonding catalysts, β -isocupreidine (β -ICD) and cupreidine (CPD) were capable of stereoselective kinetic resolution ROP of *rac*-lactide, however, the furnished enantiomeric excess values (*ee*) and polymerization constants for the *S*- and *R*-enantiomer polymerization could be significantly improved. The catalyst improvement

strategy included the incorporation of a thiourea moiety into the β -ICD structure. A series of monofunctional chiral TU catalysts (figure 5) exhibited significantly improved characteristics during the ROP, particularly catalyst **1** that yielded $k_S/k_R = 10$ and $ee = 63\%$ upon the following ROP conditions: [*rac*-LA] = 1.67 M, in DCM, at 25 °C, [M]/[Cat]/[I] = 100/1/1. For the contrast, the same polymerization conditions (with the exception [M]/[Cat]/[I] = 50/1/1) mediated by β -ICD and CPD, furnished, respectively, $k_S/k_R = 3.8$ and $ee = 40\%$ and $k_S/k_R = 3.6$ and $ee = 33\%$.¹⁶

The following step was to introduce the second chiral moiety into the chiral TU catalyst. The second chiral moiety was chosen to be of the binaphthyl amine nature. In particular, a slate of bifunctional chiral TU catalysts was synthesized (figure 5). The above-mentioned polymerization conditions were applied to test the catalyst performance. The representative ROP performed by the optimized catalyst candidate **4** yielded impressive parameters of $k_S/k_R = 26$ and $ee = 83\%$ upon the following ROP conditions: [*rac*-LA] = 1.67 M, in DCM, at 25 °C, [M]/[Cat]/[I] = 100/1/1. Switching from chlorinated to fluorinated solvents improved kinetic resolution and stereoselectivity. For example, the same reaction performed in fluorobenzene and difluorobenzene (DFB), gave, respectively, $k_S/k_R = 41$ and $ee = 89\%$ and $k_S/k_R = 53$ and $ee = 91\%$. Interestingly, the *S*-enantiomer (**8**) of catalyst **4** proved to be significantly less effective when performing the enantioselective kinetic resolution ROP of *rac*-LA.¹⁶

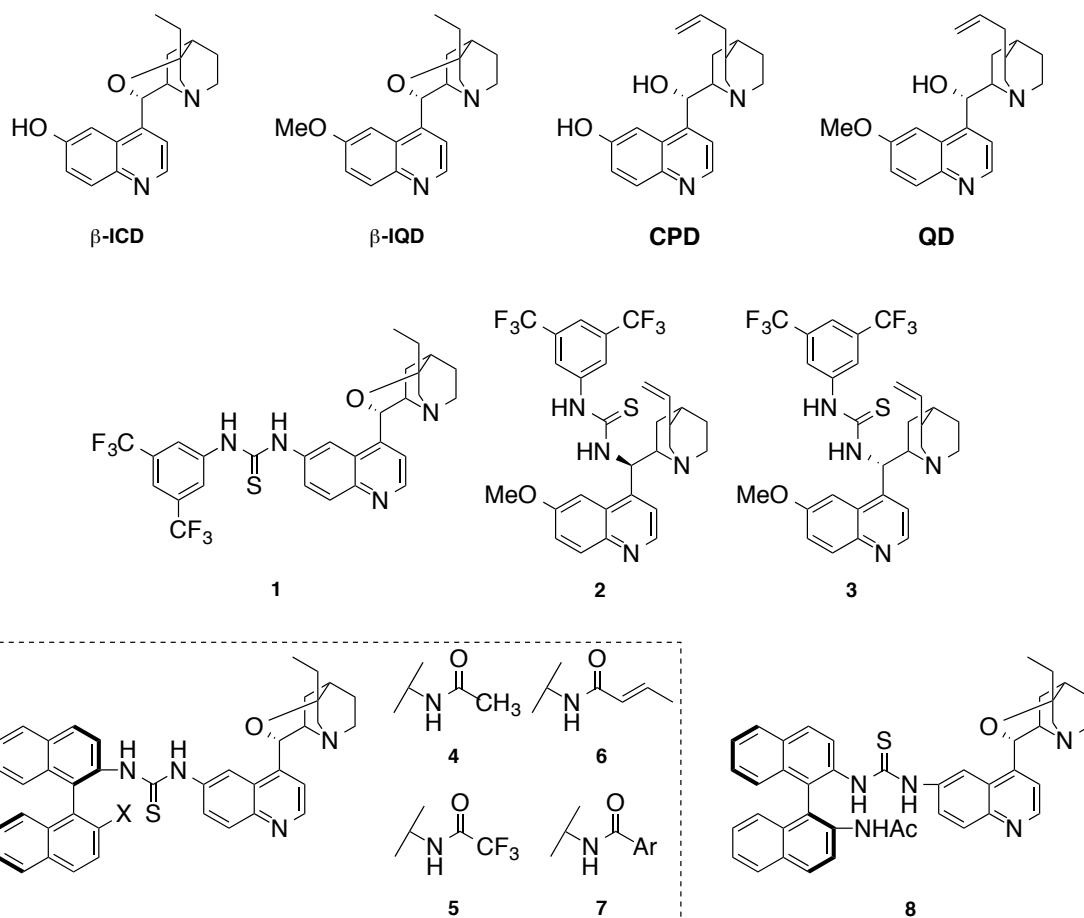


Figure 1.5. Selection of the chiral catalysts screened for kinetic resolution stereoselective ROP of *rac*-LA.

Next, an attempt was made to combine epimerization of *meso*-LA and subsequent enantioselective polymerization of *rac*-LA in one reaction vessel.¹⁶ At the first stage, *meso*-LA (0.0721 g) was epimerized, using the established pair DABCO/B(C₆F₅)₃ in toluene, and *rac*-LA/*meso*-LA in the ratio 99/1 was obtained. At the second stage, the epimerization solvent was switched to polymerization solvent, DFB, to yield the polymer with excellent results of $k_S/k_R = 35$ and $ee = 88\%$ at $[rac\text{-LA}] = 1.67\text{ M}$, at $25\text{ }^\circ\text{C}$, $[M]/[Cat]/[I] = 100/1/1$.¹⁶

The research initiative undertaken and successfully executed by Chen and coworkers furnished the armamentarium of stereoselective ring-opening polymerization with two remarkable tools. First, an affordable combination of commercially available products, DABCO/B(C₆F₅)₃, was established in the role of an extremely efficient epimerization agent converting *meso*-LA into *rac*-LA quantitatively. Second, a novel H-bonding thiourea-based catalyst with the dual chiral functionality was synthesized and successfully applied to polymerize *rac*-LA via enantioselective kinetic resolution. As an added bonus, the execution of subsequent epimerization and enantioselective ROP is a feasible operation yielding excellent polymerization characteristics.

1.7 Stereoselective Ring-Opening Polymerization Using Binaphthol-derived Phosphoric Acids

Binaphthol derivatives of phosphoric acid proved to be broadly applicable in a range of chiral transformations. The two key features of such compounds, the hydrogen-bond donating unit and a chiral motif, rendered these substances as potential organocatalysts for stereocontrolled ROP of lactide.¹⁷

The research project undertaken by Satoh and coworkers placed a number of binaphthol-derived phosphoric acids into the spotlight to exercise stereoselective ring-opening polymerization of *rac*-LA and yielded remarkable results in the enantioselective ROP of *rac*-LA.¹⁷

BINAP-derived phosphoric acids (fig.6figure 6) were used as catalysts for ROP of *rac*-LA. The polymerizations were performed in a range of conditions which differed by the initiator, monomer, and catalyst loadings as well as the reaction temperature. All the

scenarios provided polymers with target molecular weights, reasonable reaction times, and sufficiently narrow PDIs. The screening of the catalysts and polymerization conditions determined the optimal catalyst structure that exhibited the highest ratio of the polymerization rate constants for the two enantiomers of *rac*-LA.¹⁷

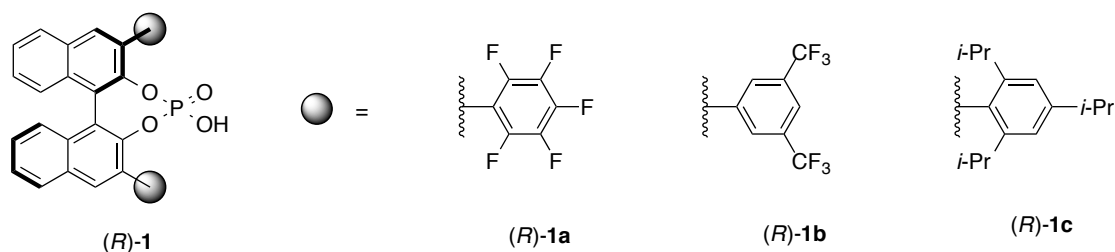
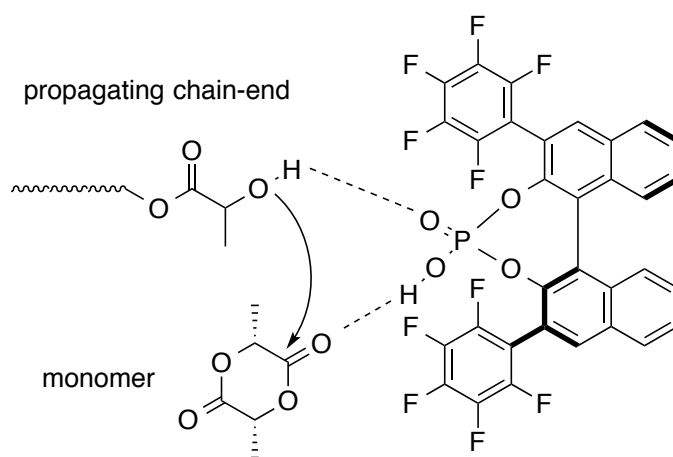


Figure 1.6. A selection of catalysts used for screening.

The most competitive performance was exhibited by catalyst **(R)-1a**. To start the quest for fine ROP conditions, the ROP of *rac*-LA at the conditions $[rac\text{-}LA]_0/[PPA]_0/[cat.] = 50/1/1$, in toluene, at 60 °C, was carried out and gave the promising results expressed by $k_D/k_L = 1.99$ and $ee = 24.4$. Next, the temperature impact on the ROP of *rac*-LA was assessed. The polymerization was done in the same reaction conditions with the exception that the temperature was gradually increased from run to run. The polymerization at 75 °C was found to be optimal since the highest $k_D/k_L = 28.3$ and $ee = 80.6$ were obtained. A further increase in the reaction temperature led to decreased performance indicators. For example, at 80 °C, $k_D/k_L = 17.3$ and $ee = 74.8$ whereas there was even sharper a drop in the kinetic resolution at 90 °C, $k_D/k_L = 9.60$ and $ee = 74.9$.¹⁷

The mechanism of polymerization was proposed to take the dual route (scheme 122). The two activating sites located in the catalyst structure are the acidic and basic moieties. By authors' proposal, the acidic moiety electrophilically activates the incoming LA monomer, whereas the basic moiety of the catalyst nucleophilically activates the growing polymer chain for the attack and subsequent ring-opening of the monomer.¹⁷



Scheme 1.12. Proposed mechanism of LA ROP catalyzed by a chiral (*R*)-1a.

The mechanistic hypothesis was bolstered via ¹³C NMR and IR studies of the interaction between the enantiomers of LA and catalyst (*R*)-1a. The interaction between catalyst (*R*)-1a and D-LA was visualized, whereas it was not established for L-LA, via ¹³C NMR spectroscopy. The carbonyl carbon shift of pure D-LA was measured to be 166.55 ppm. Then, the mixtures [(*R*)-1a]/[D-LA] = 1.0 and 3.0 were prepared and the same chemical shift moved downfield to 166.58 and 166.61, respectively, in the two mixtures. The chemical shift in the analogous experiment with L-LA did not change. Another confirmation for the mechanistic hypothesis was an IR study in which the

signal of the carbonyl group of pure LA acquired a lower wavenumber upon mixing of the monomer with (R)-**1a** in equal concentrations; a shift from 1755 cm⁻¹ to 1746 cm⁻¹ was detected in the spectrum.¹⁷

The mode of stereocontrol in the polymerization was postulated to be enantiomer-selective. To elucidate the stereoselectivity mode, the representative ROP in the optimized conditions was quenched at ~ 50% monomer conversion, and the unreacted monomer was extracted from the polymerization reaction mixture. The said unreacted monomer was subjected to the chiral HPLC analysis and the enantiomers traces demonstrated depletion in the content of one enantiomer. Thereby, the preference of the catalyst for a particular enantiomer of LA in ROP and root of the subsequent kinetic resolution of *rac*-LA were established.¹⁷

The project successfully accomplished by Satoh and coworkers added one more brick into the nascent foundation of stereoselective organocatalytic polymerization of cyclic esters.

1.8 Stereoselective Ring-Opening Polymerization of *rac*-Lactide Using Cinchona Alkaloids

A project undertaken by Chen and Miyake explored the abilities of natural products, cinchona alkaloids, in the stereoselective ring-opening polymerization of *rac*-LA. An optimal alkaloid was established as an effective catalyst for partial kinetic resolution polymerization of *rac*-LA.¹⁸

To begin with, a set of catalysts and initiators was chosen (fig.7figure 7). The catalyst CD proved to be inactive for ROP of *rac*-LA after a variety of polymerization

conditions was screened, including the application of external initiators, prolonged reaction times, and neat, monomer melt environment at an elevated temperature.¹⁸

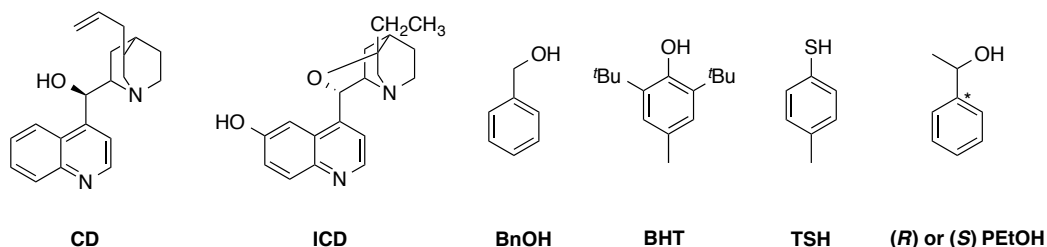


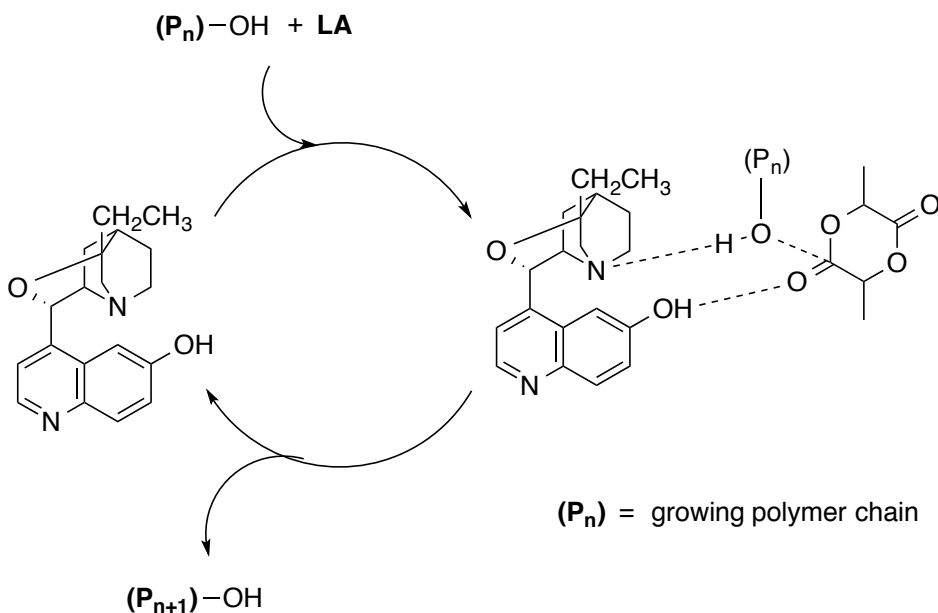
Figure 1.7. A selection of catalysts and initiators employed for the study.

The relative weakness of the amino group in CD compared with ICD and the supposition that the hydroxy group of CD is not acidic enough compared with ICD to activate the monomer, CD was rendered incapable of ROP of LA and the spotlight was turned onto another alkaloid from the pool. Consequently, the workers moved down the line of the catalyst selection and applied ICD as a bifunctional catalyst candidate for stereoselective ROP of L-LA. The general conditions for the polymerizations screening were as follows: DCM 5 mL, $T \sim 25\text{ }^{\circ}\text{C}$, $[\text{L-LA}] = 1.93\text{ M}$, $[\text{ICD}] = [\text{initiator}] = 19.3\text{ mM}$, conversion tracked by NMR, M_w/M_n determined by GPC. The absence of initiator brought satisfying starting results in the general ROP conditions: the 57.9% conversion was achieved in 126 hours, $MWD = 1.31$. The application of the initiating benzyl alcohol (BnOH) accelerated the reaction and improved the control over the polymer architecture: conversion of 86.3% was achieved in 31.5 hours, $MWD = 1.12$. Gratifyingly, the MALDI-TOF analysis did not show any observable transesterification.¹⁸

The next step taken was to apply the general polymerization conditions to ROP of *rac*-LA. This screening employed the measurement by NMR of probability of isotactic polymer chain propagation, the P_m value. ICD utilized without the initiator was notably slower than in the event of L-LA yet capable of 26.4% conversion in 73.0 hours with a moderate $P_m = 0.69$ and $MWD = 1.25$. The usage of 1.0 equivalent of initiating BnOH yielded the conversion of 90.4% in 61.5 hours with comparable $P_m = 0.68$ and a slightly improved $MWD = 1.12$. Higher loadings of the initiator (10 equivalents of BnOH) gave the conversion of 91.2 in 14.0 hours with $MWD = 1.11$ and the highest in the screen $P_m = 0.75$. The identical process at 0 °C in 10 mL of DCM furnished the conversion = 84.7% in 76.0 hours.¹⁸

The question of high importance was to identify if the catalyst ICD controls ROP of *rac*-LA through the chain-end or enantiosite control mechanism. To attempt to answer the question, the polymerization was run to ~50% conversion. The isolation of the unreacted monomer with a 1:1 hexanes:ⁱPrOH mixture and HPLC analysis of the isolate allowed the determination of the stereoselectivity factor s (k_S/k_R). Intriguingly, the fact that the values of s across the polymerizations were higher than unity pointed to the catalyst enantiosite control mechanism in place during the stereoselective ROP of *rac*-LA. The application of ICD as a sole bifunctional catalyst in the general polymerization conditions for ROP of *rac*-LA offered the conversion of 26.4% in 73.0 hours with ee (of the unreacted monomer) = 7.5% and $s = 1.6$. The utilization of 1.0 equivalent of BnOH in the identical conditions for ROP yielded the conversion of 48.4% in 16.4 hours, whereas $ee = 45.1%$ and $s = 4.4$, the highest stereoselectivity! The same reaction carried out with 5 equivalents of BnOH furnished the conversion of 86.8% in

14.0 hours, the highest $ee = 71.8\%$ yet lower $s = 2.2$. It is interesting to note that the utilization of the chiral initiators did not improve the factor s that was in the range 2.2 – 3.3. The decrease of the temperature to 0 °C or the usage of toluene as the solvent did not increase the s factor. The mechanism for ROP of LA was proposed¹⁸ (sscheme 313).



Scheme 1.13. Proposed mechanism of ICD-mediated ROP of LA.

Overall, the polymerizations proceeded through the preferential polymerization of L-LA and led to the production of isotactically-enriched PLA. The polymer obtained upon the reaction at the general conditions and employment of 10 equivalents of BnOH ($s = 1.9$, $ee = 71.1$) was subjected to DSC analysis and demonstrated three T_m points at 148 °C, 132 °C, and 120 °C, which likely correspond to regions of the polymer with various amounts of isotacticity. In conjunction with the presence of polymer parts with high isotacticity, $T_g = 34$ °C was noted.¹⁸

In conclusion, the successful step accomplished by Chen and Miyake, showcased effective application of an alkaloid from the cinchona family for enantioselective ROP of *rac*-LA, even though the achieved selectivity levels were unostentatious. The project nevertheless contributed a significant development into the field of stereoselective ROP of cyclic esters.

1.9 Stereoselective Ring-Opening Polymerization of *rac*-Lactide Using Unnatural Densely Substituted Amino Acids

A team of researchers from Spain developed a series of unnatural densely substituted amino acids capable of excellently stereocontrolled ROP of *rac*-LA.¹⁹ The inspiration for this project stemmed from previous successes achieved with chiral amino acids employed for asymmetric synthesis, chiefly in small-molecule transformations.

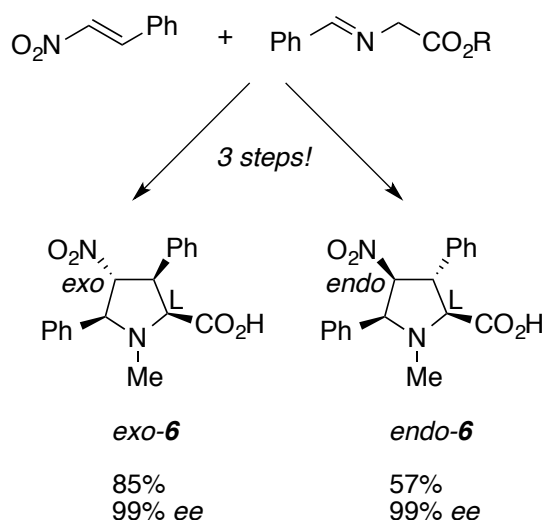
Initially, the authors deemed to try the almost proverbial catalyst, proline, for ROP of *rac*-LA since this catalyst, in particular, was a successful performer in a wide repertoire of asymmetric processes.¹⁹

The standard conditions for polymerization screening were devised: solvent DCM, [LA] = 1 M, [LA]/[BnOH]/[cat.] = 50/1/1 (unless noted otherwise), conversion was determined by NMR in CDCl₃, polymers weights were characterized by SEC, P_m values were determined by ¹³C NMR spectroscopy.¹⁹

A bulkier derivative proline, Boc-L-Pro and DBU, were used at the 5 equivalents loading to the initiator for the ROP of *rac*-LA. The ~98% conversion, gave a polymer with M_n = 8000 g/mol, PDI = 1.2, and the modest P_m = 0.65.¹⁹

In the same reaction scenario Boc-L-Pro was switched to DBU (known as a fast catalyst in itself for ROP of LA), and a slightly poorer controlled polymeric product was obtained with $M_n = 12200$ g/mol, PDI = 2.1, and the worse $P_m = 0.50$.¹⁹

After attaining unsatisfying results with the two H-bonding catalysts, the authors started pursuing the path of the proline catalyst modification. The general idea was to increase the steric bulk of this catalytic species through installation of large functional groups on the proline ring. A series of multi-step synthetic processes (sscheme 414) furnished the densely substituted amino acid catalysts, *exo-6* and *endo-6*.¹⁹



Scheme 1.14. A general synthetic scheme depicting the route towards the catalysts employed in the study.

The standard conditions were applied for ROP of L-LA: both *exo-6* and *endo-6* produced polymers with controlled molecular weights and $P_m = 1.00$ for both catalysts that signified no racemization occurrence during polymerization. The ROP of D-LA by *exo-6* and *endo-6* also furnished polymers with $P_m = 1.00$.¹⁹

Next, the challenging task was put on the line for *exo-6* and *endo-6*. The challenging ROP of *rac*-LA was accomplished with exquisite performance indicators. First, at the standard polymerization conditions *exo-6*/DBU at 50% conversion produced the polymer with $M_n = 3300$ g/mol, PDI = 1.1, and $P_m = 0.96$. Second, at the standard polymerization conditions *endo-6*/DBU at 51% conversion produced the polymer with $M_n = 3100$ g/mol, PDI = 1.2, and $P_m = 0.90$. Third, in the analogous conditions *exo-6* and *endo-6* together produced, at 98% conversion, a polymer with $M_n = 23000$ g/mol, PDI = 0.60, yet a substantially poorer $P_m = 0.60$.¹⁹

The polymers obtained from *rac*-LA at ~50% conversion were characterized for optical rotation parameters and thermal properties. Representative examples showcased $[\alpha]_D = +75.9$ which shows close characteristics of PDLA, whereas DSC characterization of the other polymer showed $T_m = 165$ °C characteristic of PLLA. These analysis items demonstrate the efficient chirality control of the polymer depending on the catalyst chirality.¹⁹

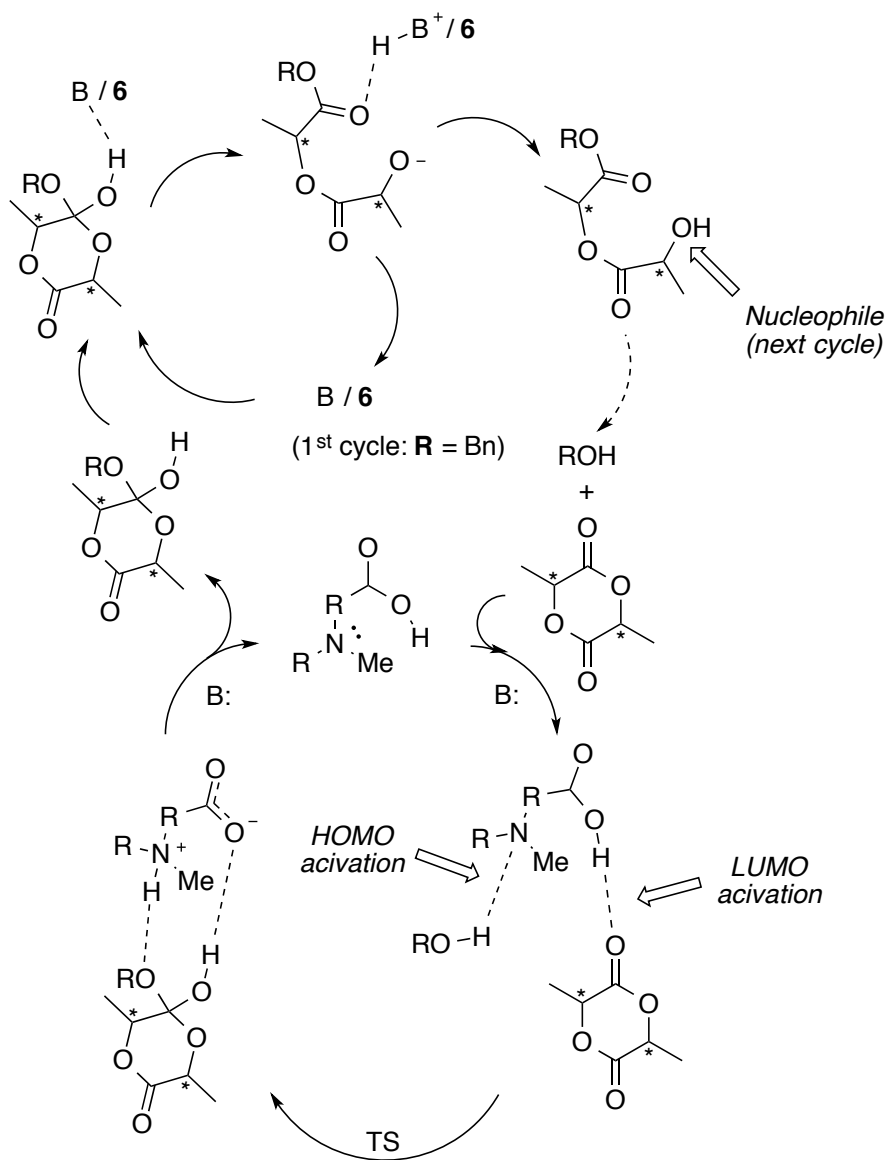
The following step after the achievement of impressive effects in ROP of *rac*-LA was to probe the mechanistic features of the polymerization process. The DOSY experiments on the 0.25 M and 1 M solutions of *exo-6* showed the existence of the increasing diffusion coefficient with the increase in concentration and thus the formation of *exo-6* was strongly suggested.¹⁹

The presence of DBU only negligibly increases the diffusion coefficient, suggesting the formation of a weak complex *exo-6*/DBU. The *exo-6*/DBU, according to the DFT calculations, most likely exists as an H-bonded complex as the formation of an

anionic complex would likely result in a higher diffusion coefficient by DOSY, which was not observed experimentally.¹⁹

The catalytic species association experiments led the authors to suggest that the formation of complexes between the cocatalysts is not strong enough to prevent the catalysts from commencing polymerization. Indeed, the COSY experiment performed on a mixture of *exo-6*, lactide, and benzyl alcohol (concentration of all was 1 M) let compute the diffusion coefficient for *exo-6*, suggesting the formation of a monomeric catalyst species in solution. These observations render *exo-6* as an active chiral catalytic species in ROP of LA.¹⁹

Extensive DFT calculations were conducted and the structures of *exo-6* and *endo-6* were shown (computationally) to preferentially attack L-LA and D-LA, respectively, during the *rac*-LA ROP process. The proposed catalytic enantioselective control cycle is presented¹⁹ below (sscheme 515).



Scheme 1.15. The proposed mechanism for ROP of LA, mediated by the unnatural densely substituted amino acid H-bonding catalyst.

The elegant project accomplished by the researchers from Spain¹⁹ constitutes a significant breakthrough in the stereoselective ROP of lactide. The novel catalyst can be readily synthesized from common materials and the catalyst chirality is capable of

targeted polymerization of either enantiomer in *rac*-LA with excellent levels of stereoselectivity resulting in fine-tuned architectures of the produced polymers.

1.10 Conclusion

The state of the art of stereoselective ring-opening polymerization of cyclic esters has been highlighted and as of right now, it is present in a rather nascent stage. However, the course of research in this underexplored and challenging field has seen substantial evolution. The attempts to achieve stereoselective ROP of *rac*-LA were constantly undertaken and various organocatalytic systems were utilized. Probably the first examples can be represented by N-heterocyclic carbenes as the agents of stereocontrolled ROP of *rac*-LA via chain-end mechanism, yielding moderate isotacticity of the polymeric product.²⁰ Everlasting explorations of hydrogen-bond donating thioureas bearing chiral motifs produced harbingers of using these compounds as potential catalysts for stereoselective ROP of *rac*-LA. For example, chiral thioureas proved to be efficient in dynamic kinetic resolution of other cyclic esters, azlactones.²¹
²² The chain-end control systems got enhanced over time to afford remarkable isotacticities of polymers, as was demonstrated by the advent of phosphazenes as ROP catalysts.¹¹ Further research efforts in the area offered catalytic systems capable of enantiosite control over ROP of *rac*-LA with excellent performance indicators, as was demonstrated by chiral binaphthyl phosphoric acids.¹⁷

The attention was later drawn to chiral cinchona alkaloids that were capable of partial kinetic resolution ROP of *rac*-LA.¹⁸ Interestingly, the work with alkaloids burgeoned into the project intertwinning alkaloid, binaphthyl, and thiourea motifs to

produce powerful organocatalytic systems for ROP of *rac*-LA.¹⁶ Circa the time this review was being written, the research pendulum swung towards the unnatural chiral amino acids established as potent catalysts for stereoselective ROP of *rac*-LA.¹⁹ The scope of enantioselective H-bonding catalytic systems for ROP of *rac*-LA appears to ever increase and it is possible to expect the emergence of new players on the stage in the foreseeable future. Additionally, there is also an emerging tendency in the expansion of chiral *monomers* scope, that will be a springboard to take the stereocontrolled ROP field to the next level towards new chiral polymeric materials.²³

This review chapter, as I trust, outlines the major milestones of research efforts in stereoselective ROP of *rac*-LA. My research aspiration is to implement innovation into the field and broaden the scope of metal-free catalytic processes of stereoselective ROP in particular and ROP in general.

1.11 References

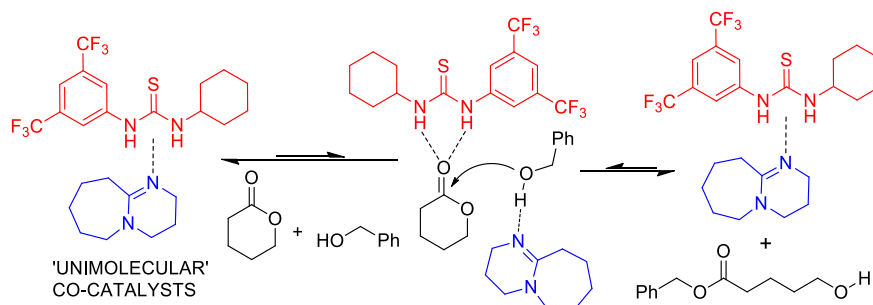
- (1) Tsuji, H. *Macromol. Biosci.* **2005**, *5*, 569–597.
- (2) Kamber, N. E.; Jeong W.; Pratt, R. C.; Lohmeijer, B. G. G; Hedrick J. L.; Waymouth R. M. *Chem. Rev.* **2007**, *107*, 5813–5840.
- (3) Thomas, C.; Bibal, B. *Green Chem.* **2014**, *16*, 1687–1699.
- (4) Coates, G. W. *Chem. Rev.* **2000**, *100*, 1223–1252.
- (5) Ovitt, T. M.; Coates, G. W. *J. Am. Chem. Soc.* **1999**, *121*, 4072–4073.
- (6) Kiesewetter, M. K.; Shin, E. J.; Hedrick, J. L.; Waymouth, R. M. *Macromolecules* **2010**, *43*, 2093–2107.
- (7) Lunt, J. *Polym. Degrad. Stab.* **1998**, *59*, 145–152.
- (8) Drumright, R. E.; Gruber P. R.; Henton, D. E. *Adv. Mater.* **2000**, *12*, 1841–1846.

- (9) Dechy-Cabaret, O.; Martin-Vaca, B.; Bourissou, D. *Chem. Rev.* **2004**, *104*, 6147–6176.
- (10) Dove, A. P.; Pratt, R. C.; Lohmeijer, B. G. G.; Waymouth R. M.; Hedrick J. L. *J. Am. Chem. Soc.* **2005**, *127*, 13798–13799.
- (11) Zhang, L.; Nederberg, F.; Messman, J. M.; Pratt, R. C.; Hedrick, J. L.; Wade, C. G. *J. Am. Chem. Soc.* **2007**, *129*, 12610–12611.
- (12) Jensen, T.R.; Breyfogle, L. E.; Hillmyer, M. A.; Tolman, W. B. *Chem. Commun.* **2004**, *21*, 2504–2505.
- (13) Dove, A. P.; Li, H.; Pratt, R. C.; Lohmeijer, B. G. G.; Culkin, D. A.; Waymouth, R. M.; Hedrick, J. L. *Chem. Commun.* **2006**, *27*, 2881–2883.
- (14) Stephan, D. W.; Erker, G. *Angew. Chem. Int. Ed.* **2010**, *49*, 46–76.
- (15) Shuklov, I. A.; Jiao, H.; Schulze, J.; Tietz, W.; Kühlein, K.; Börner, A. *Green Chem.* **2014**, *16*, 1687–1699.
- (16) Zhu, J.; Chen, E. Y.-X. *J. Am. Chem. Soc.* **2015**, *137*, 12506–12509.
- (17) Makiguchi, K.; Yamanaka, T.; Kakuchi, T.; Terada, M.; Satoh, T. *Chem. Commun.* **2014**, *50*, 2883–2885.
- (18) Miyake, G. M.; Chen, E. Y.-X. *Macromolecules* **2011**, *44*, 4116–4124.
- (19) Sanchez-Sanchez, A.; Rivilla, I.; Agirre, M.; Basterretxea, A.; Etxeberria, A.; Veloso, A.; Sardon, H.; Mecerreyes, D.; Cossío, F. *J. Am. Chem. Soc.* **2017**, *139*, 4805–4814.
- (20) Stanford, M. J.; Dove, A. P. *Chem. Soc. Rev.* **2010**, *39*, 486–494.
- (21) Berkessel, A.; Mukherjee, S.; Cleemann, F.; Müller, T. N.; Lex, J. *Chem. Commun.* **2005**, *14*, 1898–1900.
- (22) Berkessel, A.; Cleemann, F.; Mukherjee, S.; Müller, T. N.; Lex, J. *Angew. Chem. Int. Ed.* **2005**, *44*, 807–811.
- (23) Thomas, C. M. *Chem. Soc. Rev.* **2010**, *39*, 165–173.

INTENTIONALLY BLANK PAGE

Chapter 2

Cooperative Hydrogen-Bond Pairing in Organocatalytic Ring-Opening Polymerization

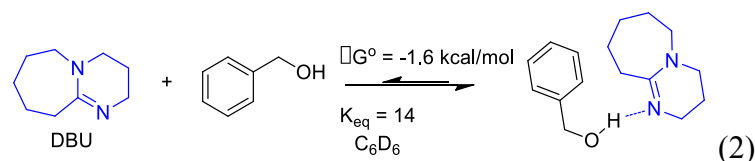
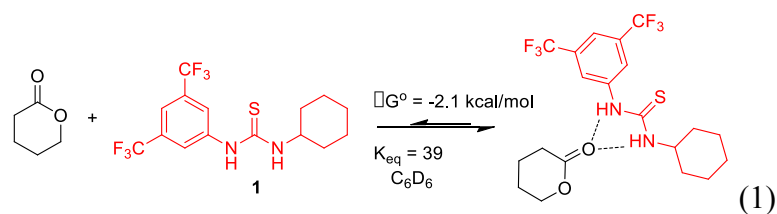


2.1 Abstract

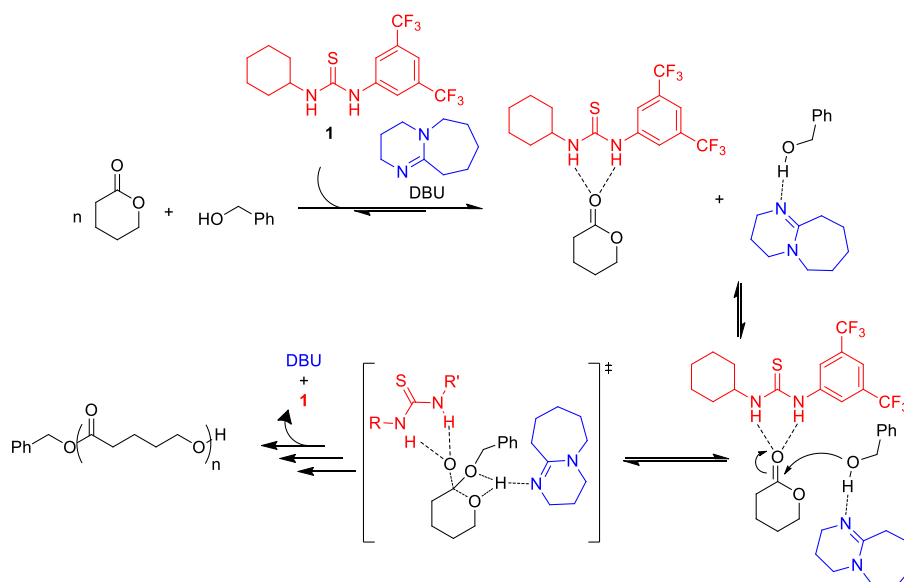
Thiourea (TU)/amine base cocatalysts are commonly employed for well-controlled, highly active ‘living’ organocatalytic ring-opening polymerizations (ROPs) of cyclic esters and carbonates. In this work, several of the most active cocatalyst pairs are shown by ¹H-NMR binding studies to be highly associated in solution, dominating all other known non-covalent catalyst/reagent interactions during ROP. One strongly-binding catalyst pair behaves kinetically as a unimolecular catalyst species. The high selectivity and activity exhibited by these ROP organocatalysts is attributed to the strong binding between the two cocatalysts, and the predictive utility of these binding parameters is applied for the discovery of a new, highly active cocatalyst pair.

2.2 Introduction

The multitude of polymer architectures and constructs that can be generated via organocatalytic ring-opening polymerization (ROP) is largely driven by the precise level of reaction control engendered by the catalysts.¹⁻³ The asymmetrical thiourea, **1** in Scheme 1, is believed to selectively activate cyclic esters and carbonates for ROP



(eq. 1)⁴; it is conveniently synthesized, highly active, and has become a preferred hydrogen bond donor for ROP.⁴⁻¹⁰ A more varied slate of base cocatalysts (H-bond acceptors) is used to activate the initiating/propagating alcohol for nucleophilic attack (eq. 2)^{4,6,8} and stronger bases are generally more active as cocatalysts for ROP.¹¹ The imine bases, particularly 1,8-diazabicyclo[5.4.0]undec-7-ene (DBU in scheme 2.1), have found common implementation in ROP.^{1,3,4,7,12} The preponderance of experimental^{4,10,13,14} and computational^{13,15,16} evidence suggests that bimolecular hydrogen bond activation of lactone and initiating/propagating alcohol facilitates the rapid ROP of lactone monomers exhibited by **1**/DBU, Scheme 1.^{3,4,17} The exact balance of interactions that must exist for a ‘living’ ROP to occur is impressive,⁵ and deep mechanistic insights into the robust and diverse set of H-bonding ROP organocatalysts will be the driving force for the development of the improved catalysts which precede new materials. In the following, we present evidence that **1** and amine base cocatalysts are highly associated in solution and that this binding is productive rather than inhibitory toward the high activity and selectivity of these **1**/amine base systems. This increased mechanistic understanding is applied to the discovery of a new cocatalyst pair for ROP.



Scheme 2.1. H-Bonding Mechanism for the ROP of δ -Valerolactone.

2.3 Results and Discussion

2.3.1 Chemical Kinetics

Kinetic studies were undertaken to help elucidate the roles of **1** and DBU in the ROP of δ -valerolactone (VL). While holding the concentration of VL (2M, 1.00 mmol) and benzyl alcohol (0.04 M, 0.020 mmol) constant in C_6D_6 , the concentrations of **1** and DBU were varied from $[1] = [DBU] = 0.05$ to 0.20 M, see Experimental Section (ES). The resulting plot, Figure 1, of observed rate constant, k_{obs} , versus ($[1] + [DBU]$), where $[1] = [DBU]$, is linear which describes an ROP reaction that is first order in cocatalysts: $Rate = k_{obs} [VL]$, where $k_{obs} = k_p([1] + [DBU])[benzyl\ alcohol]$, and k_p is the polymerization rate constant. This observation is in contrast to a previous report which assumed for purposes of kinetic fitting that rate is proportional to both $[1]$ and $[base]$ (i.e. $k_{obs} = k_p [1][base][benzyl\ alcohol]$).⁴ The ROP rate being proportional to ($[1] +$

[DBU]) suggests a cocatalyst system that behaves as a discrete catalyst species, yet the role of the individual cocatalyst moieties is unclear.

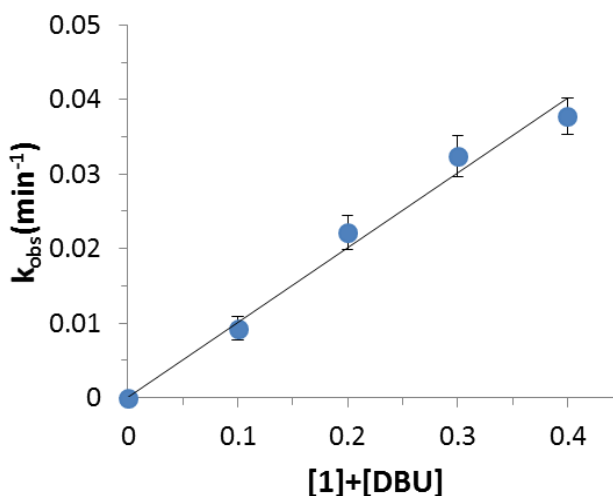


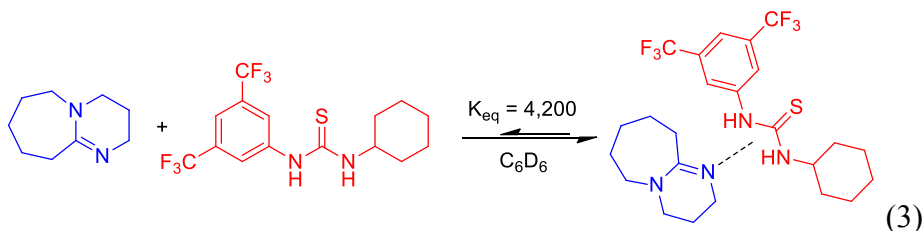
Figure 2.1. For the ROP of VL, observed rate constant (k_{obs}) vs $[1] + [\text{DBU}]$. Conditions: VL (2 M, 100 mg):benzyl alcohol 50:1 in C_6D_6 . Rate = $k_{\text{obs}}[\text{VL}]$, where $k_{\text{obs}} = k_{\text{p}}([1] + [\text{DBU}])[\text{benzyl alcohol}]$.

Kinetic studies were also undertaken when $[1] \neq [\text{DBU}]$. For the case where **1** is in excess, the observed rate constant is insensitive to $[1]$ (within error) for the concentration range examined (see ES). The thiourea, **1**, is known to self-bind at high concentrations,⁵ and any increased monomer activation may be attenuated by catalyst self-inhibition (due to **1**•**1**) at $[1] > 0.2$ M. In the case of $[\text{DBU}] > [1]$, the data describe a reaction that is inverse first order in $[\text{DBU}]$ for the entire concentration range examined (100 mM $< [\text{DBU}] < 400$ mM; $[1] = 50$ mM), see ES. The fact that both cocatalysts must be present for ROP to occur suggests that DBU facilitates catalysis.

However, the empirical rate dependences upon [1] and [DBU] imply an inhibitory role for DBU which would occur upon a strong binding interaction between **1** and DBU.

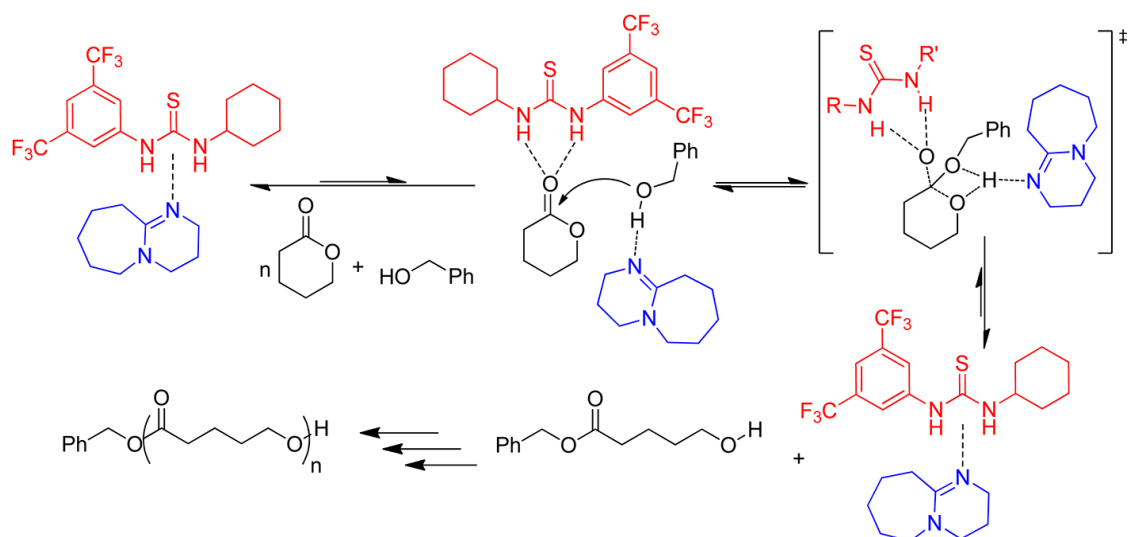
2.3.2 Cocatalyst Binding

Inhibitory interactions by amine base cocatalysts upon **1** have been suggested by other researchers to decrease ROP rate.⁵ In an illuminating study of several cocatalysts, it was found via ¹H-NMR binding studies that **1** and sparteine, an erstwhile favorite catalyst pair for the ROP of lactide,⁹ exhibit a moderate binding constant of $K_{\text{eq}}(\text{CDCl}_3) = 6 \pm 1$.^{5,18} This magnitude of binding constant was not thought to be inhibitory to catalysis, but the same study ascribed the reduced activity of some more strongly binding cocatalysts to an undesirable H-bond equilibrium that reduces the effective concentration of catalyst through self-inhibition.^{5,7} The potent H-bonding ability of DBU¹⁹ and high activity of **1**/DBU for ROP belie this concept.



A ¹H-NMR binding study²⁰ conducted in our laboratory by serial dilution of a 1:1 mixture of DBU and **1** (from 5 mM to 0.125 mM) reveals a strong **1**•DBU binding constant of $K_{\text{eq}} = 4,200 \pm 170$ (eq 3), see ES. Such strong interactions have previously been posited (*vide infra*) between coulombically tethered cocatalysts,¹⁴ and strong cocatalyst binding is not necessarily inhibitory to ROP. All binding processes are reversible and rapid on the NMR timescale, and the ROP is determined by the approach to the equilibrium monomer concentration, $[\text{VL}]_{\text{eq}}$. The strong **1**•DBU binding constant

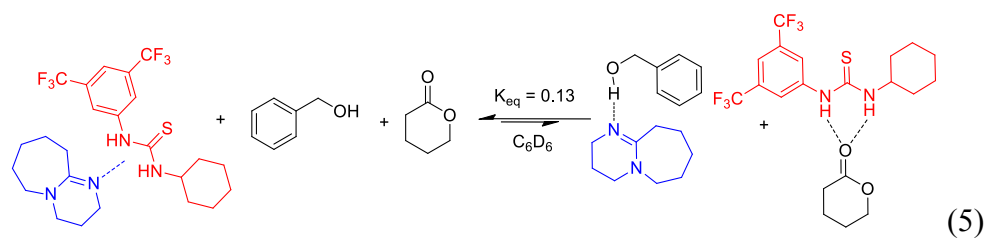
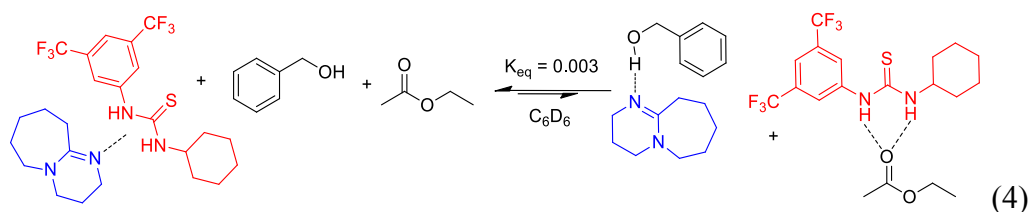
may simply act in concert with other known interactions (**1**•VL and DBU•benzyl alcohol; eqs 1 and 2) to hold all reagents in close proximity during a rapid exchange of binding partners thereby accelerating the reaction.²¹ However, the kinetic data suggest that the strong binding could serve to make a distinct catalytic species.²² The binding and kinetic data collectively describe a reaction process where highly self-associated cocatalysts can be cooperatively interrupted by VL and alcohol to result in a reaction turnover, scheme 2.2.



Scheme 2.2. Proposed Cocatalyst Binding Mechanism for the ROP of VL.

The selectivity of **1**/DBU for monomer in the ROP of VL can be rationalized by the magnitude of the **1**•DBU binding constant. This selectivity has previously been attributed to the preference of **1** to bind to *s*-cis esters (monomers) versus *s*-trans esters (polymer backbone);⁴ however some **1**/amine base combinations result in almost zero transesterification of the resultant polymer after 4 h.²³ The very dependence of post-polymerization transesterification upon the identity of the base cocatalyst suggests that

factors other than the **1**•ester binding constants control ROP selectivity. Indeed, the identity of the base cocatalyst dominates the equilibria which describe the ability of ethyl acetate (a surrogate for polymer, which exhibits a small but non-zero binding to **1**)⁴ to interrupt the **1**•DBU pair (eq 4) versus that of VL (eq 5). These values ($K_{\text{eq}} = 0.003$ vs $K_{\text{eq}} = 0.13$, respectively), which can be found through thermodynamic sums, could account for the high selectivity of the ROP reaction. Further, altering the base cocatalyst would be expected to drastically alter the cocatalyst selectivity for monomer, as empirically observed.^{1-3,23}



Our study was continued on a variety of base cocatalysts (with **1**) for ROP, and a relationship between cocatalyst binding and ROP activity was discovered. Binding constants to **1** in C_6D_6 were measured either by the dilution or titration method²⁴⁻²⁷ for bases previously evaluated as cocatalysts in the ROP literature: DBU, MTBD (7-methyl-1,5,7-triazabicyclo[4.4.0]dec-5-ene), pyridine, proton sponge (1,8-bis(dimethylamino)naphthalene), and DMAP (4-dimethylaminopyridine). The k_{obs} values were also measured for each of these bases (see ES) in the **1** (0.1 M, 0.050 mmol) and base (0.1 M, 0.050 mmol) catalyzed ROP of cyclic ester monomers (2 M, 1.00 mmol) from benzyl alcohol (0.04 M, 0.020 mmol); the results of these experiments are

shown in table 2.1. In general, a strong **1**·base binding constant is associated with rapid ROP, and weakly binding cocatalysts exhibit very low or zero ROP activity.

Table 2.1. Binding constants and observed rate constants for the bases studied.

base	K_{eq} ^a	k_{obs} ^b x 10^{-3} , min ⁻¹
proton sponge	0	0 ^c
pyridine	9 ± 1	0 ^c
DMAP	170 ± 30	4.1±0.2 ^c
BEMP	1,200 ± 40	17.8±0.3
MTBD	1,500 ± 100	20.0±0.1
DBU	4,200 ± 170	16.2±0.1

^aBinding constant (at 292 K) for base + **1** in equilibrium with **1**·base as measured with NMR titration/dilution experiments. ^bObserved rate constant, k_{obs} , for the **1**/base catalyzed ROP of VL from benzyl alcohol. Conditions VL:base:**1**:benzyl alcohol:100 (100 mg, 2 M):5:5:2 in C₆D₆. ^cObserved rate constant (at 100 h) for the ROP of LA, same experimental conditions as footnote b.

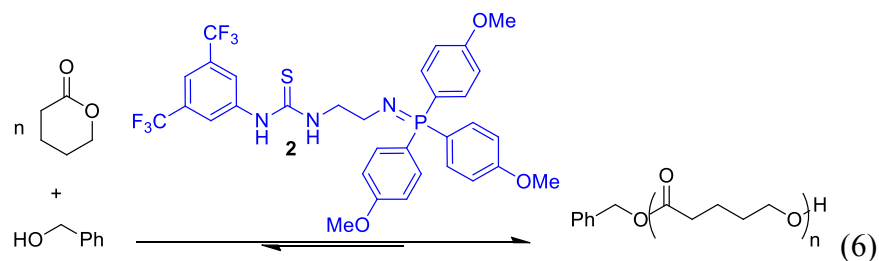
In the low binding constant regime, K_{eq} correlates with polymerization rate, and cocatalyst binding constant appears to be a better predictor of catalytic activity than does pK_a . The k_{obs} for the systems that exhibited weak binding (**1** with DMAP, pyridine or proton sponge) were measured for the **1**/base catalyzed ROP of L-lactide (LA) (Table 1) as they are not active for the ROP of VL. Of these cocatalysts, only **1**/DMAP exhibits ROP activity: k_{obs} (LA)= 4.1 x 10⁻³ min⁻¹. Both **1**/pyridine and **1**/proton sponge are inactive for the ROP of LA, but **1**·pyridine displays weak binding (**1**·pyridine K_{eq} = 9 ± 1) whereas **1**·proton sponge exhibits none. The binding constant observed for **1**·DMAP was the strongest of the three (**1**·DMAP K_{eq} = 170 ± 30). A pK_a explanation of ROP

activity is unsuccessful for the case of DMAP vs proton sponge (in acetonitrile: DMAP-H⁺ pK_a = 18.2,²⁸ proton sponge-H⁺ pK_a = 18.7),^{29,30} yet their ROP activities correlate well with the strength of their binding to **1**. For the **1**/pyridine system, its moderate binding constant yet lack of ROP activity could indicate that ROP is only feasible when cocatalyst binding becomes competitive with **1**·VL K_{eq} (C₆D₆) = 44,⁴ **1**·LA K_{eq} (CDCl₃) = 2)⁵ such that the cocatalysts are closely associated in solution.

The binding constant between **1** and DBU was the strongest measured, but this catalyst pair is not the most active of those examined for the ROP of VL. **1**/MTBD exhibited a faster rate for the ROP of VL than **1**/DBU, which is reasonably predicted by pK_a: MTBD-H⁺ pK_a^{MeCN} = 25.4;³⁰ DBU-H⁺ pK_a^{MeCN} = 24.3.³⁰ As Bibal *et al.* noted, strong cocatalyst binding is anticipated to be inhibitory to ROP,^{5,6} and one interpretation of the **1**/DBU vs **1**/MTBD reactions is that ROP activity (*k*_{obs}) becomes attenuated due to catalyst inhibition if the cocatalyst binding constant becomes too large, 1,500 < K_{eq} < 4,200.

2.3.4 BEMP/**1** Catalyzed ROP

One of the most powerful applications of reaction mechanism elucidation is in the discovery of new catalyst species, and we sought to ply our increased understanding of **1**/base catalyzed ROP to this end. While this work was ongoing, Dixon *et al.* reported the ROP of VL by a phosphazene-inspired bifunctional TU-iminophosphorane catalyst, **2** in eq 6.³¹



The bifunctional catalyst **2** exhibits ‘living’ ROP behavior, the usual relative monomer reactivity ($k_{LA} > k_{VL} \gg k_{CL}$), and good selectivity for monomer.³¹ While the application of phosphazene bases like BEMP (2-*tert*-butylimino-2-diethylamino-1,3-dimethylperhydro-1,3,2-diazaphosphorine) to the ROP of LA is known,³² this superbase is not active for the ROP of VL except in neat monomer where reaction control is poor (2 days, 93% conversion, $M_w/M_n = 1.23$).³³

The binding constant of BEMP and **1** was measured in C_6D_6 , $K_{eq} = 1,200 \pm 40$. Within the set of K_{eq} vs k_{obs} data, the strength of the **1**·BEMP binding constant suggests its VL ROP activity should be similar to that of **1**/MTBD. Indeed, the observed rate constant for the **1**/BEMP catalyzed ROP of VL ($k_{obs}(VL) = 17.8 \times 10^{-3} \text{ min}^{-1}$) is slightly less than that of **1**/MTBD, as would be expected by the **1**·BEMP K_{eq} value. This result would not be anticipated by a pK_a argument: $BEMP-H^+ pK_a^{MeCN} = 27.6$,³⁴ $MTBD-H^+ pK_a^{MeCN} = 25.4$.³⁰ Further studies show that **1**/BEMP is active for the ROP of VL, ϵ -caprolactone (CL), and trimethylene carbonate (TMC) but is inactive for β -butyrolactone (BL), Table 2.2. The **1**/BEMP catalyzed ROP of VL from pyrenebutanol exhibits the characteristics of a ‘living’ ROP: linear evolution of M_n with conversion (see ES), evidence of end group fidelity (overlapping RI and UV signals by GPC), and M_n that is predictable by $[M]_0/[I]_0$. The evidence of H-bonding for both BEMP-to-alcohol³³ and **1**-to-VL⁴ taken with these experimental observations suggest an H-bond

mediated ‘living’ ROP of VL. The ROP activity (for VL) of the cocatalyst systems **1**/BEMP, **1**/DBU and **1**/MTBD is only slightly attenuated in THF.

Table 2.2. The **1**/BEMP catalyzed ROP of cyclic monomers.^a

monomer	[M] ₀ /[I] ₀	time (h)	% conv.	M _n (GPC)	M _w /M _n
BL ^b	100	48	0	--	--
VL	50	0.75	88	6,200	1.05
VL	100	2	92	14,600	1.03
VL	200	3	83	32,200	1.01
VL	500	5	98	92,600	1.01
CL ^b	50	42	98	8,900	1.03
CL ^b	100	75	94	17,000	1.02
TMC ^b	50	0.2	99	2,800	1.07
TMC ^b	100	0.3	97	7,600	1.03

^aReaction conditions: monomer (2 M, 100 mg), pyrenebutanol, 5 mol % BEMP and 5 mol % **1**. Reactions conducted in dry toluene in a glovebox (N₂) and quenched at the given time by the addition of 2 mol equiv of benzoic acid to BEMP. ^bReactions performed in C₆D₆.

2.4 Conclusion

For the organocatalytic ROP cocatalysts examined, the magnitude of the cocatalyst binding constant has been shown to be proportional to the ROP rate. For the bases studied, cocatalyst binding constant is a far better predictor of catalytic activity than pK_a. The strongly binding **1**/DBU system behaves kinetically as a unimolecular catalyst species, and it could be representative of a hydrogen-bonding analogue of so-called ‘cooperative ion pairing’ in asymmetric organocatalysis.²² We agree with the conclusion of Bibal *et al.* that TU/amine base binding can be inhibitory to ROP^{5,6} but

submit that: 1) the phenomenon is much more general than first proposed; 2) the magnitude of the interaction may be a good predictor of cocatalyst activity; and 3) the point at which cocatalyst binding becomes counterproductive to catalysis is significantly higher than once believed. As organocatalysis strives to mimic the awe-inspiring catalytic abilities of nature, it is important to fully understand the catalytic systems being employed. As it would happen, the roles of **1** and DBU in the ROP of VL are not very dissimilar from those of enzyme and cofactor. Further mechanistic studies are ongoing; such studies have already revealed one new catalyst system for ROP (**1**/BEMP) and they are expected to yield dividends in the form of more new catalyst systems.

2.5 Experimental Section

2.5.1 General Considerations

All manipulations were performed in an MBRAUN stainless steel glovebox equipped with a gas purification system under a nitrogen atmosphere. All chemicals were purchased from Fisher Scientific and used as received unless stated otherwise. Toluene and THF were dried on an Innovated Technologies solvent purification system with alumina columns and nitrogen working gas. Benzene- d_6 was supplied by Cambridge Isotope Laboratories and distilled from CaH_2 under nitrogen atmosphere. δ -valerolactone (VL; 99%) and ϵ -caprolactone (CL; 99%) were distilled from CaH_2 under high vacuum. Benzyl alcohol was distilled from CaH_2 under high vacuum. L-lactide was supplied by Acros Organics and recrystallized from dry toluene prior to use. 1-[3,5-Bis(trifluoromethyl)phenyl]-3-cyclohexylthiourea (**1**) was synthesized and

purified according to literature procedures.⁴ 1,8-diazabicyclo[5.4.0]undec-7-ene (DBU) and 7-methyl-1,5,7-triazabicyclo[4.4.0]dec-5-ene (MTBD) were purchased from TCI. NMR experiments were performed on a Bruker Avance 300 MHz spectrometer. Size exclusion chromatography (SEC) was performed at 40°C in dichloromethane (DCM) using a Agilent Infinity GPC system equipped with three Agilent PLGel columns 7.5 mm x 300mm (5µm, pore sizes: 10³ Å, 10⁴ Å, 10⁵ Å). Molecular weight and M_w/M_n were determined versus PS standards (500 g/mol – 3,150 kg/mol; Polymer Laboratories).

2.5.2 Determination of Binding Constant by the Dilution Method

A stock solution containing **1** (2.8 mg, 0.0075 mmol) and DBU (0.0011 mL, 0.0075 mmol) was prepared in deuterated benzene (1.5 mL). This solution was distributed to 6-10 NMR tubes, and each NMR tube was diluted with benzene-d₆ to give final concentrations ranging from 5 mM to 0.313 mM. ¹H-NMR spectra (referenced to residual benzene-H) were acquired for each tube at multiple temperatures and the chemical shift of the *ortho*-protons of **1** was noted. The K_{eq} values were determined from the linearized (Lineweaver-Burke) forms of the binding equations (see ES), which are a powerful means of accurately measuring binding constants with fewer samples (versus curve fitting).²⁵ The binding constant for each **1**/base pair was determined at elevated temperatures (303 - 323 K). The enthalpy and entropy of binding were determined by plotting $\ln K_{eq}$ versus 1/T to conduct a Van't Hoff analysis, and error was determined from linear regression at the 95% confidence interval.

2.5.6 Example Determination of k_{obs}

In a glovebox under nitrogen atmosphere, one vial (baked at 140°C overnight) was loaded with a stir bar and δ -valerolactone (VL) (0.0927 mL, 1.00 mmol). A second dried vial was loaded with benzyl alcohol (0.0021 mL, 0.020 mmol), **1** (18.5 mg, 0.050 mmol), and DBU (0.0075 mL, 0.050 mmol). 200 μL of deuterated benzene was added to the first vial, and 300 μL of deuterated benzene was added to the second vial. The solutions were stirred until homogeneous. The reaction was started by transferring the solution of VL into the vial containing catalyst solution and stirred to mix before transferring to an NMR tube. The change in the concentration of the monomer was monitored by $^1\text{H-NMR}$. Rate constants were extracted from a plot of $\ln([\text{VL}]_0/[\text{VL}])$ versus time; the reaction is linear on this plot to 3+ half-lives. The slope of this plot is k_{obs} , and the error was determined by propagation of NMR integration error at $\pm 5\%$. Only [**1**] and [DBU] were varied between individual kinetic runs.

2.5.7 Example ring-opening polymerization.

In a typical polymerization, VL (0.100 g, 0.999 mmol) was added to a 20 mL glass vial containing a stir bar, both of which were baked at 140°C overnight. In another dried 20 mL glass vial with stir bar, **1** (0.0185 g, 0.499 mmol), BEMP (14.45 μL , 0.499 mmol) and pyrenebutanol (9.96 μmol) were added. Solvent (for C_6D_6 0.4744 g, 2 M in VL) was added to both vials to bring the total mass of solvent to the desired level, approximately equal portions of solvent per vial. After stirring for 5 minutes, the VL solution was transferred via pipette to the vial containing catalysts and initiator. To quench the reaction, benzoic acid (2 mol equivalents to base) was added. The vial was

removed from the glovebox and the polymer solution was treated with hexanes to precipitate the polymer. The hexanes supernatant was decanted, and the polymer removed of volatiles under reduced pressure. Yield, 90%; $M_w/M_n = 1.03$; $M_n(\text{GPC}) = 16,800$. $^1\text{H NMR}$ (C_6D_6) δ 7.22-7.17 (2H, d, benzyl aryls), 7.13-7.05 (3H, m, benzyl aryls), 4.97 (2H, s, benzylic), 3.91 (193H, t, $-\text{C}(\text{O})\text{OCH}_2-$), 2.04 (193H, t, $-\text{CH}_2\text{C}(\text{O})\text{O}$), 1.58-1.30 (386H, m, $\text{C}(\text{O})\text{CH}_2\text{CH}_2\text{CH}_2\text{CH}_2\text{O}-$).

2.5.8 Equations used for binding studies.

$$\text{For dilution: } \Delta\delta/[\text{base}] = -2K_{\text{eq}}\Delta\delta + K_{\text{eq}} \delta_{\text{C}}$$

$$\text{For titration: } \Delta\delta/[\text{base}] = -K_{\text{eq}}\Delta\delta + K_{\text{eq}} \delta_{\text{C}}$$

Where³⁵⁻³⁷:

$\Delta\delta$ is the difference between the chemical shift of the observed *ortho*-protons in the TU-Base mixture and of pure TU;

δ_{C} is the chemical shift of the *ortho*-protons of TU in the complex, TU-Base;

K_{eq} is the binding constant between **1** and a Base.

The determination of binding constants from the slope of the linear (Lineweaver-Burke) forms of the binding equation (above) has several benefits over fitting the binding curve.³⁵ It should be noted that the linearized form of the binding equations are rigorously true and can be derived from the equilibrium expression using simple algebra.³⁷ Very accurate data can be obtained with fewer data points (versus curve fitting) because experimental errors from inaccurate concentration are attenuated in the linearized form. For this method, the accuracy of K_{eq} versus number of data points has been tested in the literature and shown to be highly accurate with 5 data points.³⁶ These

studies even omitted the plateau of the binding curve,³⁶ which was never the case in our studies. Further, computationally fitting the binding curve introduces indeterminable error from the fitting approximations. Error in the slope of the linear form (K_{eq}) is solely determined by the scatter in data (from residual error in concentration), and the error in K_{eq} is exactly the error in the slope of the line, which can be determined from linear regression.³⁷

Table 2.3. Thermodynamic Values of Binding between **1** and various bases.

Value \ Base	Proton Sponge	Pyridine	DMAP	BEMP	MTBD	DBU
K_{eq} (292K)	0	9	170±30	1,200±40	1,500±100	4,200±170
ΔH° (kcal/mol)	--	--	-8.8±1.1	-2.7±0.4	-4.2±0.3	-10.7±2.0
ΔS° (cal/mol·K)	--	--	-20.1±3.6	5.0±1.4	0.1±1.1	-20.4±6.4

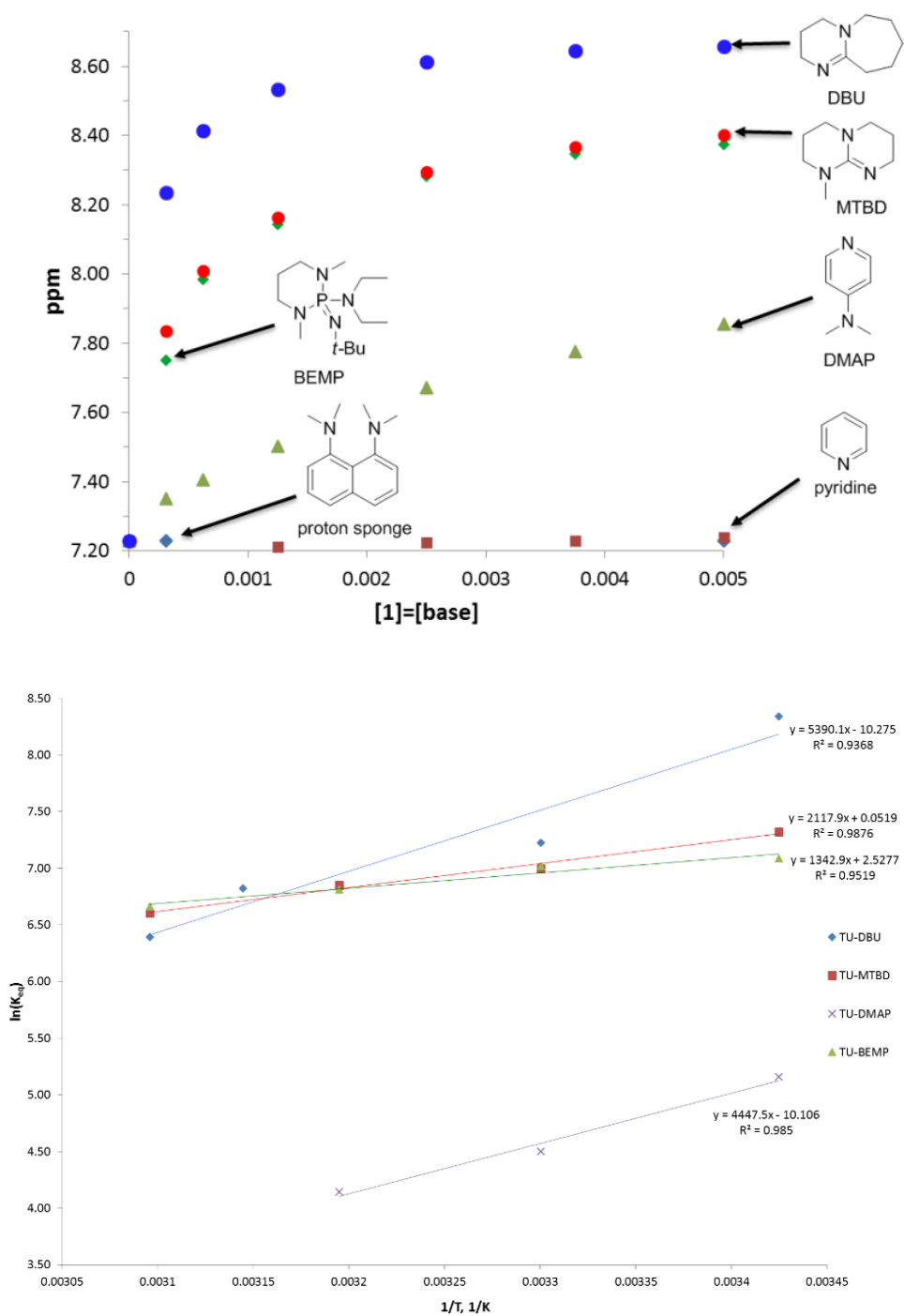


Figure 2.2. (upper) The bases studied along with the respective binding curves to **1**. (lower) Van't Hoff plots of binding between **1** and various bases.

2.5.9 Kinetic Plots

For all plots $[VL] = 2M$, $[\text{benzyl alcohol}] = 0.04 M$ in C_6D_6 .

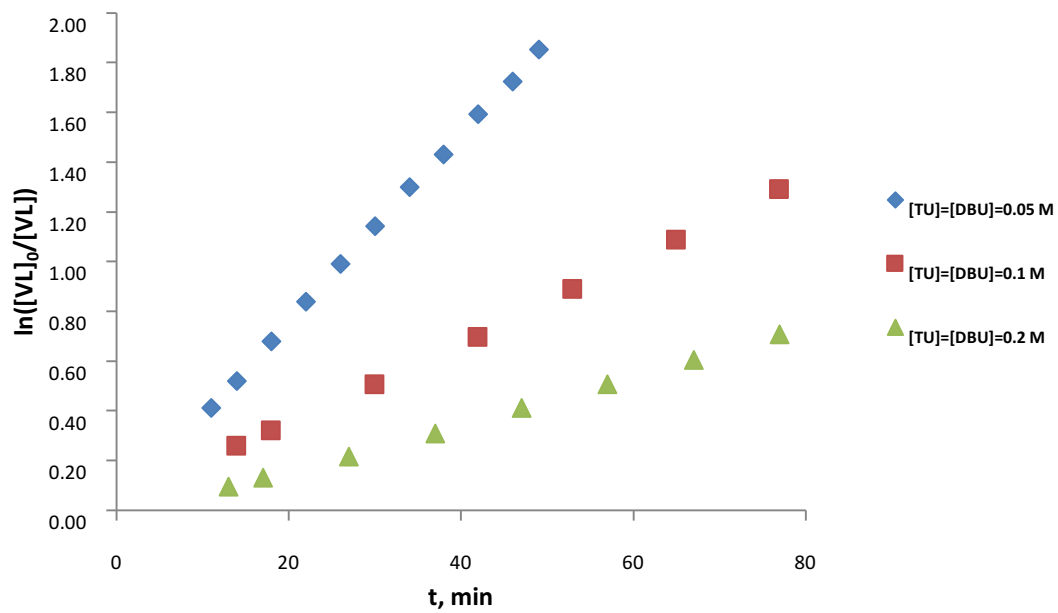


Figure 2.3. First order evolution of $[VL]$ vs time when $[1] = [DBU]$.

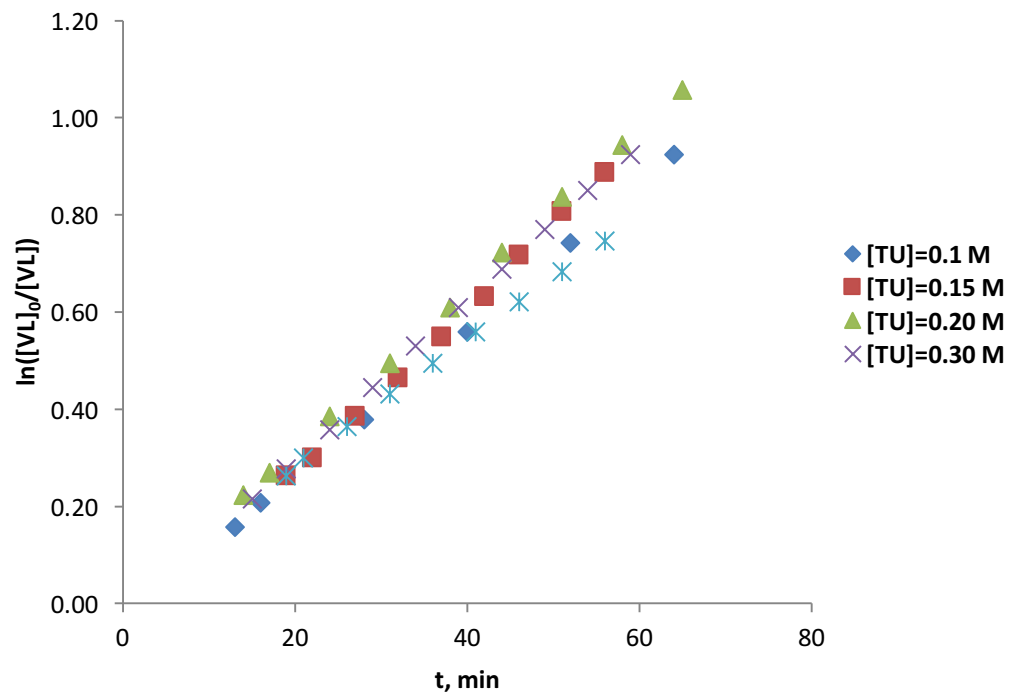


Figure 2.4. First order evolution of [VL] vs time when [1] > [DBU] = 0.05 M.

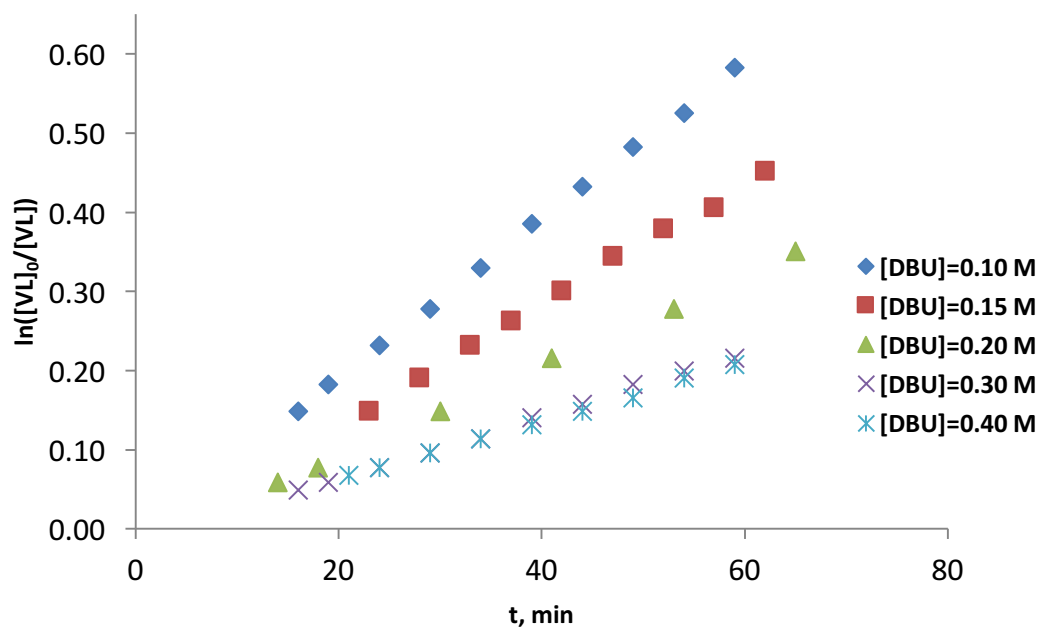


Figure 2.5. First order evolution of [VL] vs time when [1] = 0.05 M < [DBU].

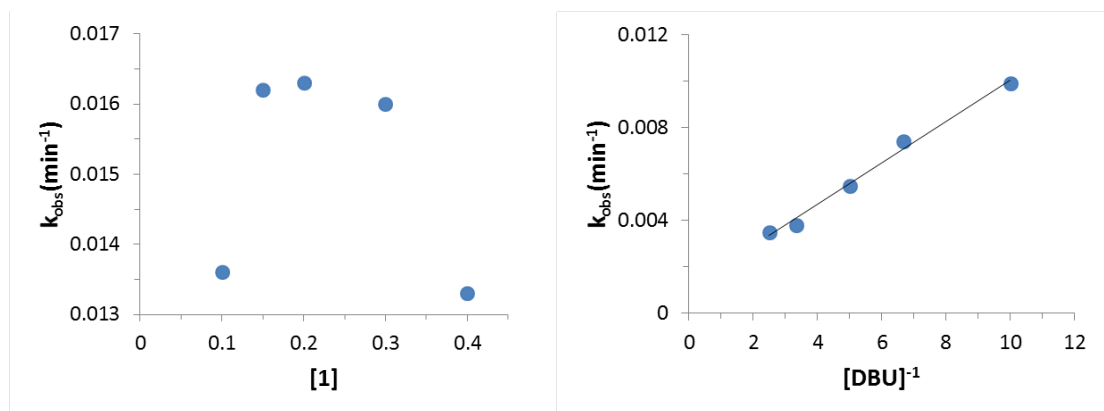


Figure 2.6. For the ROP of VL: (left) observed rate constant vs [1] when [1] > [DBU] = 50 mM; (right) observed rate constant vs [DBU]⁻¹ when [DBU] > [1] = 50 mM. Conditions: VL (2 M, 100 mg):benzyl alcohol 50:1 in C₆D₆. Rate = k_{obs} [VL]; where k_{obs} = kP[1 +DBU][benzyl alcohol]

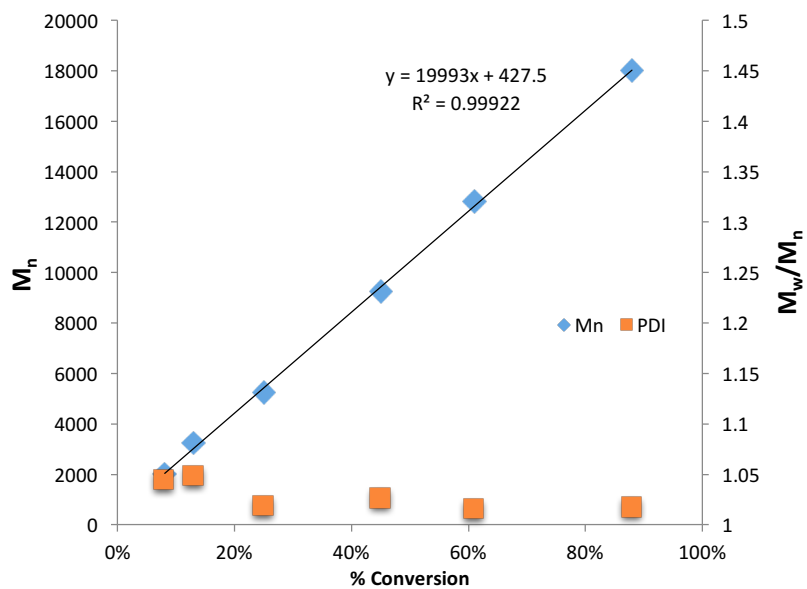


Figure 2.7. Mn (GPC) and Mw/Mn vs percent conversion for the 1/BEMP catalyzed ROP of VL. Reaction conditions: VL (2 M, 100 mg): 1: BEMP: benzyl alcohol :: 100: 5: 5: 1 in toluene.

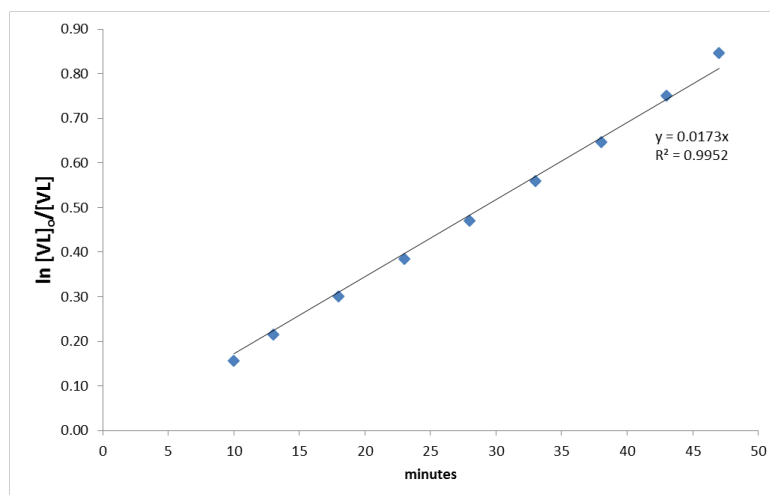


Figure 2.8. First order evolution of [VL] vs time for the **1**/BEMP catalyzed ROP of VL. Conditions: VL (2M, 100 mg): **1**: BEMP: benzyl alcohol :: 100: 5: 5: 2 in C₆D₆.

2.6 References

- (1) (a) Dove, A. P. *ACS Macro Lett.* **2012**, *1*, 1409. (b) Bourissou, D.; Moebs-Sanchez, S.; Martin-Vaca, B. C. *R. Chim.* **2007**, *10*, 775.
- (2) Kamber, N. E.; Jeong, W.; Waymouth, R. M.; Pratt, R. C.; Lohmeijer, B. G. G.; Hedrick, J. L. *Chem. Rev.* **2007**, *107*, 5813.
- (3) Kiesewetter, M. K.; Shin, E. J.; Hedrick, J. L.; Waymouth, R. M. *Macromolecules* **2010**, *43*, 2093.
- (4) Lohmeijer, B. G. G.; Pratt, R. C.; Leibfarth, F.; Logan, J. W.; Long, D. A.; Dove, A. P.; Nederberg, F.; Choi, J.; Wade, C.; Waymouth, R. M.; Hedrick, J. L. *Macromolecules* **2006**, *39*, 8574.
- (5) Koeller, S.; Kadota, J.; Peruch, F.; Deffieux, A.; Pinaud, N.; Pianet, I.; Massip, S.; Léger, J. M.; Desvergne, J. P.; Bibal, B. *Chem. Eur. J.* **2010**, *16*, 4196.
- (6) Thomas, C.; Bibal, B. *Green Chem.* **2014**, *16*, 1687.

- (7) Thomas, C.; Peruch, F.; Bibal, B. *RSC Adv.* **2012**, *2*, 12851.
- (8) Lippert, K. M.; Hof, K.; Gerbig, D.; Ley, D.; Hausmann, H.; Guenther, S.; Schreiner, P. R. *Eur. J. Org. Chem.* **2012**, 5919.
- (9) Todd, R.; Rubio, G.; Hall, D. J.; Tempelaar, S.; Dove, A. P. *Chem. Sci.* **2013**, *4*, 1092.
- (10) Dove, A. P.; Pratt, R. C.; Lohmeijer, B. G. G.; Waymouth, R. M.; Hedrick, J. L. *J. Am. Chem. Soc.* **2005**, *127*, 13798.
- (11) Pratt, R. C.; Lohmeijer, B. G. G.; Long, D. A.; Lundberg, P. N. P.; Dove, A. P.; Li, H.; Wade, C. G.; Waymouth, R. M.; Hedrick, J. L. *Macromolecules* **2006**, *39*, 7863.
- (12) Misaka, H.; Kakuchi, R.; Zhang, C.; Sakai, R.; Satoh, T.; Kakuchi, T. *Macromolecules* **2009**, *42*, 5091.
- (13) Zhang, L.; Pratt, R. C.; Nederberg, F.; Horn, H. W.; Rice, J. E.; Waymouth, R. M.; Wade, C. G.; Hedrick, J. L. *Macromolecules* **2010**, *43*, 1660.
- (14) Coady, D. J.; Fukushima, K.; Horn, H. W.; Rice, J. E.; Hedrick, J. L. *Chem. Commun.* **2011**, *47*, 3105.
- (15) Horn, H. W.; Jones, G. O.; Wei, D. S.; Fukushima, K.; Lecuyer, J. M.; Coady, D. J.; Hedrick, J. L.; Rice, J. E. *J. Phys. Chem. A* **2012**, *116*, 12389.
- (16) Coady, D. J.; Horn, H. W.; Jones, G. O.; Sardon, H.; Engler, A. C.; Waymouth, R. M.; Rice, J. E.; Yang, Y. Y.; Hedrick, J. L. *ACS Macro Lett.* **2013**, *2*, 306.
- (17) Becker, J. M.; Tempelaar, S.; Stanford, M. J.; Pounder, R. J.; Covington, J. A.; Dove, A. P. *Chem. Eur. J.* **2010**, *16*, 6099.
- (18) The units of binding constant in this paper are M⁻¹. The chemical convention of unitless K_{eq} is used throughout.

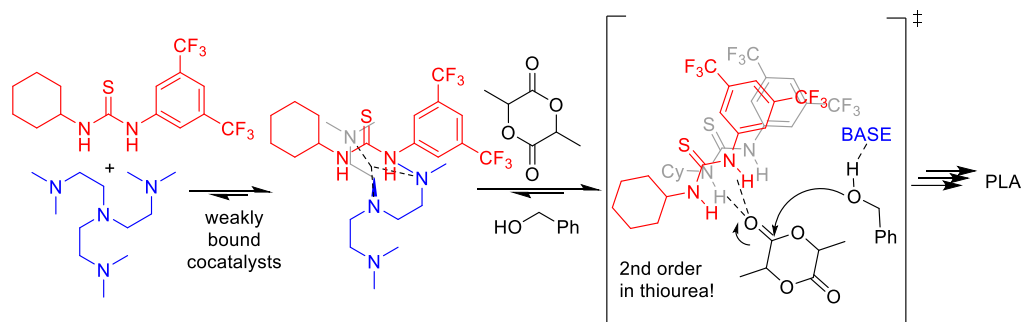
- (19) Laurence, C.; Brameld, K. A.; Graton, J.; Le Questel, J. Y.; Renault, E. *J. Med. Chem.* **2009**, *52*, 4073.
- (20) The ortho-protons were monitored for all studies as the NH protons of **1** are not always observed. The large chemical shifts of the NH protons upon binding and rapid exchange rates broaden those resonances into the baseline.
- (21) Rebek, J. *Angew. Chem., Int. Ed.* **2005**, *44*, 2068.
- (22) Briere, J. F.; Oudeyer, S.; Dalla, V.; Levacher, V. *Chem. Soc. Rev.* **2012**, *41*, 1696.
- (23) Coady, D. J.; Engler, A. C.; Horn, H. W.; Bajjuri, K. M.; Fukushima, K.; Jones, G. O.; Nelson, A.; Rice, J. E.; Hedrick, J. L. *ACS Macro Lett.* **2012**, *1*, 19.
- (24) Deranleau, D. A. *J. Am. Chem. Soc.* **1969**, *91*, 4044.
- (25) Horman, I.; Dreux, B. *Anal. Chem.* **1983**, *55*, 1219.
- (26) Peters, S. J.; Stevenson, C. D. *J. Chem. Educ.* **2004**, *81*, 715.
- (27) Kelly, T. R.; Kim, M. H. *J. Am. Chem. Soc.* **1994**, *116*, 7072.
- (28) Augustin-Nowacka, D.; Chmurzynski, L. *Anal. Chim. Acta* **1999**, *381*, 215.
- (29) Koppel, I. A.; Koppel, J. B.; Pihl, V. O. *Org. React.* **1987**, *24*, 387.
- (30) Kaljurand, I.; Kütt, A.; Sooväli, L.; Rodima, T.; Mäemets, V.; Leito, I.; Koppel, I. *J. Org. Chem.* **2005**, *70*, 1019.
- (31) Goldys, A. M.; Dixon, D. J. *Macromolecules* **2014**, *47*, 1277.
- (32) Zhang, L.; Nederberg, F.; Messman, J. M.; Pratt, R. C.; Hedrick, J. L.; Wade, C. G. *J. Am. Chem. Soc.* **2007**, *129*, 12610.
- (33) Zhang, L.; Nederberg, F.; Pratt, R. C.; Waymouth, R. M.; Hedrick, J. L.; Wade, C. G.; V, S. U.; February, R. V.; Re, V.; Recci, M.; April, V. *Macromolecules* **2007**, *40*, 4154.

- (34) Schwesinger, R.; Schlempep, H.; Hasenfratz, C.; Willaredt, J.; Dambacher, T.; Breuer, T.; Ottaway, C.; Fletschinger, M.; Boele, J.; Fritz, H.; Putzas, D.; Rotter, H. W.; Bordwell, F. G.; Satish, A. V.; Ji, G.; Peters, E.; Peters, K.; Schnering, H. G.; Von Walz, L. *Liebigs Ann.* **1996**, 1055.
- (35) Deranleau, D. A. *J. Am. Chem. Soc.* **1969**, *91*, 4044.
- (36) Horman, I.; Dreux, B. *Anal. Chem.* **1983**, *55*, 1219.
- (37) Peters, S. J.; Stevenson, C. D. *J. Chem. Educ.* **2004**, *81*, 715.

INTENTIONALLY BLANK PAGE

Chapter 3

Cocatalyst Binding Effects in Organocatalytic Ring-Opening Polymerization of L-Lactide

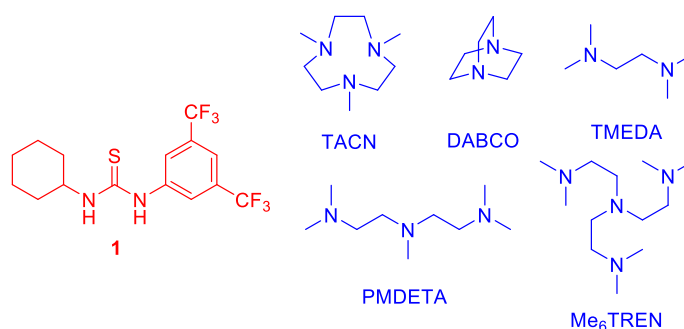


3.1 Abstract

Thiourea/alkylamine cocatalysts have previously been shown to be effective systems for the ring-opening polymerization (ROP) of lactide, but an experimental explanation for the varied activity and selectivity of these structurally similar alkylamine cocatalysts combined with thiourea is elusive. In this work, several alkylamine bases are shown to be weakly associated with a thiourea cocatalyst in solution, and the nature of cocatalyst interactions vary with the identity of the alkylamine. Kinetic analyses of the organocatalytic ROP reactions reveal noninhibitory behavior in [alkylamine] and a new mode of activity for thiourea. Reactivity patterns are proposed based on computed cocatalyst geometries, and a new cocatalyst pair for the ROP of lactide is disclosed.

3.2 Introduction

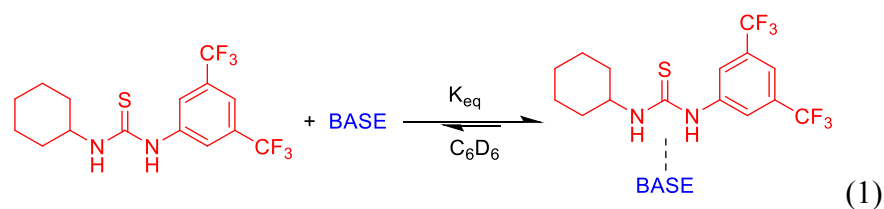
Since the beginning of the century, research in the area of organocatalytic polymerization has evolved a large number of catalyst systems for ring-opening polymerization. ¹⁻⁴ Among these catalysts, some of the most fascinating systems are the numerous bimolecular H-bonding cocatalysts which are varied in their chemical composition but consist of an H-bond donor, usually thiourea **1** (in scheme 3.1), and an H-bond accepting base. ^{4,5} These systems are believed to effect catalysis through H-bond mediated activation of thiourea (TU) upon monomer and of base upon alcohol, respectively. ¹⁻⁸ This broad class of cocatalyst systems ¹ is typified by the precise level of reaction control exhibited by the catalysts and the remarkably “living” character of their polymerization reactions. ⁶ Despite the extent to which the exquisite level of control exhibited by these cocatalysts has been used to construct well-defined materials, our understanding of the diverse and sometimes conflicting modes of action



Scheme 3.1. Common H-Bonding Cocatalysts for the ROP of Lactide.

exhibited by these catalysts in solution is still evolving. ^{4,7,8} An explanation of the varied reactivity of the alkylamine bases, along with **1** cocatalyst, in the ROP of esters is

elusive. The application of strong amidine or phosphazene bases in combination with **1** is known to effect the ROP of δ -valerolactone (VL). Strong binding between **1**



and strong base cocatalysts was reported by our group to be an energetically dominating interaction during the ROP of VL, $K_{eq} = 1200\text{--}4200$ in eq 1.⁸ The strength of cocatalyst binding was shown to be proportional to the activity of the cocatalysts in the ROP of VL, but the strongest binding base cocatalyst (to **1**) exhibited inhibitory behavior.⁸ These observations provided a rationale for the varied activity and selectivity of **1** cocatalyzed ROP when used with a set of structurally diverse bases.⁸ In contrast, the application of amidine or phosphazene bases alone is sufficient to effect the ROP of lactide (LA), but these ROPs are generally uncontrolled. The controlled ROP of LA can be accomplished with **1** in combination with a weak base cocatalyst (e.g., alkylamines).^{6,10} The panel of base cocatalysts shown in Scheme 1 came into prominence for ROP (especially of LA) after the worldwide shortage of the chiral bisamine(–)-sparteine.^{5,9,10} The similar structures and mild basicities of these compounds (Scheme 1) belie the varied rate and selectivity exhibited by them in the base/**1** catalyzed ROP of lactide. Computational explanations have been offered,¹⁰ but experimentally observable differences in the modes of action of these alkylamine/**1** cocatalysts have not yet been put forward. We posited that cocatalyst interactions may account for the differing activities and selectivities of the structurally similar alkylamine bases when applied with **1** for the ROP of lactide. Herein, we propose an explanation

for the different activities based on cocatalyst interactions exhibited by several alkylamine/**1** cocatalysts.

3.3 Results and Discussion

3.3.1 Cocatalyst Binding Thermodynamics

The binding constants, K_{eq} in eq 1, between the alkylamine cocatalysts in Scheme 1 and **1** are of similar magnitude and do not predict cocatalyst activity. The binding constants of each alkylamine/**1** pair were determined in C_6D_6 by 1H NMR titrations according to published methods^{11–13} (Table 1). Additionally, the observed rate constants for the formation of polymer, k_{obs} in eq 2, for the base/**1** (0.025 mmol each) catalyzed ROP of Lactide (L-LA, 0.5 mmol, 1 M) from benzyl alcohol (0.01 mmol) were determined from the first-order evolution of [L-LA] versus time (Table 1). The alkylamine/**1** binding constants are narrowly dispersed in magnitude, $\Delta\Delta G^\circ = 0.95$ kcal/mol ($K_{eq} = 6.4\text{--}32$), and unlike amidine base/**1** catalyzed ROP of VL,⁸ binding constant does not correlate with ROP activity. However, all cocatalyst pairs exhibit a $K_{eq} > 1$ which indicates that the cocatalysts are preassembled in solution.¹⁴

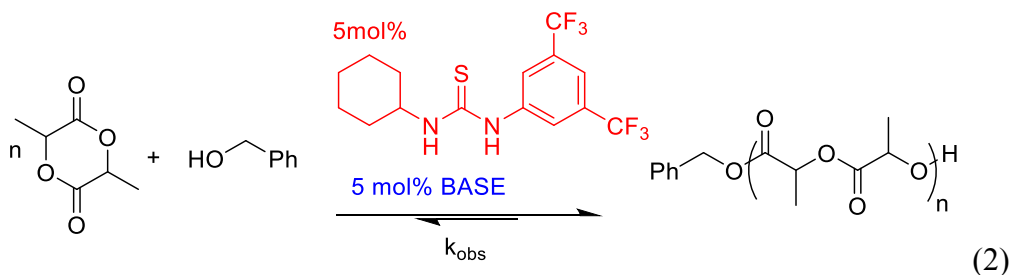


Table 3.1. Thermodynamics of Cocatalyst Binding and Observed Rate Constants for the ROP of L-Lactide.

Base	K_{eq}^a	% complex ^b	ΔH° (kcal/mol) ^c	ΔS° (cal/mol·K) ^c	$k_{obs} (h^{-1})^d$
TACN	6 ± 0.3	20	3.5 ± 0.3	15.5 ± 0.9	1.370 ± 0.130
Me ₆ TREN	49 ± 6	53	0.8 ± 0.5	2.5 ± 1.7	0.329 ± 0.011
PMDETA	23 ± 1.5	41	-3.5 ± 1.4	-6.1 ± 4.5	0.038 ± 0.001
DABCO	10 ± 0.4	27	-4.6 ± 1.0	-11.2 ± 3.2	0.037 ± 0.001
TMEDA	23 ± 0.7	40	-8.4 ± 0.5	-22.6 ± 1.6	0.010 ± 0.001

a) Binding constant (at 292 K) for base + **1** in equilibrium with **1**•base (eq 1) as measured with NMR titration in C₆D₆. b) Percent of each cocatalyst occupied in base/TU complexes under ROP concentrations, calculated in the absence of LA and alcohol. c) From temperature dependent measurement of K_{eq} . d) Observed rate constant, k_{obs} , for the **1**/base (5 mol% each) catalyzed ROP of LA (1 equiv, 1M) from benzyl alcohol (2 mol%).

The enthalpy and entropy of cocatalyst binding exhibit compensation-like behavior. Temperature-dependent measurement of K_{eq} for each cocatalyst pair allowed for the determination of the thermodynamic parameters of binding (table 3.1). While the enthalpy and entropy of binding are different for each cocatalyst pair, the ΔH° and ΔS° exhibit identical trends (in sign). This phenomenon is akin to the enthalpy–entropy compensation effect often observed in enzyme catalysis which renders the enzyme–substrate binding affinities (ΔG°) and hence reactivity identical upon structural perturbation of either partner.^{15,16} In the case of ROP, however, the binding constant does not describe the affinity of substrate for active site but can be interpreted to describe the extent to which the cocatalysts are associated in solution, which is effectively the creation of an “active site”. The most active alkylamine cocatalysts possess the least enthalpically favorable binding to **1** while the least active cocatalysts bind to **1** with the strongest H-bond enthalpy (table 3.1); all cocatalyst binding constants are exergonic, $K_{eq} > 1$.

3.3.2. Kinetics

The alkylamines do not behave as inhibitors in the ROP of L-LA. Kinetic evaluation of the ROP of L-LA (1 M, 0.5 mmol) catalyzed by Me₆TREN/**1** from benzyl alcohol (0.010 mmol) under conditions where [Me₆TREN] < [**1**] and [**1**] = 0.05 M suggests that the ROP displays a first-order dependence upon [Me₆TREN]. However, under conditions where [Me₆TREN] > [**1**] and [**1**] = 0.05 M, the ROP displays zero-order behavior in [Me₆TREN] (Figure 1). This suggests that additional base (in excess of [**1**]) does not alter the reaction kinetics or transition state. This is in contrast to previous disclosures which have suggested that all cocatalyst interactions are inhibitory to catalysis^{4,7,17} and contrary to kinetic evaluations of strongly binding amidine base/**1** cocatalyzed ROP which exhibits inverse dependence in [base] (K_{eq} DBU/**1** = 4200 but K_{eq} Me₆TREN/**1** = 32 at r. t.).⁸ The transition from first- to zero-order behavior in [Me₆TREN] at equal concentrations of **1** and Me₆TREN (a tetraamine) suggests 1:1 stoichiometry under catalytic conditions, as is commonly employed.^{1-6,8,10,23} These observations reinforce the conclusion that the magnitude and nature of cocatalyst interactions have a dramatic effect on the ROP reaction.

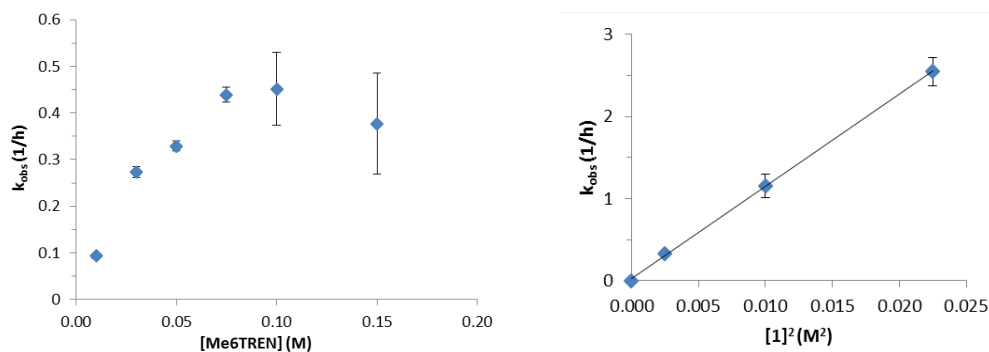


Figure 3.1. Observed rate constant, k_{obs} , vs concentration in the $\text{Me}_6\text{TREN}/\mathbf{1}$ catalyzed ROP of L-LA (1 M, 0.5 mmol) from benzyl alcohol (0.010 mmol) when (left) $[\mathbf{1}] = 0.05$ M and $[\text{Me}_6\text{TREN}] > [\mathbf{1}]$; and (right) $[\text{Me}_6\text{TREN}] = 0.05$ M and $[\text{Me}_6\text{TREN}] < [\mathbf{1}]$.

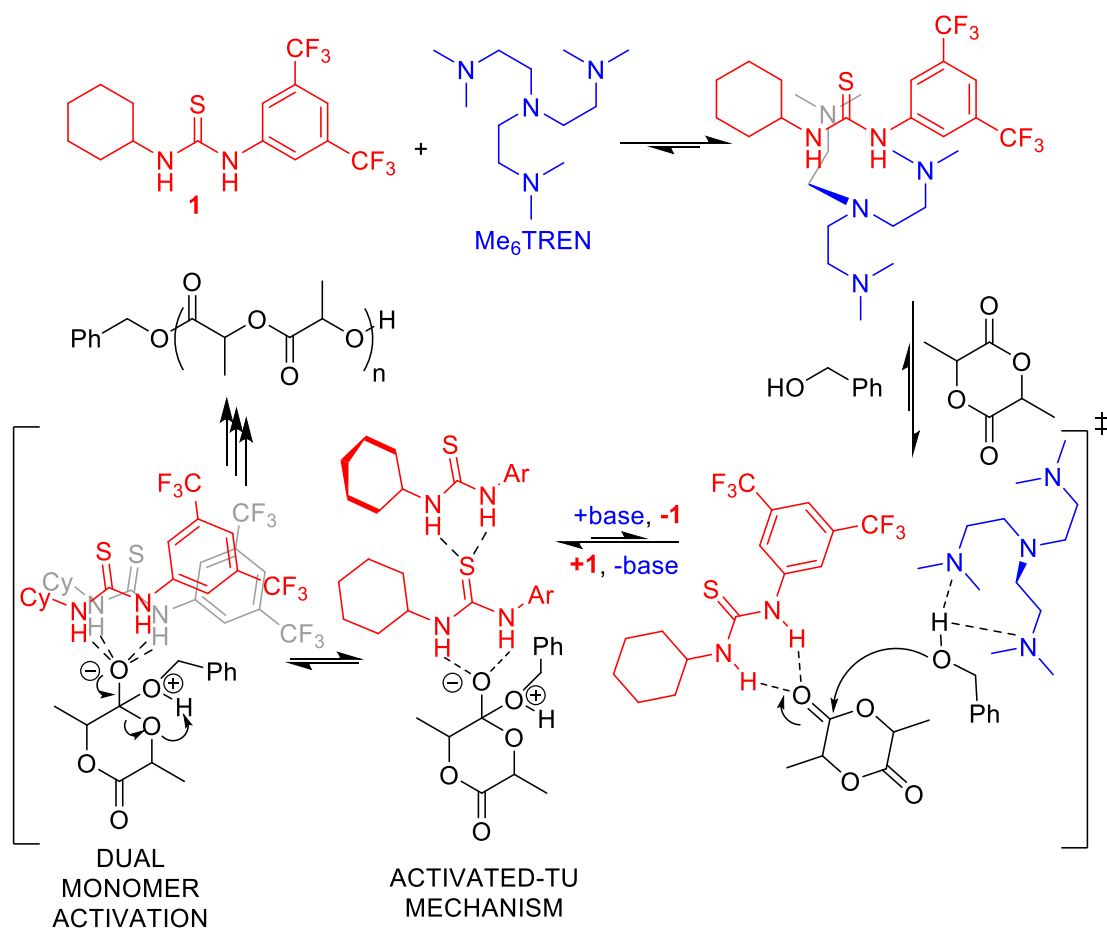
Kinetic studies were extended to conditions where $[\mathbf{1}] > [\text{Me}_6\text{TREN}]$ and $[\text{Me}_6\text{TREN}] = 0.05$, and this resulted in the surprising observation of a second-order dependence exhibited by $[\mathbf{1}]$ in the ROP of L-LA. This suggests a mechanism that may involve two $\mathbf{1}$ moieties in the transition state of the ring-opening. In the absence of short strong hydrogen bonds, H-bonds are electrostatic in nature,¹⁶ and multiple H-bonds at a single carbonyl are feasible. Thus, while the exact nature of this transition state remains unclear, the role of two molecules of $\mathbf{1}$ could be to directly stabilize the highly charged transition state via dual monomer activation. However, this data does not rule out an activated-thiourea (TU) mechanism¹⁸ one where the $\mathbf{1}$ /monomer complex is itself being activated by the second molecule of $\mathbf{1}$.

Kinetic evaluation of the $\mathbf{1}/\text{Me}_6\text{TREN}$ catalyzed ROP of LA under conditions where $[\mathbf{1}] = [\text{Me}_6\text{TREN}]$ produces two equivalent rate dependences in [catalysts]: both k_{obs} vs $[\mathbf{1}]^2$ and k_{obs} vs $[\mathbf{1}][\text{Me}_6\text{TREN}]$ are linear (fig. 3.1).¹⁹ Because this ROP requires the presence of both $\mathbf{1}$ and base, the latter scenario provides the more robust conclusion

that the rate-determining step is proximal to the nucleophilic attack of alcohol on monomer, catalyzed by independent activation by base and **1**, respectively. However, the former scenario is consistent with the observation of zero-order behavior in [Me₆TREN] (when in excess of [**1**]) which suggests a rate-determining step after the nucleophilic attack of alcohol upon LA (i.e., no rate dependence in base). Such a mechanism would be supported by published computational studies on ROP by H-bonding catalysts which have suggested that all steps subsequent to and including nucleophilic attack by alcohol upon ester are similarly destabilized relative to reactants or products.²⁰ Certainly, the involvement of two H-bond donor moieties and the presence/absence of base would be expected to alter the relative energy of these transition state structures and hence the identity of the transition state complex.

The kinetic dependence upon [alkylamine] and [**1**] in the ROP of L-LA varies with the identity of the base cocatalyst. Unlike the Me₆TREN/**1** or DBU/**1**⁸ catalyzed reactions, the TMEDA/**1** catalyzed ROP of L-LA (0.5 mmol, 1 M) from benzyl alcohol exhibits first-order dependence in [**1**] (when [TMEDA] = 0.05 M and [TMEDA] < [**1**]) and a zero-order dependence in [TMEDA] (when [**1**] = 0.05 M and [TMEDA] > [**1**]) (see ES). The same reaction exhibits a first-order dependence in overall catalyst loading ([**1**] = [TMEDA]) such that both k_{obs} vs [**1**] and k_{obs} vs ([TMEDA] + [**1**]) are linear (see ES).¹⁹ Both the Me₆TREN/**1** and TMEDA/**1** catalyzed ROP of L-LA implicate a strong rate dependence in [**1**] and a weak (possibly zero) dependence in [base]. This latter observation is consistent with the remarkable performance of these systems as bimolecular catalysts.^{9,21-23} The observed orders in [base] and [**1**] in combination with cocatalyst binding data suggest that the rate-determining step of this exothermic ROP is

proximal to nucleophilic attack by the alcohol upon the lactide ring in the reaction coordinate (Scheme 2). Because H-bonds are electrostatic in nature and multiple H-bonds can be involved at a single TU (e.g.) site,¹⁶ the geometry of catalyst–catalyst and catalyst–reagent interactions are not clear. The role of a second TU may be to activate the first TU in an activated-TU mechanism (Scheme 2)¹⁸ or provide additional stabilization by directly binding monomer in the transition state in a dual monomer activation mechanism (scheme 3.2). Other possibilities, like TU binding to base away from the transesterification event, are not expected to be kinetically relevant. Further studies of these H-bond mediated ROP reactions may elucidate the complex, base-dependent roles of the cocatalysts in determining the course of a ROP reaction.



Scheme 3.2. Proposed mechanism for the Me₆TREN/**1** catalyzed ROP of L-LA; the ROP reaction exhibits 2nd order behavior in [**1**] and zero order behavior in [Me₆TREN].

3.3.3. Effect of Alkylamine Base upon Calculated Cocatalyst Geometry

For the ROP of esters in nonpolar solvent, the a priori selection of a base cocatalyst which does not allow all its nitrogen atoms to bind to the **1** cocatalyst is predicted to provide the best ROP rate but lowest selectivity for monomer. The similar composition of PMDETA and TACN ($\pm 2\text{H}$) makes their behavior particularly illuminating. Geometry optimization studies at the DFT/B3LYP 6-31G** level of theory qualitatively show that PMDETA is able to cradle the electrophilic face of **1** and

allow all three nitrogen lone pairs to H-bond (figure 3.2).²⁴ For the case of TACN, the constricted geometry enforced by the ring does not allow all N lone pairs to H-bond simultaneously (Figure 2), even when it is enforced prior to computational minimization. The four-nitrogen base, Me₆TREN, is structurally flexible, but computational modeling indicates that only three of the N lone pairs are able to coordinate to **1** upon binding (see ES). DABCO is ostensibly an outlier in the set in that it is a base that does not allow for simultaneous coordination of both N lone pairs, yet this base displays slower rate of ROP than Me₆TREN or TACN. However, the manner of coordination of DABCO is different than TACN or Me₆TREN. In order to coordinate the second nitrogen to **1**, DABCO would have to dissociate and recoordinate at the other nitrogen while the other bases can simply perform a geometry modification while bound, analogous to a Berry pseudorotation.²⁵ Clearly, the identity of the base is a strong influence on cocatalyst interactions and hence ROP dynamics.

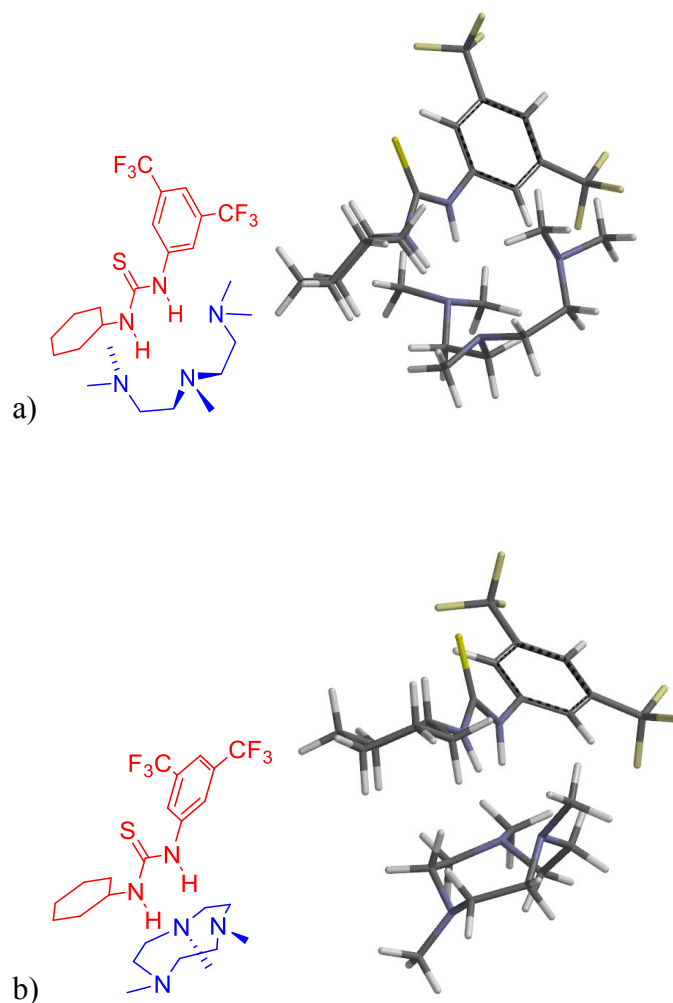
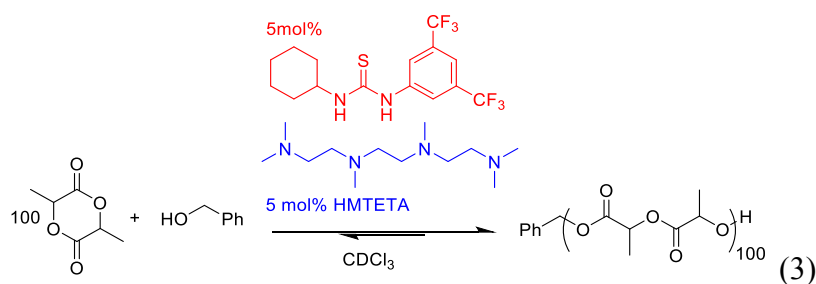


Figure 3.2. DFT/B3LYP 6-31G* geometry optimized structures of **1** bound to a) PMDETA and b) TACN. Note that all Ns can simultaneously H-bond to **1** in the case of PMDETA and only two in the case of TACN. Structurally flexible bases that can bind all basic Ns to **1** form the most enthalpically stable **1**/base adducts.

HMTETA, a linear constitutional isomer of Me₆TREN, has not previously been reported as a cocatalyst for ROP. Geometry optimization of the HMTETA/**1** adduct at the (DFT) B3LYP/6-31G** level of theory suggests that the structurally flexible HMTETA cradles the electrophilic face of **1** with all four nitrogens (see ES). This would

be expected to render HMTETA less efficacious a cocatalyst than Me₆TREN. This prediction is supported by experimental binding data which shows that the binding strength of HMTETA to **1** is less enthalpically favored than that of Me₆TREN. For HMTETA/**1**, $\Delta H^\circ = -4.7 \pm 5.8$ kcal/mol, $\Delta S^\circ = -7.1 \pm 19.2$ cal/(mol·K), and K_{eq} (292 K) = 90 ± 9 . When HMTETA and **1** (0.025 mmol) were applied to the ROP of LA (0.5 mmol, 1 M) initiated from benzyl alcohol (0.01 mmol) (eq 3) in chloroform-d, the observed rate constant was lower than that for Me₆TREN under identical conditions: k_{obs} (HMTETA) = 0.127 ± 0.004 h⁻¹ and k_{obs} (Me₆TREN) = 0.329 ± 0.011 h⁻¹. The HMTETA reaction was quenched at 94% conversion and precipitated with hexanes to isolate the resulting polymer which was characterized by NMR and GPC: $M_n = 16\,000$, $M_w/M_n = 1.055$ (see ES). When the reaction is left to stir for 1 h after full conversion, the M_w/M_n is observed to minimally broaden ($M_w/M_n = 1.056$), which suggests a similar degree of selectivity to that exhibited by Me₆TREN.¹⁰



3.3.4. Comparison of Monomers and Base Cocatalysts

The multitude of competing and complementary interactions that occur during a “simple” transesterification event renders definitive conclusions regarding the effect of catalyst structure upon activity difficult. Taking the VL⁸ and current LA studies

collectively, cocatalyst binding constant appears to be the most important factor when accounting for the activity of the cocatalyst pair for ROP as it is representative of how tightly the cocatalysts are associated in solution. However, this observation cannot be divorced from the different energetics of the respective monomers ($[VL]_{eq} > [LA]_{eq}$).²⁷ In the case of VL, strong base cocatalysts are required for ROP, and strong binding constants to **1** are expected due to their increased basicity. In contrast, the alkylamine cocatalysts employed with **1** for the ROP of LA should be expected to exhibit weaker binding to **1** due to their reduced (vs amidine bases) basicity, as observed. Within a particular set of bases (strong or alkylamine), the effects of the base cocatalyst upon rate and selectivity do not follow trends in pK_a. In this study, the three nitrogen base TACN was superior in reaction rate to the four nitrogen bases while a second three-nitrogen base, PMDETA, was slower still (see Table 1). Again, this suggests that pK_a is not as important as cocatalyst binding in determining catalyst activity. However, when cocatalyst binding constants, K_{eq}, are approximately equal in magnitude, as with the alkylamines, the enthalpy of cocatalyst binding is a better predictor of activity than binding constant proper. This is an extension of the previous observation.⁸ For example, if the driving force for the association of a cocatalyst pair, like TACN to **1** or Me₆TREN to **1** ($\Delta H^\circ > 0$), is the exclusion of solvent that occurs upon binding ($\Delta S^\circ > 0$),¹⁶ then the reactivity exhibited by these cocatalysts would be expected to be markedly different than those cocatalyst pairs that are enthalpically bound (HMTETA, DABCO, PMDETA or TMEDA to **1**). The former alkylamine/**1** pairs are “preassembled” due to their mutual dislike of solvent and should be expected to be rapid ROP cocatalysts due to their enthalpically favorable binding to monomer/alcohol ($\Delta H^\circ < 0$),²³ as observed.

3.4 Conclusion

For the base/**1** combinations examined herein and previously,⁸ the cocatalysts possess a binding constant greater than unity which may be interpreted to be representative of the ability of a particular cocatalyst pair to assemble an “active site” in solution. The alkylamine/**1** systems exhibit similar binding constants (K_{eq} , eq 1) to each other and display an enthalpy–entropy compensation effect analogous to enzyme catalysis. The Me₆TREN/**1** and TMEDA/**1** cocatalyst systems exhibit remarkably different rate dependencies in their respective ROP reactions. Contrary to amidine base cocatalyzed ROP, Me₆TREN and TMEDA do not exhibit inhibitory behavior. The **1**/Me₆TREN catalyzed ROP of LA displays second-order kinetics in [**1**], and the same reaction catalyzed by **1**/TMEDA does not. Clearly, the identity of the base has dramatic ramifications on the ROP reaction due to perturbations in cocatalysts interactions, changing the location of the transition state along the reaction coordinate, and potentially other unidentified factors. These mechanistic observations suggest new modes of action for H-bonding catalysts for ROP.²⁸

3.5 Experimental Section

3.5.1 General Considerations

All manipulations were performed in a glovebox or via standard Schlenk technique under a nitrogen atmosphere in glassware baked overnight. All chemicals were purchased from Fisher Scientific and used as received unless stated otherwise. THF and toluene were dried on an Innovative Technologies solvent purification system

with activated alumina columns and nitrogen working gas. Benzyl alcohol, chloroform-d, and benzene-d₆ were dried for 12 h over CaH₂ prior to distillation under an inert atmosphere. L-Lactide was supplied by Acros Organics and recrystallized from dry toluene prior to use. 1-[3,5-Bis(trifluoromethyl)phenyl]-3-cyclohexylthiourea (**1**) was synthesized and purified according to literature procedures.²³ NMR experiments were performed on a Bruker Avance 300 MHz spectrometer. Size exclusion chromatography (SEC) was performed at 30 °C in dichloromethane (DCM) using an Agilent Infinity GPC system equipped with three Agilent PLGel columns 7.5 mm Å~ 300 mm (5 µm, pore sizes: 103, 104, and 105 Å). Molecular weight and Mw/Mn were determined versus PS standards (500–3150 kg/mol; Polymer Laboratories). The Spartan'14 software package running on a 64 bit Windows 7 operating system was used for computations.

3.5.2. Binding Studies

Binding constants (K_{eq}) between **1** and alkylamine bases were determined in benzene-d₆ by the titration method and curve fitting as previously described.^{12,13} The K_{eq} values were determined by fitting the binding curve to the quadratic form of the binding equation with K_{eq} and $\Delta\delta$ as variables.²⁶ The binding constant for each **1**/base pair was determined at elevated temperatures (298–318 K). The enthalpy and entropy of binding were determined by Van't Hoff analysis, and error was determined from linear regression at the 95% confidence interval.

3.5.3 Example Kinetic Reaction

An 8 mL vial was charged with 0.0721 g (0.5 mmol, 1 M) of L-lactide and 300 μL of chloroform-d. Another 8 mL vial was charged with 1.04 μL (0.010 mmol) of benzyl alcohol, 1 (9.3 mg, 0.025 mmol), and Me6TREN (6.68 μL , 0.025 mmol). Chloroform-d (200 μL) was added to the second vial. The contents of the first vial were transferred to the second vial, shaken to mix, and transferred to an NMR tube. The reaction conversion was monitored by ^1H NMR. Rate constants were extracted from a plot of eq 4; the data are linear on this plot to 3+ half-lives. The slope of this plot is k_{obs} , where k_{obs} is defined in eq. 5, and the error was determined by propagation of NMR integration error at $\pm 10\%$. Only [1] and [base] were varied (from 5 to 25 mol % to L-lactide) between individual kinetic runs.

3.5.4. Computations

Chemical computations were performed to gain a qualitative insight into cocatalysts interactions. Structures were built in the Spartan builder interface and geometry optimized using DFT at the B3LYP//6-31G** level of theory starting from the PM3 optimized structures. Geometry optimizations were performed in the gas phase. Cartesian coordinates of the optimized structures and their energies are given below.

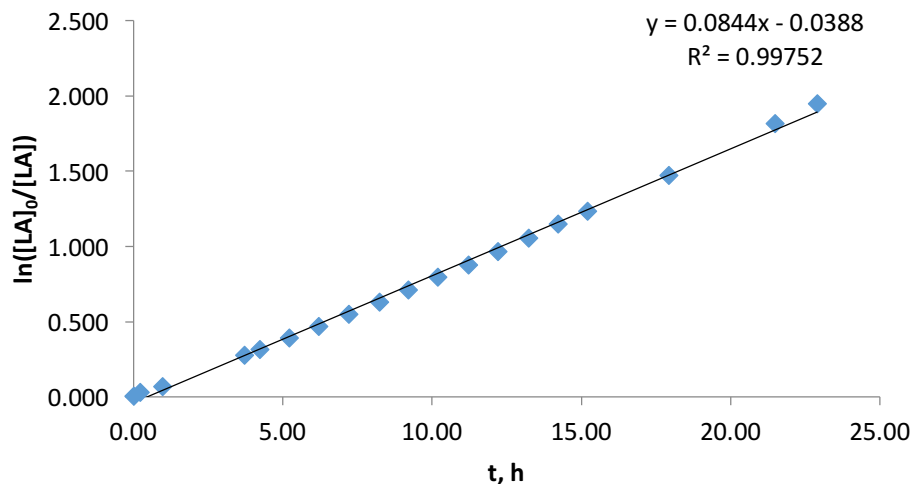


Figure 3.3. First order evolution of [LA] versus time in the **1**/HMTETA catalyzed ROP of LA from benzyl alcohol in CDCl₃. [LA]₀ = 0.5 mmol; [HMTETA]₀ = [**1**]₀ = 0.025 mmol; [benzyl alcohol]₀ = 0.010 mmol.

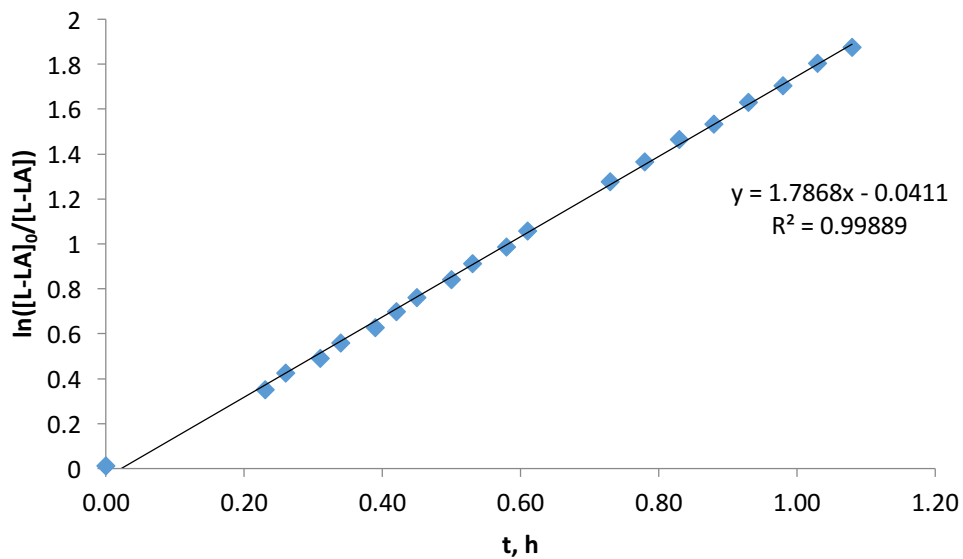


Figure 3.4. First order evolution of [LA] versus time in the **1**/Me6TREN catalyzed ROP of LA from benzyl alcohol in CDCl₃. [LA]₀ = 0.5 mmol; [Me6TREN]₀ = [**1**]₀ = 0.050 mmol; [benzyl alcohol]₀ = 0.010 mmol.

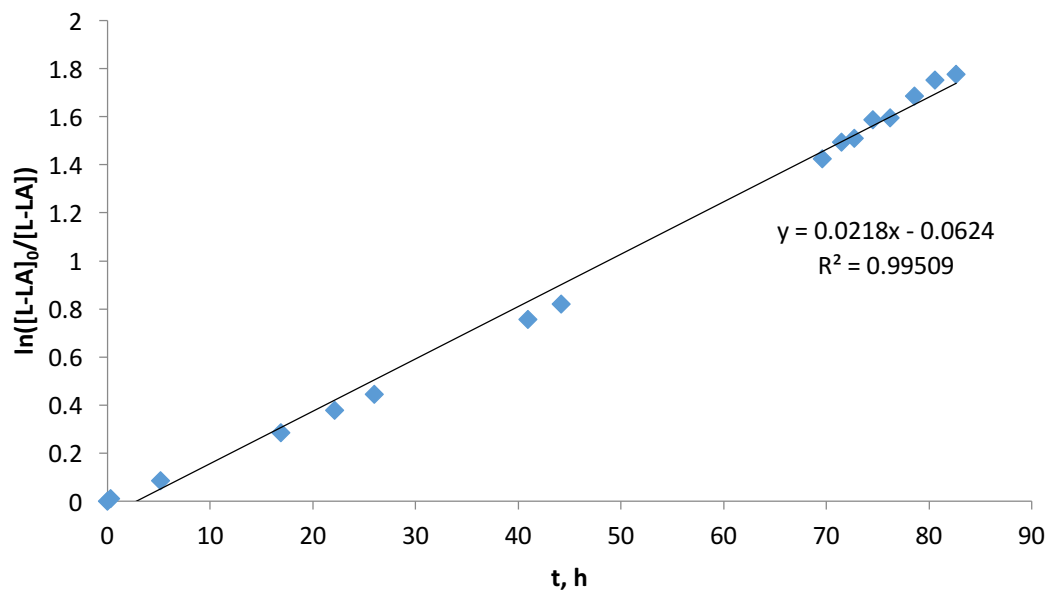
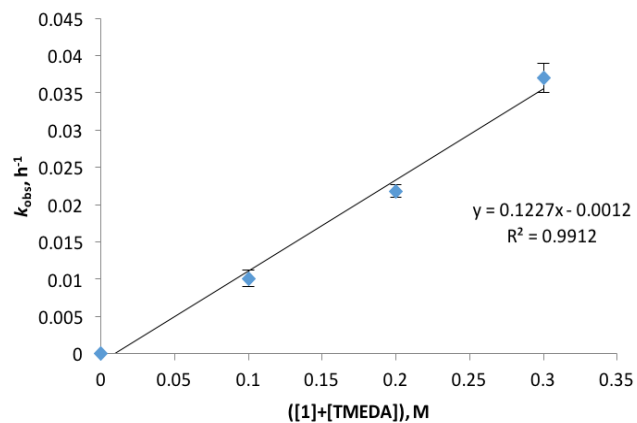
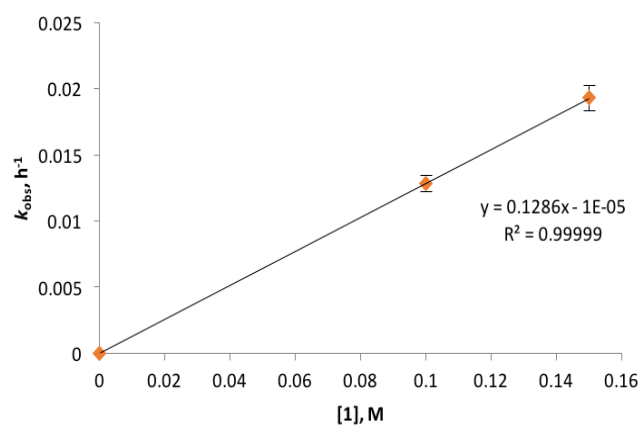


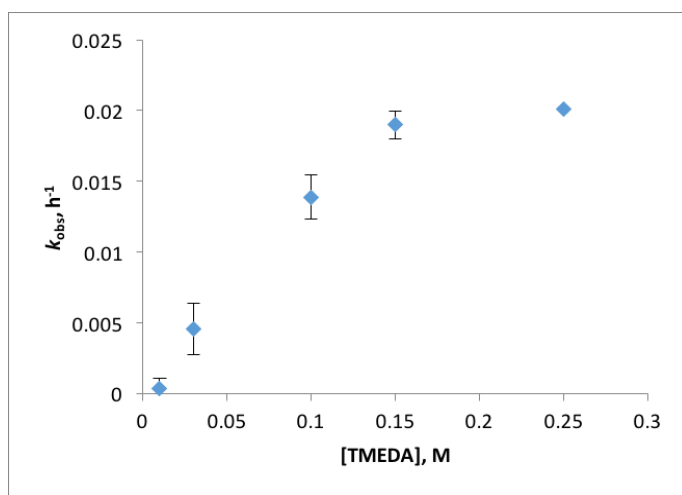
Figure 3.5. First order evolution of [LA] versus time in the **1**/TMEDA catalyzed ROP of LA from benzyl alcohol in $CDCl_3$. $[LA]_0 = 0.5$ mmol; $[TMEDA]_0 = [1]_0 = 0.050$ mmol; $[benzyl\ alcohol]_0 = 0.010$ mmol.



A)



B)



C)

Figure 3.6. Observed rate constant (k_{obs}) vs concentration plots for the **1**/TMEDA catalyzed ROP of L-LA: A) $[1] = [TMEDA]$, B) $[1] > [TMEDA]$, $[TMEDA] = 0.05$ M, C) k_{obs} vs $[TMEDA]$, $[1] = 0.05$ M (bottom).

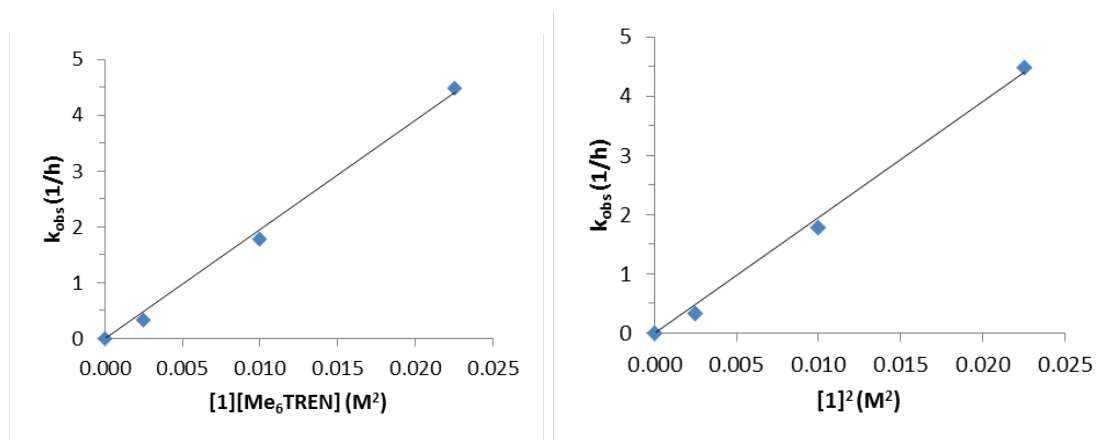


Figure 3.7. (left) Observed rate constant (k_{obs}) vs $[1][\text{Me}_6\text{TREN}]$, and (right) observed rate constant (k_{obs}) vs $[1]^2$ for the $1/\text{Me}_6\text{TREN}$ catalyzed ROP of L-LA.

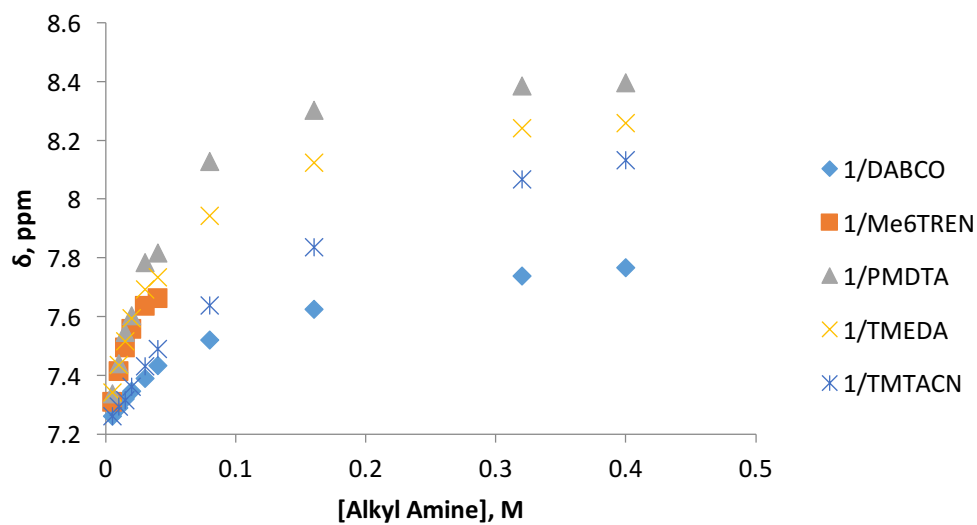


Figure 3.8. Binding curves for the association of **1** with alkylamine cocatalysts. The curve fitting method was used to extract binding constants, see Experimental Section. The chemical shift is of the *ortho*-protons of **1**.

3.5.5 Equation Used for Binding Studies

$$\delta_{\text{obs}} = \delta_{\text{H}} - (\Delta\delta/2[\text{H}]_0)\{[\text{H}]_0 + [\text{G}]_0 + 1/K - ((([\text{H}]_0 + [\text{G}]_0 + 1/K)^2 - 4[\text{H}]_0[\text{G}]_0)^{1/2})\}$$

Where²⁹⁻³¹:

δ_{obs} is the observed chemical shift of the TU in the presence of base;

δ_{H} is the chemical shift of free TU in the absence of base;

$\Delta\delta$ is the difference in the chemical shift of host and complex, ($\Delta\delta = \delta_{\text{C}} - \delta_{\text{H}}$);

K is the binding constant, K_{eq} .

The binding constants were determined by fitting the binding curve with the quadratic form of the binding equation shown above (K_{eq} and $\Delta\delta$ variables).²⁹⁻³⁰ The value of the binding constants determined from curve fitting are within experimental error of those determined from the slope of the linear (Lineweaver-Burke) forms of the binding equation.³²⁻³³

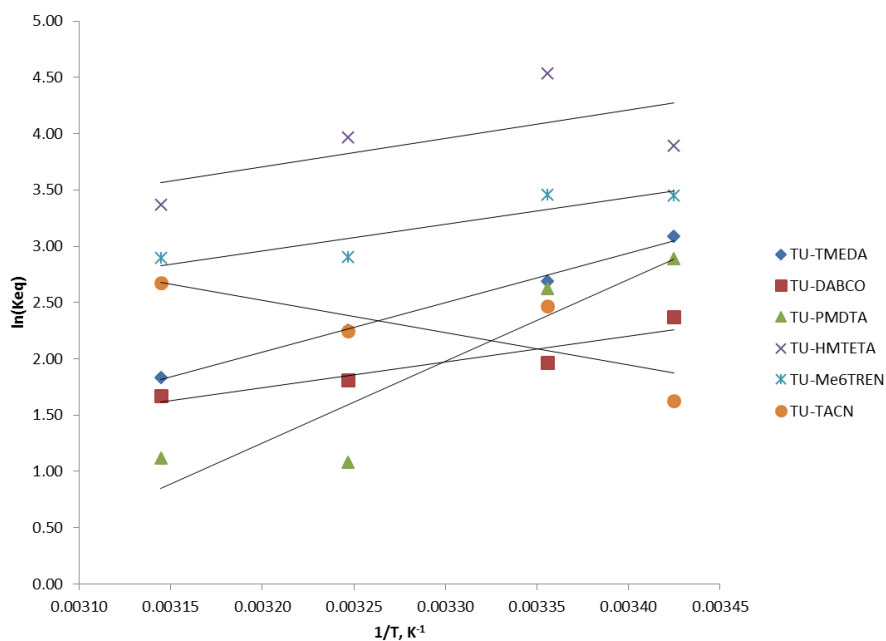


Figure 3.9. Temperature-dependent binding.

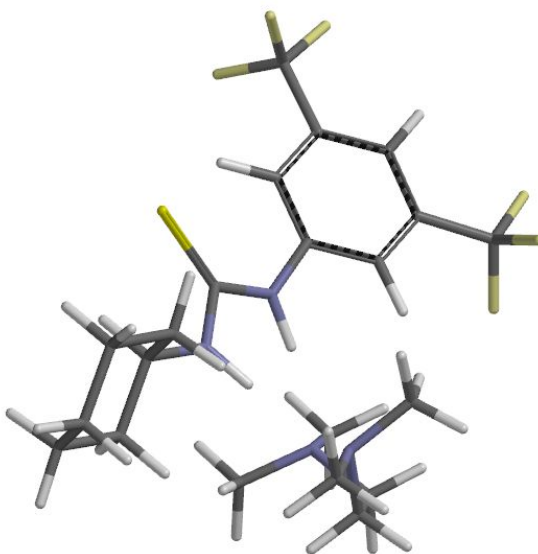


Figure 3.10. **1** + TMEDA. See Experimental Section for computational details and below for optimized coordinates.

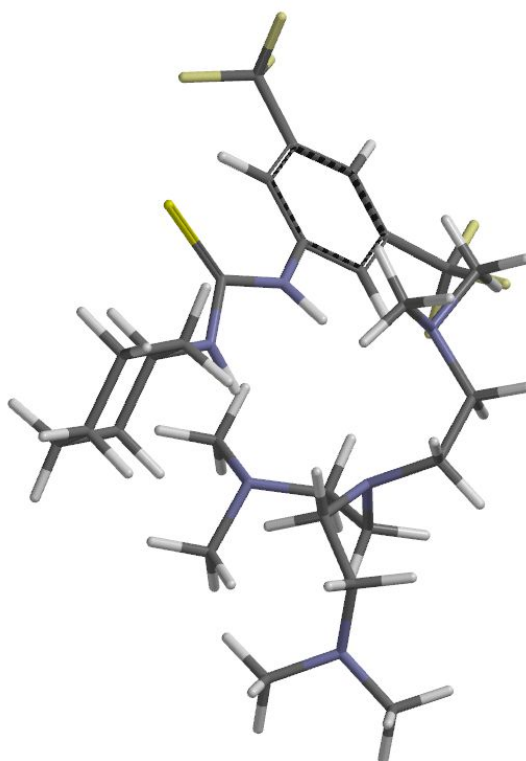


Figure 3.11. **1** + Me₆TREN. See Experimental Section for computational details and below for optimized coordinates.

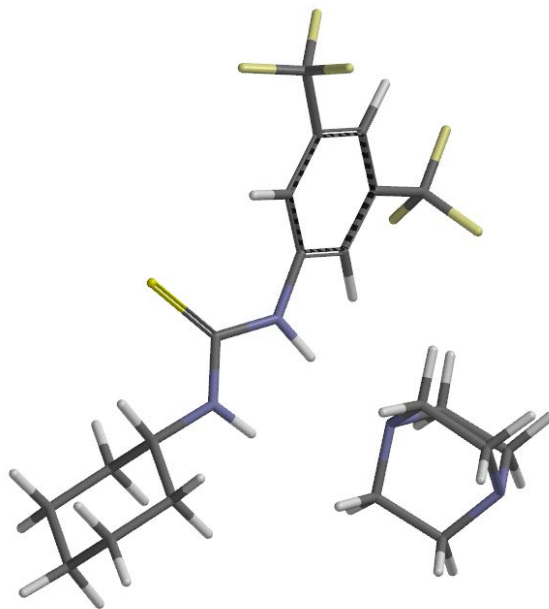


Figure 3.12. **1** + DABCO. See Experimental Section for computational details and below for optimized coordinates.

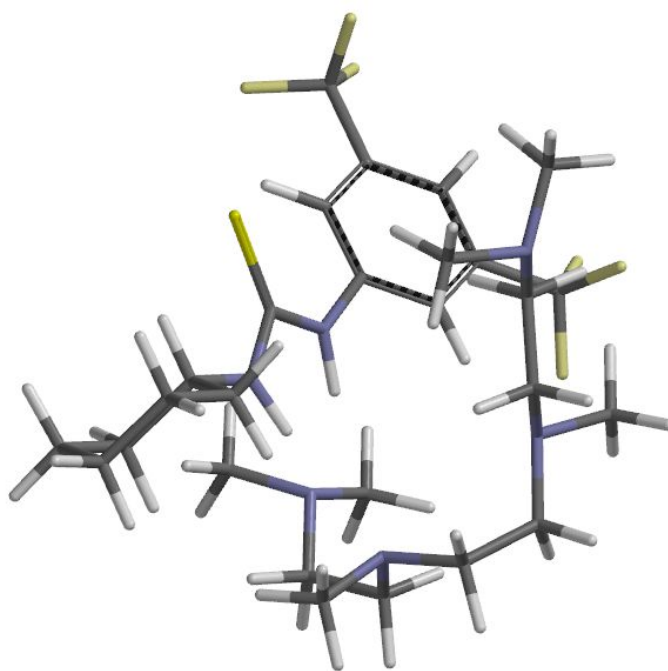


Figure 3.13. **1** + HMTETA. See Experimental Section for computational details and below for optimized coordinates.

3.4.5. Optimized Energies and Atomic Coordinates

1 + HMTETA

Atom	Cartesian Coordinates (Angstroms)		
	X	Y	Z
1 C C16	0.9894109	-1.4727979	-0.8215657
2 S S1	0.6430497	-3.1250735	-0.7542201
3 N N2	2.2567399	-0.9719702	-0.8520693
4 H H10	2.3673275	0.0235565	-0.6697293
5 N N3	0.0487468	-0.4735353	-0.8389453
6 H H27	0.3951613	0.4802393	-0.9934503
7 C C17	-1.3536643	-0.5391003	-0.7540792
8 C C18	-4.1633420	-0.3832505	-0.6479231
9 C C19	-1.9865385	0.5674783	-0.1699250
10 C C20	-2.1363603	-1.5750872	-1.2837411
11 C C21	-3.5270611	-1.4876128	-1.2149658
12 C C22	-3.3773418	0.6461909	-0.1317388
13 H H28	-1.3716619	1.3511466	0.2606122
14 H H30	-1.6591248	-2.4294477	-1.7419244
15 H H33	-5.2436517	-0.3196712	-0.6245901
16 C C23	3.4701700	-1.7767561	-0.9681170
17 C C24	5.5695445	-2.1977026	-2.3280808
18 C C25	5.5868573	-2.5902270	0.1753813
19 C C26	6.4142148	-2.1636308	-1.0458813
20 C C27	4.3109634	-1.7460253	0.3199323
21 C C28	4.2993162	-1.3453127	-2.1899404
22 H H36	5.2810725	-3.2358982	-2.5429145
23 H H37	5.3070792	-3.6475100	0.0713954
24 H H38	6.7954007	-1.1439239	-0.8892658
25 H H39	4.5881530	-0.7059347	0.5478426
26 H H40	4.5825388	-0.2874051	-2.0865219
27 H H41	3.1194264	-2.8008227	-1.1250681
28 H H42	6.1596642	-1.8546386	-3.1858855
29 H H43	6.1865864	-2.5166078	1.0900585
30 H H44	7.2930945	-2.8102422	-1.1530313
31 H H45	3.7014172	-2.1056411	1.1552688
32 H H46	3.6812193	-1.4246690	-3.0915252
33 C C29	-4.0219879	1.8357875	0.5235128
34 C C30	-4.3547243	-2.6287743	-1.7476187
35 F F1	-5.5818693	-2.2155149	-2.1391270
36 F F2	-3.7685601	-3.2213670	-2.8097864
37 F F3	-4.5413966	-3.5874171	-0.8127692
38 F F4	-5.2949743	2.0148487	0.1170267

39 F F5	-4.0544452	1.7135871	1.8754090
40 F F6	-3.3459894	2.9820225	0.2594708
41 N N1	2.6702447	2.5108853	-0.0118602
42 C C1	2.6570347	2.9767424	1.3897007
43 H H4	3.2432810	3.9126873	1.4845602
44 H H5	3.1977183	2.2290948	1.9783196
45 C C13	2.0303958	3.4807450	-0.9151633
46 C C3	4.0732986	2.3157114	-0.3913989
47 H H3	4.5422410	1.5921227	0.2811281
48 H H11	4.1548068	1.9264769	-1.4083824
49 C C4	1.7418670	2.9416491	-2.3207297
50 H H12	2.5907757	2.3487832	-2.6729730
51 H H13	1.6614474	3.8004166	-3.0132225
52 C C5	1.3082839	3.2790767	2.0514547
53 H H14	0.8102258	4.0953529	1.5175889
54 H H15	1.5640309	3.6946784	3.0481068
55 N N4	0.5390989	2.1003618	-2.4028408
56 N N5	0.3383679	2.1868039	2.1794641
57 C C7	0.5648099	1.2835707	-3.6206611
58 H H17	-0.3264400	0.6517953	-3.6579922
59 H H21	1.4424875	0.6313873	-3.6100076
60 H H22	0.5926992	1.8941239	-4.5403678
61 C C8	-0.6814797	2.9130532	-2.3783385
62 H H18	-0.7233249	3.6257529	-3.2220017
63 H H23	-0.7539024	3.4803785	-1.4475546
64 H H24	-1.5575433	2.2633073	-2.4307914
65 C C11	0.8643401	1.1098113	3.0334914
66 H H32	1.0817197	1.4774447	4.0546627
67 H H34	1.8121501	0.7804380	2.6016355
68 C C12	-0.9051967	2.7439296	2.7220489
69 H H1	-1.2482672	3.5624784	2.0830226
70 H H19	-0.7831571	3.1389513	3.7484449
71 H H47	-1.6979603	1.9967027	2.7363261
72 H H48	1.0878049	3.7985586	-0.4684969
73 H H49	2.6541594	4.3908863	-1.0099409
74 H H7	4.6567605	3.2541004	-0.3405876
75 C C2	-0.0642334	-0.1064021	3.1496429
76 H H6	-0.2826709	-0.5014797	2.1411538
77 H H8	-1.0186322	0.2058965	3.5825641
78 N N6	0.4913164	-1.1243020	4.0439486
79 C C6	1.5968539	-1.8693305	3.4473450
80 H H9	2.4082860	-1.1931472	3.1644554
81 H H16	1.2996867	-2.4454297	2.5515433
82 H H20	1.9997711	-2.5700019	4.1857611
83 C C9	-0.5421762	-2.0403384	4.5146340
84 H H2	-0.1055393	-2.7459537	5.2285419

85 H H25	-1.0128186	-2.6285078	3.7041436
86 H H26	-1.3292775	-1.4814082	5.0312808

1 + TACN

Atom	Cartesian Coordinates (Angstroms)		
	X	Y	Z
-----	-----	-----	-----
1 N N1	-3.9631626	-2.3050019	-1.2539444
2 C C1	-4.8886767	-2.7814741	-2.2730449
3 H H3	-5.5106800	-3.5872821	-1.8699328
4 H H4	-4.3243359	-3.1905683	-3.1182340
5 H H5	-5.5550754	-1.9903955	-2.6683066
6 C C2	-4.6096232	-1.8619147	-0.0203063
7 H H6	-5.6039747	-2.3225152	0.0330960
8 H H7	-4.7757403	-0.7694037	-0.0149363
9 C C3	-3.8746646	-2.2736638	1.2660706
10 H H8	-3.8345144	-3.3724584	1.3112164
11 H H9	-4.5039855	-1.9550676	2.1068505
12 C C4	-2.9845535	-1.3540467	-1.7997892
13 H H10	-2.7762733	-0.5859165	-1.0547378
14 H H11	-3.4073089	-0.8360211	-2.6780426
15 C C5	-1.6507800	-1.9842827	-2.2135349
16 H H12	-1.1336123	-1.2736685	-2.8697925
17 H H13	-1.8429327	-2.8933942	-2.8147716
18 N N2	-2.5174451	-1.7051403	1.4518723
19 N N3	-0.7363163	-2.2714848	-1.0950480
20 C C6	-1.4589247	-2.7161697	1.2812582
21 H H16	-1.6359694	-3.5752216	1.9584852
22 H H17	-0.5164651	-2.2576495	1.6011561
23 C C7	-1.2717620	-3.2679231	-0.1336680
24 H H18	-0.5711350	-4.1095125	-0.0553601
25 H H19	-2.2159496	-3.6737321	-0.5068160
26 C C9	-2.3824622	-1.1029927	2.7873490
27 H H1	-2.4718091	-1.8446681	3.6018546
28 H H20	-3.1523584	-0.3409928	2.9316040
29 H H21	-1.4072375	-0.6139913	2.8755968
30 C C10	-0.3709184	1.6522465	0.3890683
31 N N4	-1.7127224	1.4628076	0.5120385
32 H H24	-2.0527609	0.5029743	0.5790606
33 N N5	0.3114036	0.4779938	0.1573701
34 H H23	-0.2268353	-0.3721215	-0.0515139
35 S S1	0.3784710	3.1575981	0.5371844
36 C C11	1.7128331	0.2948509	0.1134650
37 C C12	4.4596054	-0.3015849	-0.0435930

38 C C13	2.5710317	1.1149817	-0.6330972
39 C C14	2.2432870	-0.8095529	0.7840138
40 C C15	3.6013244	-1.1177585	0.6858338
41 C C16	3.9322063	0.8202717	-0.6889279
42 H H22	2.1729769	1.9686009	-1.1632310
43 H H26	1.5910922	-1.4331372	1.3862344
44 H H29	5.5147685	-0.5351550	-0.1154477
45 C C17	-2.7057116	2.5371246	0.5439967
46 C C18	-4.4297349	3.8392205	-0.7904108
47 C C19	-4.7568961	3.4715049	1.6987798
48 C C20	-5.4518274	3.6477860	0.3404729
49 C C21	-3.7303318	2.3278134	1.6697620
50 C C22	-3.4024262	2.6982701	-0.8204078
51 H H25	-3.9029409	4.7934909	-0.6477641
52 H H30	-4.2443530	4.4054508	1.9697636
53 H H31	-6.0635677	2.7572660	0.1300492
54 H H32	-4.2580361	1.3728265	1.5166967
55 H H33	-3.9058246	1.7560227	-1.0849440
56 H H34	-2.1403753	3.4499352	0.7527893
57 H H35	-4.9412813	3.9077456	-1.7585613
58 H H36	-5.4983013	3.2842202	2.4854917
59 H H37	-6.1436403	4.4987462	0.3773559
60 H H38	-3.2086290	2.2558407	2.6319109
61 H H39	-2.6431580	2.8818684	-1.5896707
62 C C23	4.8568765	1.7480689	-1.4331844
63 C C24	4.0915529	-2.3847066	1.3275451
64 F F1	5.3363983	2.7196332	-0.6264127
65 F F2	5.9269385	1.0900910	-1.9361994
66 F F3	4.2354730	2.3572002	-2.4653152
67 F F4	3.6783539	-3.4756434	0.6285434
68 F F5	3.6082901	-2.5308782	2.5819912
69 F F6	5.4354727	-2.4444453	1.3964676
70 C C8	0.5642315	-2.6952970	-1.6307742
71 H H2	0.9890776	-1.8953792	-2.2459015
72 H H14	0.4902535	-3.6060394	-2.2524422
73 H H15	1.2628477	-2.8976087	-0.8149270

1 + Me₆TREN

		Cartesian Coordinates (Angstroms)		
Atom		X	Y	Z
-----		-----	-----	-----
1 C	C16	-0.3565532	-1.9654632	0.2387363
2 S	S1	-1.1207598	-3.4475029	0.4941631
3 N	N2	0.9719516	-1.8466738	-0.0174063
4 H	H10	1.3074932	-0.9566372	-0.3934779
5 N	N3	-0.9757238	-0.7252759	0.3006581
6 H	H27	-0.3722192	0.0499826	0.5924125
7 C	C17	-2.3084752	-0.3440481	0.0937992
8 C	C18	-4.9143951	0.6752252	-0.3453424
9 C	C19	-2.5400110	1.0365476	-0.0393070
10 C	C20	-3.4058028	-1.2145768	-0.0150334
11 C	C21	-4.6815944	-0.6950182	-0.2357005
12 C	C22	-3.8227716	1.5347176	-0.2418054
13 H	H28	-1.7038945	1.7235529	0.0202816
14 H	H30	-3.2512939	-2.2800549	0.0797111
15 H	H33	-5.9121122	1.0599851	-0.5086353
16 C	C23	1.9047760	-2.9753131	-0.0214730
17 C	C24	3.9118105	-4.0150346	-1.1615347
18 C	C25	3.5684324	-4.3331403	1.3300990
19 C	C26	4.5990173	-4.1959931	0.1998898
20 C	C27	2.5911907	-3.1492103	1.3452993
21 C	C28	2.9328753	-2.8305365	-1.1526160
22 H	H36	3.3649591	-4.9328453	-1.4169447
23 H	H37	3.0021816	-5.2645983	1.1939824
24 H	H38	5.2411063	-3.3255996	0.3987345
25 H	H39	3.1309476	-2.2249158	1.5961858
26 H	H40	3.4964247	-1.8965405	-1.0226784
27 H	H41	1.2995863	-3.8676532	-0.2122285
28 H	H42	4.6595808	-3.8707964	-1.9502402
29 H	H43	4.0723748	-4.4156428	2.3001553
30 H	H44	5.2591200	-5.0710342	0.1762892
31 H	H45	1.8230726	-3.2920537	2.1125161
32 H	H46	2.4117507	-2.7557165	-2.1139955
33 C	C29	-3.9911292	3.0223452	-0.3838011
34 C	C30	-5.8441155	-1.6536240	-0.2865727
35 F	F1	-6.9221760	-1.1022743	-0.8889782
36 F	F2	-5.5367901	-2.7824334	-0.9584769
37 F	F3	-6.2325557	-2.0272279	0.9540142
38 F	F4	-5.2849372	3.3972487	-0.3886396
39 F	F5	-3.3818722	3.6903011	0.6312191
40 F	F6	-3.4330444	3.4828813	-1.5279053

41 N N1	2.6712172	1.5729156	0.5387792
42 C C1	2.4560060	2.2769173	1.8008238
43 H H4	2.9756586	3.2532645	1.8337622
44 H H5	2.9036435	1.6771309	2.5998396
45 C C13	2.4717650	2.4043496	-0.6619079
46 C C3	3.9041124	0.7766860	0.5408367
47 H H3	3.8188353	0.0434604	1.3526992
48 H H11	3.9299761	0.1963593	-0.3851796
49 C C4	1.3290279	1.9414201	-1.5757468
50 H H12	1.1942213	2.7081642	-2.3651848
51 H H13	0.4026557	1.9235519	-0.9922123
52 C C5	0.9979294	2.5652812	2.1696056
53 H H14	0.5474077	3.2436689	1.4341452
54 H H15	1.0343664	3.1274073	3.1237948
55 C C6	5.2465570	1.5178999	0.7283457
56 H H6	5.9922056	0.8054275	1.1358054
57 H H16	5.1170011	2.2891301	1.4946283
58 N N4	1.4987514	0.6069992	-2.1665485
59 N N5	0.1108668	1.3975211	2.2981623
60 N N6	5.7523458	2.1697795	-0.4862453
61 C C7	2.6255564	0.5539074	-3.0974384
62 H H17	2.7280786	-0.4630850	-3.4868588
63 H H21	3.5582265	0.8182945	-2.5967624
64 H H22	2.4975802	1.2371232	-3.9578844
65 C C8	0.2784606	0.2019085	-2.8696812
66 H H18	0.0455305	0.8600357	-3.7268575
67 H H23	-0.5735378	0.2176121	-2.1878272
68 H H24	0.3922826	-0.8189360	-3.2462111
69 C C9	6.3856359	1.2148333	-1.3900349
70 H H9	6.6921431	1.7228455	-2.3095486
71 H H25	5.6870614	0.4206208	-1.6679526
72 H H26	7.2800528	0.7354826	-0.9471517
73 C C10	6.6751609	3.2558425	-0.1697362
74 H H20	7.5785419	2.9141576	0.3701598
75 H H29	6.1713257	4.0042144	0.4494834
76 H H31	7.0001824	3.7443355	-1.0935897
77 C C11	0.6890679	0.3261788	3.1143348
78 H H2	-0.0559571	-0.4643574	3.2360790
79 H H32	0.9924531	0.6695158	4.1201041
80 H H34	1.5535040	-0.1122512	2.6122861
81 C C12	-1.1598265	1.8303244	2.8902341
82 H H1	-1.6168627	2.6163775	2.2837463
83 H H19	-1.0278637	2.2212039	3.9152612
84 H H47	-1.8559628	0.9887315	2.9319240
85 H H48	2.2310503	3.4327438	-0.3603208
86 H H49	3.4117858	2.4835209	-1.2165070

1 + DABCO

		Cartesian Coordinates (Angstroms)		
Atom		X	Y	Z

1	C C16	1.2089310	-1.5514649	-0.1404124
2	S S1	0.8434249	-3.1945276	-0.1898216
3	N N2	2.4839571	-1.0697456	-0.1091368
4	H H10	2.5995125	-0.0695143	-0.2185575
5	N N3	0.2805404	-0.5364245	-0.1334519
6	H H27	0.6405493	0.4273059	-0.1680656
7	C C17	-1.1231022	-0.6064949	-0.1231761
8	C C18	-3.9363673	-0.4603232	-0.0478571
9	C C19	-1.8078393	0.4069801	-0.8032659
10	C C20	-1.8601259	-1.5672325	0.5860731
11	C C21	-3.2515290	-1.4878668	0.6055873
12	C C22	-3.1983255	0.4888863	-0.7479374
13	H H28	-1.2475707	1.1302262	-1.3853439
14	H H30	-1.3468037	-2.3653039	1.1036452
15	H H33	-5.0167641	-0.4085715	-0.0159565
16	C C23	3.6965505	-1.8707133	-0.2670929
17	C C24	5.4163840	-2.7844409	-1.8990332
18	C C25	6.1208369	-2.1025689	0.4379769
19	C C26	6.5465478	-2.2095660	-1.0337670
20	C C27	4.8250903	-1.2914282	0.5990594
21	C C28	4.1212951	-1.9734941	-1.7429378
22	H H36	5.2260834	-3.8256228	-1.6051630
23	H H37	5.9612217	-3.1111195	0.8431719
24	H H38	6.8160151	-1.2103320	-1.4057236
25	H H39	5.0145221	-0.2480021	0.3004993
26	H H40	4.2744714	-0.9583744	-2.1393945
27	H H41	3.4393165	-2.8710308	0.0937622
28	H H42	5.7153918	-2.8097876	-2.9532068
29	H H43	6.9195667	-1.6499140	1.0368580
30	H H44	7.4472147	-2.8280928	-1.1219844
31	H H45	4.5093513	-1.2703692	1.6483144
32	H H46	3.3067623	-2.4256999	-2.3177468
33	C C29	-3.8628339	1.6414512	-1.4475148
34	C C30	-4.0248454	-2.4831993	1.4323407
35	F F1	-5.3007159	-2.6062559	1.0033055
36	F F2	-3.4637370	-3.7081607	1.4066213
37	F F3	-4.0813457	-2.1009652	2.7308812
38	F F4	-5.2067203	1.5672760	-1.4105526
39	F F5	-3.5085914	2.8255572	-0.8790857
40	F F6	-3.4904649	1.7191521	-2.7451072

41 N N1	1.7151695	4.6739524	1.2927295
42 C C1	1.3708245	3.7165088	2.3580458
43 H H1	0.5246207	4.1222409	2.9221435
44 H H4	2.2209661	3.6473364	3.0450267
45 C C2	0.5816590	4.7728135	0.3582372
46 H H3	-0.2885464	5.1329969	0.9165792
47 H H7	0.8213070	5.5280997	-0.3977503
48 C C3	2.8906327	4.1757897	0.5619933
49 H H2	3.1281182	4.8907931	-0.2329674
50 H H9	3.7438368	4.1539792	1.2483343
51 C C4	1.0234908	2.3222680	1.7437244
52 H H5	-0.0134969	2.0350674	1.9452258
53 H H11	1.6649400	1.5290914	2.1428162
54 C C5	2.5997029	2.7557482	-0.0261382
55 H H12	3.2678858	2.0048223	0.4133317
56 H H13	2.7378696	2.7304746	-1.1127498
57 C C6	0.2926558	3.3842379	-0.2965406
58 H H6	0.4519217	3.4090504	-1.3802941
59 H H14	-0.7396619	3.0674558	-0.1226144
60 N N5	1.2031124	2.3573292	0.2707544

1 + PMDETA

Atom	Cartesian Coordinates (Angstroms)		
	X	Y	Z
-----	-----	-----	-----
1 C C16	0.9400661	-1.6040524	-0.1443843
2 S S1	0.6157847	-3.2162549	0.2401523
3 N N2	2.2057303	-1.1049881	-0.2575092
4 H H10	2.3141278	-0.0911790	-0.2229078
5 N N3	-0.0108788	-0.6399799	-0.3807524
6 H H27	0.3343899	0.2770472	-0.6868464
7 C C17	-1.4092661	-0.6787211	-0.2598552
8 C C18	-4.2218703	-0.4910748	-0.1243812
9 C C19	-2.0383473	0.5523458	-0.0232264
10 C C20	-2.2035871	-1.8246631	-0.4249482
11 C C21	-3.5913786	-1.7169660	-0.3403202
12 C C22	-3.4281184	0.6437516	0.0248336
13 H H28	-1.4219558	1.4304084	0.1326002
14 H H30	-1.7344506	-2.7785990	-0.6159406
15 H H33	-5.3010874	-0.4212929	-0.0872832
16 C C23	3.4183721	-1.9007813	-0.0703383
17 C C24	5.7270086	-2.4321396	-0.9765603
18 C C25	5.2956182	-2.5397073	1.5180724
19 C C26	6.3278211	-2.2347944	0.4230170

20 C C27	4.0166113	-1.7098841	1.3349931
21 C C28	4.4496489	-1.6002796	-1.1700992
22 H H36	5.4894708	-3.4951540	-1.1209284
23 H H37	5.0368427	-3.6067652	1.4842987
24 H H38	6.6714782	-1.1951208	0.5269876
25 H H39	4.2444625	-0.6444970	1.4896057
26 H H40	4.7079942	-0.5325104	-1.1504086
27 H H41	3.1001953	-2.9429187	-0.1617691
28 H H42	6.4607054	-2.1711481	-1.7482931
29 H H43	5.7220720	-2.3553794	2.5108448
30 H H44	7.2138715	-2.8683412	0.5475669
31 H H45	3.2636358	-1.9894235	2.0795107
32 H H46	4.0035875	-1.8023337	-2.1506696
33 C C29	-4.0458593	1.9966866	0.2443854
34 C C30	-4.4263740	-2.9663093	-0.4550219
35 F F1	-5.6740186	-2.6933512	-0.9032544
36 F F2	-3.8798602	-3.8647042	-1.3008540
37 F F3	-4.5643934	-3.5810240	0.7412260
38 F F4	-5.3903503	1.9704658	0.1667490
39 F F5	-3.7241858	2.5068657	1.4596089
40 F F6	-3.6055217	2.8959611	-0.6722761
41 N N1	2.8609581	2.3232232	0.1154391
42 C C1	2.8324698	2.8795208	1.4825166
43 H H4	3.3972421	3.8318341	1.5240012
44 H H5	3.3833560	2.1789626	2.1187197
45 C C13	2.1499982	3.1758319	-0.8518909
46 C C3	4.2707428	2.1880077	-0.2664492
47 H H3	4.7820072	1.5175267	0.4301727
48 H H11	4.3692558	1.7649898	-1.2679621
49 C C4	1.8813542	2.4867485	-2.1994069
50 H H12	2.6878678	1.7830710	-2.4216918
51 H H13	1.9043376	3.2447585	-3.0040595
52 C C5	1.4701625	3.1761508	2.1151257
53 H H14	0.9893280	4.0149546	1.5984064
54 H H15	1.6979940	3.5487139	3.1362736
55 N N4	0.6135739	1.7393036	-2.2390926
56 N N5	0.5113127	2.0753433	2.1537552
57 C C7	0.6267775	0.7602926	-3.3320572
58 H H17	-0.3204841	0.2153006	-3.3448300
59 H H21	1.4317413	0.0383152	-3.1681518
60 H H22	0.7680299	1.2284546	-4.3219965
61 C C8	-0.5242007	2.6520569	-2.4038536
62 H H18	-0.4622074	3.2210297	-3.3488124
63 H H23	-0.5689471	3.3689083	-1.5800036
64 H H24	-1.4605974	2.0905281	-2.3978799
65 C C11	1.0194452	0.9197221	2.8888881

66 H H2	0.2541795	0.1394243	2.9140273
67 H H32	1.2893103	1.1646713	3.9346331
68 H H34	1.8998185	0.5035958	2.3953640
69 C C12	-0.7404767	2.5366942	2.7525669
70 H H1	-1.1437064	3.3791766	2.1825798
71 H H19	-0.6162055	2.8633433	3.8027732
72 H H47	-1.4825717	1.7356678	2.7315969
73 H H48	1.1920571	3.4624643	-0.4169104
74 H H49	2.7141533	4.1115312	-1.0283118
75 H H7	4.8012259	3.1582719	-0.2578458

1 + TMEDA

Atom	Cartesian Coordinates (Angstroms)		
	X	Y	Z
1 C C16	1.1570678	1.2675919	0.0222826
2 S S1	0.9494085	2.9278905	-0.1958706
3 N N2	2.3798598	0.6712669	0.0681768
4 H H10	2.4168497	-0.3418869	-0.0773393
5 N N3	0.1397676	0.3487417	0.1844900
6 H H27	0.4285296	-0.5907202	0.4873435
7 C C17	-1.2463911	0.4684560	0.0007023
8 C C18	-4.0591293	0.4444004	-0.3149723
9 C C19	-1.9394608	-0.7225780	-0.2674805
10 C C20	-1.9850429	1.6566730	0.1120983
11 C C21	-3.3702227	1.6287463	-0.0599405
12 C C22	-3.3234370	-0.7358615	-0.4065835
13 H H28	-1.3856709	-1.6495293	-0.3627610
14 H H30	-1.4722421	2.5833396	0.3279167
15 H H33	-5.1343914	0.4411501	-0.4313642
16 C C23	3.6490887	1.3944767	-0.0070741
17 C C24	6.0307823	1.4967964	0.8554797
18 C C25	5.5076252	2.2557995	-1.5057231
19 C C26	6.5519716	1.6083247	-0.5845087
20 C C27	4.1672180	1.5070433	-1.4515880
21 C C28	4.6921368	0.7433315	0.9151919
22 H H36	5.8905068	2.5048970	1.2687728
23 H H37	5.3486534	3.2986839	-1.1992757
24 H H38	6.7925174	0.6028516	-0.9597954
25 H H39	4.2967586	0.4965878	-1.8645439
26 H H40	4.8532592	-0.3016587	0.6106266
27 H H41	3.4402613	2.4057996	0.3544496
28 H H42	6.7684484	0.9975785	1.4947389
29 H H43	5.8759867	2.2893798	-2.5376754

30 H H44	7.4864250	2.1809629	-0.6053528
31 H H45	3.4120860	2.0149830	-2.0592718
32 H H46	4.3094525	0.7201953	1.9423092
33 C C29	-3.9890580	-2.0548644	-0.6841672
34 C C30	-4.1151725	2.9351552	0.0475203
35 F F1	-5.4541487	2.7654965	-0.0240372
36 F F2	-3.8500760	3.5608646	1.2160605
37 F F3	-3.7646131	3.7875439	-0.9398024
38 F F4	-5.3327373	-1.9729156	-0.6611308
39 F F5	-3.6323375	-2.5501557	-1.8920969
40 F F6	-3.6250475	-2.9925675	0.2316921
41 N N1	2.4744326	-2.4736675	-0.7590856
42 C C1	1.4257689	-2.6453258	-1.7682042
43 H H4	1.4777839	-3.6292553	-2.2680308
44 H H5	1.5248856	-1.8680463	-2.5305927
45 C C13	2.4072905	-3.4928987	0.2970583
46 C C3	3.7886831	-2.5355159	-1.4060932
47 H H3	3.8584624	-1.7634978	-2.1766666
48 H H11	4.5778705	-2.3578008	-0.6696665
49 C C4	1.1151918	-3.5298157	1.1183454
50 H H12	1.2566766	-4.3107199	1.8900617
51 H H13	0.2841926	-3.8723424	0.4923204
52 N N4	0.7107028	-2.2572025	1.7318656
53 C C7	1.7242025	-1.7384717	2.6566403
54 H H17	1.3706376	-0.7971667	3.0857834
55 H H21	2.6553437	-1.5311150	2.1275283
56 H H22	1.9358424	-2.4377437	3.4850554
57 C C8	-0.5607377	-2.4327048	2.4463774
58 H H18	-0.4708125	-3.1394883	3.2900595
59 H H23	-1.3335598	-2.8056676	1.7693349
60 H H24	-0.8937992	-1.4696026	2.8423802
61 H H48	2.5410912	-4.5074014	-0.1261331
62 H H49	3.2616450	-3.3258903	0.9616365
63 H H7	3.9791157	-3.5137009	-1.8831872
64 H H51	0.4370790	-2.5424611	-1.3193358

3.5 References

- (1) Nederberg, F.; Connor, E. F.; Möller, M.; Glauser, T.; Hedrick, J. L. *Angew. Chem., Int. Ed.* **2001**, *40*, 2712.
- (2) (a) Kamber, N. E.; Jeong, W.; Waymouth, R. M.; Pratt, R. C.; Lohmeijer, B. G. G.; Hedrick, J. L. *Chem. Rev.* **2007**, *107*, 5813. (b) Bourissou, D.; Moebs-Sanchez, S.; Martin-Vaca, B. *C. R. Chim.* **2007**, *10*, 775.
- (3) Dove, A. P. *ACS Macro Lett.* **2012**, *1*, 1409.
- (4) Thomas, C.; Bibal, B. *Green Chem.* **2014**, *16*, 1687.
- (5) Pratt, R. C.; Lohmeijer, B. G. G.; Long, D. A.; Lundberg, P. N. P.; Dove, A. P.; Li, H.; Wade, C. G.; Waymouth, R. M.; Hedrick, J. L. *Macromolecules* **2006**, *39*, 7863.
- (6) Kiesewetter, M. K.; Shin, E. J.; Hedrick, J. L.; Waymouth, R. M. *Macromolecules* **2010**, *43*, 2093.
- (7) Koeller, S.; Kadota, J.; Peruch, F.; Deffieux, A.; Pinaud, N.; Pianet, I.; Massip, S.; Léger, J.-M.; Desvergne, J.-P.; Bibal, B. *Chem. - Eur. J.* **2010**, *16*, 4196.
- (8) Kazakov, O. I.; Datta, P. P.; Isajani, M.; Kiesewetter, E. T.; Kiesewetter, M. K. *Macromolecules* **2014**, *47*, 7463.
- (9) Todd, R.; Rubio, G.; Hall, D. J.; Tempelaar, S.; Dove, A. P. *Chem. Sci.* **2013**, *4*, 1092.
- (10) Coady, D. J.; Engler, A. C.; Horn, H. W.; Bajjuri, K. M.; Fukushima, K.; Jones, G. O.; Nelson, A.; Rice, J. E.; Hedrick, J. L. *ACS Macro Lett.* **2012**, *1*, 19.
- (11) Horman, I.; Dreux, B. *Anal. Chem.* **1983**, *55*, 1219.
- (12) Webb, J. E. A.; Crossley, M. J.; Turner, P.; Thordarson, P. *J. Am. Chem. Soc.* **2007**, *129*, 7155.

- (13) Thordarson, P. *Chem. Soc. Rev.* **2011**, *40*, 1305.
- (14) All K_{eq} and free energy values are reported at 298 K. The units of binding constant in this paper are M^{-1} . The chemical convention of unitless K_{eq} is used throughout.
- (15) Cornish-Bowden, A. J. *Biosci.* **2002**, *27*, 121.
- (16) Anslyn, E. V.; Dougherty, D. A. *Mod. Phys. Org. Chem.* **2006**, 145–222.
- (17) Thomas, C.; Peruch, F.; Bibal, B. *RSC Adv.* **2012**, *2*, 12851.
- (18) Jones, C. R.; Dan Pantos, G.; Morrison, A. J.; Smith, M. D. *Angew. Chem., Int. Ed.* **2009**, *48*, 7391.
- (19) A plot of k_{obs} vs $[\text{base}]^n$ is also linear. However, this ROP is zero order in $[\text{base}]$, and this interpretation does not seem tenable.
- (20) Simón, L.; Goodman, J. M. *J. Org. Chem.* **2007**, *72*, 9656.
- (21) Nederberg, F.; Lohmeijer, B. G. G.; Leibfarth, F.; Pratt, R. C.; Choi, J.; Dove, A. P.; Waymouth, R. M.; Hedrick, J. L. *Biomacromolecules* **2007**, *8*, 153.
- (22) Dove, A. P.; Pratt, R. C.; Lohmeijer, B. G. G.; Waymouth, R. M.; Hedrick, J. L. *J. Am. Chem. Soc.* **2005**, *127*, 13798.
- (23) Lohmeijer, B. G. G.; Pratt, R. C.; Leibfarth, F.; Logan, J. W.; Long, D. A.; Dove, A. P.; Nederberg, F.; Choi, J.; Wade, C.; Waymouth, R. M.; Hedrick, J. L. *Macromolecules* **2006**, *39*, 8574.
- (24) These models were constructed in the gas phase and were not meant to provide quantitative energetic data which can be difficult to extract from reactions that exhibit low energy changes.
- (25) Berry, S. J. *J. Chem. Phys.* **1960**, *32*, 933.

(26) Binding equation from references: $\delta_{\text{obs}} = \delta_{\text{H}} - (\Delta\delta/2[\text{H}]_0)\{[\text{H}]_0 + [\text{G}]_0 + 1/\text{K} - (([\text{H}]_0 + [\text{G}]_0 + 1/\text{K})^2 - 4[\text{H}]_0[\text{G}]_0)^{1/2}\}$; $\Delta\delta$ is the difference in the chemical shift of host and complex; δ_{obs} is the observed chemical shift of the TU in the presence of base; δ_{H} is the chemical shift of free TU in the absence of base.

(27) Duda, A.; Kowalski, A. In *Handbook of Ring-Opening Polymerization*; Dubois, P., Coulembier, O., Raquez, J.-M., Eds.; Wiley-VCH: Weinheim, Germany, 2009; pp 1–52.

(28) Spink, S. S.; Kazakov, O. I.; Kiesewetter, E. T.; Kiesewetter, M. K. *Macromolecules*, **2015**, *48* (17), 6127–6131.

(29) Webb, J. E. A.; Crossley, M. J.; Turner, P.; Thordarson, P. *J. Am. Chem. Soc.* **2007**, *129*, 7155.

(30) Thordarson, P. *Chem. Soc. Rev.* **2011**, *40*, 1305.

(31) Deranleau, D. A. *J. Am. Chem. Soc.* **1969**, *91*, 4044.

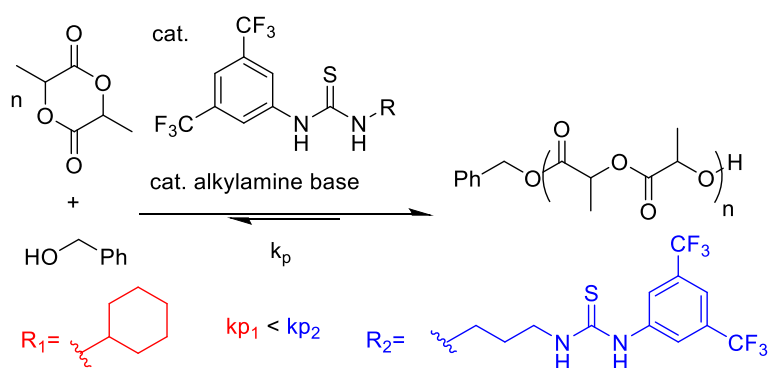
(32) Horman, I.; Dreux, B. *Anal. Chem.* **1983**, *55*, 1219.

(33) Peters, S. J.; Stevenson, C. D. *J. Chem. Educ.* **2004**, *81*, 715.

INTENTIONALLY BLANK PAGE

Chapter 4

Rate Accelerated Organocatalytic Ring-Opening Polymerization of L-Lactide via the Application of a Bis(thiourea) H-bond Donating Cocatalyst

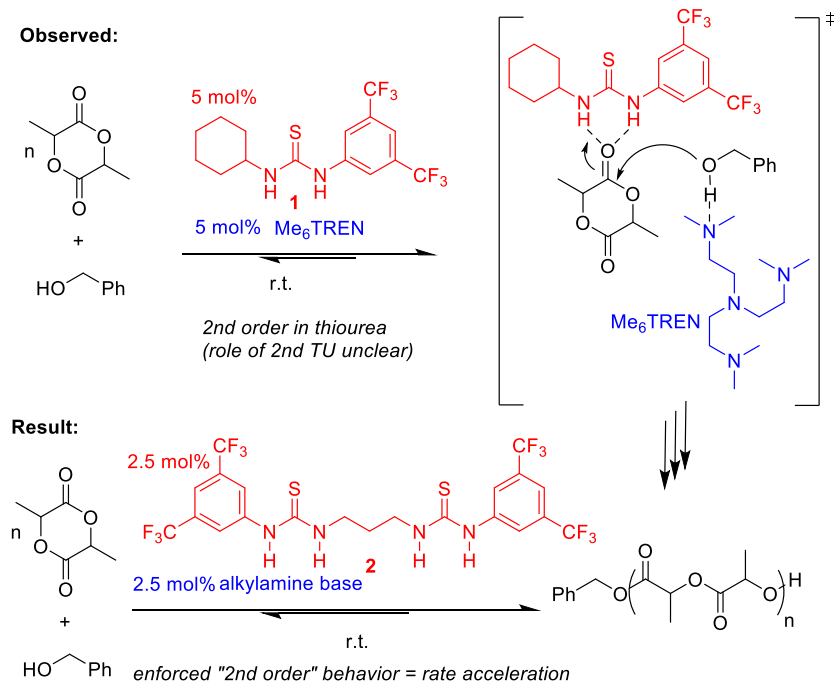


4.1. Abstract

A cocatalyst system consisting of an alkylamine base and a bis(thiourea) featuring a linear alkane tether is shown to dramatically increase the rate of ring-opening polymerization (ROP) of L-lactide versus previously disclosed monothiourea H-bond donors. Rate acceleration occurs regardless of the identity of the alkylamine cocatalyst, and the ROP remains controlled yielding poly(lactide) with narrow molecular weight distributions, predictable molecular weights and high selectivity for monomer. This H-bond mediated ROP of L-lactide constitutes a rare, clear example of rate acceleration with bis(thiourea) H-bond donors versus monothioureas, and the bis(thiourea) is shown to remain highly active for ROP at fractional percent catalyst loadings. Activation at a single monomer ester by both thiourea moieties is implicated as the source of rate acceleration.

4.2. Introduction

Thiourea (TU) H-bond donors¹ have been a workhorse of organocatalytic transformations.²⁻⁵ This class of compounds features a wide array of functional motifs and geometries and has been employed in a multitude of reactions including Henry reactions, hydroaminations, conjugate additions and ringopening polymerization (ROP).⁶⁻¹² While the wealth of chemistry offered by H-bonding catalysts has attracted numerous research groups, these systems can require high catalyst loadings and/or long reaction times. A general means of producing rate-accelerated reactions with this widely used class of catalysts has been elusive. The thiourea **1** (scheme 4.1), with a slate of base cocatalysts, has been widely applied to the synthesis of polyesters and polycarbonates via ROP.^{13,14} These systems are believed to effect “living” ROP via dual activation of monomer by **1** and of growing polymer chain by base, Scheme 1.^{15,16} Herein, we show a strategy for the rate enhancement of the ROP of L-lactide (L-LA) using bis(thiourea) H-bond donors with a variety of alkylamine cocatalysts, Figure 1. Such a rate acceleration is not usually observed upon switching from monothiourea to bis(thiourea) H-bond donating catalysts in small molecule systems.^{7,17}



Scheme 4.1. Second Order Behavior in **1** Inspires Tethered H-Bond Donor **2**.

4.3. Results and Discussion

Our approach was inspired by the use of bis(thiourea) catalysts in small molecule transformations as well as our own investigations into the nature of **1**/base catalyzed ROP.²⁰ During the course of mechanistic studies into the **1**/base catalyzed ROP of lactide initiated from benzyl alcohol, we observed that some **1**/alkylamine combinations, like **1**/Me₆TREN in Scheme 1, exhibit second order kinetics in [**1**].²¹ This observation suggests that two **1** molecules are kinetically relevant in the rate-determining step. The kinetic orders of the previously studied ROP reactions are base dependent,²¹ which hints at the possibility of exploiting these differences for the

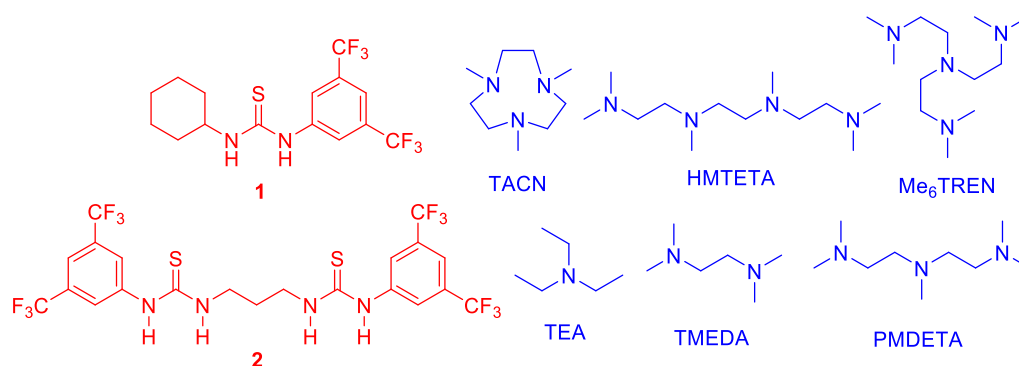
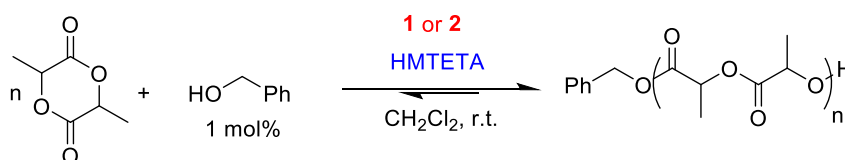


Figure 4.1. Alkylamine and thiourea cocatalysts evaluated for the ROP of L-LA.

development of advanced catalyst systems. We reasoned that tethering two thiourea moieties could enhance the rate of the **1**/base cocatalyzed ROPs which exhibit second order dependence upon [**1**] and possibly enforce dual thiourea activation in the others, likewise enhancing rate.

Table 4.1. HMTETA and Bis(thiourea) cocatalyzed ROP of L-LA.^a

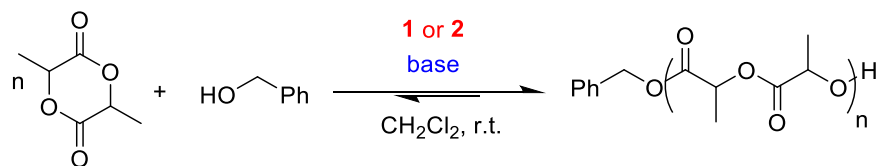


entry	TU	mol% (bis)TU	mol% base	conv. ^b (%)	time (min)	M _n ^c (g/mol)	M _w /M _n ^c
1	1	5	5	94	90	16,300	1.05
2	1	5	2.5	88	198	16,800	1.06
3	2	2.5	2.5	90	15	15,400	1.03
4	2	2.5	5	90	20	17,100	1.04

^aReaction conditions: 1 M (0.7 mmol) L-LA, 0.007 mmol benzyl alcohol, CH₂Cl₂ (0.7 mL) and given amount of catalyst. Aliquots of the reaction were quenched with benzoic acid and characterized by GPC and ¹H NMR. ^bConversion to polymer obtained by ¹H NMR. ^cDetermined by GPC vs polystyrene standards.

Bis(thiourea)^{2,7} combined with the alkyl amine base HMTETA (fig. 4.1), significantly accelerates the ROP of L-LA (1 M in CH₂Cl₂), initiated from benzyl alcohol ([M]₀/[I]₀ = 100) versus the **1**/HMTETA cocatalyzed ROP. Only the concentration of cocatalysts are varied between runs. The ROP of L-LA from benzyl alcohol achieves 90% conversion in 15 min when catalyzed by **2**/HMTETA (2.5 mol % each), whereas the **1**/HMTETA (5 mol % each) catalyzed reaction reaches 94% conversion in 90 min. This ROP is accelerated with **2** versus **1** when controlling for the concentrations of cocatalysts or the concentration of thiourea moiety present, Table 1. The reaction rate slows with a stoichiometric excess of HMTETA to **2** (Table 1, entries 3 and 4), which suggests that 1:1 stoichiometry of base:**2** is optimal for ROP.

The rate acceleration exhibited by **2** vs **1** is a general trend and is independent of the identity of the alkylamine cocatalyst being employed. Several commercially available alkylamines in combination with **1** have been shown previously to be effective cocatalysts for the ROP of lactide.^{21,22} The effects of base cocatalyst identity upon ROP have been explained computationally²² and experimentally²¹ in terms of chelating H-bonding interactions with alcohol or varied cocatalyst interactions, respectively. A selection of these cocatalysts were evaluated in the **2**/base cocatalyzed ROP of L-LA (table 4.2). For all base cocatalysts examined, the **2**/base cocatalyzed ROP was faster than the comparative **1**/base catalyzed ROP. This rate acceleration occurs regardless of base identity or the reaction order in [**1**] exhibited in the **1**/base catalyzed ROP of L-LA.²¹ This H-bond mediated ROP of L-LA constitutes a rare, clear example of rate acceleration with bis(thiourea) H-bond donors versus monothioureas.

Table 4.2. Comparison of Alkylamine and (bis)TU Cocatalyzed ROPs of L-Lactide.^a

entry	base	TU	$[M]_0/[I]_0$	conv. (%)	time (min)	M_n^e (g/mol)	M_w/M_n^e
1 ^b	Me ₆ TREN	1	100	94	50	18,400	1.04
2 ^c	Me ₆ TREN	2	100	94	10	17,500	1.03
3 ^c	Me ₆ TREN	2	50	94	8	9,700	1.05
4 ^c	Me ₆ TREN	2	200	95	20	32,200	1.02
5 ^b	TACN	1	100	90	20	16,900	1.04
6 ^c	TACN	2	100	89	6	16,200	1.05
7 ^b	PMDETA	1	100	94	60	16,400	1.04
8 ^c	PMDETA	2	100	88	15	16,200	1.04
9 ^{b,d}	TMEDA	1	100	60	24 h ^f	9,200	1.07
10 ^{c,d}	TMEDA	2	100	81	24 h ^f	14,600	1.04
11 ^{b,d}	TEA	1	100	40	24 h ^f	6,200	1.11
12 ^{d,g}	TEA	2	100	90	24 h ^f	17,600	1.04

^aReactions conducted in CH₂Cl₂ at 1 M (0.7 mmol) L-LA, except in the case in footnote d. ^b5 mol % each base and **1**. ^c2.5 mol % each base and **2**. ^d2 M L-LA. ^e M_n and M_w/M_n determined by GPC in CH₂Cl₂ vs polystyrene standards. ^fReaction stopped at 24h. ^g2.5 mol % **2** and 5 mol % TEA.

Despite the increased rate, the ROPs cocatalyzed by **2** remain controlled and exhibit the characteristics of a “living” polymerization. In the **2**/Me₆TREN catalyzed ROP of L-LA, the M_n is predictable by $[M]_0/[I]_0$ and M_w/M_n is narrow, < 1.05, Table 2, Entries 2– 4. When initiated from pyrenebutanol, the RI and UV/vis signals overlap in the GPC trace of the resulting polymer which suggests end group fidelity, see Experimental Section. This conclusion is supported by MALDI–TOF analysis of a PLA sample which shows only the repeat pattern associated with PLA initiated from benzyl alcohol (see Experimental Section). Further, the sequential addition of LA monomer to a single polymerization solution results in quantitative chain-extension, see

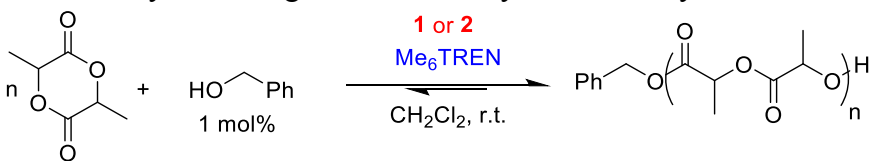
Experimental Section. These observations are consistent with those typically observed for the **1**/base-catalyzed ROP of lactide.^{16,22}

Previously, the best means of effecting higher rates of ROP were to employ stronger bases which typically result in the rapid post polymerization broadening of M_w/M_n .^{3,15} However, the higher rates of these **2**/base-catalyzed ROPs are not associated with loss of selectivity for monomer; MALDI–TOF analysis confirms the remarkable selectivity of **2**/base systems for monomer as multiples of 72 m/z which are associated with random chain scission are vanishingly small, see Experimental Section. The absence of these peaks in the MALDI–TOF suggests that near zero postpolymerization transesterification is occurring. Further, when the reaction solution was left to stir for 1 h after full conversion, the most active **2**/base systems resulted in only modest erosion of M_w/M_n . After 1 h of stirring past full conversion, the initial M_w/M_n for the **2**/HMTETA (Table 1, entry 3) and **2**/Me₆TREN (Table 2, Entry 2) experiments broadened only slightly to $M_w/M_n = 1.06$ for both samples. The ¹³C NMR spectrum of poly(L-lactide) shows only one resonance in the methine region, which suggests that the stereochemistry of the monomer is retained in the polymerization.

The bis(thiourea) (**2**) cocatalyst remains highly active at low concentrations which typically halt **1**/alkylamine cocatalyzed ROP of lactide. For the ROP of L-lactide, the **2**/Me₆TREN (0.5 mol %, table 4.3, entry 2) catalyzed reaction proceeded to 98% conversion in 45 min ($M_n = 17\ 000$; $M_w/M_n = 1.05$) whereas the **1**/Me₆TREN (1 mol %, Table 3, entry 1) catalyzed reaction only progressed to 3% conversion in 24 h. The same ROP with **2**/Me₆TREN cocatalysts (0.1 mol %, table 4.3, entry 4) progressed to full conversion in 180 min. The development of highly selective catalysts for ROP

which remain highly active at low catalyst loadings is vitally important to the increased applicability of these systems.²³

Table 4.3. Low Catalyst Loadings in the TU/Alkylamine Catalyzed ROP of L-LA.^a



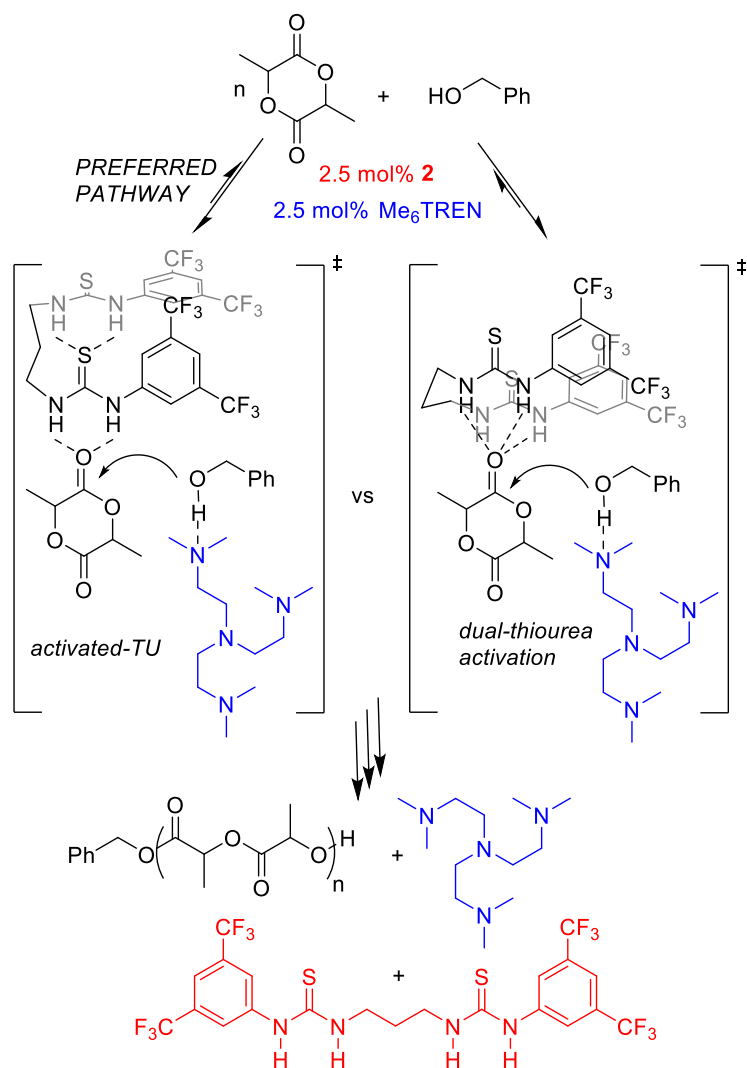
entry	TU	mol% cats. (each) ^a	conv. ^b (%)	time (min)	M _n ^c (g/mol)	M _w /M _n ^c
1	1	1	3	24 h ^d	--	--
2	2	0.5	98	45	17,000	1.05
3	2	0.25	93	80	20,000	1.02
4	2	0.10	98	180	17,900	1.03

^aReactions conducted in CH₂Cl₂ at 2 M (0.7 mmol) L-LA with the given mol % (to LA) of each catalyst. ^bConversion determined by ¹H NMR. ^cM_n and M_w/M_n determined by GPC in CH₂Cl₂ vs polystyrene standards. ^dReaction stopped at 24 h.

Tethered bis(thiourea)s, to our knowledge, have not been evaluated as ROP cocatalysts; however, such systems have been evaluated with mixed results as catalysts for small molecule transformations. Enhanced reaction rates have been observed when activation of two substrates is a possibility.¹⁷ However, rate acceleration with bis(thiourea)s is not general,^{7,18,19} although the introduction of chiral linkers facilitates increased enantioselectivity in some cases.^{6,19} The bis(thiourea) **2** does not feature a chiral linker and was not expected to alter the stereoselectivity of the ROP vis-a-vis monothiourea **1**. The polymers resulting from the **1**/Me₆TREN and **2**/Me₆TREN catalyzed ROP of rac-LA from benzyl alcohol (conditions from Table 2, entries 1 and 2) were analyzed by ¹³C NMR (see Experimental Section). The ¹H decoupled ¹³C NMR spectra suggested similar tacticities (P_m (**1**) = 0.69; P_m (**2**) = 0.66; where P_m is the probability of propagating with the retention of stereochemistry).^{16,24–26} This is

consistent with previous suggestions that organocatalytic H-bonding catalysts display chain-end controlled stereochemistry.¹⁶

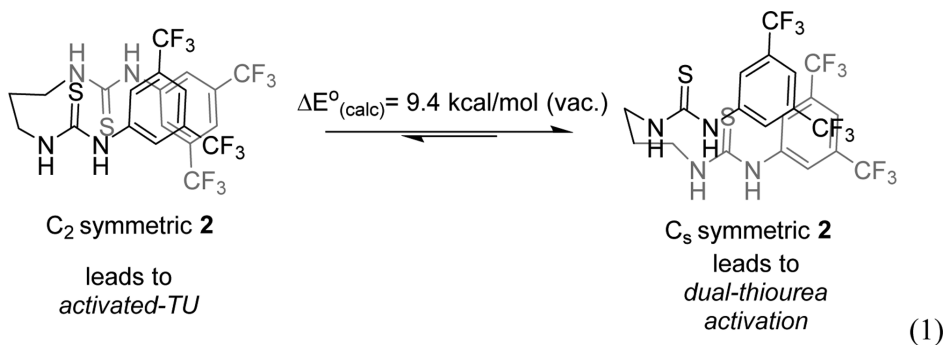
The source of the rate acceleration exhibited by bis(thiourea) **2** is proposed to be the activation at a single monomer ester by both thiourea moieties. While the possibility of **2** simultaneously binding base and monomer or simultaneous binding of monomer and polymer cannot be ruled out, the observed second order dependence upon [**1**] for some **1**/alkylamine catalyzed ROPs of L-LA strongly indicates that both thiourea moieties of **2** are involved in the activation of a single ester moiety in the transition state.²⁷ Presumably, the role of **2** is to enforce this favorable catalytic mode even in those **1**/alkylamine systems which do not display second order dependence upon [**1**], Scheme 2. This suggestion is consistent with computational studies of a bis(thiourea) catalyzed Morita-Baylis-Hillman reaction wherein a bisTU-nitrate complex is believed to react with an uncomplexed aldehyde rather than bind both reagents prior to reaction.^{28,29} With the exception of the short-strong variety, H-bonds are electrostatic in nature and do not require orbital overlap,³⁰ hence the mode of the **2**-lactide activation could be due to direct, dual-thiourea activation of a single ester moiety or an activated-TU mechanism³¹ (scheme 4.2). However, other unenvisioned processes are possible.



Scheme 4.2. Proposed Mechanism for the **2**/ Me_6TREN Catalyzed ROP of L-Lactide.

Computational studies were conducted to differentiate between these mechanistic possibilities. Energies from geometry optimized structures (B3LYP/6-31G**) in CH_2Cl_2 solvent and the gas phase suggest that the C_2 symmetric **2** structure leading to the activated-TU transition state is more stable than the C_s structure required for a dual-thiourea activation mechanism by 5.7 or 9.4 kcal/mol, respectively, eq. 1 (see Experimental Section). Further, computations suggest that LA activation via the

activated-TU structure (scheme 4.2, left) is lower in energy than the dual-thiourea activation structure (scheme 4.2, right), see Experimental Section. Future studies will be aimed at experimentally determining the source of this increased activity.



4.4. Conclusion

Achiral, bis(thiourea) H-bond donating molecules have been shown to be highly effective cocatalysts for the ROP of lactide. The rate accelerated **2**/alkylamine systems retain ROP control, exhibiting the characteristics of a “living” polymerization, a high selectivity for monomer and marked activity at low catalyst loadings. The reaction rate enhancement is postulated to occur via an activated-TU mechanism, but ongoing mechanistic studies are expected to provide further insight into the source of the potency of the bis(thiourea) systems. The addition of a second thiourea moiety to these H-bond donating systems introduces the possibility of a multitude of structural variations, each of which could have dramatic ramifications on the course of the ROP.

4.5. Experimental Section

4.5.1. General Considerations

All manipulations were performed in an MBRAUN stainless steel glovebox equipped with a gas purification system under a nitrogen atmosphere. All chemicals were purchased from Fisher Scientific and used as received unless stated otherwise. Dichloromethane, toluene and THF (HPLC grade) were dried on an Innovative Technology solvent purification system with activated alumina columns. Thiourea catalysts were prepared as previously described.^{7,15} L-lactide and rac-lactide from Acros Organics were recrystallized from dry toluene prior to use. Benzyl alcohol was distilled from CaH₂ under high vacuum. Dialysis bags (MWCO = 3,000) were purchased from SpectraPor and stored in aqueous NaN₃ solution. NMR experiments were performed on a Bruker Avance 300 MHz spectrometer except decoupled experiments which were performed on a Varian 500 MHz NMR spectrometer. Size exclusion chromatography (SEC) was performed at 30 °C in dichloromethane (DCM) at 1.0 mL/min using a Agilent Infinity GPC system equipped with three Agilent PLGel columns 7.5 mm Å~300 mm (5 µm; pore sizes = 103, 104, and 105 Å) and multiwavelength detector (set to 254 nm) and refractive index detector connected in series. Molecular weight and M_w/M_n were determined versus PS standards (500 g/mol to 3150 kg/mol; Polymer Laboratories). MALDI–TOF data was acquired at the University of Akron Mass Spectrometry Center.

4.5.2. Example ROP of L-Lactide

In a typical polymerization, L-LA (100 mg, 0.7 mmol) was added to a 20 mL glass vial containing a stir bar, both of which were baked at 140 °C overnight. In another dried 20 mL glass vial with stir bar, **2** (17.5 μmol), Me₆TREN (17.5 μmol) and benzyl alcohol (0.007 mmol) were added. Solvent (CH₂Cl₂, 1 M in L-LA) was added to both vials to bring the total volume of solvent to the desired level, approximately equal portions of solvent per vial. After stirring for 5 min, the L-LA solution was transferred via pipet to the vial containing catalysts and initiator. Aliquots were removed from the reaction with a micropipet at predetermined time points and quenched by the addition of benzoic acid (2 mol equivalents to base). The vial was removed from the glovebox, solvent removed under vacuum, conversion determined via ¹H NMR, and the polymer was precipitated from CH₂Cl₂ by treatment with hexanes. The hexanes supernatant was decanted, and the polymer removed of volatiles under reduced pressure. Yield: 80%. M_w/M_n = 1.03; M_n (GPC) = 17 500. Comparative reactions were run side-by-side at room temperature.

For Determination of Selectivity for Monomer. An aliquot of the reaction mixture was allowed to stir for 1 h past full conversion and the polymer was reanalyzed by GPC: M_w/M_n = 1.06; M_n (GPC) = 17,100.

For the Chain-Extension Experiment. The **2**/Me₆TREN (2.5 mol %) catalyzed ROP of LA (0.69 mmol, 1 equiv, 0.5 M in CH₂Cl₂) from benzyl alcohol (2 mol %) was stirred to full conversion (30 min) and an aliquot withdrawn. An additional 0.60 mmol of LA (to account for aliquot volume) was added to the reaction, and the process repeated at 60 min with a third addition of LA (0.49 mmol). Aliquot 1: M_n = 13700

g/mol, $M_w/M_n = 1.04$. Aliquot 2: $M_n = 29000$ g/mol, $M_w/M_n = 1.02$. Aliquot 3: $M_n = 43700$ g/mol, $M_w/M_n = 1.02$.

4.5.3. Determination of P_m

The standard polymerization procedure was repeated but with rac-LA (100 mg, 0.7 mmol). The polymerization solution was stirred for enough time to achieve 90% conversion (to minimize postpolymerization reactivity). The reaction was quenched by the addition of benzoic acid and conversion determined by ^1H NMR. The polymer was then dialyzed in methanol for 24 h to remove any trace of monomer impurity. The pure monomer was dissolved in chloroform-d and analyzed by ^1H -decoupled ^{13}C NMR at 70 °C. The procedure for determining P_m is thoroughly described elsewhere.^{16,24-26} Briefly, the experimental intensities of the five tetrads resulting from the ROP of rac-lactide were simulated using MNova software. The theoretical intensities of these resonances are determined from Markovian statistics from the P_m value. A calculated value of P_m was determined using Excel by systematically varying P_m subject to the minimization in the difference between the experimental and calculated tetrad intensities.

4.5.4. Computational Details

Computational experiments were performed in Spartan '14 (Windows 7). Structures were geometry optimized at the DFT B3LYP/6-31G** level of theory in the gas phase. Energies in CH_2Cl_2 solvent were calculated as Single Point energies from the DFT-optimized structures. Energies, computed structures, and coordinates of optimized structures are given in the Experimental Section.

Table 4.4. Tacticity analysis of poly(lactide)s.

		mmm	mmr	rmm	rmr	mrm	P _m	error
2/Me ₆ TREN	exper.	0.548	0.111	0.111	0.049	0.181	0.66	0.27
	calc.	0.547	0.112	0.112	0.058	0.170		
1/Me ₆ TREN	exper.	0.586	0.110	0.110	0.047	0.147	0.69	0.09
	calc.	0.586	0.106	0.106	0.047	0.147		

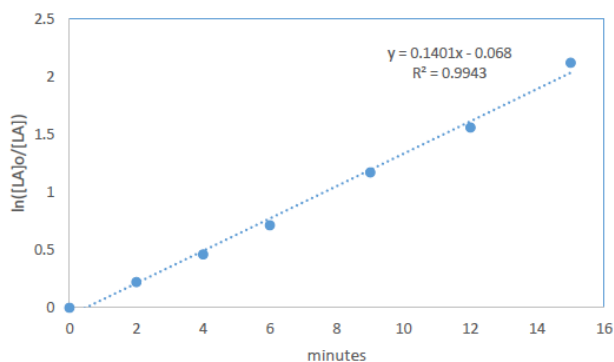


Figure 4.2. First order evolution of [LA] versus time for the reaction given in the example ROP experiment (see experimental).

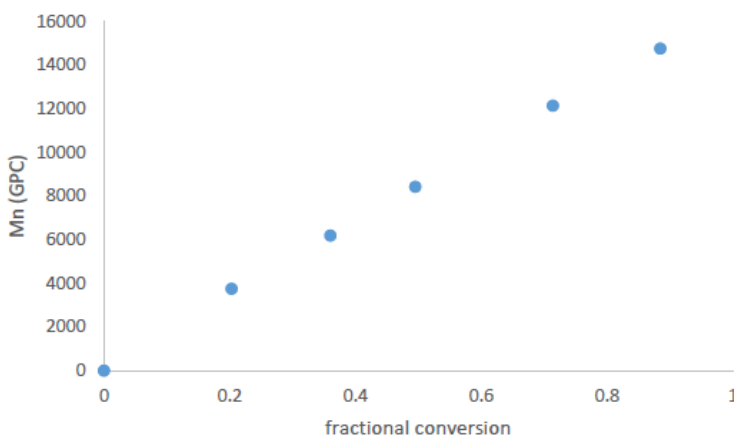


Figure 4.3. Molecular weight versus conversion plot for the ROP of L-LA from benzyl alcohol in DCM catalyzed by 2/HMTETA. Reaction conditions: 1M LA (100 mg, 0.70 mmol), 0.7 mg (7 mmol) benzyl alcohol, and 17.5 mmol each of 2 and HMTETA.

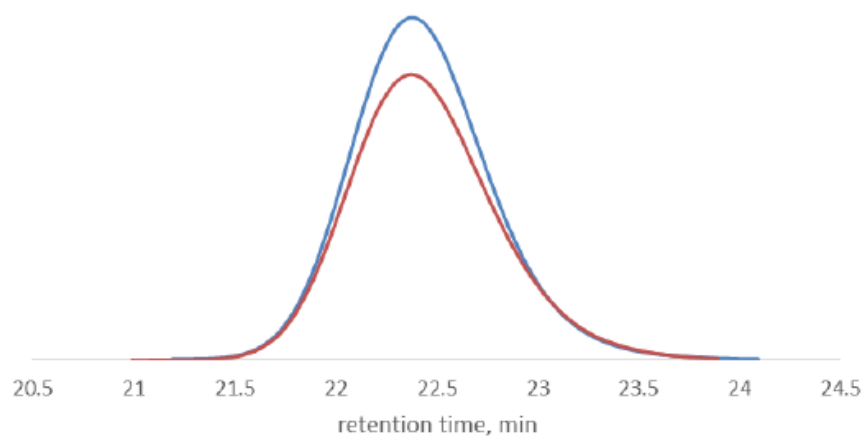


Figure 4.4. GPC traces of the ROP of LA from pyrenebutanol catalyzed by Me₆TREN/2 in CH₂Cl₂. The UV trace is shown in blue and the RI trace shown in red.

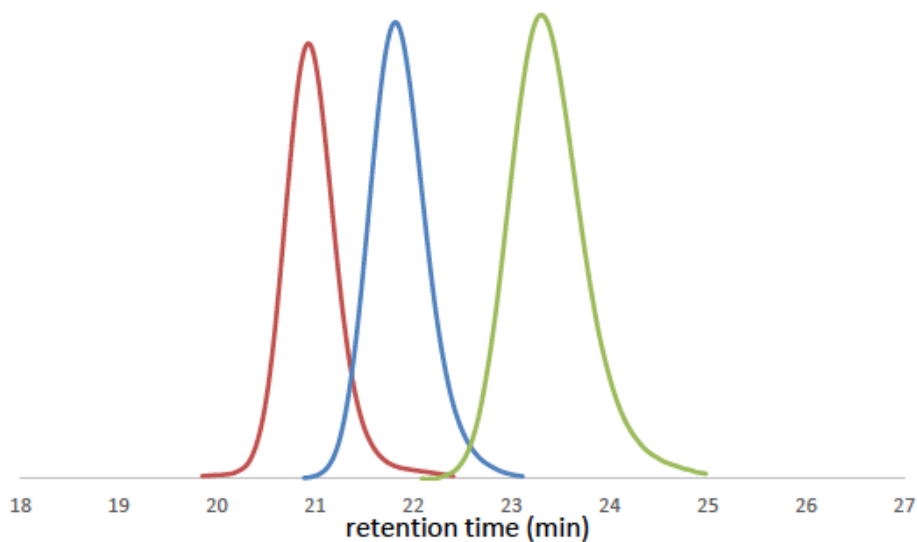


Figure 4.5. GPC traces showing chain-extension of PLA by sequential addition of LA to a single reaction mixture. Green: $M_n = 13,700$ g/mol, $M_w/M_n = 1.04$; blue: $M_n = 29,000$ g/mol, $M_w/M_n = 1.02$; red: $M_n = 43,700$ g/mol, $M_w/M_n = 1.02$.

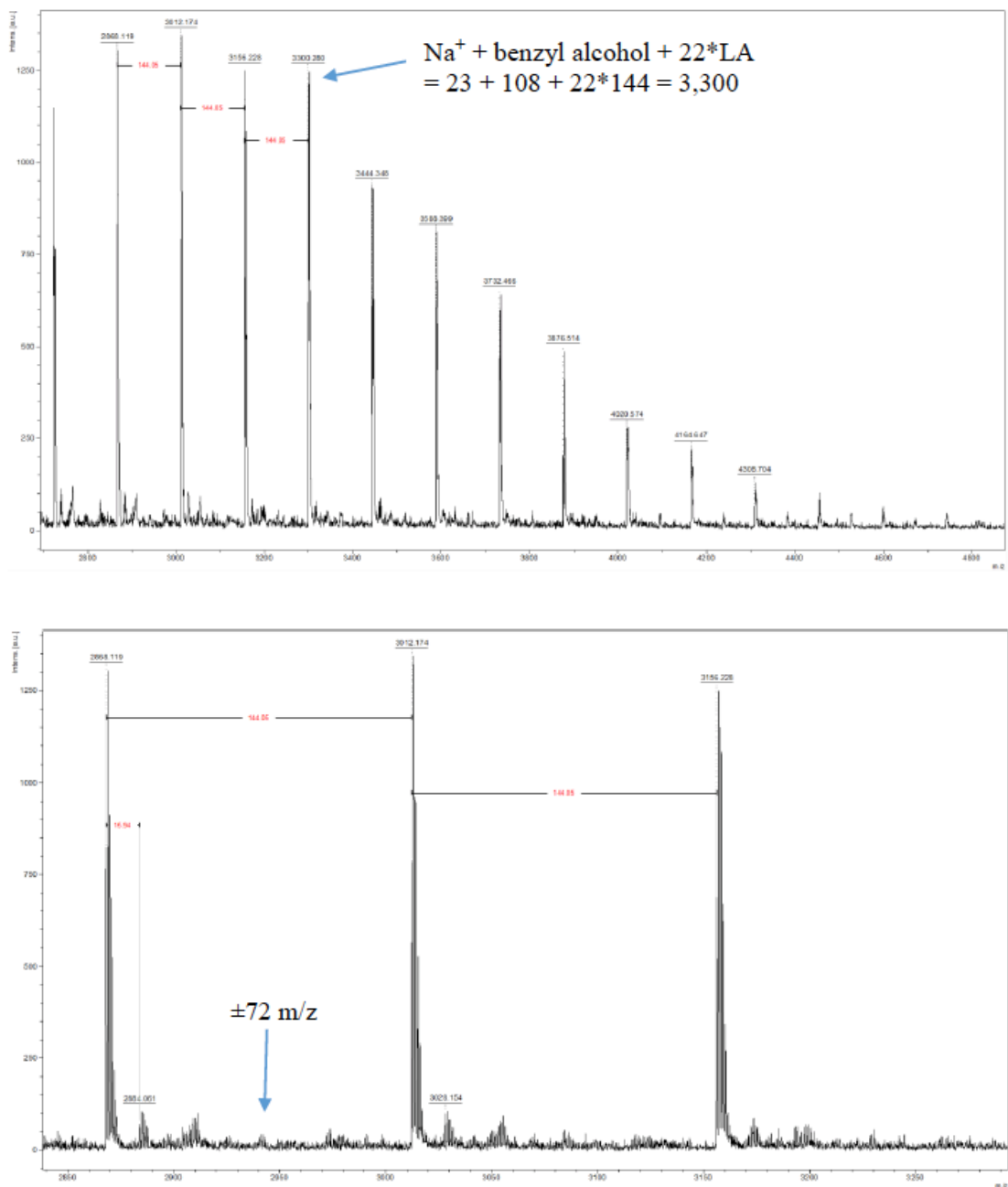


Figure 4.6. MALDI-TOF of PLA polymerized from benzyl alcohol (BA) by 2/Me₆TREN. The dominate repeat units are due to BA+Na++LAn. (lower) Expansion of upper MALDI-TOF shows the vanishingly small peak due to 72 m/z repeat units caused by random chain scission post polymerization.

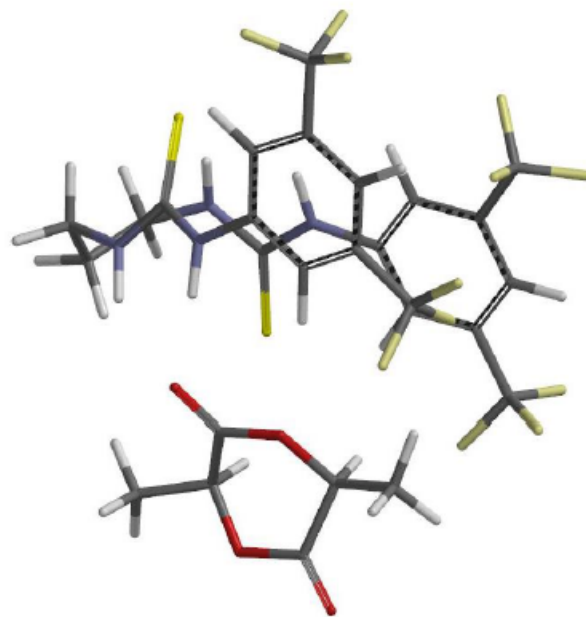


Figure 4.7. Activated-TU 2 + LA, energy: -3557.804353 hartrees, coordinates below:

Cartesian Coordinates (Angstroms)

Atom	X	Y	Z
1 C C1	-0.9064691	0.6846702	3.3422887
2 S S1	0.4192201	0.0301055	4.1949981
3 N N1	-1.3272381	1.9613370	3.4919925
4 H H4	-2.0471126	2.2850412	2.8508883
5 N N2	-1.6351373	-0.0028529	2.4068516
6 H H3	-2.2636191	0.5697678	1.8414300
7 C C2	-1.4780186	-1.3181307	1.9206151
8 C C4	-1.3038299	-3.8951451	0.8080621
9 C C3	-1.7748179	-1.5316252	0.5691335
10 C C6	-1.1197484	-2.4069990	2.7256285
11 C C5	-1.0269254	-3.6773567	2.1578210
12 C C7	-1.6870244	-2.8108177	0.0227054
13 H H6	-2.0717837	-0.6953297	-0.0568783
14 H H7	-0.9188341	-2.2652772	3.7778617
15 H H10	-1.2220315	-4.8860978	0.3809107
16 C C10	-0.8457889	2.9595460	4.4431934
17 H H11	-0.1755043	2.4553571	5.1422695
18 H H14	-1.7150846	3.3104923	5.0127339
19 C C12	1.3173693	3.9812031	3.4086266
20 H H15	1.9135280	3.9356177	4.3266389
21 H H18	1.6651523	4.8326381	2.8196401
22 N N3	1.6183205	2.7623162	2.6706815
23 H H20	1.6661459	1.9199290	3.2474230
24 C C13	1.4780444	2.5924212	1.3342440
25 N N4	1.6623718	1.2748073	0.9710184
26 H H22	1.7528072	0.6379554	1.7600355
27 C C14	1.7160574	0.6088321	-0.2633706
28 C C15	1.8287702	-0.9475978	-2.6155482
29 C C16	1.5229688	1.2067387	-1.5172077
30 C C17	1.9853931	-0.7697328	-0.2054152
31 C C18	2.0471149	-1.5308062	-1.3686901
32 C C19	1.5681644	0.4203871	-2.6682415
33 H H21	1.3404154	2.2686838	-1.5827162
34 H H23	2.1520584	-1.2483267	0.7554837
35 H H26	1.8630883	-1.5452289	-3.5184394
36 S S2	1.1168314	3.8768980	0.2908220
37 C C9	-0.1679943	4.1665045	3.7636679
38 H H5	-0.7248628	4.4323456	2.8578305
39 H H66	-0.2380748	5.0277572	4.4404427
40 C C8	-0.5671232	-4.8240902	3.0216398
41 C C11	-1.9744697	-2.9752598	-1.4453065
42 C C20	2.3046859	-3.0125800	-1.2677503
43 C C21	1.3565925	1.0658446	-4.0129449
44 F F1	3.1164132	-3.3055093	-0.2300955
45 F F2	2.8768813	-3.4975814	-2.3882139
46 F F3	1.1589809	-3.7102889	-1.0786183
47 F F4	0.7566504	2.2789674	-3.9048034
48 F F5	0.5664127	0.3035958	-4.8039630
49 F F6	2.5136272	1.2560414	-4.6756229
50 F F7	0.7814041	-4.8666486	3.1050135
51 F F8	-0.9738333	-6.0151593	2.5325270
52 F F9	-1.0368931	-4.7197210	4.2836780

53 F F10	-1.9493708	-4.2598572	-1.8394920
54 F F11	-3.1866648	-2.4689161	-1.7720297
55 F F12	-1.0679095	-2.3013080	-2.2037286
56 C C22	-3.1907221	3.1229399	-2.9513261
57 O O1	-3.6966169	3.2451065	-4.0352113
58 O O2	-3.3561429	4.0680901	-1.9919003
59 C C23	-2.3277516	1.9295066	-2.5390790
60 H H1	-1.2751458	2.2357811	-2.5617918
61 O O3	-2.6404405	1.5535075	-1.1555368
62 C C24	-2.5971988	3.9423515	-0.7662014
63 H H2	-1.5317549	4.1098812	-0.9816187
64 C C25	-2.7206399	2.5194683	-0.2377145
65 O O4	-2.8851868	2.2349830	0.9364524
66 C C26	-2.5428099	0.7106989	-3.4119400
67 H H8	-3.5943131	0.4128686	-3.4100730
68 H H9	-1.9313489	-0.1220950	-3.0597691
69 H H12	-2.2508463	0.9531915	-4.4358677
70 C C27	-3.1072836	4.9937494	0.2004829
71 H H13	-3.0175891	5.9808068	-0.2596645
72 H H16	-2.5088662	4.9755004	1.1140498
73 H H17	-4.1546034	4.8117343	0.4557507

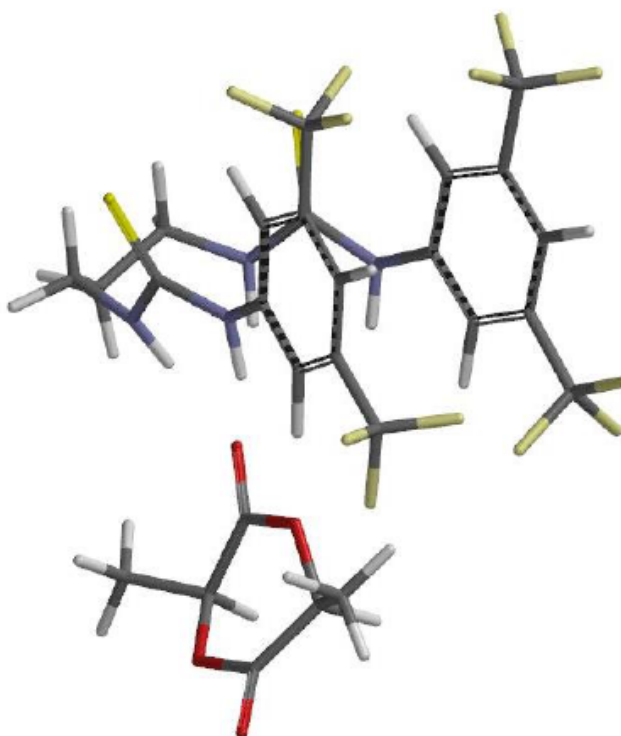


Figure 4.8. Dual monomer activated **2** + LA, energy: -3557.7617345 hartrees, coordinates below:

Cartesian Coordinates (Angstroms)

Atom	X	Y	Z
1 C C1	-0.9381617	1.6178948	2.3132458
2 S S1	0.0181904	2.3119203	3.4654796
3 N N1	-2.2047113	2.1172305	1.9756591
4 H H4	-2.6973114	1.7347856	1.1787906
5 N N2	-0.6171000	0.4728896	1.5338553
6 H H3	-1.3859136	0.0101139	1.0895209
7 C C2	0.4711157	-0.4352163	1.7880448
8 C C4	2.5891011	-2.2516107	2.0312077
9 C C3	0.2697995	-1.7927238	1.4955578
10 C C6	1.7303413	0.0107879	2.2105624
11 C C5	2.7760260	-0.9030296	2.3163689
12 C C7	1.3284296	-2.6843509	1.6239882
13 H H6	-0.7129724	-2.1576403	1.1569514
14 H H7	1.8823114	1.0743305	2.4880919
15 H H10	3.4111921	-2.9745450	2.1197481
16 C C10	-2.6079963	3.4867962	2.3737624
17 H H11	-1.7109327	4.0446847	2.7402103
18 H H14	-3.2767143	3.3709617	3.2520747
19 C C12	-2.4167944	4.8713512	0.2213362
20 H H15	-1.4689189	5.2539414	0.6736655
21 H H18	-2.9149436	5.7458778	-0.2455846
22 N N3	-2.0906994	3.9483684	-0.8895497
23 H H20	-2.7941696	3.2597887	-1.0711390
24 C C13	-0.7616067	3.6369181	-1.2258247
25 N N4	-0.7118606	2.5551941	-2.1480383
26 H H22	-1.5847621	2.0907713	-2.3080876
27 C C14	0.3954439	1.6511230	-2.3162639
28 C C15	2.4556488	-0.2002736	-2.7544159
29 C C16	1.7280270	2.0174202	-2.0770564
30 C C17	0.1006788	0.3629956	-2.7848997
31 C C18	1.1310745	-0.5486353	-2.9951413
32 C C19	2.7372341	1.0865101	-2.2973961
33 H H21	1.9485402	3.0416109	-1.6875693
34 H H23	-0.9324359	0.0488072	-2.9901480
35 H H26	3.2678697	-0.9214963	-2.9183110
36 S S2	0.5197729	4.5540530	-0.7396673
37 C C9	-3.3334483	4.2536679	1.2740214
38 H H5	-4.1289890	3.6310548	0.8077036
39 H H66	-3.8772754	5.0867177	1.7655557
40 C C8	4.1482703	-0.3680791	2.7388210
41 C C11	1.1496693	-4.1711494	1.3136771
42 C C20	0.7492633	-1.9457941	-3.4840359
43 C C21	4.1952013	1.4572425	-2.0000697
44 F F1	-0.0908940	-2.5944447	-2.6397594
45 F F2	1.7743228	-2.8045748	-3.6653444
46 F F3	0.0904226	-1.9446559	-4.6664137
47 F F4	5.0863387	0.9207571	-2.8661439
48 F F5	4.6099635	1.0371185	-0.7828125
49 F F6	4.4655076	2.7798604	-2.0213904
50 F F7	4.1486060	0.2294283	3.9512367
51 F F8	4.6393056	0.5652426	1.8920507
52 F F9	5.1270912	-1.2976082	2.8214429
53 F F10	1.9297381	-4.6072589	0.2981512
54 F F11	1.4548560	-4.9830003	2.3511076
55 F F12	-0.1021464	-4.5414780	0.9558210
56 O O1	-3.5412788	0.8941049	-0.2500775

57 C	C22	-4.1898246	-0.1321099	-0.3523945
58 O	O2	-3.3390653	-1.1766652	-0.4947430
59 C	C23	-5.7017149	-0.3116108	-0.3413540
60 H	H1	-6.0636901	-0.2356963	-1.3963786
61 C	C24	-6.3892342	0.7240380	0.5384444
62 H	H8	-6.1197208	1.7411477	0.2226850
63 H	H12	-6.1128529	0.6172752	1.5963690
64 H	H13	-7.4816969	0.6297443	0.4744770
65 C	C25	-3.9012182	-2.4710286	-0.7675379
66 H	H2	-4.0268417	-2.5372746	-1.8758724
67 C	C26	-2.8851507	-3.4929502	-0.2821856
68 H	H17	-1.9113594	-3.3570788	-0.7766023
69 H	H19	-3.2309640	-4.5114743	-0.5043951
70 H	H24	-2.7117857	-3.4310654	0.8016436
71 O	O3	-6.0866423	-1.5958812	0.1526129
72 C	C27	-5.2665254	-2.6589549	-0.1152990
73 O	O4	-5.8058109	-3.6786260	0.2381610

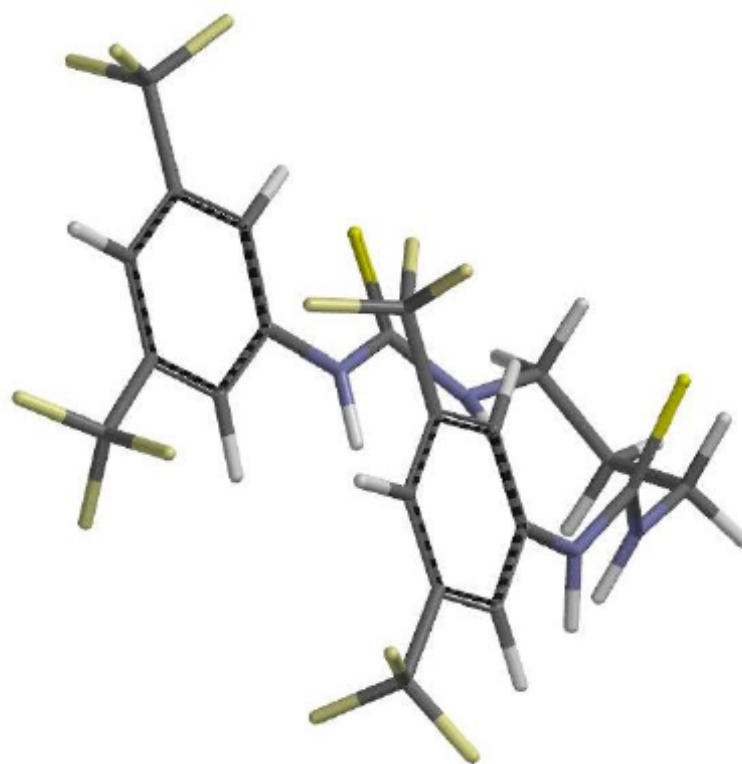


Figure 4.9. Dual monomer activated **2** vacuum, energy: -3023.4279491 hartrees, coordinates below:

Cartesian Coordinates (Angstroms)

Atom	X	Y	Z
1 C C2	0.0482247	-3.3159490	1.0079086
2 S S1	-1.0701303	-4.5440223	0.8333826
3 N N1	1.3974924	-3.5347540	1.0922058
4 H H5	1.9855157	-2.7492843	0.8474222
5 N N2	-0.2348436	-1.9659738	1.1373462
6 H H6	0.5292158	-1.4103960	1.5035376
7 C C3	-1.4013051	-1.2125301	0.9213351
8 C C4	-3.5819635	0.5162106	0.4771447
9 C C5	-1.4004085	0.0943057	1.4322607
10 C C6	-2.5085043	-1.6530507	0.1835169
11 C C7	-3.5818396	-0.7862834	-0.0209755
12 C C8	-2.4765410	0.9482908	1.2071913
13 H H7	-0.5511599	0.4512042	2.0084192
14 H H8	-2.5288002	-2.6548134	-0.2211614
15 H H10	-4.4216792	1.1759687	0.2988841
16 C C10	2.0227240	-4.8299883	0.8312859
17 H H11	1.8504005	-5.1315517	-0.2113714
18 H H14	1.5325881	-5.5763950	1.4618289
19 C C12	4.4005441	-3.9193107	0.2219398
20 H H15	4.1935712	-4.1277373	-0.8292658
21 H H18	5.4592842	-4.1380766	0.4070699
22 N N3	4.1811392	-2.4848580	0.4182178
23 H H20	4.3611801	-2.1377814	1.3538365
24 C C13	3.6721550	-1.6053917	-0.5003257
25 N N4	3.5387736	-0.3347888	0.0432189
26 H H22	4.1547735	-0.1166089	0.8182600
27 C C14	2.7222387	0.7474459	-0.3487589
28 C C15	1.0587330	2.9608572	-0.8474369
29 C C16	1.5544008	0.5944904	-1.1098179
30 C C17	3.0548952	2.0139071	0.1470742
31 C C18	2.2234012	3.1062894	-0.0973364
32 C C19	0.7419719	1.6989339	-1.3519895
33 H H21	1.2802328	-0.3717107	-1.5062365
34 H H23	3.9639207	2.1522713	0.7259605
35 H H26	0.4083156	3.8084506	-1.0255582
36 S S2	3.2415152	-2.0330190	-2.0565829
37 C C9	3.5265072	-4.7954937	1.1409901
38 H H9	3.6788461	-4.5046430	2.1900702
39 H H66	3.9009642	-5.8225072	1.0507811
40 C C11	-4.7965180	-1.2951299	-0.7559767
41 C C20	-2.4001653	2.3637435	1.7170616
42 C C21	2.5575907	4.4416785	0.5172903
43 C C22	-0.4915357	1.5359001	-2.2073931
44 F F1	2.0957466	5.4644047	-0.2286036
45 F F2	3.8930191	4.6041922	0.6571479
46 F F3	2.0155105	4.5668772	1.7496735
47 F F4	-1.5298980	2.2447651	-1.7155797
48 F F5	-0.8798288	0.2472384	-2.2910007
49 F F6	-0.2739560	1.9758045	-3.4654823
50 F F7	-4.4691733	-2.1935177	-1.7074328
51 F F8	-5.4736121	-0.2917524	-1.3568222
52 F F9	-5.6595917	-1.9042152	0.0878737
53 F F10	-1.6736819	3.1573179	0.8923795
54 F F11	-3.6186281	2.9267640	1.8341938
55 F F12	-1.8020053	2.4216034	2.9294171

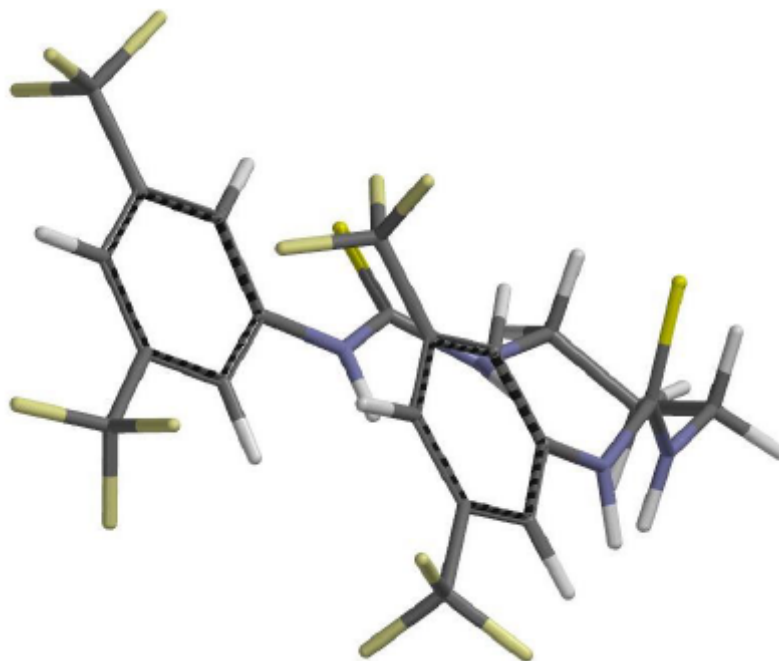


Figure 4.10. Dual monomer activated 2 methylene chloride solvent, energy: -3023.4693565

hartrees, coordinates below:

Atom	X	Y	Z
1 C C2	0.0482247	-3.3159490	1.0079086
2 S S1	-1.0701303	-4.5440223	0.8333826
3 N N1	1.3974924	-3.5347540	1.0922058
4 H H5	1.9855157	-2.7492843	0.8474222
5 N N2	-0.2348436	-1.9659738	1.1373462
6 H H6	0.5292158	-1.4103960	1.5035376
7 C C3	-1.4013051	-1.2125301	0.9213351
8 C C4	-3.5819635	0.5162106	0.4771447
9 C C5	-1.4004085	0.0943057	1.4322607
10 C C6	-2.5085043	-1.6530507	0.1835169
11 C C7	-3.5818396	-0.7862834	-0.0209755
12 C C8	-2.4765410	0.9482908	1.2071913
13 H H7	-0.5511599	0.4512042	2.0084192
14 H H8	-2.5288002	-2.6548134	-0.2211614
15 H H10	-4.4216792	1.1759687	0.2988841
16 C C10	2.0227240	-4.8299883	0.8312859
17 H H11	1.8504005	-5.1315517	-0.2113714
18 H H14	1.5325881	-5.5763950	1.4618289
19 C C12	4.4005441	-3.9193107	0.2219398
20 H H15	4.1935712	-4.1277373	-0.8292658
21 H H18	5.4592842	-4.1380766	0.4070699
22 N N3	4.1811392	-2.4848580	0.4182178
23 H H20	4.3611801	-2.1377814	1.3538365
24 C C13	3.6721550	-1.6053917	-0.5003257
25 N N4	3.5387736	-0.3347888	0.0432189
26 H H22	4.1547735	-0.1166089	0.8182600
27 C C14	2.7222387	0.7474459	-0.3487589

28 C	C15	1.0587330	2.9608572	-0.8474369
29 C	C16	1.5544008	0.5944904	-1.1098179
30 C	C17	3.0548952	2.0139071	0.1470742
31 C	C18	2.2234012	3.1062894	-0.0973364
32 C	C19	0.7419719	1.6989339	-1.3519895
33 H	H21	1.2802328	-0.3717107	-1.5062365
34 H	H23	3.9639207	2.1522713	0.7259605
35 H	H26	0.4083156	3.8084506	-1.0255582
36 S	S2	3.2415152	-2.0330190	-2.0565829
37 C	C9	3.5265072	-4.7954937	1.1409901
38 H	H9	3.6788461	-4.5046430	2.1900702
39 H	H66	3.9009642	-5.8225072	1.0507811
40 C	C11	-4.7965180	-1.2951299	-0.7559767
41 C	C20	-2.4001653	2.3637435	1.7170616
42 C	C21	2.5575907	4.4416785	0.5172903
43 C	C22	-0.4915357	1.5359001	-2.2073931
44 F	F1	2.0957466	5.4644047	-0.2286036
45 F	F2	3.8930191	4.6041922	0.6571479
46 F	F3	2.0155105	4.5668772	1.7496735
47 F	F4	-1.5298980	2.2447651	-1.7155797
48 F	F5	-0.8798288	0.2472384	-2.2910007
49 F	F6	-0.2739560	1.9758045	-3.4654823
50 F	F7	-4.4691733	-2.1935177	-1.7074328
51 F	F8	-5.4736121	-0.2917524	-1.3568222
52 F	F9	-5.6595917	-1.9042152	0.0878737
53 F	F10	-1.6736819	3.1573179	0.8923795
54 F	F11	-3.6186281	2.9267640	1.8341938
55 F	F12	-1.8020053	2.4216034	2.9294171

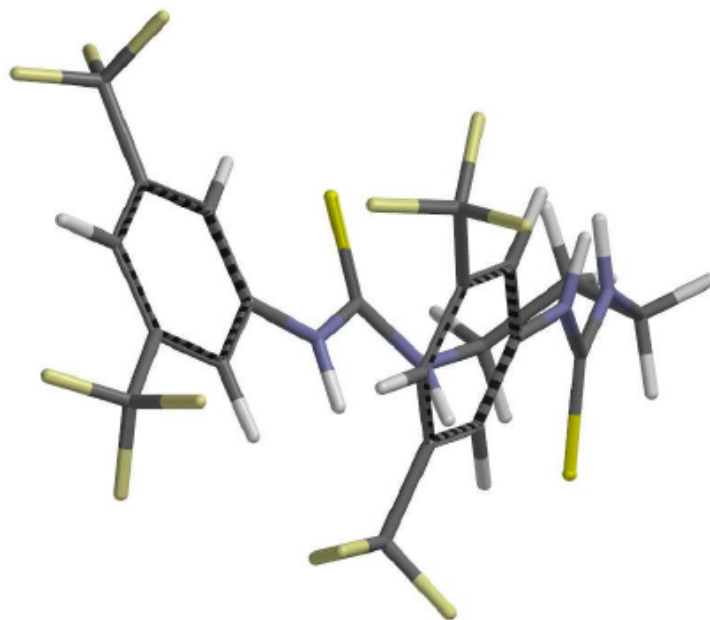


Figure 4.11. Activated-TU 2 vacuum, energy: -3023.442880 hartrees, coordinates below:

Atom	X	Y	Z
1 C C1	-1.4039848	3.3557331	0.2319456
2 S S1	-1.5471836	3.4262345	1.9187244
3 N N1	-0.8161008	4.3380521	-0.4956312
4 H H4	-0.5977440	4.1360828	-1.4637171
5 N N2	-1.8642420	2.3296774	-0.5584579
6 H H3	-1.8408791	2.5202114	-1.5525524
7 C C2	-2.2854073	1.0122725	-0.2823326
8 C C4	-3.0533943	-1.6821046	0.0174598
9 C C3	-2.6155382	0.2296610	-1.4023052
10 C C6	-2.3677079	0.4420919	0.9907854
11 C C5	-2.7363989	-0.8989211	1.1201915
12 C C7	-2.9991129	-1.0959417	-1.2494392
13 H H6	-2.5581002	0.6519390	-2.4009399
14 H H7	-2.1529321	1.0382627	1.8653522
15 H H10	-3.3236972	-2.7230712	0.1379471
16 C C10	-0.3292703	5.6316029	-0.0128533
17 H H11	-0.6965855	5.7535902	1.0076950
18 H H14	-0.7983192	6.4062662	-0.6307592
19 C C12	1.9995733	5.1039306	1.0379985
20 H H15	1.7693091	5.5881872	1.9927928
21 H H18	3.0662098	5.2285377	0.8391172
22 N N3	1.7376473	3.6837580	1.2263125
23 H H20	0.9132907	3.4751332	1.7888216
24 C C13	2.2647876	2.6913582	0.4614445
25 N N4	1.7788739	1.4525915	0.8333446
26 H H22	1.1678204	1.4707861	1.6410616
27 C C14	1.9830464	0.1497809	0.3442095
28 C C15	2.2419214	-2.5366837	-0.4763003
29 C C16	2.7588316	-0.1754640	-0.7774055
30 C C17	1.3419551	-0.8836104	1.0494577
31 C C18	1.4751754	-2.2077170	0.6406604
32 C C19	2.8737368	-1.5083250	-1.1711056
33 H H21	3.2760424	0.6053116	-1.3157302
34 H H23	0.7357836	-0.6568717	1.9215287
35 H H26	2.3546240	-3.5677754	-0.7840965
36 S S2	3.3813283	2.9941132	-0.7637320
37 C C9	1.1999702	5.7770240	-0.0908704
38 H H5	1.5625568	5.4071654	-1.0561918
39 H H66	1.4348566	6.8483122	-0.0611207
40 C C8	-2.7550829	-1.4778977	2.5121218
41 C C11	-3.4053505	-1.9052003	-2.4543052
42 C C20	0.7470089	-3.2883071	1.3982983
43 C C21	3.6624723	-1.8224552	-2.4173174
44 F F1	-0.5654309	-3.3375091	1.0541947
45 F F2	0.7945182	-3.0864114	2.7307650
46 F F3	1.2615303	-4.5100584	1.1498005
47 F F4	4.1179869	-3.0939344	-2.4163412
48 F F5	4.7269871	-1.0065215	-2.5579416
49 F F6	2.9031296	-1.6738796	-3.5281796
50 F F7	-3.1643164	-2.7583451	2.5297886
51 F F8	-3.5695423	-0.7712000	3.3250668
52 F F9	-1.5201748	-1.4341862	3.0733770
53 F F10	-2.9323791	-3.1657199	-2.3877436
54 F F11	-4.7505696	-1.9918709	-2.5524765
55 F F12	-2.9556891	-1.3575034	-3.6050227

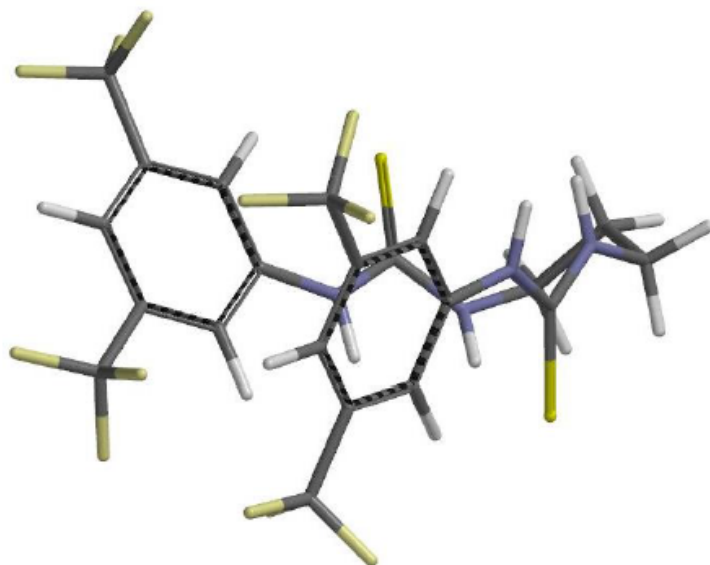


Figure 4.12. Activated-TU **2** methylene chloride solvent, energy: -3023.4784099 hartrees, coordinates below:

Atom	X	Y	Z
1 C C1	2.4754083	2.5516519	-0.6381515
2 S S1	2.5125799	3.2336940	0.9123764
3 N N1	3.5992317	2.2016292	-1.3122670
4 H H4	3.4886693	1.6289945	-2.1402327
5 N N2	1.3354885	2.2967161	-1.3626896
6 H H3	1.4984277	2.0388257	-2.3280996
7 C C2	-0.0311136	2.2288265	-1.0206796
8 C C4	-2.7920892	1.9259703	-0.5467173
9 C C3	-0.9020267	1.8536415	-2.0582500
10 C C6	-0.5576662	2.4759643	0.2499008
11 C C5	-1.9265233	2.3073034	0.4707602
12 C C7	-2.2627000	1.7112822	-1.8215595
13 H H6	-0.5146433	1.6561063	-3.0531386
14 H H7	0.0907570	2.8002104	1.0504178
15 H H10	-3.8475882	1.7876193	-0.3518489
16 C C10	4.9868596	2.4421324	-0.9122681
17 H H11	4.9632701	3.1284559	-0.0639025
18 H H14	5.4800112	2.9578334	-1.7445972
19 C C12	5.5084603	0.5533798	0.8101684
20 H H15	5.8698011	1.2432300	1.5800372
21 H H18	6.0661144	-0.3814767	0.8988206
22 N N3	4.1138691	0.2798695	1.1283905
23 H H20	3.5891066	1.0867627	1.4646233
24 C C13	3.4202317	-0.8066836	0.6970818
25 N N4	2.0996278	-0.7575645	1.1002660
26 H H22	1.8751690	0.0314931	1.6945141
27 C C14	0.9940748	-1.6005888	0.8873857
28 C C15	-1.3500917	-3.1397229	0.5819426

29 C C16	1.0030764	-2.7515378	0.0868342
30 C C17	-0.1988929	-1.2317329	1.5331756
31 C C18	-1.3520082	-1.9965808	1.3800295
32 C C19	-0.1653828	-3.4992623	-0.0557590
33 H H21	1.9181199	-3.0603119	-0.3971751
34 H H23	-0.2308619	-0.3445638	2.1586924
35 H H26	-2.2440531	-3.7397431	0.4751741
36 S S2	4.1401135	-2.0373609	-0.2010190
37 C C9	5.7603371	1.1538986	-0.5836394
38 H H5	5.5582006	0.3914673	-1.3438694
39 H H66	6.8314239	1.3820357	-0.6502878
40 C C8	-2.4319446	2.5334019	1.8730662
41 C C11	-3.1914733	1.3646439	-2.9568362
42 C C20	-2.6233682	-1.5546090	2.0584257
43 C C21	-0.1433240	-4.6962163	-0.9726233
44 F F1	-3.2267644	-0.5485548	1.3749824
45 F F2	-2.3938382	-1.0970329	3.3059941
46 F F3	-3.5201080	-2.5581058	2.1479342
47 F F4	-1.1050383	-5.5898421	-0.6553023
48 F F5	1.0416633	-5.3388015	-0.9325677
49 F F6	-0.3499242	-4.3312651	-2.2597978
50 F F7	-3.7651311	2.3884511	1.9675809
51 F F8	-2.1173328	3.7708044	2.3129527
52 F F9	-1.8618289	1.6604652	2.7418964
53 F F10	-4.1346048	0.4808838	-2.5740655
54 F F11	-3.8377645	2.4616256	-3.4103809
55 F F12	-2.5283947	0.8298391	-4.0059448

4.6. References

- (1) Lippert, K. M.; Hof, K.; Gerbig, D.; Ley, D.; Hausmann, H.; Guenther, S.; Schreiner, P. R. *Eur. J. Org. Chem.* 2012, 2012, 5919–5927.
- (2) Thomas, C.; Bibal, B. *Green Chem.* 2014, 16, 1687.
- (3) Kieseewetter, M. K.; Shin, E. J.; Hedrick, J. L.; Waymouth, R. M. *Macromolecules* 2010, 43, 2093–2107.
- (4) Kamber, N. E.; Jeong, W.; Waymouth, R. M.; Pratt, R. C.; Lohmeijer, B. G. G.; Hedrick, J. L. *Chem. Rev.* 2007, 107, 5813–5840.
- (5) Dove, A. P. *ACS Macro Lett.* 2012, 1, 1409–1412.
- (6) Doyle, A. G.; Jacobsen, E. N. *Chem. Rev.* 2007, 107, 5713–43.
- (7) Bertucci, M. A.; Lee, S. J.; Gagne, M. R. *Chem. Commun.* 2013, 49, 2055–2057.
- (8) Nakayama, Y.; Gotanda, T.; Ito, K. *Tetrahedron Lett.* 2011, 52, 6234–6237.
- (9) Klauber, E. G.; De, C. K.; Shah, T. K.; Seidel, D. *J. Am. Chem. Soc.* 2010, 132, 13624–13626.
- (10) Berkessel, A.; Roland, K.; Neudörfl, J. M. *Org. Lett.* 2006, 8, 4195–4198.
- (11) Li, B. J.; Jiang, L.; Liu, M.; Chen, Y. C.; Ding, L. S.; Wu, Y. *Synlett.* 2005, 603–606.
- (12) Knowles, R. R.; Lin, S.; Jacobsen, E. N. *J. Am. Chem. Soc.* 2010, 132, 5030–5032.
- (13) Becker, J. M.; Tempelaar, S.; Stanford, M. J.; Pounder, R. J.; Covington, J. A.; Dove, A. P. *Chem. Eur. J.* 2010, 16, 6099–6105.
- (14) Koeller, S.; Kadota, J.; Peruch, F.; Deffieux, A.; Pinaud, N.; Pianet, I.; Massip, S.; Léger, J.-M.; Desvergne, J.-P.; Bibal, B. *Chem. - Eur. J.* 2010, 16, 4196–4205.

- (15) Lohmeijer, B. G. G.; Pratt, R. C.; Leibfarth, F.; Logan, J. W.; Long, D. A.; Dove, A. P.; Nederberg, F.; Choi, J.; Wade, C.; Waymouth, R. M.; Hedrick, J. L. *Macromolecules* 2006, 39, 8574–8583.
- (16) Pratt, R. C.; Lohmeijer, B. G. G.; Long, D. A.; Lundberg, P. N. P.; Dove, A. P.; Li, H.; Wade, C. G.; Waymouth, R. M.; Hedrick, J. L. *Macromolecules* 2006, 39, 7863–7871.
- (17) Sohtome, Y.; Tanatani, A.; Hashimoto, Y.; Nagasawa, K. *Tetrahedron Lett.* 2004, 45, 5589–5592.
- (18) Li, X.; Luo, S.; Cheng, J. P. *Eur. J. Org. Chem.* 2008, 2008, 4350–4356.
- (19) Shi, Y.; Lin, A.; Mao, H.; Mao, Z.; Li, W.; Hu, H.; Zhu, C.; Cheng, Y. *Chem. Eur. J.* 2013, 19, 1914–1918.
- (20) Kazakov, O. I.; Datta, P. P.; Isajani, M.; Kiesewetter, E. T.; Kiesewetter, M. K. *Macromolecules* 2014, 47, 7463–7468.
- (21) Kazakov, O. I. Kiesewetter, M. K. *Macromolecules*, **2015**, 48 (17), 6121–6126.
- (22) Coady, D. J.; Engler, A. C.; Horn, H. W.; Bajjuri, K. M.; Fukushima, K.; Jones, G. O.; Nelson, A.; Rice, J. E.; Hedrick, J. L. *ACS Macro Lett.* 2012, 1, 19–22.
- (23) Helou, M.; Miserque, O.; Brusson, J. M.; Carpentier, J. F.; Guillaume, S. M. *Chem. Eur. J.* 2010, 16, 13805–13813.
- (24) Chamberlain, B. M.; Cheng, M.; Moore, D. R.; Ovitt, T. M.; Lobkovsky, E. B.; Coates, G. W.; V, C. U.; York, N.; Recci, V. *J. Am. Chem. Soc.* 2001, 123, 3229–3238.
- (25) Thakur, K. M.; Kean, R. T.; Hall, E. S.; Kolstad, J. J.; Lindgren, T. A.; Doscotch, M. A.; Siepmann, J. I.; Munson, E. J. *Macromolecules* 1997, 30, 2422–2428.
- (26) Ovitt, T. M.; Coates, G. W. *J. Am. Chem. Soc.* 2002, 124, 1316–1326.

(27) The simultaneous activation of both ester moieties of lactide by **2** is a geometric possibility, but such dual-ester activation would not be expected to display the observed rate dependence in [**1**].

(28) Breugst, M.; Houk, K. N. *J. Org. Chem.* 2014, 79, 6302–6309.

(29) Sohtome, Y.; Nagasawa, K. *Synlett* 2010, 2010, 1–22.

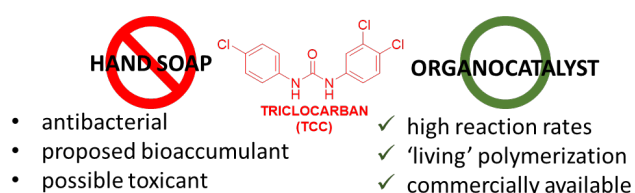
(30) Anslyn, E.; Dougherty, D. A. *Modern Physical Organic Chemistry*; University Science Books: Mill Valley, CA, 2006145206

(31) Jones, C. R.; Dan Pantos, G.; Morrison, A. J.; Smith, M. D. *Angew. Chem., Int. Ed.* 2009, 48, 7391–7394.

INTENTIONALLY BLANK PAGE

Chapter 5

Triclocarban: Commercial Antibacterial and Highly Effective H-Bond Donating Catalyst for Ring-Opening Polymerization



5.1 Abstract

The antibacterial compound, triclocarban (TCC), is shown to be a highly effective H-bond donating catalyst for ring-opening polymerization (ROP) when applied with an H-bond accepting base cocatalyst. These ROPs exhibit the characteristics of “living” polymerizations. TCC is shown to possess the high activity characteristic of urea (vs thiourea) H-bond donors. The urea class of H-bond donors is shown to remain highly active in H-bonding solvents, a trait that is not displayed by the corresponding thiourea H-bond donors. Two H-bond donating ureas that are electronically similar to TCC are evaluated for their efficacy in ROP, and a mechanism of action is proposed. This “off-the-shelf” H-bond donor is among the most active and most controlled organocatalysts for the ROP of lactones.

5.2 Introduction

H-bond mediated ring-opening polymerization (ROP) has attracted interest due to the highly controlled nature of these transformations.¹⁻⁴ These mild, highly functional group tolerant catalysts, especially the bimolecular systems consisting of a

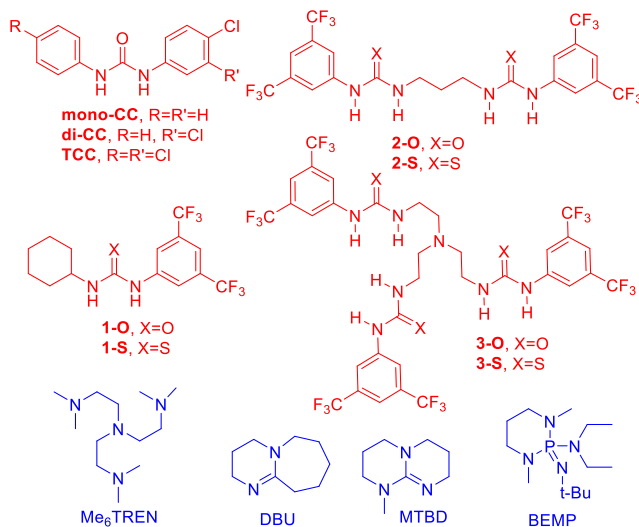
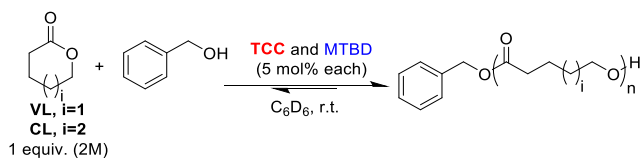


Figure 5.1. Base and (thio)urea cocatalysts evaluated for ROP.

(thio)urea H-bond donor plus H-bond accepting base, have facilitated the construction of precise polymer architectures, multiblocks, and well-defined systems.^{3,5-8} Targeted efforts by several groups toward rate-accelerated, H-bond mediated ROP seek to address a critical shortcoming of the field: low activity.⁹⁻¹² For example, our group has recently disclosed the utility of urea H-bond donors for rate accelerated ROP;¹³ thiourea H-bond donors have been used in organocatalytic ROP for more than a decade, but are less active.³ Another barrier to the wide implementation of this chemistry is the paucity of commercially available H-bond donors. Most (thio)urea catalysts are synthesized via a

“click” reaction of an appropriate amine and iso(thio)cyanate.^{3,14,15} While simple, this stands in contrast to the wide array of

Table 5.1. MTBD and TCC Catalyzed ROP of VL and CL^a.



entry	mon.	$[\text{M}]_0/[\text{I}]_0$	time (min)	conv. ^b (%)	M_n^c (g/mol)	M_w/M_n^c
1 ^d	VL	100	81	90	18 900	1.06
2		100	22	91	19 900	1.05
3		50	14	90	8 500	1.08
4		200	46	90	35 900	1.09
5		500	125	90	72 900	1.02
6	CL	100	132	90	21 200	1.06

^aReaction conditions: VL or CL (1.0 mmol, 1 equiv, 2M), benzyl alcohol, C₆D₆.

^bMonomer conversion was monitored via ¹H NMR. ^cM_n and M_w/M_n were determined by GPC (CH₂Cl₂) vs polystyrene standards. ^dDBU (5 mol %, 0.05 mmol) cocatalyst was employed (no MTBD).

readily available H-bond accepting base cocatalysts and adds a synthetic step prior to conducting polymerization chemistry. Certainly, the ready availability of chemical reagents and catalysts facilitates the wide implementation of chemical transformations. In this context, the antibacterial compound, triclocarban (TCC, figure 5.1), recently banned as a hand soap additive by the FDA, captured our attention.¹⁶ It is an electron-deficient biaryl urea, similar to the slate of urea and multiurea H-bond donating catalysts that we recently showed to be highly active for ROP.¹³ While TCC has attracted

considerable scientific interest as an antibacterial compound, possible bioaccumulate, and possible environmental toxin, we believe that this readily available compound has not previously been employed as a catalyst.¹⁷⁻¹⁹

5.3 Results and Discussion

The efficacy of TCC/amidine base combinations for the ROP of lactone monomers was evaluated, table 5.1. All reactions were conducted in C₆D₆ and conversion monitored by ¹H NMR. The guanidine base, MTBD, exhibited faster rates than the imine base, DBU, and it was used for further experimentation. The ROP of δ -valerolactone (VL) from benzyl alcohol is highly controlled, exhibiting the characteristics of a living polymerization: linear evolution of M_n vs conversion, first order consumption of monomer and M_n predictable from [M]₀/[I]₀, (see figures 5.2 and 5.3). This behavior is typical among organocatalysts for ROP.^{1,3} Initiation of a VL (1.0 mmol) ROP catalyzed by TCC/MTBD (0.05 mmol each) from 1-pyrenebutanol (0.02 mmol) and subsequent addition of a second monomer portion (1.0 mmol) exhibits overlapping UV and refractive index traces in the gel permeation chromatogram (GPC) of the resulting polymer (see Figure S3), suggesting end group fidelity and a chain end that is susceptible to chain-extension. The TCC/MTBD (5 mol %) cocatalysts are also effective for the ROP of ϵ -caprolactone (CL), producing a similarly well-behaved ROP. The ROP rates exhibited by TCC/MTBD represent a significant advance over those exhibited by **1-S**/MTBD, yet the reactions remain highly controlled. By comparison, for [M]₀ / [I]₀ = 50 from benzyl alcohol in C₆D₆, the **1-S**/MTBD-catalyzed ROPs of VL and CL achieve full conversion in 110 min and 45 h, respectively (c.f. Table 5.1).¹³

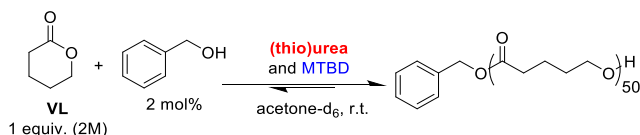
Entry 2 (Table 5.1) was attempted on a 200 mg scale, producing nearly identical polyvalerolactone (24 min, 90% conv, $M_n = 18100$, $M_w/M_n = 1.04$), which suggests that scale-up is feasible.

We have embarked on a research program aimed at mitigating the low activity of H-bond mediated transformations without sacrificing the precise control typical of these catalysts. In this vein, electron deficient aryl ureas have proved to be particularly efficacious; our lab previously disclosed the rapid rates exhibited by mono-, bis-, and tris-urea H-bond donors for the ROP of lactones.¹³ In general, urea H-bond donors are more active for ROP than their corresponding thioureas. This trend extends to the urea anions which, besides being remarkably active and controlled catalysts for ROP, are much more active than the corresponding thiourea anions.^{10,12} The uncharged H-bond donor **3-O**, in combination with MTBD (0.017 mmol each), effects the ROP of VL (1.0 mmol) from benzyl alcohol (0.02 mmol) in C_6D_6 in 3 min.¹³ While the analogous reaction with TCC/MTBD (0.05 mmol each) achieves full conversion in a slower 14 min, the commercial availability of the TCC catalyst is expected to be a boon to the wider application of this and similar systems. Additionally, the TCC/MTBD cocatalysts exhibit high selectivity for monomer (vs polymer). When a fully converted PVL reaction solution remains unquenched, the M_n and M_w/M_n are minimally altered over an hour: 20 min, $M_n = 22300$, $M_w/M_n = 1.02$; 60 min, $M_n = 23900$, $M_w/M_n = 1.03$ (c.f. table 5.1, entry 2), which may constitute an advantage versus other highly active systems for ROP.^{10,12,13}

Urea H-bond donors remain active in polar, H-bond accepting solvent. A long-standing limitation of H-bond mediated catalysis is the often narrow window of

nonpolar solvents in which these catalysts are operable.^{20,21} We had previously observed that the urea H-bond donor **3-O** remains active in THF and hypothesized that TCC would exhibit similar behavior, and a solvent screen was conducted for the

Table 5.2. Urea or Thiourea Plus MTBD Cocatalyzed ROP of VL in Acetone.^a



entry	TU or U (mol%)	time (min)	conv. ^b (%)	M_n^c (g/mol)	M_w/M_n^c
1	TCC (5%)	13	89	10 000	1.09
2	1-S (5%)	1200	89	9 500	1.21
3	1-O (5%)	60	91	11 900	1.08
4	2-S (2.5%)	1020	90	11 400	1.28
5	2-O (2.5%)	20	90	10 800	1.15
6	3-S (1.7%)	7440	89	12 100	1.16
7	3-O (1.7%)	20	89	10 300	1.13

^aReaction conditions: VL (1.0 mmol, 1 equiv, 2M), benzyl alcohol (2 mol %), and MTBD (same mol % as U/TU), acetone-d₆. ^bMonomer conversion was monitored via ¹H NMR. ^c M_n and M_w/M_n were determined by GPC (CH₂Cl₂) vs polystyrene standards.

TCC/MTBD catalyzed ROP of VL (see table 5.5). In DMF, the reaction time is extremely attenuated, and the reaction does not achieve >83% conversion. In THF, the ROP remains highly active (90% conv in 30 min), but M_w/M_n (= 1.23) broadens. The result in acetone is surprising in that the reaction rate does not slow versus C₆D₆, and the M_w/M_n remains narrow, table 5.2.

The ROP rates for all thiourea H-bond donors drop considerably versus their rates in C₆D₆,¹³ table 5.2. The TCC/MTBD catalyzed ROP of VL in acetone-d₆ remains controlled and exhibits the characteristics of a “living” polymerization (see fig. 5.8). The polymer samples resulting from the initiation of a VL (1.0 mmol, 2 M) ROP from 1-pyrenebutanol (0.02 mmol) catalyzed by TCC/MTBD (0.05 mmol each) and subsequent chain extension show overlapping UV and RI traces in the GPC (see fig. 5.9), which suggests end-group fidelity and that there is no initiation from the enol form of acetone-d₆.

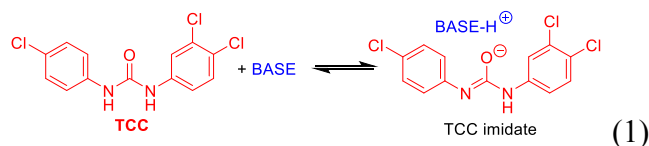
When TCC and Me₆TREN cocatalysts (5 mol % each) are applied for the ROP of L-lactide (1.0 mmol) from benzyl alcohol (0.01 mmol) in acetone-d₆, the ROP reaction exhibits “living” behavior (see figures 5.12 and 5.13). In contrast to the ROP of VL, CL, or carbonate monomers, mild base cocatalysts are required for the ROP of lactide.^{21–24} The poly(lactide) was isolated and analyzed by selectively decoupled ¹H NMR, revealing the polylactide (PLA) to be ~ 90% isotactic (see fig. 5.17), which suggests minor epimerization. The MALDI-TOF analysis of the same PLA sample shows the presence of ± 72 m/z repeat units, indicating that postpolymerization transesterification is occurring to a minor extent. This latter observation is in contrast to **2-S** H-bond donating catalyst, which effects the ROP of LA in the virtual absence of postpolymerization transesterification.²³

H-bond donating biaryl ureas were synthesized and applied in catalytic ROP to determine the origin of the enhanced rates of TCC (vs **1-O**). These catalysts, here dubbed monoclocarban (mono-CC)^{25,26} and diclocarban (di-CC)²⁶ in figure 5.1, were applied to the ROP of VL in C₆D₆; we believe these molecules have not previously been

used as catalysts. The TCC/MTBD (5 mol % each) cocatalyzed ROP of VL (1.0 mmol, 2 M) from benzyl alcohol (0.01 mmol) in C₆D₆ reaches 91% conversion in 22 min (table 5.1). The H-bond donors di-CC or mono-CC plus MTBD (5 mol % each) exhibit similar activity to TCC, but di-CC is the most active of the three H-bond donors (88% conversion in 15 min for di-CC and 37 min for mono-CC). The ROP of VL catalyzed by di-CC/MTBD exhibits the characteristics of a “living” polymerization (see fig. 5.18). The similar rates exhibited by TCC and di-CC toward ROP may suggest that the additional chlorine atom in TCC (vs di-CC) is not essential for catalysis or that the additional electron withdrawing effects from the “extra” chlorine atom in TCC versus di-CC are inhibitory to catalysis. The latter possibility recalls similar effects that have been observed for extremely electron deficient thioureas,^{27,28} and these observations suggest that the augmented activity of the biaryl TCC (vs **1-O**) can be approximated by functionalization at a single aryl ring. Certainly, the increased efficacy of TCC (vs **1-O**) for ROP calls into question the primacy of the bis(trifluoromethyl)aryl group, at least for urea H-bond donors.²⁷ While the commercial availability of TCC may be a boon to the application of H-bond mediated transformations in polymer synthesis laboratories, we expect that the development of advanced catalyst architectures will benefit from the more synthetically modular catalyst scaffold of di-CC.

The enhanced efficacy of TCC and all urea H-bond donors in C₆D₆ could be attributed to the stronger binding of ureas vs thioureas to monomer.²⁰ The limited solubility of TCC and **n-O** in nonpolar solvent in the absence of base cocatalyst limits the extent to which we can quantitatively probe this hypothesis by measuring binding

constants to monomer. For example, TCC is insoluble in benzene in the absence of H-bond acceptor, and binding constants for this compound could not be measured. However, the binding constants of **1-O** and **1-S** to CL were independently measured in C₆D₆ and are consistent with the long-held hypothesis: for **1-O**, $K_{\text{eq}} = 41 \pm 1$ (300 K) and for **1-S**, $K_{\text{eq}} = 28 \pm 1$ (300 K).²⁴ However, a binding constant rationale cannot be used to explain the ROP activity observed in acetone. As expected, when the **1-O** /monomer binding study is repeated in acetone-d₆, there is no observed change in chemical shift of **1-O** up to ~ 1000 equiv of monomer, which suggests very weak ($K_{\text{eq}} \sim 1$) or no binding in acetone-d₆. While we have previously observed **1-S** to exhibit a marked effect on a ROP reaction in the near absence of binding to monomer,^{29,30} these questions collectively reinforce a recently proposed mechanism.¹²

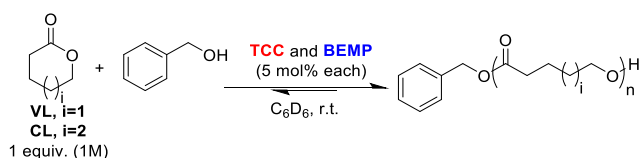


While this study was ongoing, “hyperactive” urea anions for ROP, generated by the action of alkoxides upon aryl and alkyl ureas, were disclosed; these systems are incredibly active yet controlled, exhibiting rates that rival traditional metal-based systems.¹² The proposed mechanism of action whereby an active urea anion catalyst is generated by the deprotonation of a urea by alkoxide is distinct from traditional H-bond mediated ROP by neutral catalysts, and we sought to investigate the feasibility of this mechanism for TCC/imine bases. As opposed to the quantitative deprotonation of TCC by potassium methoxide, one could envisage an equilibrium established between urea plus base and the corresponding salt, eq 1. ¹H NMR spectra in acetone-d₆ of TCC and TCC plus MTBD or DBU (5 mM each species) show an upfield shift of the TCC

resonances upon treatment with base that would be associated with the formation of an anionic character at the urea (see Figure 5.21). Repeating this experiment with highly basic BEMP (Figure 1, BEMP-H+ $pK_a^{\text{MeCN}} = 27.6$)³¹ establishes a pattern of increased upfield shift with increasing pK_a (MTBD-H+ $pK_a^{\text{MeCN}} = 25.4$; DBU-H+ $pK_a^{\text{MeCN}} = 24.3$).³² Repeating the TCC/BEMP ¹H NMR experiment with a deficient amount of BEMP (2.5 mM) shows only one set of resonances for TCC, suggesting that the equilibrium in eq 1 is dynamic on the ¹H NMR time scale.

The ¹H NMR experiments suggest that TCC/BEMP would be the most imidate-like species (i.e., eq 1 further to the right) and presumably the most active TCC/organic base catalyst pair yet examined herein. Indeed, the BEMP/TCC (0.05 mmol) catalyzed ROP of VL (1 M, 1 mmol) from benzyl alcohol (0.01 mmol) in benzene achieves full conversion in 3 min (table 5.3).

Table 5.3. Triclocarban Plus BEMP Cocatalyzed ROP of VL and CL.^a

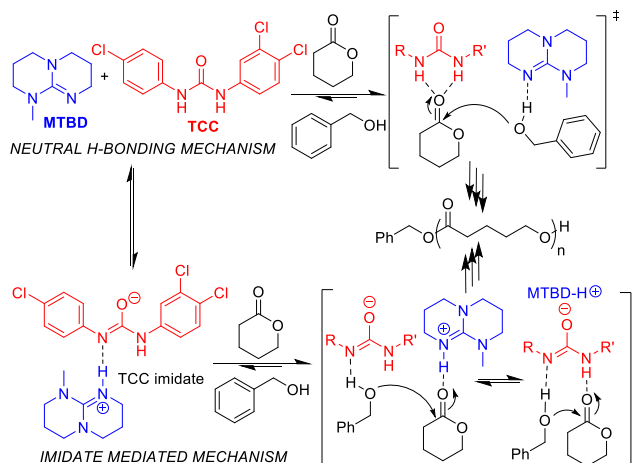


entry	mon.	$[M]_0/[I]_0$	time (min)	conv. ^b (%)	M_n^c (g/mol)	M_w/M_n^c
1	VL	50	1	87	11 900	1.04
2		100	3	90	22 400	1.04
3		200	6	90	47 900	1.06
4		500	10	90	108 800	1.05
5 ^d	CL	100	6	90	16 500	1.04

^aReaction conditions: VL or CL (1.0 mmol, 1 equiv, 1M), benzyl alcohol, C₆D₆.

^bMonomer conversion was monitored via ¹H NMR. ^c M_n and M_w/M_n were determined by GPC (CH₂Cl₂) vs polystyrene standards. ^dCL (1.0 mmol, 1 equiv, 2 M).

Higher reaction concentrations can be employed, but the reaction becomes difficult to monitor, fully converting within seconds at 2 M VL. The same ROP of VL fails to reach full conversion in THF or acetone- d_6 within 30 min. In C_6D_6 , the ROP is highly controlled and exhibits the characteristics of a “living” polymerization (see fig. 5.10), and the $[M]_0/[I]_0$ series (table 5.3) is notable for the high predictability of M_n even when considered against other organocatalytic systems. Further, M_w/M_n broadens slowly postpolymerization (Table 3, entry 2: 3 min, $M_n = 22400$, $M_w/M_n = 1.04$; 6 min, $M_n = 24100$, $M_w/M_n = 1.07$; 15 min, $M_n = 24700$, $M_w/M_n = 1.15$; 90% conv. for all aliquots). TCC/BEMP is ineffective for the ROP of β -butyrolactone, consistent with other urea and thiourea H-bond donors.^{13,20}



Scheme 5.1. Proposed Mechanism for TCC/Base Cocatalyzed ROP.

5.4 Mechanistic Considerations

We propose that the TCC/base cocatalyzed ROP of ester monomers proceeds through a mixed mechanism where the identity of the dominate catalyst largely depends on the pK_a of the cocatalysts. The 1H NMR spectrum of TCC plus Me_6TREN shows very slight downfield shift of the TCC resonances and broadening of the N-H

resonances which could be attributed to H-bonding; there is no evidence to suggest the formation of imidate character at the urea for this cocatalyst pair (c.f. TCC/BEMP, fig. 5.21). Accordingly, we propose that TCC/base cocatalyzed ROP is capable of effecting ROP through a classic dual H-bond mechanism mediated by neutral catalysts or an imidate mediated mechanism, the primary determination of which mode is dominant rests with the pK_a of the base. In the case of TCC plus Me_6TREN , we proposed a primarily neutral catalyst mechanism versus BEMP, which may proceed primarily through an imidate mechanism, scheme 5.1. Certainly, the rate of the TCC/BEMP ROP recalls that of the alkoxide-generated urea anions.¹² This mechanistic proposal is an extension of the recent work with “hyperactive” urea anion catalysts for ROP, taking into account weakly basic cocatalysts.¹² For the present system, it is unclear if the conjugate acid of the base serves as a H-bond donor or primarily serves to deprotonate the urea. The complicated and sensitive interplay of cocatalyst/reagent interactions requires more study to be thoroughly understood.

5.5 Conclusion

The antibacterial TCC has been shown to be a highly effective cocatalyst for ring-opening polymerization. The commercially available H-bond donor, when applied with an H-bond accepting base cocatalyst, is among the most active organic catalysts for the ROP of esters, yet it exhibits the characteristics of a “living” polymerization, producing well-defined polymers. The activity of this catalyst can be approximated by other mono- and dichloro biaryl urea H-bond donor(s), which adds synthetic flexibility for the generation of future H-bond donating ureas. We suspect that the ROP of lactone

monomers is just one application that can offer new roles to old reagents, in this case, the antibacterial compound now banned in hand soap, TCC.

5.6 Experimental Section

5.6.1 General Considerations

All chemicals were purchased from Fisher Scientific and used as received unless stated otherwise. Triclocarban (TCC), 7-methyl-1,5,7-triazabicyclo[4.4.0]dec-5-ene (MTBD) and 1,8-diazabicyclo[5.4.0]undec-7-ene (DBU) were purchased from TCI. Tris[2-(dimethylamino)ethyl]amine (Me₆TREN) and 2-*tert*-butylimino-2-diethylamino-1,3-dimethylperhydro-1,3,2-diazaphosphorine (BEMP) were purchased from Alfa Aesar. Benzyl alcohol and 1,2-dichlorobenzene were distilled under high vacuum from calcium hydride. THF was dried on an Innovative Technology solvent purification system. DMF was dried over 4 Å molecular sieves for 48 h prior to use. 1-pyrenebutanol was purchased from Sigma Aldrich. δ -valerolactone (VL), ϵ -caprolactone (CL) and β -butyrolactone (BL) were distilled from calcium hydride under high vacuum. L-Lactide (L-LA) was purchased from Acros Organics and recrystallized from dry toluene. Benzene-*d*₆ and chloroform-*d* were purchased from Cambridge Isotope Laboratories and distilled from calcium hydride. Acetone-*d*₆ was purchased from Cambridge Isotope Laboratories and stored over 4 Å molecular sieves for 48 h prior to use. Experiments were conducted using pre-dried glassware in an MBRAUN or INERT stainless steel glovebox or using a Schlenk line under nitrogen atmosphere. NMR experiments were conducted on a Bruker Avance III 300 MHz or 400 MHz

spectrometer or a Varian 500 MHz spectrometer. Gel Permeation Chromatography (GPC) was performed at 40 °C using HPLC grade dichloromethane eluent on an Agilent Infinity GPC system equipped with three Agilent PLGel columns 7.5 mm × 300 mm (5 μm, pore sizes: 103, 104, 50 Å). M_n and M_w/M_n were determined versus polystyrene standards (500 g/mol-3150 kg/mol, Polymer Laboratories). Mass spectrometry was performed using a Thermo Scientific (San Jose, CA, USA) LTQ Orbitrap XL mass spectrometer affixed with either an atmospheric-pressure chemical ionization (APCI) or electrospray ionization (ESI) interface, positive ions were produced and introduced into the S2 instrument. Tune conditions for infusion experiments (5 μL/min flow, sample concentration 5 μg/mL in 50/50 v/v water/methanol) were as follows: ionspray voltage, 5 kV; capillary temperature, 275 °C; sheath gas (N₂, arbitrary units), 8; auxiliary gas (N₂, arbitrary units), 2; capillary voltage, 35 V; and tube lens, 90 V. Prior to analysis, the instrument was calibrated for positive ions using Pierce LTQ ESI positive ion calibration solution (lot #PC197784). Ion trap experiments used N₂ as a collision gas with normalized collision energies (NCE) between 10-25 eV for multistage fragmentation. High-energy collision (HCD) experiments were performed with He as the collision gas with a NCE of 25 eV.

5.6.2. Example ring-opening polymerization of VL

To a 7 mL vial, TCC (15.7 mg, 0.05 mmol), VL (100 mg, 1.0 mmol) and benzene-*d*₆ (250 μL) were added. The contents were stirred until the solution became homogenous. To a second 7 ml vial, benzyl alcohol (4.3 mg, 0.04 mmol), MTBD (7.6 mg, 0.05 mmol) and benzene-*d*₆ (250 μL) were added. The contents in the second vial

were transferred to the first vial via Pasteur pipette, and the contents were agitated to mix. The reaction solution was then transferred to an NMR tube, and the progress of the reaction monitored by ^1H NMR. The reaction was quenched by the addition of benzoic acid (6.1 mg, 0.05 mmol). Polymer isolated by precipitation with hexanes contains residual TCC that can be removed by repeated precipitation or washing with methanol. PVL was removed of volatiles under high vacuum prior to characterization. Yield 89%, M_n (GPC)= 5,400, $M_w/M_n = 1.09$, M_n (NMR) = 2,700.

5.6.3 Example post-polymerization transesterification.

To a 7 mL vial, TCC (15.7 mg, 0.05 mmol), VL (100 mg, 1.0 mmol) and benzene- d_6 (250 μL) were added. The contents were stirred until the solution became homogenous. To a second 7 ml vial, benzyl alcohol (1.1 mg, 0.01 mmol), MTBD (7.6 mg, 0.05 mmol) and benzene- d_6 (250 μL) were added. The contents in the second vial were transferred to the first vial via Pasteur pipette, and the contents were agitated to mix. Three 50 μL aliquots from the reaction were quenched at 20 min, 45 min and 60 min using benzoic acid (6.2 mg, 0.05 mmol). Polymer in each aliquot was then isolated by precipitation with hexanes. PVL was removed of volatiles under high vacuum prior to characterization by GPC: $M_n = 22,300, 23,900, 23,900$, $M_w/M_n = 1.02, 1.03, 1.03$ respectively.

5.6.4. Example chain extension experiment.

To a 7 mL vial, TCC (15.7 mg, 0.05 mmol), VL (100 mg, 1.0 mmol) and benzene- d_6 (250 μL) were added. The contents were agitated until the solution became

homogenous. To a second 7 ml vial, 1-pyrenebutanol (5.5 mg, 0.02 mmol), MTBD (7.6 mg, 0.05 mmol) and benzene- d_6 (250 μ L) were added. The contents of the second vial were transferred to the first vial via Pasteur pipette, and the contents were agitated to mixed. After 13 min, a 100 μ L aliquot from the reaction was quenched using benzoic acid (6.2 mg, 0.05 mmol), and VL (100 mg, 1.0 mmol) was added to the reaction vial. A second 100 μ L aliquot from the reaction vial was quenched in 27 min using benzoic acid (6.2 mg, 0.05 mmol). Conversion of VL in the two aliquots were then determined by ^1H NMR, followed by the isolation of PVL and characterization by GPC.

5.6.5. Example ring-opening polymerization of L-Lactide.

A first 7 mL vial was charged with TCC (15.8 mg, 0.05 mmol), Me_6TREN (13.4 μ L, 0.05 mmol) and benzyl alcohol (1.0 μ L, 0.01 mmol). A second 7 mL vial was charged with L-LA (144.1 mg, 1 mmol) and acetone- d_6 (1000 μ L). The contents of the second vial were added to the first vial, and the resulting mixture was vigorously shaken until homogenous. The reaction mixture was transferred to an NMR tube via pipette, and the reaction progress was monitored by ^1H NMR. The reaction was quenched with benzoic acid (0.1 mmol). The reaction mixture was removed of volatiles under reduced pressure, dissolved in minimal dichloromethane, and the polylactide (PLA) was precipitated with the addition of hexanes. The supernatant was decanted, and the precipitate was subjected to high vacuum to remove volatiles.

5.6.6. Example binding experiment.

For the titration of **1-O** with CL, stock solutions of **1-O** and CL were prepared in benzene- d_6 . Into several NMR tubes, varying amounts of each solution were added to each tube along with neat benzene- d_6 such that the final volume of each sample was 0.4 mL. The final concentrations were $[\mathbf{1-O}] = 0.005 \text{ M}$ and $0.25 \text{ M} < [\text{CL}] < 2.25 \text{ M}$. $^1\text{H-NMR}$ spectra (referenced to residual benzene-H) were acquired for each tube at 300 K and the chemical shift of the *ortho*-protons of **1-O** was noted. Binding constants were determined by the curve fitting method,³³⁻³⁵ and these values match those determined from the Lineweaver-Burke method.^{36, 37} Binding curves are shown below.

5.6.7. Example synthesis of 1-(4-chlorophenyl)-3-phenylurea (mono-CC).

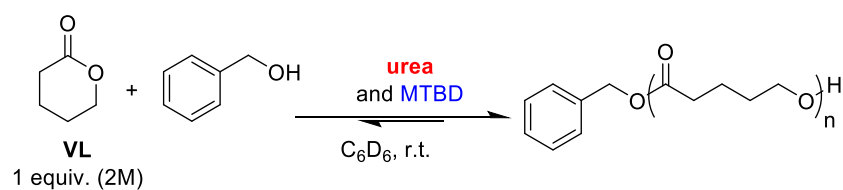
A dried Schlenk flask was charged with 4-chlorophenylisocyanate (598.2 mg, 3.90 mmol) and ~10 mL dried DCM. Next, aniline (0.36 mL, 3.95 mmol) was added via syringe. Immediately upon addition of aniline, a white precipitate formed. The reaction mixture was filtered and rinsed 3 times with cold DCM to provide a pure white powder (846.1 mg, 3.43 mmol, 88.1 % yield). Characterization matches literature,³⁸ NMR spectra below; $^{13}\text{C NMR}$ (CD_3OD , 100 MHz): $\delta = 155.2, 140.3, 139.5, 129.5, 129.4, 128.5, 124.0, 121.6, 120.5$.

5.6.8. Example synthesis of 1-(3,4-dichlorophenyl)-3-phenylurea (mono-CC).

A dried Schlenk flask was charged with 3,4-dichlorophenylisocyanate (731.8 mg, 3.89 mmol) and ~10 mL dried DCM. Next, aniline (0.36 mL, 3.95 mmol) was added via syringe. Immediately upon addition of aniline a white precipitate formed. The

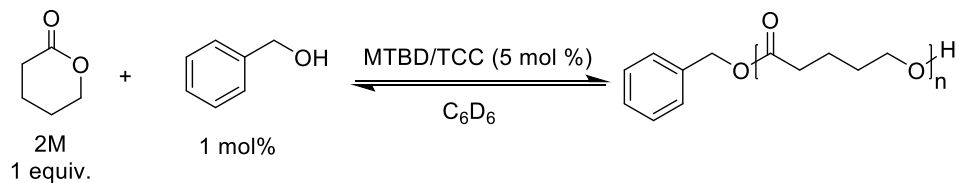
reaction mixture was filtered and rinsed 3 times with cold DCM to provide a pure white powder (1.01 g, 3.59 mmol, 92.7 % yield). Characterization matches literature;³⁹ NMR spectra below; ¹³C NMR (CD₃OD, 100 MHz): δ = 154.87, 140.81, 140.16, 133.32, 131.48, 129.89, 126.14, 124.12, 121.39, 120.53, 119.60.

Table 5.4. Chain Length Variation for the TCC or di-CC plus MTBD cocatalyzed ROP of VL.



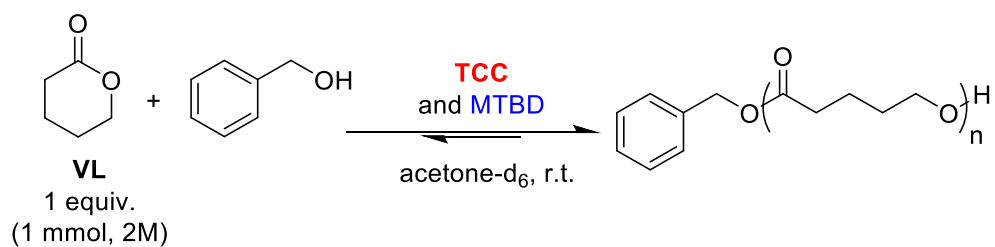
Entry	urea	[M] ₀ /[I] ₀	time (min)	conv. (%) ^a	M_n^b	M_w/M_n^b
1	TCC	50	14	90	8500	1.08
2		100	22	91	19900	1.05
3		200	46	90	35900	1.0
4		500	125	90	72900	1.02
5	di-CC	50	15	88	6000	1.04
6		100	20	89	12000	1.04
7		200	78	94	25000	1.03
8		500	180	89	64000	1.06

a. Conversion determined by ¹H NMR. b. M_n and M_w were obtained by GPC.

Table 5.5. Solvent Screen of TCC/MTBD cocatalyzed ROP of VL.

Entry	Solvent	time (min)	conv. (%) ^a	M_n^b	M_w/M_n^b
1	benzene- <i>d</i> ₆	22	91	19,900	1.06
2	acetone- <i>d</i> ₆	22	89	19,400	1.11
3	chloroform- <i>d</i>	273	89	19,100	1.08
4	THF	30	89	14,700	1.23
5	DMF	600	83	9,000	1.41

a. Conversion determined by ¹H NMR. b. M_n and M_w were obtained by GPC.

Table 5.6. Chain Length Variation for the TCC/MTBD cocatalyzed ROP of VL in acetone-*d*₆.

Entry	$[M]_0/[I]_0$	time (min)	conv. (%) ^a	M_n^b	M_w/M_n^b
1	50	13	88	7400	1.11
2	100	20	88	14100	1.10
3	200	32	89	22600	1.09
4	500	45	89	44700	1.08

a. Conversion determined by ¹H NMR. b. M_n and M_w were obtained by GPC.

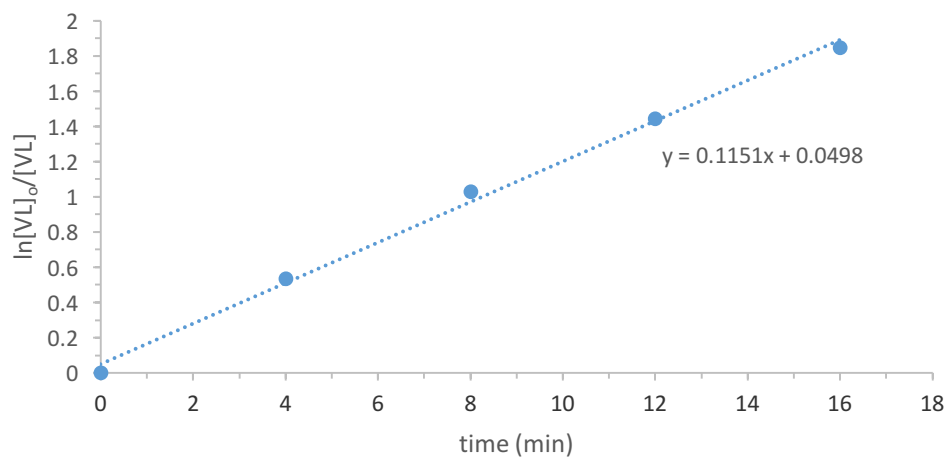


Figure 5.2. First order evolution of VL vs time for the TCC/MTBD catalyzed ring-opening polymerization of VL. Conditions: VL (2 M, 1 mmol), benzyl alcohol (1mol%, 0.01 mmol), TCC (5mol%, 0.05 mmol), MTBD (5 mol%, 0.05 mmol) in benzene- d_6 .

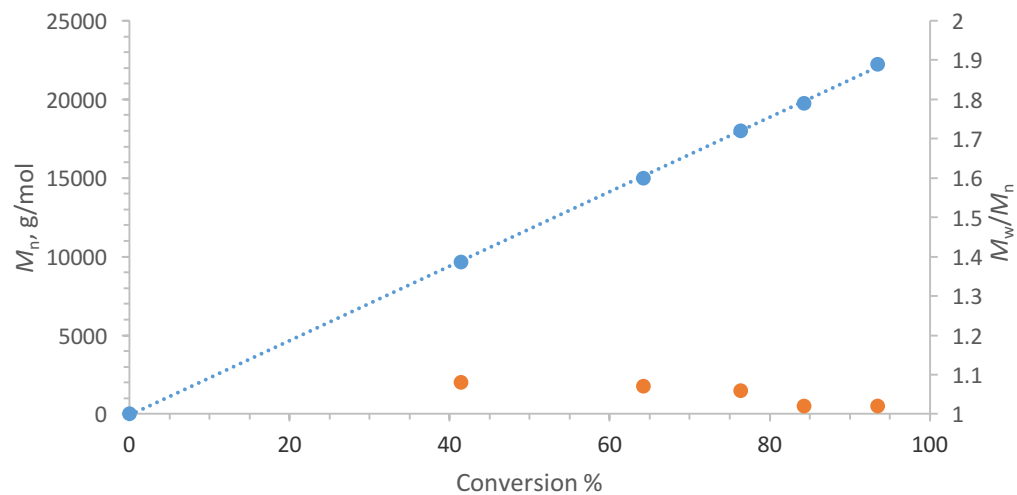


Figure 5.3. M_n (blue) and M_w/M_n (orange) vs conversion for the TCC/MTBD catalyzed ring-opening polymerization of VL. Conditions: VL (2 M, 1 mmol), benzyl alcohol (1mol%, 0.01 mmol), TCC (5mol%, 0.05 mmol), MTBD (5 mol%, 0.05 mmol) in benzene- d_6 .

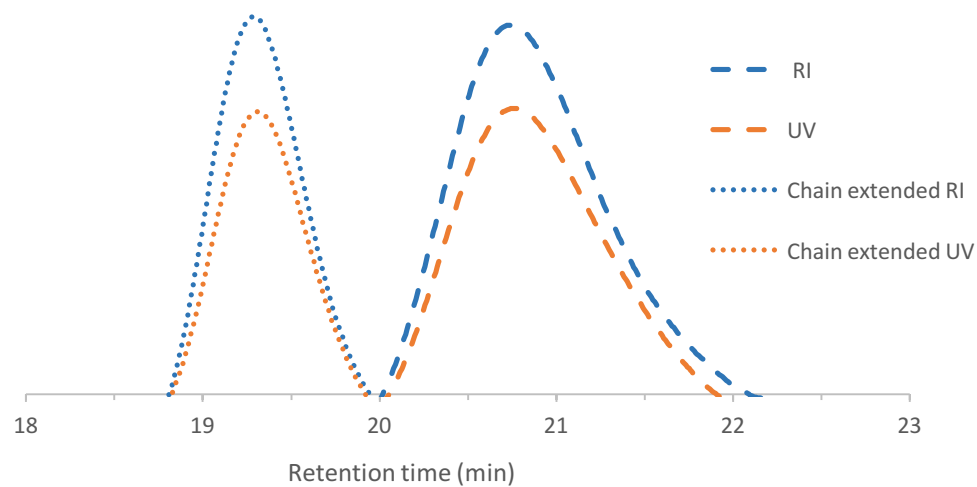


Figure 5.4. GPC traces of the polymers resulting from the chain extension experiment of VL. Conditions: VL (2 M, 1mmol), 1-pyrenebutanol (2mol%, 0.02mmol), TCC (5mol%, 0.05 mmol), MTBD (5 mol%, 0.05 mmol) in benzene-*d*₆, and subsequent chain extension by the addition of VL (1mmol).

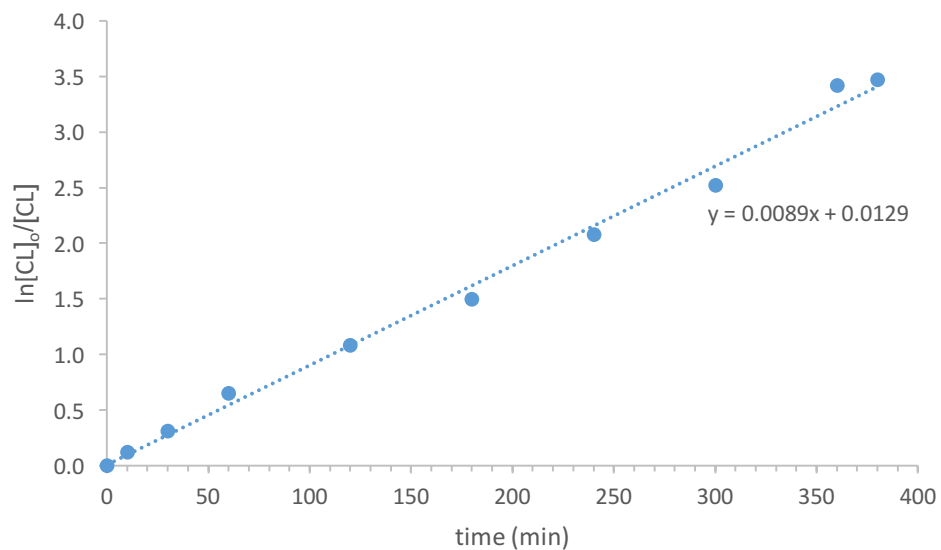


Figure 5.5. First order evolution of CL vs time for the TCC/MTBD catalyzed ring-opening polymerization of CL. Conditions: CL (2 M, 1 mmol), benzyl alcohol (1mol%, 0.01mmol), TCC (5mol%, 0.04 mmol), MTBD (5 mol%, 0.04 mmol) in benzene- d_6 .

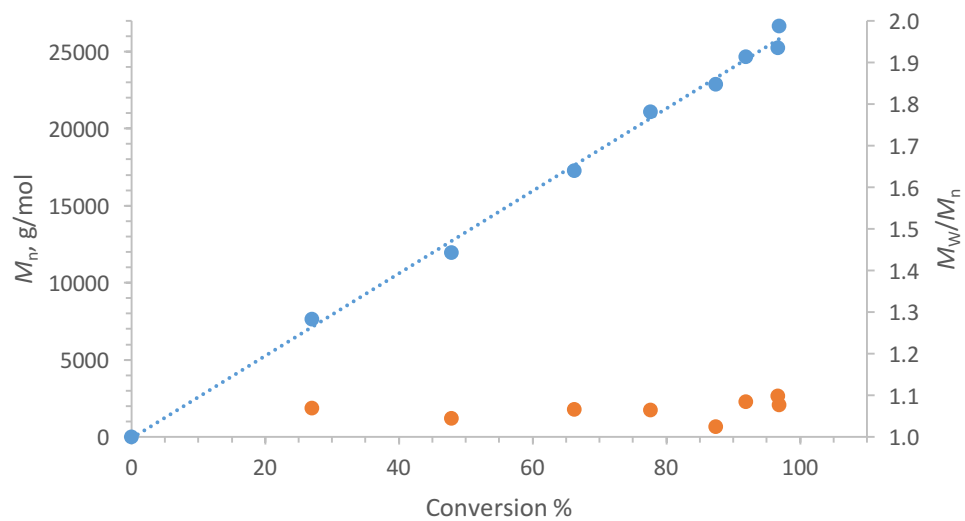


Figure 5.6. M_n (blue) and M_w/M_n (orange) catalyzed ring-opening polymerization of CL. Conditions: CL (2 M, 1mmol), benzyl alcohol (1mol%, 0.01 mmol), TCC (5mol%, 0.04 mmol), MTBD (5 mol%, 0.04 mmol) in benzene- d_6 .

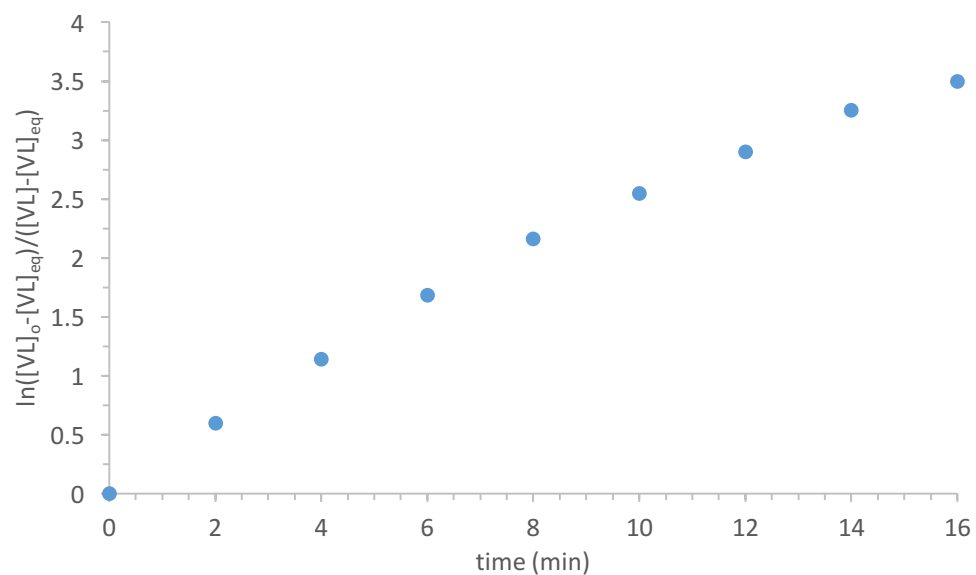


Figure 5.7. Approach to equilibrium evolution of [VL] vs time for the TCC/MTBD catalyzed ring-opening polymerization of VL. Conditions: VL (2.1 M, 2mmol, 1 equiv.), benzyl alcohol (1mol%, 0.02 mmol), TCC (5mol%, 0.1 mmol), MTBD (5 mol%, 0.1 mmol) in acetone- d_6 . $[VL]_{eq} = 0.22$ M

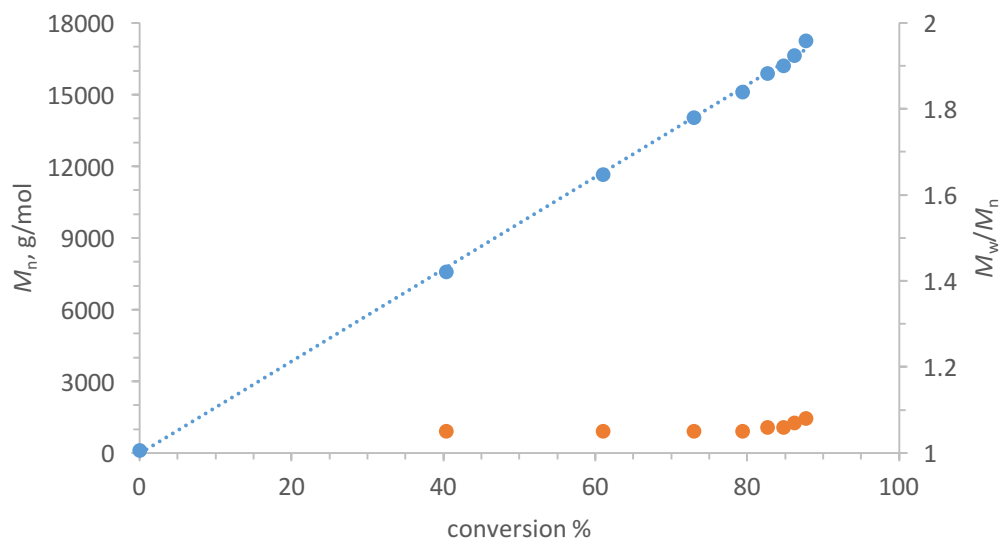


Figure 5.8. M_n (blue) and M_w/M_n (orange) vs conversion for the TCC/MTBD catalyzed ring-opening polymerization of VL. Conditions: VL (2.1 M, 2 mmol, 1 equiv.), benzyl alcohol (1 mol. %, 0.02 mmol), TCC (5 mol. %, 0.1 mmol), MTBD (5 mol. %, 0.1 mmol) in acetone- d_6 .

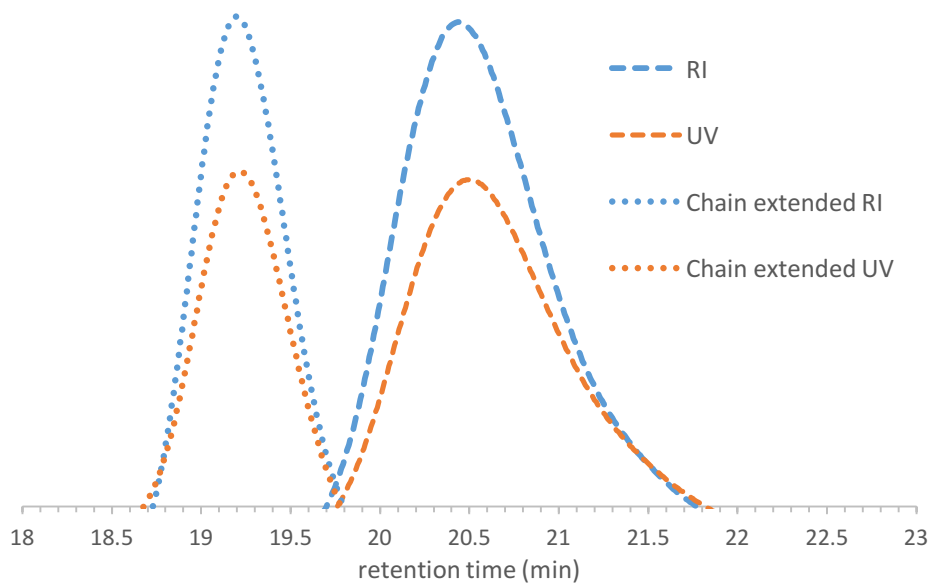


Figure 5.9. GPC traces of the polymers resulting from the chain extension of PVL in acetone. Conditions: VL (2 M, 1 mmol), 1-pyrenebutanol (2 mol%, 0.02mmol), TCC (5 mol%, 0.05 mmol), MTBD (5 mol%, 0.05 mmol) in acetone- d_6 , and subsequent chain extension by the addition of VL (1 mmol).

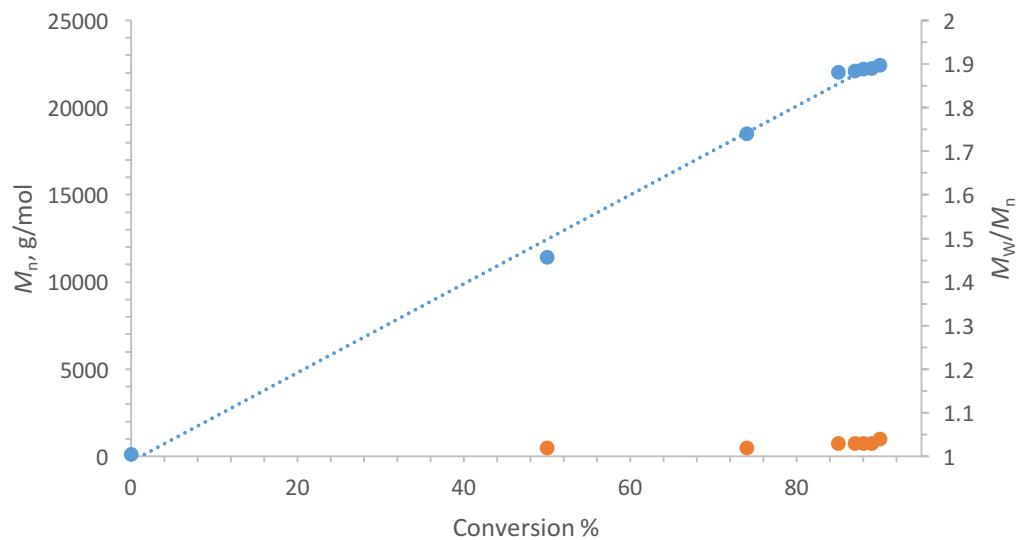


Figure 5.10. M_n (blue) and M_w/M_n (orange) vs conversion for the TCC/BEMP catalyzed ring-opening polymerization of VL. Conditions: VL (1M, 1 mmol), benzyl alcohol (1 mol%, 0.01 mmol), TCC (5 mol%, 0.05 mmol), BEMP (5 mol%, 0.05 mmol) in benzene- d_6 .

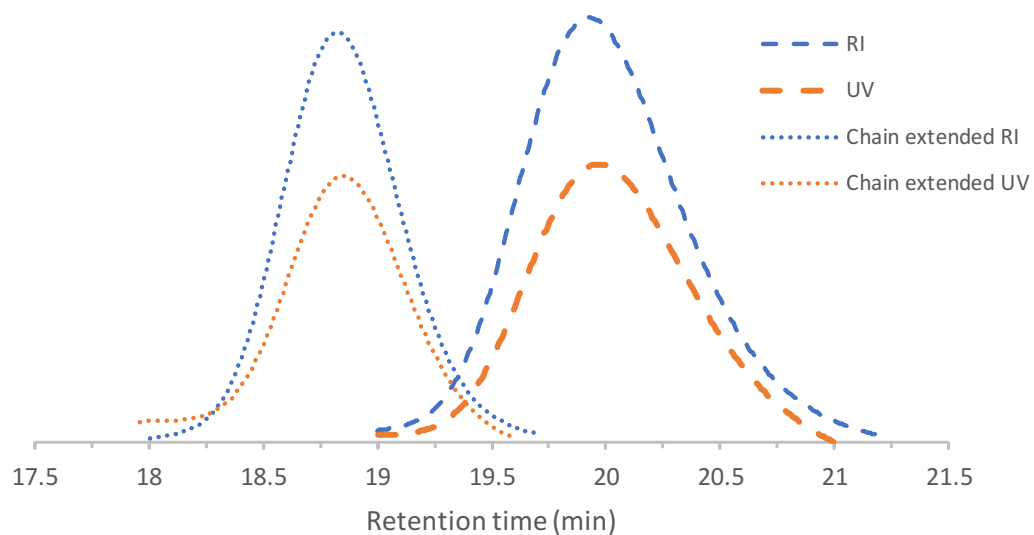


Figure 5.11. GPC traces of the polymers resulting from the chain extension experiment of VL. Conditions: VL (1 M, 1 mmol), 1-pyrenebutanol (2 mol%, 0.02mmol), TCC (5 mol%, 0.05 mmol), BEMP (5 mol%, 0.05 mmol) in benzene-*d*6, and subsequent chain extension by the addition of VL (1 mmol).

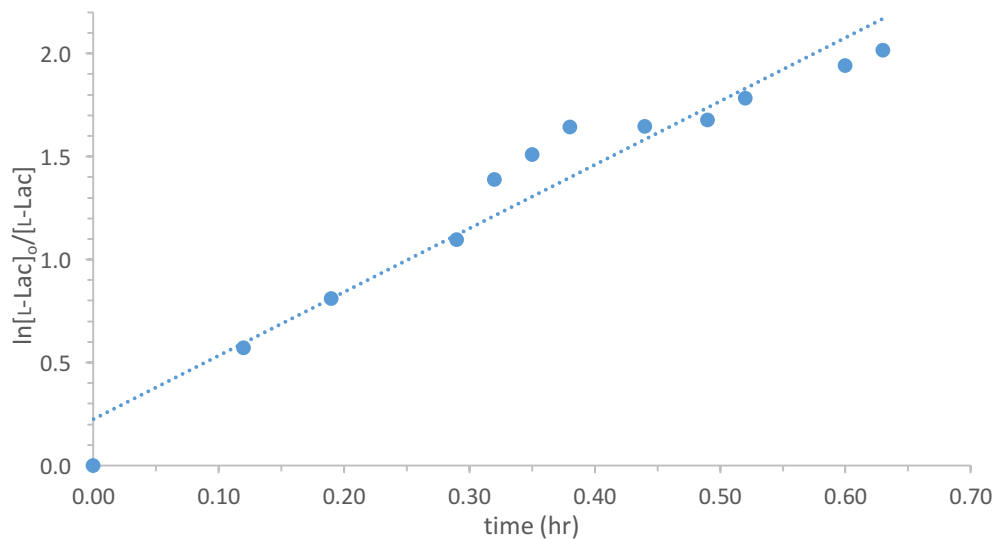


Figure 5.12. First order evolution of [L-LA] vs time for the TCC/Me₆TREN catalyzed ring-opening polymerization. Conditions: L-LA (1 M, 1 mmol), benzyl alcohol (1 mol %, 0.01 mmol), TCC (5 mol %, 0.05 mmol), Me₆TREN (5 mol %, 0.05 mmol) in acetone-*d*₆.

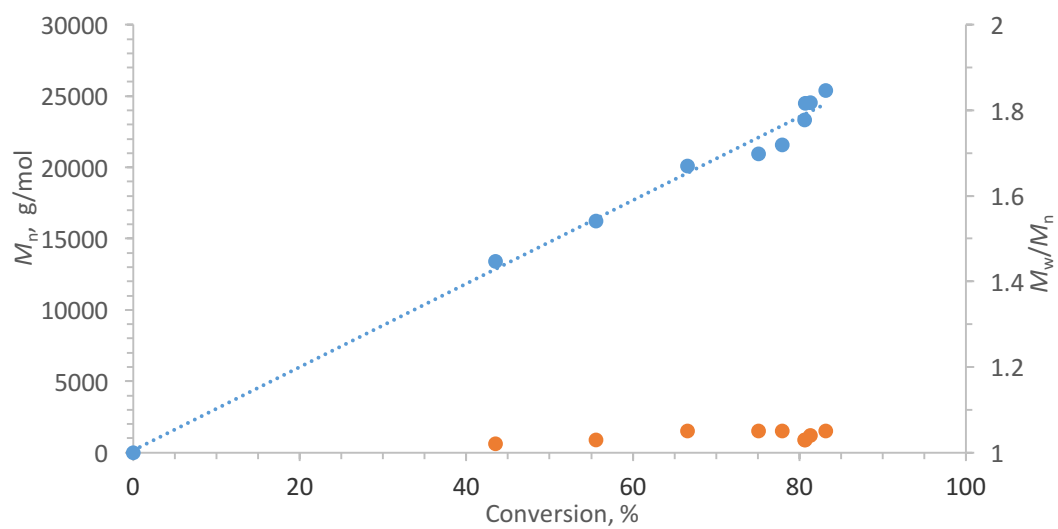


Figure 5.13. M_n (blue) and M_w/M_n (orange) vs conversion for the TCC/Me₆TREN catalyzed ring-opening polymerization of L-LA. Conditions: L-LA (1 M, 1 mmol), benzyl alcohol (1 mol. %, 0.01 mmol), TCC (5 mol. %, 0.05 mmol), Me₆TREN (5 mol. %, 0.05 mmol) in acetone-*d*₆.

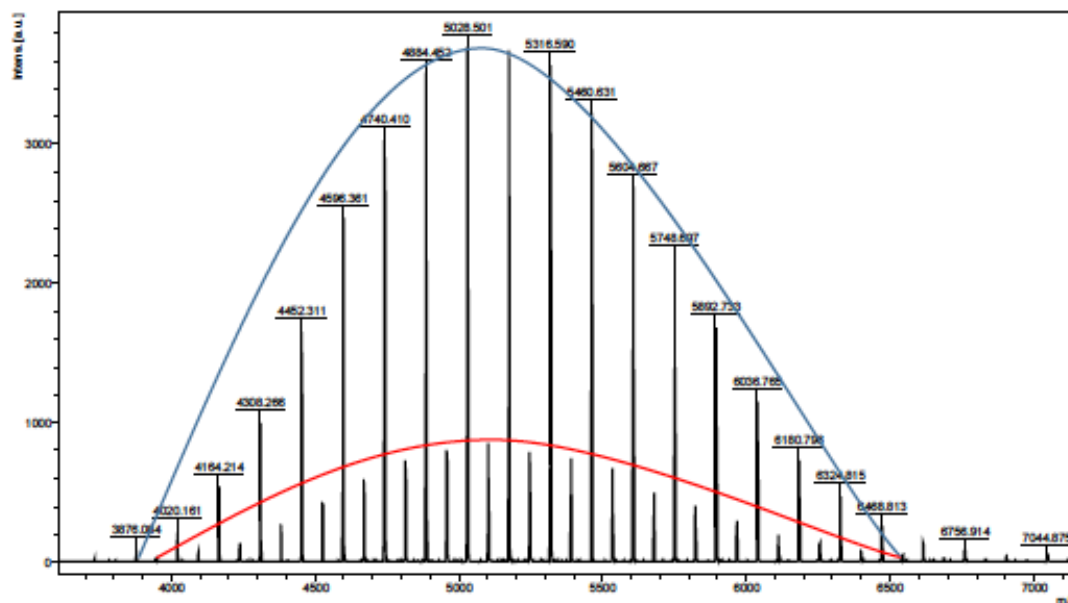


Figure 5.14. MALDI-TOF of the PLLA resulting from TCC/Me₆TREN cocatalyzed ROP of L-lactide. The major pattern (blue line) is due to whole repeat units $m/z = (\text{Na}^+ + \text{benzyl alcohol} + n \cdot \text{LA})$ while the minor pattern (red line) is due to half repeat units generated by post-polymerization transesterification $m/z = (\text{Na}^+ + \text{benzyl alcohol} + (n+1/2) \cdot \text{LA})$. All m/z bear a benzyl alcohol initiator.

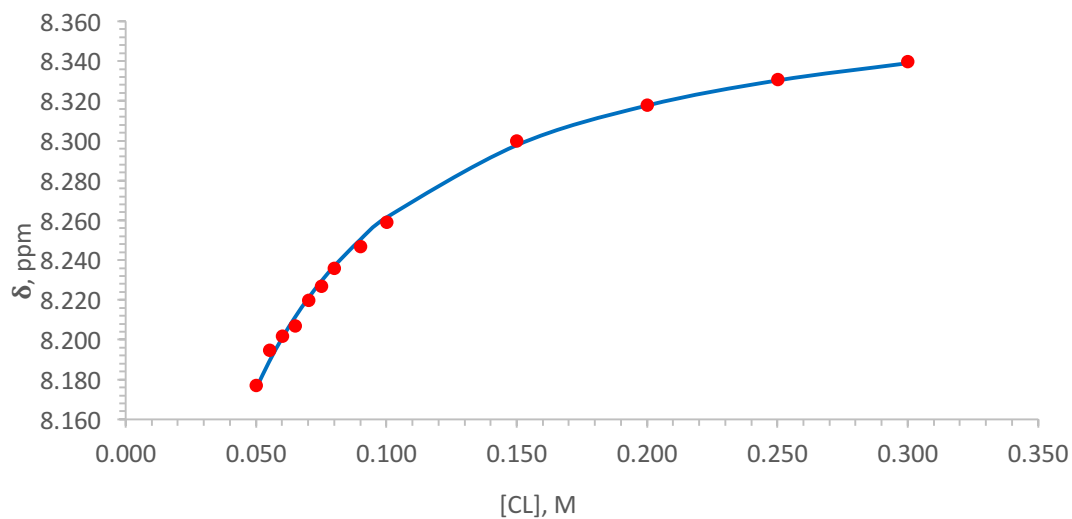


Figure 5.15. Titration binding curve for the CL/1-O binding in benzene- d_6 . Chemical shift of the *o*-phenyl protons vs [CL]; solid line is the fit from the binding equation.

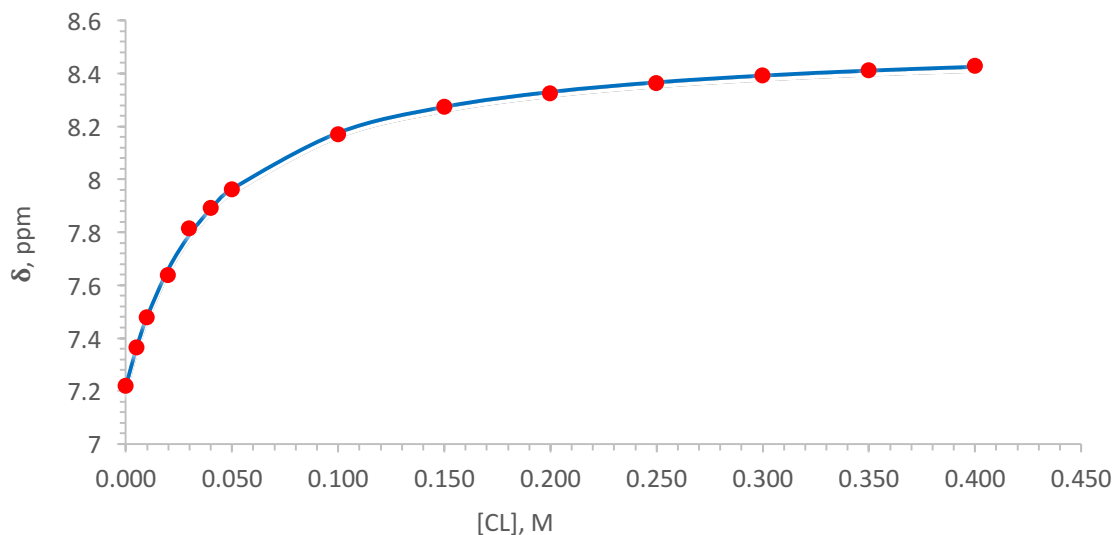


Figure 5.16. Titration binding curve for the CL/1-S binding in benzene- d_6 . Chemical shift of the *o*-phenyl protons vs [CL]; solid line is the fit from the binding equation.

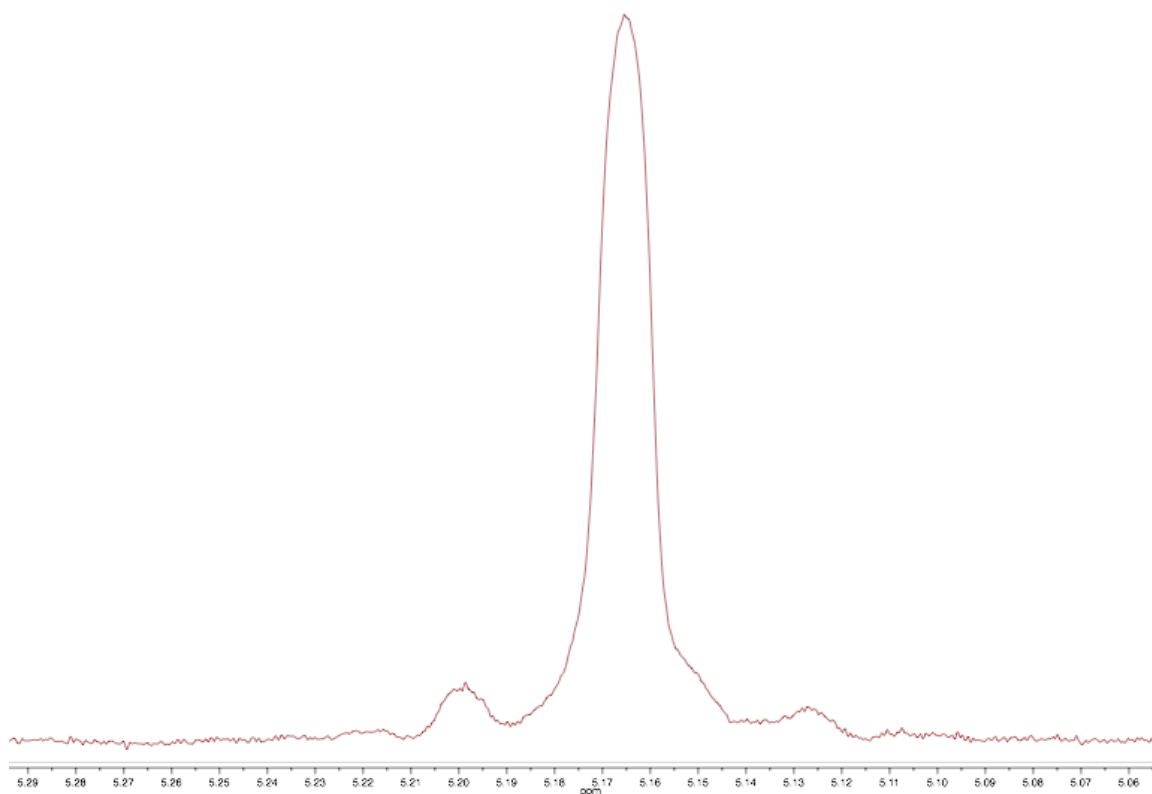


Figure 5.17. Methine region of the methyl-decoupled ^1H NMR spectrum of PLLA obtained via TCC/ Me_6TREN cocatalyzed ROP of L-LA (500 MHz, 25 °C).

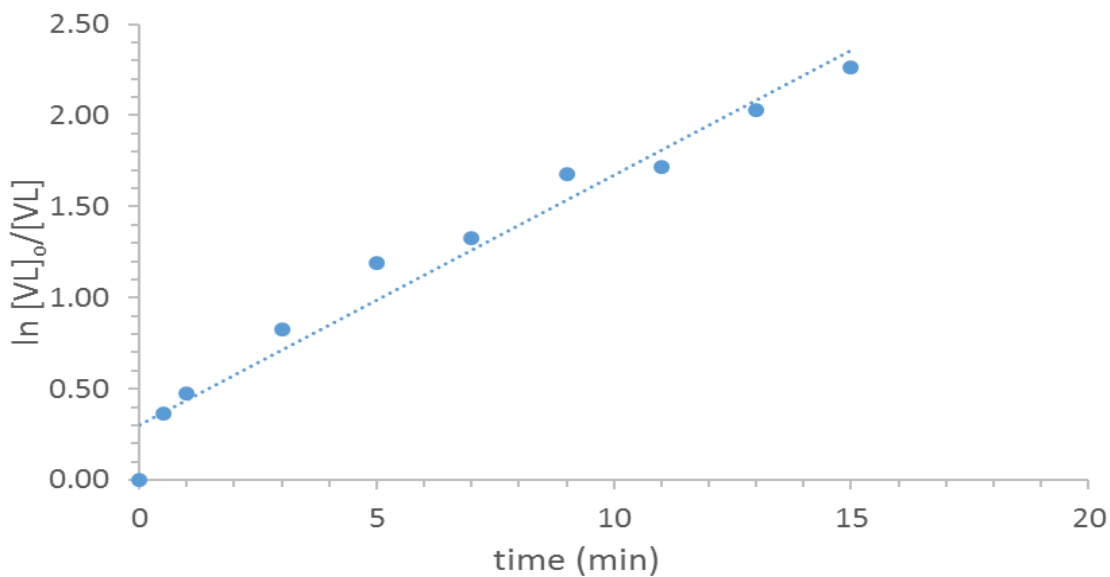
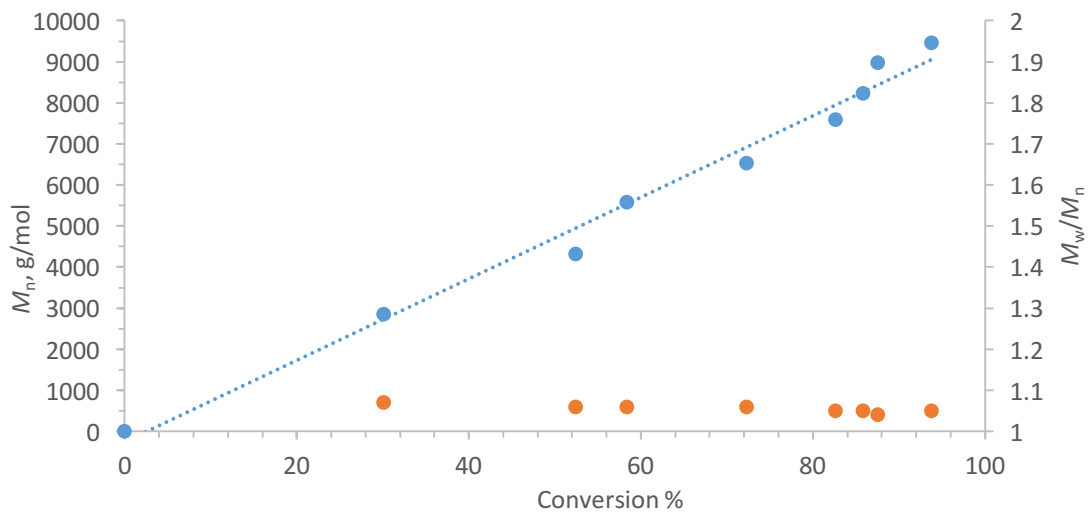


Figure 5.18. (upper) First order evolution of $[VL]$ vs time for the di-CC/MTBD catalyzed ROP of VL. (lower) The ROP displays a linear evolution of M_n (blue) vs conversion and narrow M_w/M_n (orange). Conditions: VL (2 M, 1.0 mmol), benzyl alcohol (2.0 mol%, 0.02mmol), di-CC (5.0 mol%, 0.05 mmol), MTBD (5 mol%, 0.05 mmol) in benzene- d_6 .

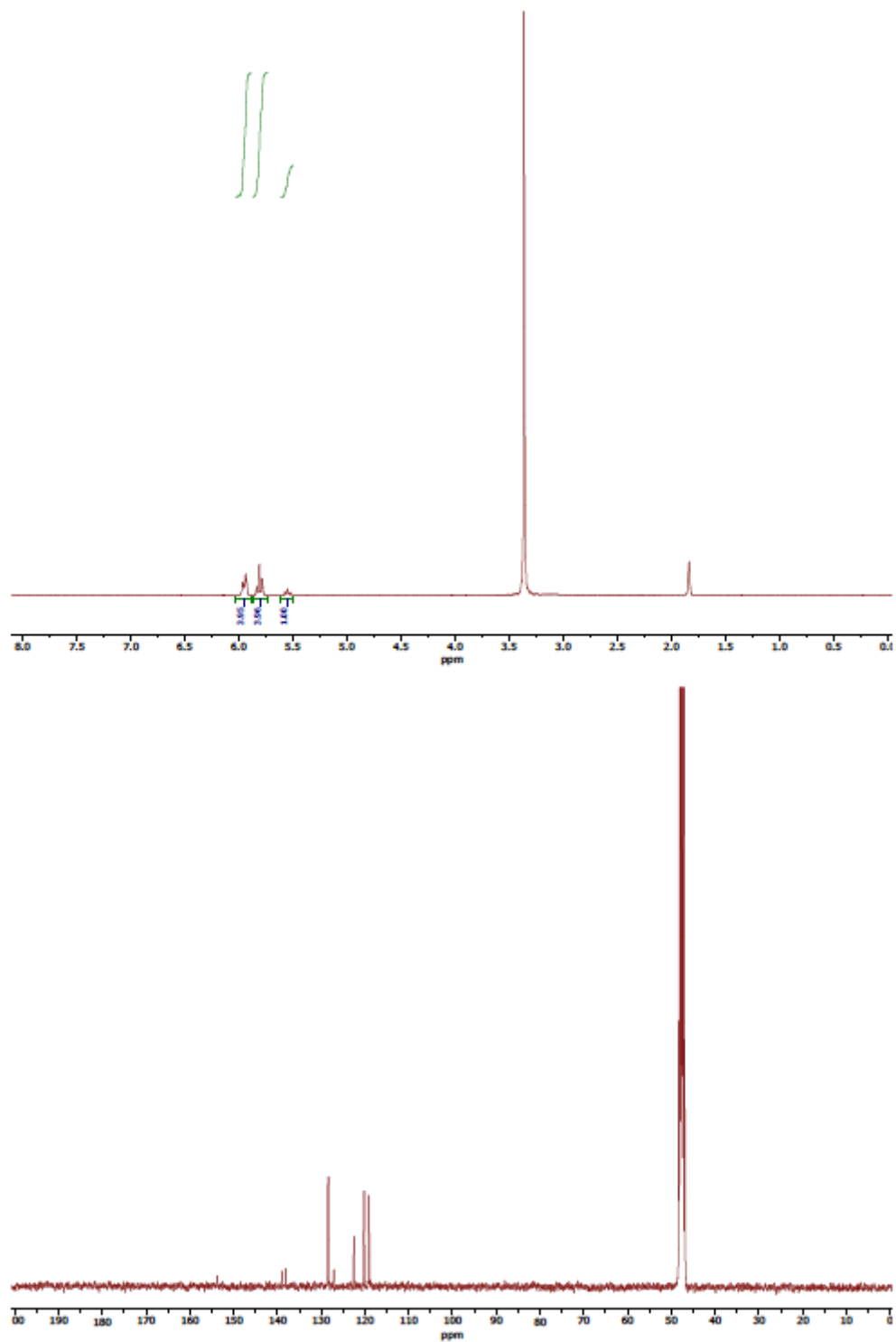


Figure 5.19. (upper) ^1H NMR (CD₃OD, 400 MHz) spectrum of mono-CC. (lower) ^{13}C NMR (CD₃OD, 100 MHz) spectrum of mono-CC.

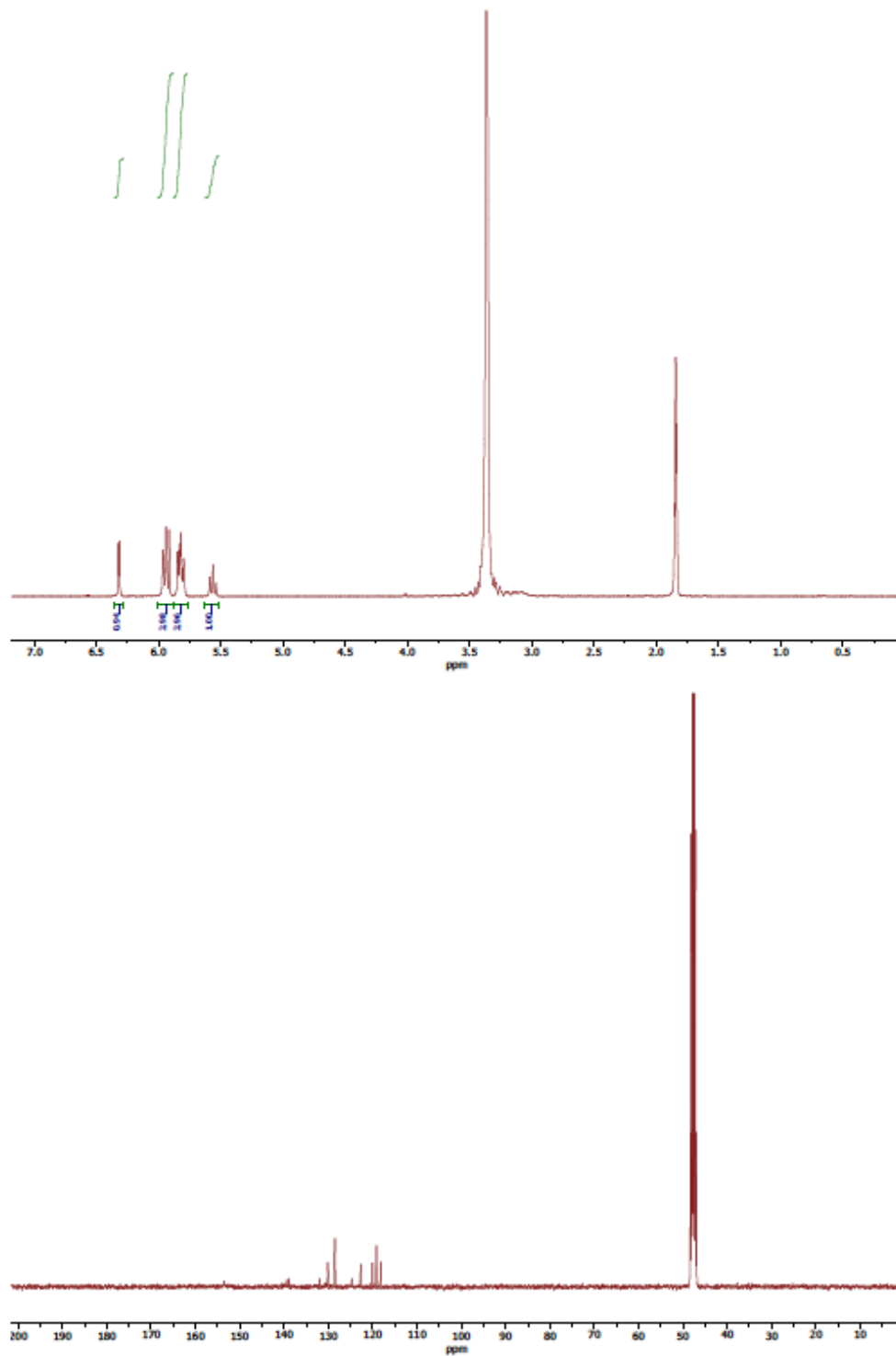


Figure 5.20. (upper) ^1H NMR (CD_3OD , 400 MHz) spectrum of di-CC. (lower) ^{13}C NMR (CD_3OD , 100 MHz) spectrum of di-CC.

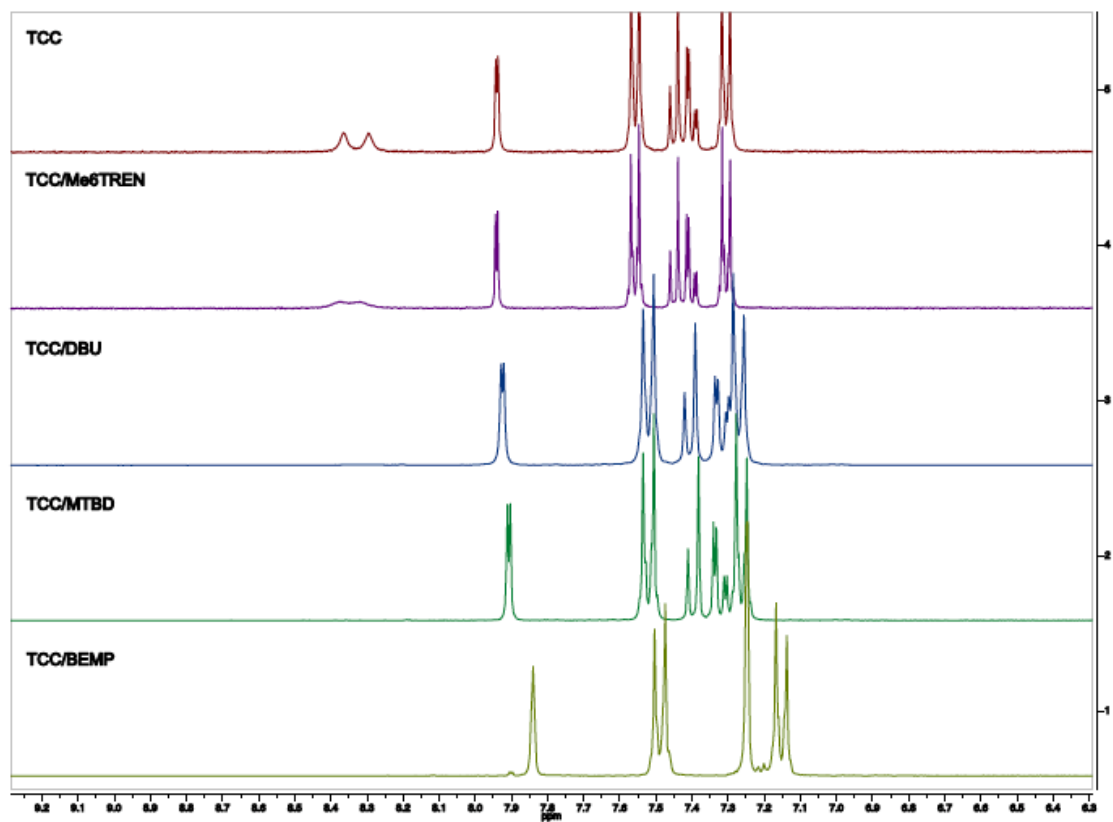


Figure 5.21. Downfield portion of the ¹H NMR spectra of TCC plus base ([TCC] = [base] = 5 mM) in acetone-*d*₆.

5.7. References

- (1) Kieseewetter, M. K.; Shin, E. J.; Hedrick, J. L.; Waymouth, R. M. Organocatalysis: Opportunities and Challenges for Polymer Synthesis. *Macromolecules* **2010**, *43*, 2093–2107.
- (2) Kamber, N. E.; Jeong, W.; Waymouth, R. M.; Pratt, R. C.; Lohmeijer, B. G. G.; Hedrick, J. L. Organocatalytic Ring-Opening Polymerization. *Chem. Rev.* **2007**, *107*, 5813–5840.
- (3) Pratt, R. C.; Lohmeijer, B. G. G.; Long, D. A.; Lundberg, P. N. P.; Dove, A. P.; Li, H.; Wade, C. G.; Waymouth, R. M.; Hedrick, J. L. Exploration, Optimization, and Application of Supramolecular Thiourea–Amine Catalysts for the Synthesis of Lactide (Co)polymers. *Macromolecules* **2006**, *39*, 7863–7871.
- (4) Kazakov, O. I.; Datta, P. P.; Isajani, M.; Kieseewetter, E. T.; Kieseewetter, M. K. Cooperative Hydrogen-Bond Pairing in Organocatalytic Ring-Opening Polymerization. *Macromolecules* **2014**, *47*, 7463–7468.
- (5) Csihony, S.; Culkin, D. A.; Sentman, A. C.; Dove, A. P.; Waymouth, R. M.; Hedrick, J. L. Single-Component Catalyst/initiators for the Organocatalytic Ring-Opening Polymerization of Lactide. *J. Am. Chem. Soc.* **2005**, *127*, 9079–9084.
- (6) McKinlay, C. J.; Waymouth, R. M.; Wender, P. A. Cell- Penetrating, Guanidinium-Rich Oligophosphoesters: Effective and Versatile Molecular Transporters for Drug and Probe Delivery. *J. Am. Chem. Soc.* **2016**, *138*, 3510–3517.
- (7) Blake, T. R.; Waymouth, R. M. Organocatalytic Ring-Opening Polymerization of Morpholinones: New Strategies to Functionalized Polyesters. *J. Am. Chem. Soc.* **2014**, *136*, 9252–9255.

- (8) Miyake, G. M.; Chen, E. Y. X. Cinchona Alkaloids as Stereoselective Organocatalysts for the Partial Kinetic Resolution Polymerization of Rac-Lactide. *Macromolecules* **2011**, *44*, 4116–4124.
- (9) (a) Naumann, S.; Scholten, P. B. V.; Wilson, J. A.; Dove, A. P. Dual Catalysis for Selective Ring-Opening Polymerization of Lactones: Evolution toward Simplicity. *J. Am. Chem. Soc.* **2015**, *137*, 14439–14445. (b) Xu, S.; Sun, H.; Liu, J.; Xu, J.; Pan, X.; Dong, H.; Liu, Y.; Li, Z.; Guo, K. Internal Lewis pair enhanced H-bond donor: boronateurea and tertiary amine co-catalysis in ring-opening polymerization. *Polym. Chem.* **2016**, *7*, 6843.
- (10) Zhang, X.; Jones, G. O.; Hedrick, J. L.; Waymouth, R. M. Fast and Selective Ring-Opening Polymerizations by Alkoxides and Thioureas. *Nat. Chem.* **2016**, *8*, 1047–1053.
- (11) Guillaume, S. M.; Kirillov, E.; Sarazin, Y.; Carpentier, J. F. Beyond Stereoselectivity, Switchable Catalysis: Some of the Last Frontier Challenges in Ring-Opening Polymerization of Cyclic Esters. *Chem. - Eur. J.* **2015**, *21*, 7988–8003.
- (12) Lin, B.; Waymouth, R. M. Urea Anions: Simple, Fast, and Selective Catalysts for Ring-Opening Polymerizations. *J. Am. Chem. Soc.* **2017**, *139*, 1645–1652.
- (13) Fastnacht, K. V.; Spink, S. S.; Dharmaratne, N. U.; Pothupitiya, J. U.; Datta, P. P.; Kiesewetter, E. T.; Kiesewetter, M. K. Bis- and Tris-Urea H-Bond Donors for Ring-Opening Polymerization: Unprecedented Activity and Control from an Organocatalyst. *ACS Macro Lett.* **2016**, *5*, 982–986.
- (14) Kolb, H. C.; Finn, M. G.; Sharpless, K. B. Click Chemistry: Diverse Chemical Function from a Few Good Reactions. *Angew. Chem., Int. Ed.* **2001**, *40*, 2004–2021.

- (15) Dove, A. P.; Pratt, R. C.; Lohmeijer, B. G. G.; Waymouth, R. M.; Hedrick, J. L. Thiourea-Based Bifunctional Organocatalysis: Supramolecular Recognition for Living Polymerization. *J. Am. Chem. Soc.* **2005**, *127*, 13798–13799.
- (16) Erickson, B. E. FDA Bans Antibacterials in Consumers Soaps. *Chem. Eng. News* **2016**, *94*, 16.
- (17) DeLeo, P. C.; Sedlak, R. I. Comment on “On the Need and Speed of Regulating Triclosan and Triclocarban in the United States. *Environ. Sci. Technol.* **2014**, *48*, 11021–11022.
- (18) Pycke, B. F. G.; Roll, I. B.; Brownawell, B. J.; Kinney, C. A.; Furlong, E. T.; Kolpin, D. W.; Halden, R. U. Transformation Products and Human Metabolites of Triclocarban and Triclosan in Sewage Sludge across the United States. *Environ. Sci. Technol.* **2014**, *48*, 7881–7890.
- (19) Pycke, B. F. G.; Geer, L. A.; Dalloul, M.; Abulafia, O.; Jenck, A. M.; Halden, R. U. Human Fetal Exposure to Triclosan and Triclocarban in an Urban Population from Brooklyn, New York. *Environ. Sci. Technol.* **2014**, *48*, 8831–8838.
- (20) Doyle, A. G.; Jacobsen, E. N. Small-Molecule H-Bond Donors in Asymmetric Catalysis. *Chem. Rev.* **2007**, *107*, 5713–5743.
- (21) Kazakov, O. I.; Kiesewetter, M. K. Cocatalyst Binding Effects in Organocatalytic Ring-Opening Polymerization of L-Lactide. *Macromolecules* **2015**, *48*, 6121–6126.
- (22) Coady, D. J.; Engler, A. C.; Horn, H. W.; Bajjuri, K. M.; Fukushima, K.; Jones, G. O.; Nelson, A.; Rice, J. E.; Hedrick, J. L. Catalyst Chelation Effects in Organocatalyzed Ring-Opening Polymerization of Lactide. *ACS Macro Lett.* **2012**, *1*, 19–22.

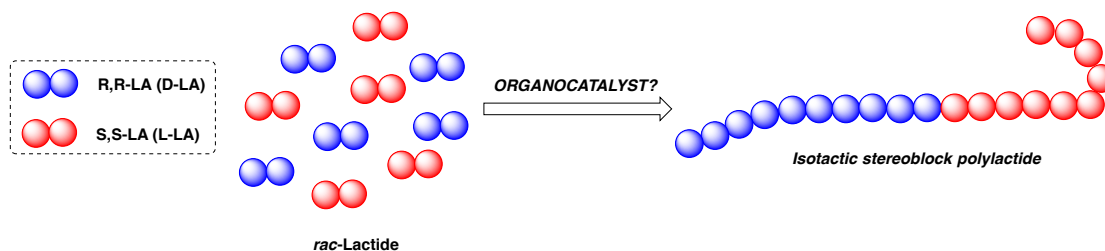
- (23) Spink, S. S.; Kazakov, O. I.; Kiesewetter, E. T.; Kiesewetter, M. K. Rate Accelerated Organocatalytic Ring-Opening Polymerization of L-Lactide via the Application of a Bis(thiourea) H-Bond Donating Cocatalyst. *Macromolecules* **2015**, *48*, 6127–6131.
- (24) Lohmeijer, B. G. G.; Pratt, R. C.; Leibfarth, F.; Logan, J. W.; Long, D. A.; Dove, A. P.; Nederberg, F.; Choi, J.; Wade, C.; Waymouth, R. M.; Hedrick, J. L. Guanidine and Amidine Organocatalysts for Ring-Opening Polymerization of Cyclic Esters. *Macromolecules* **2006**, *39*, 8574–8583.
- (25) Kulkarni, A. R.; Garai, S.; Thakur, G. A. Scalable, One-Pot, Microwave-Accelerated Tandem Synthesis of Unsymmetrical Urea Derivatives. *J. Org. Chem.* **2017**, *82*, 992.
- (26) Beaver, D. J.; Roman, D. P.; Stoffel, P. J. The Preparation and Bacteriostatic Activity of Substituted Ureas. *J. Am. Chem. Soc.* **1957**, *79*, 1236–1245.
- (27) Lippert, K. M.; Hof, K.; Gerbig, D.; Ley, D.; Hausmann, H.; Guenther, S.; Schreiner, P. R. Hydrogen-Bonding Thiourea Organocatalysts: The Privileged 3,5-Bis(trifluoromethyl)phenyl Group. *Eur. J. Org. Chem.* **2012**, *30*, 5919–5927.
- (28) Zhang, Z.; Schreiner, P. R. (Thio)urea Organocatalysis—What Can Be Learnt from Anion Recognition? *Chem. Soc. Rev.* **2009**, *38*, 1187–1198.
- (29) Datta, P. P.; Kiesewetter, M. K. Controlled Organocatalytic Ring-Opening Polymerization of ϵ -Thionocaprolactone. *Macromolecules* **2016**, *49*, 774–780.
- (30) Bannin, T. J.; Kiesewetter, M. K. Poly(thioester) by Organocatalytic Ring-Opening Polymerization. *Macromolecules* **2015**, *48* (16), 5481–5486.
- (31) Schwesinger, R.; Schlempep, H.; Hasenfratz, C.; Willaredt, J.; Dambacher, T.; Breuer, T.; Ottaway, C.; Fletschinger, M.; Boele, J.; Fritz, H.; Putzas, D.; Rotter, H. W.; Bordwell,

- F. G.; Satish, A. V.; Ji, G.; Peters, E.; Peters, K.; Schnering, H. G. V.; Walz, L. Extremely Strong, Uncharged Auxiliary Bases; Monomeric and Polymer-Supported Polyaminophosphazenes (P2-P5). *Liebigs Ann.* **1996**, *1996*, 1055–1081.
- (32) Kaljurand, I.; Kütt, A.; Sooväli, L.; Rodima, T.; Mäemets, V.; Leito, I.; Koppel, I. A. Extension of the Self-Consistent Spectrophotometric Basicity Scale in Acetonitrile to a Full Span of 28 pKa Units: Unification of Different Basicity Scales. *J. Org. Chem.* **2005**, *70*, 1019–1028.
- (33) Webb, J. E. A.; Crossley, M. J.; Turner, P.; Thordarson, P. Pyromellitimide Aggregates and Their Response to Anion Stimuli. *J. Am. Chem. Soc.* **2007**, *129*, 7155.
- (34) Thordarson, P. Determining association constants from titration experiments in supramolecular chemistry. *Chem. Soc. Rev.* **2011**, *40*, 1305.
- (35) Deranleau, D. A. Theory of the measurement of weak molecular complexes. II. Consequences of multiple equilibria. *J. Am. Chem. Soc.* **1969**, *91*, 4044.
- (36) Horman, I.; Dreux, B. Estimation of association constants of bimolecular complexes. Reply to comments. *Anal. Chem.* **1983**, *55*, 1219.
- (37) Peters, S. J.; Stevenson, C. D. The Complexation of Na⁺ by 18-crown -6 studied via nuclear magnetic resonance. *J. Chem. Educ.* **2004**, *81*, 715.
- (38) Lee, H-G.; Kim, M-J.; Park, S-E.; Kin, J-J.; Kim, B. R.; Lee, S-G.; Yoon, Y-J. Phenyl 4,5-dichloro-6-oxopyridazine-1(6H)-carboxylate as carbonyl source: facile and selective synthesis of carbamates and ureas under mild conditions. *Synlett* **2009**, *17*, 2809.
- (39) Khan, K. M.; Saeed, S.; Ali, M.; Gohar, M.; Zahid, J.; Khan, A.; Perveen, S.; Choudhary, M. I. Unsymmetrically disubstituted urea derivatives: A potent class of antiglycating agents. *Bioorg. Med. Chem.* **2009**, *17*, 2447.

INTENTIONALLY BLANK PAGE

Chapter 6

Effects of Catalysts on Polymer Tacticity in Ring-Opening Polymerization of *rac*-Lactide



6.1 Abstract

A slate of thiourea (TU) hydrogen-bonding (H-bonding) catalysts exhibited various effects on the tacticity of polymers obtained upon ring-opening polymerization (ROP) of *rac*-lactide (*rac*-LA). The catalysts involved in the study differed based on TU H-bonding functionalities connected to diverse chiral groups in one molecule. The impact of the functional groups on catalyst performance was investigated. Depending on the structural features comprising the screened catalysts, various isotacticity patterns (expressed by the probability of isotactic enchainment, P_m) were achieved in resulting poly-*rac*-lactides (PracLAs). The study ushers the way towards generation of selective H-bonding catalytic systems for stereocontrolled ROP of *rac*-LA.

6.2 Introduction

The field of ROP with TU-based catalysts has experienced substantial growth and witnessed a number of breakthroughs capable of advancing the field since its recent genesis.^{1,2,3} Utilization of TU catalytic systems in ROP of cyclic esters showcased, as a

significant achievement, an opportunity to carry out traditional ROP without metal-based catalysts.¹ Exquisite precision in polymerization control was a great benefit in the generation of polymeric materials for fine applications (microelectronics, biomedical devices) despite the manageable deficiencies, such as only a fledgling monomer pool for effective ROP by organocatalysts, inability to conduct enantioselective polymerization, and economic difficulties associated with organocatalytic ROP implementation on a wide industrial scale.^{1,2} The state of the art of TU H-bonding catalysis changed substantially in the past decade. The monomers pool for controlled ROP deepened significantly,^{4,5} the TU catalytic systems underwent designer changes targeted to introduce faster yet controlled catalysis unfathomable before in the slate of organocatalytic systems for ROP.^{6,7} One of the tasks still to be addressed is stereoselective ring-opening polymerization of racemic monomers.^{8,9,10} The importance of stereoselective ROP lies in the ability thereof to afford a variety of polymer architectures depending on the arrangement of stereocenters in the polymer backbone.^{11,12} For example, polymerization of *rac*-LA can afford an array of stereoregular polymers, such as syndiotactic, heterotactic, and isotactic kinds.^{11,12} All of these polymeric species are differentiated on the basis of stereocenters sequenced in the polymer chain. Positioning of stereocenters at the microlevel leads to drastically different physical properties of the respective polymers at the macrolevel.¹³ For instance, the melting points T_m for various lactide stereopolymers vary widely: $T_m = 100$ °C for heterotactic PLA, $T_m = 140$ °C for syndiotactic PLA, $T_m = 160$ °C for purely isotactic L- or D-PLA, and $T_m = 220$ °C for isotactic stereoblock PLA.¹³ The variable physical properties of PLAs differing in the sequence of stereocenters in the polymer backbone are very valuable from the standpoint of industrial applications of such polymers.¹⁴ That makes the goal of

harnessing control over the stereocenters sequencing in PLA a lucrative one to pursue.

6.3 Results and Discussion

Efforts aimed at the kinetic resolution of chiral cyclic esters are well-known.^{16, 17} Previous works devoted to chain-end controlled^{15, 18, 19} and catalyst-controlled²⁰⁻²³ dynamic kinetic resolution (DKR) ROP of *rac*-LA provide the foundation for the expansion of armamentarium of methodologies of stereoselective ROP of *rac*-LA. A wide range of hydrogen-bonding catalysts (figure 6.1) was screened as candidates for stereoselective ROP of *rac*-LA. Both commercially available and newly synthesized catalysts were employed in the study and important structure-activity relationships impacting the resulting polymeric products were revealed.

The polymer analysis was carried out using decoupled ¹H NMR spectroscopic experiments using the established methods.^{12,15} The region of the polymer in the NMR spectrum corresponding to different stereosequences was noted, the respective peaks were fitted¹⁵ under the spectrum region using the MNova NMR software, and the probability for isotactic enchainment in the polymer, P_m , was calculated according to Bernoullian statistics.^{12,15}

6.3.1 Catalysts Screening

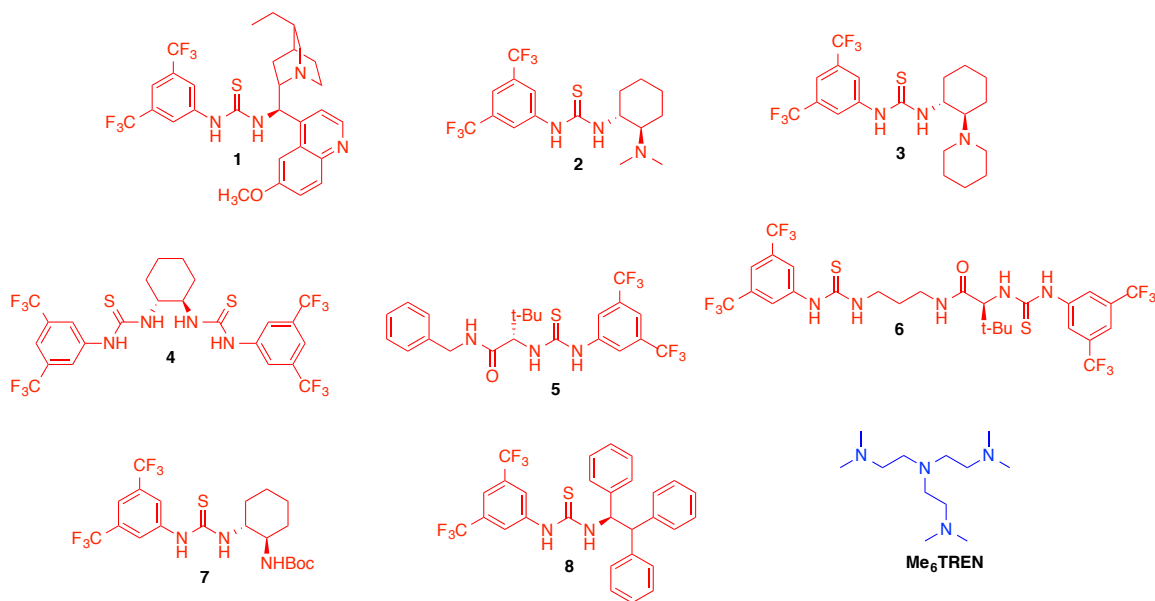


Figure 6.1. Chiral TU catalysts applied in the study.

Small molecule mediated asymmetric synthesis is well-established and offers a wide assortment of catalysts.²⁴ First, commercially available TU catalysts were applied for ROP of *rac*-LA in our study. The catalyst screening commenced with the chiral alkaloid based TU **1** that, satisfyingly, produced a poly-*rac*-LA (*Prac*LA) with $P_m = 0.81$! Since the precedent of H-bonding chiral resolving agents for cyclic esters exists^{16,17}, we decided to subject **1** to the respective experiment to elucidate its *rac*-LA resolution ability. The catalyst was combined with *rac*-LA in the 1:1 ratio (10 mM each) in an NMR tube in chloroform-*d*, and the ¹H NMR signal of the *rac*-LA methine protons was noted. To our delight, the splitting of the quartet was observed (figure 6.2), signifying possible formation of the complex between **1** and either enantiomer of *rac*-LA. Such complexation may signify the propensity of **1** for DKR ROP of *rac*-LA. It should be noted that in our catalyst screening only **1** demonstrated the *rac*-LA methine signal resolution.

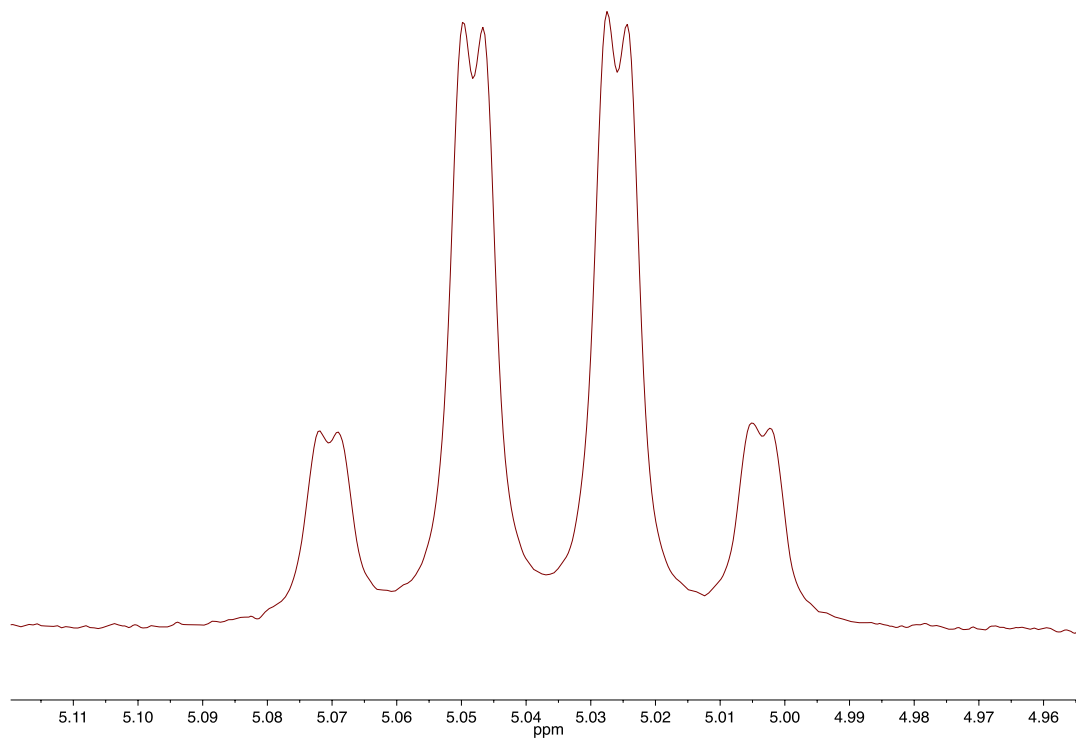


Figure 6.2. Resolution of *rac*-LA methine protons signal by **1** ($[rac\text{-LA}] = [\mathbf{1}] = 10 \text{ mM}$, chloroform-*d*, ^1H NMR, 300 MHz).

Inspired by this result, we turned our attention to the distinguished Takemoto catalyst **2** that demonstrated high efficiency in a range of small-molecule transformations.²⁵ The performance of **2** in ROP of *rac*-LA proved modest with the *Prac*LA showing $P_m = 0.61$.

We continued with assessment of structure-property relationships in the H-bonding catalysts slate. Catalyst **7** gave $P_m = 0.59$ (table 6.1) despite our guess that the large size of the Boc group may enhance the ROP control. However, a switch from the Boc to piperidinyll derivative **3** of Takemoto catalyst yielded a *Prac*LA with a higher $P_m = 0.71$, compared with catalyst **2**. Continuing with the notion of steric bulk increase and based on

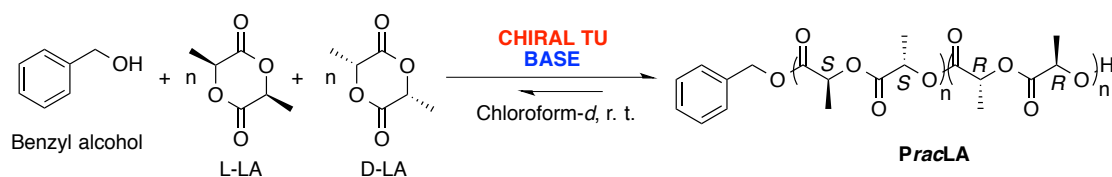
our previous rate-acceleration studies with TU catalysts,⁶ we carried out ROP of *rac*-LA, catalyzed by 2:Me₆TREN = 2:1. Gratifyingly, we were able to observe the ROP rate acceleration alongside a marked increase in isotacticity of the resulting *Prac*LA with P_m = 0.75. Interestingly, the bis-TU Nagasawa catalyst **4** did not bring about the desired P_m value increase (table 6.1). The performance of catalyst **8** possessing a bulky triaryl chiral group yielded, at the highest, P_m = 0.65 within the ROP's mediated by **8** (see ES).

A range of TU catalysts developed by Jacobsen proved to be efficient for a variety of small molecule asymmetric transformations.²⁴ Thus we selected one of Jacobsen's catalysts²⁶ - **5** - to be applied for a macromolecular transformation. However, ROP of *rac*-LA mediated by this catalyst yielded *Prac*LA with rather modest P_m = 0.61.

Having the brief screening of commercial candidates completed, we transitioned to the synthetic efforts. We decided to widen the catalyst scope by engendering new candidates for stereoselective ROP of *rac*-LA.

Our group disclosed an achiral bis-TU catalyst that proved to be a great mediator for ROP of L-LA - both fast in terms of the ROP rate and selective to the monomer.⁶ Therefore, we decided to explore the bis-TU functionality fusion with a chiral locus in one molecule (scheme 6.1) to attempt rate-accelerated *and* stereoselective ROP of *rac*-LA. The designed synthetic procedures (see ES) successfully furnished the (first in our lab) chiral bis-TU catalyst **6** (figure 6.1).

The chiral bis-TU **6** was applied for the ROP of *rac*-LA. In accord with our expectation, the polymerization proceeded in a faster manner (table 6.1) compared to other catalysts in the set. To our gladdening, when the obtained *Prac*LA was subjected to ¹H decoupled NMR analysis, a good P_m = 0.80 was calculated for the resulting polymer.

Table 6.1. ROP of *rac*-LA catalyzed by chiral TU's.

Entry	Catalyst	M/I/C/B, mol. %	Conversion, %	Time, h	P _m
1	1	100/1/5/5	88	120	0.81
2	2	100/1/5/5	58	24	0.61
3 ^a	2	100/1/10/5	88	58	0.75
4	3	100/1/5/5	96	89	0.71
5 ^b	4	100/1/5/5	88	120	0.64
6	5	100/2/5/5	40	144	0.61
7 ^c	6	100/1/1.66/1.66	94	28	0.80
8	7	100/1/5/5	83	308	0.59

Notes. I = initiator (benzyl alcohol), C = TU catalyst, B = base (Me₆TREN), M = monomer (*rac*-LA). All polymerizations were performed at room temperature, chloroform-*d* was used as a solvent, [*rac*-LA] = 1.0 M. ^{a,c}[M] = 0.95 M. ^bB = (+)-Sparteine.

Table 6.2. Solvent and base screen for ROP of *rac*-LA^a catalyzed by **1**.

Entry	Solvent	Base	Conversion, %	Time, h	P _m
1	Chloroform- <i>d</i>	Me ₆ TREN	88	120	0.81
2	Dichloromethane	Me ₆ TREN	50	70	0.71
3	Chloroform- <i>d</i>	(+)-Sparteine	99	28	0.67
4	THF	Me ₆ TREN	83	124	0.52

Notes. I = initiator (benzyl alcohol), C = TU catalyst, B = base (Me₆TREN), M = monomer (*rac*-LA). ^aAll polymerizations were performed at room temperature, [*rac*-LA] = 1.0 M, M/I/C/B, mol. % = 100/1/5/5.

Mechanistically, our intent was to use the TU motif as the activator of the monomer,¹⁵ whereas the chiral group attached to the given motif would promote dynamic kinetic resolution^{21,22} via catalyst control in ROP of *rac*-LA. ¹H NMR decoupled methine protons signals of PracLA revealed the ratio of the five tetrad peaks constituting such signals could be fit into the statistical model corresponding to the chain-end control mechanism.¹⁵ Thus, no catalyst control for these polymerizations can be proposed. The

increase in the P_m values when going from small to larger substituents in the chiral locus may be attributed to the crowded environment created at the growing chain end, that leads to the reduction of randomness in the addition of the LA enantiomers to the growing polymer chain. Hence, isotactic enchainment will be brought about.

6.4 Conclusion

The wide variety of H-bonding TU-based catalysts alongside with the flexibility of their functionalization brings forth an arsenal of small molecules that can be aimed at different goals, from small molecule transformations to polymerizations. The given project focused on surveying various chiral TU catalysts and assessing their structure-property relationships to achieve the ultimate goal of stereoselective polymerization of *rac*-LA via DKR. Based on the empirical observations, a new chiral bis-TU catalyst was developed and successfully implemented for the rate-accelerated ROP of *rac*-LA, generating a highly isotactic polymer. The resulting polymeric products, obtained via mediation by the developed catalysts, possessed a range of P_m values spanning from moderate ~ 0.6 to good ~ 0.8 . The ultimate goal of stereoselective DKR polymerization of *rac*-LA and production of highly isotactic *Prac*LAs is yet to be achieved. It was possible to explore a number of iterations that can potentially lead us to the grand aim. The mechanistic efforts towards the chiral bis-TU catalyst optimization are currently underway in our laboratory. We envision the eventual fulfillment of the goal of stereoselective DKR ROP of *rac*-LA through the application of novel organocatalysts.

6.5 Experimental Section

6.5.1 General Considerations

All chemicals were used as purchased except stated otherwise. *N,N,N',N'*-Tetramethyl-*O*-(1*H*-benzotriazol-1-yl)uronium hexafluorophosphate (HBTU) was purchased from Matrix Scientific. Triethylamine (TEA) was purchased from Sigma-Aldrich. 4 N HCl solution in 1,4-dioxane was purchased from Acros Organics. Tris[2-(dimethylamino)ethyl]amine (Me₆TREN) was purchased from Alfa Aesar. Benzyl alcohol, benzoic acid, methylene chloride, and hexanes were purchased from Fisher Scientific. Benzyl alcohol was distilled under high vacuum using calcium hydride. Methylene chloride (DCM) and tetrahydrofuran (THF) were dried on an Innovative Technology solvent purification system. *rac*-Lactide was purchased from Acros Organics and recrystallized using toluene. Chloroform-*d* was purchased from Cambridge Isotope Laboratories and distilled using calcium hydride under high vacuum. Experiments were conducted in an MBRAUN stainless steel glovebox under a nitrogen atmosphere. Routine ¹H and ¹³C NMR experiments were conducted on Bruker Avance III 300 MHz or 400 MHz spectrometers. Decoupled ¹H NMR experiments were conducted on a Varian 500 MHz spectrometer.

6.5.2 Example Ring-Opening Polymerization of *rac*-Lactide

The first 7 mL vial was charged with CA-TU (14.9 mg, 0.025 mmol), Me₆TREN (6.68 μL, 0.025 mmol), and benzyl alcohol (0.52 μL, 0.005 mmol). The second 7 mL vial was charged with *rac*-LA (72.1 mg, 0.5 mmol) and chloroform-*d* (500 μL). The contents

of the second vial were added to the first vial and the resulting mixture was vigorously shaken until homogenous whilst the vial with the mixture was closed. The obtained reaction mixture was transferred to an NMR tube, capped, and the reaction progress was monitored by NMR spectrometry. When the desired conversion of the monomer to polymer was achieved as determined by NMR spectrometry, the contents of the tube were promptly transferred into a clean vial and the reaction was quenched with at least 2 equivalents of benzoic acid to the amount of Me₆TREN. The solvent was removed by rotary evaporations, the residue was dissolved in the minimal amount of dichloromethane to obtain a homogenous solution and the synthesized polymer was precipitated with addition of hexanes. The liquids were decanted and precipitate was subjected to high vacuum to remove volatiles. The dried polymer was later washed with methanol, subjected to high vacuum, and underwent decoupled ¹H NMR analysis to determine the probability of isotactic enchainment (P_m).

Tetrad	Chemical shift, ppm	Probability
mmm	5.195	$P_m^2 + 0.5P_rP_m$
mnr	5.206	$0.5P_rP_m$
rmm	5.238	$0.5P_rP_m$
rmr	5.247	$0.5P_r^2$
mrm	5.184	$0.5(P_m^2 + P_rP_m)$

Where:

$$P_r = 1 - P_m.$$

Tetrad	Calculated	Spectrum	Weighted error	Fitted areas	Relative areas
mmm	0.791	0.793	0.029	25002	0.793
mnr	0.062	0.000	0.000	0	0.000
rmm	0.062	0.114	2.993	3587	0.114
rmr	0.011	0.021	0.021	656	0.021
mrm	0.073	0.072	0.000	2282	0.072
Sum	1.000	1.000	3.04	31527	1.000

$$P_m = 0.85.$$

In Microsoft Excel, the application of the “Solver” functionality allows to minimize the “Weighted error” by varying the P_m value.

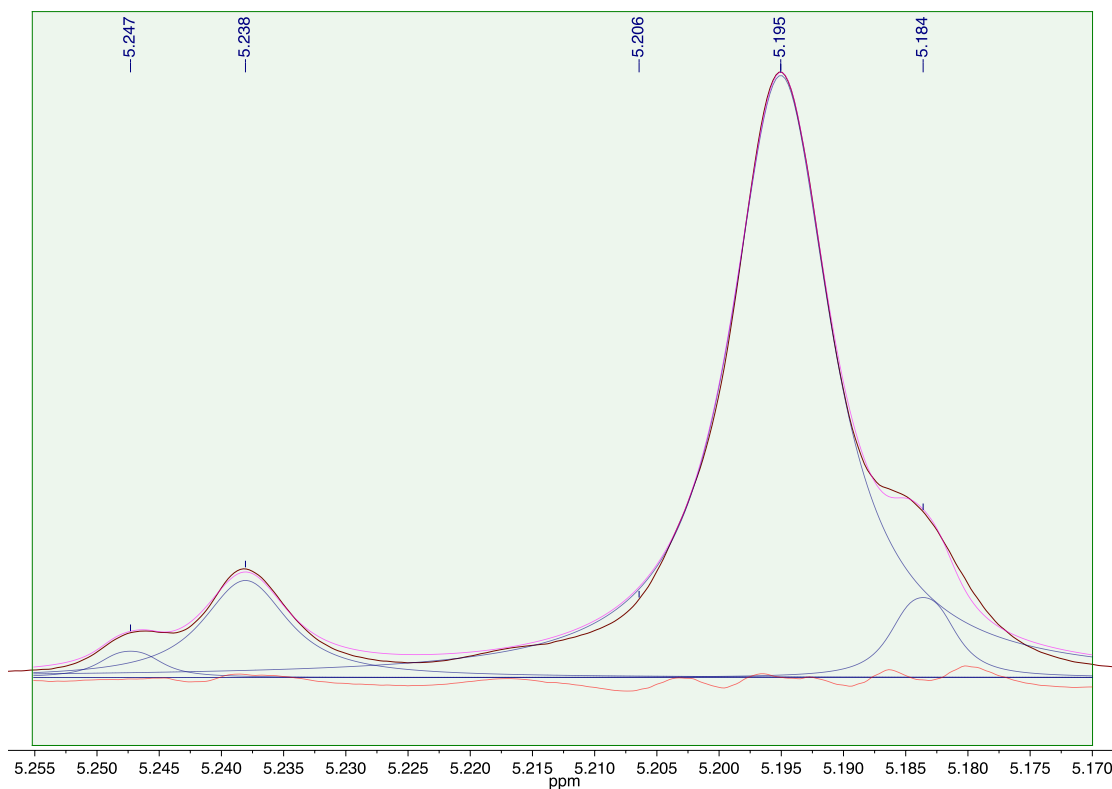


Figure 6.3. Example fitted methine protons signal of *PracLA* in homonuclear decoupled ^1H NMR for P_m calculations (table above), (500 MHz, chloroform-*d*).

6.5.3 Preparation of Catalyst 3

A 25 mL flame-dried Schlenk flask was charged with dry DCM (8 mL), then (1*R*, 2*R*)-*trans*-2-(1-piperidiny)cyclohexylamine (674 mg, 3.70 mmol) was added. The mixture was stirred under a static blanket of nitrogen until homogeneous and 3,5-bistrifluoromethylisothiocyanate (0.676 mL, 3.70 mmol) was added dropwise. The reaction mixture was stirred at ambient temperature under nitrogen overnight, the solvent was removed by rotary evaporation, and the residue was purified with column

chromatography using Methanol/DCM = 5/95 as an eluant, furnishing the target catalyst **3** (45%) as a white powder. Characterization matched the literature sources.²⁸

¹H NMR (300 MHz, CDCl₃, TMS): δ 10.08 (br s, 1H), 8.19 (s, 2H), 8.04 (br s, 1H), 7.72 (s, 1H), 4.18 (br s, 1H), 2.65 (m, 2H), 2.33 (m, 2H), 2.13 (m, 1H), 1.87 (m, 1H), 1.75 (m, 1H), 1.64 (m, 1H), 1.42 (m, 6H), 1.19 (m, 4H).

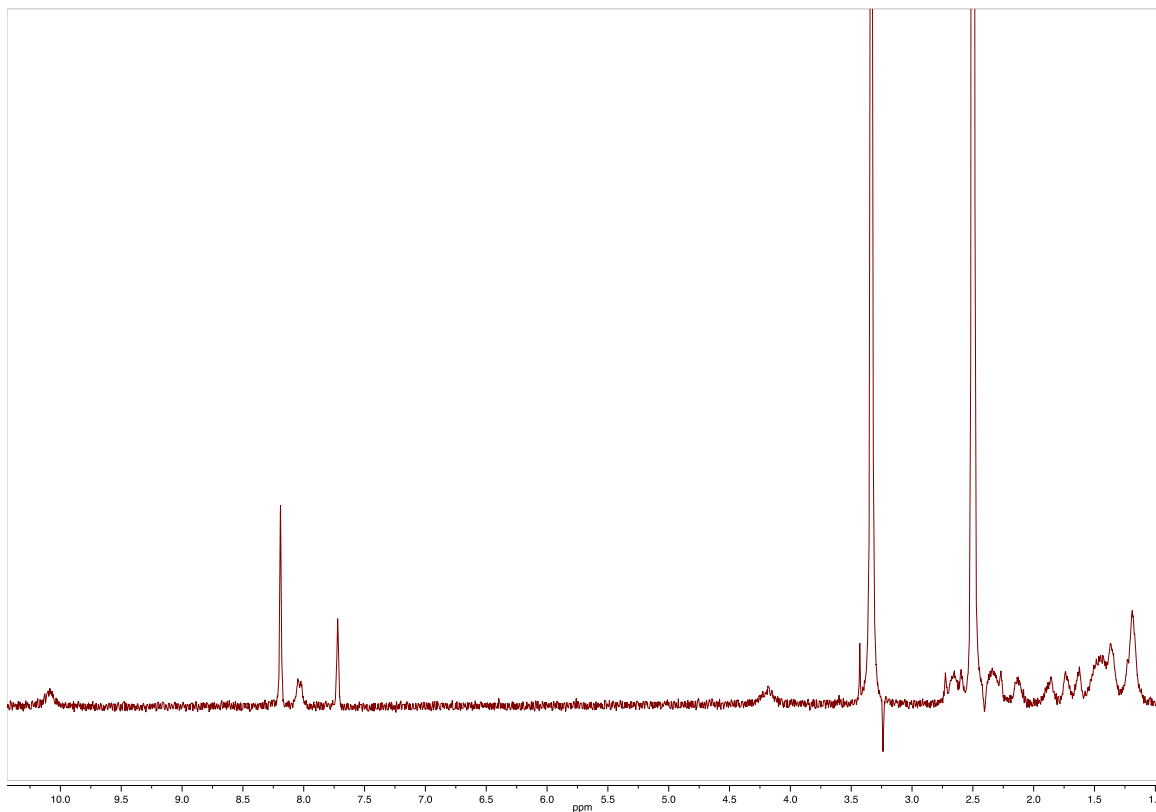


Figure 6.4. ¹H NMR of catalyst **3** (300 MHz, chloroform-*d*).

6.5.4 Preparation of Catalyst 4

A 25 mL flame-dried Schlenk flask was charged with dry THF (10 mL), then (1*R*, 2*R*)-(-)-1,2-diaminocyclohexane (0.868 mL, 0.76 mmol) was added. The mixture was stirred under a static blanket of nitrogen until homogeneous and 3,5-bistrifluoromethylisothiocyanate (0.28 mL, 1.52 mmol) was added dropwise. The reaction

mixture was stirred at ambient temperature under nitrogen overnight, the solvent was removed by rotary evaporation, and the residue was purified with column chromatography using EtOAc/Hexanes = 10/90 as an eluant, furnishing the target catalyst **4** as a white powder. Characterization matched the literature sources.²⁷

¹H NMR (300 MHz, DMSO-*d*₆, TMS): δ 7.80 (s, 4H), 7.71 (s, 2H), 6.93 (br s, 2H), 4.39 (br s, 2H), 2.21 (m, 2H), 1.82 (m, 4H), 1.36 (m, 4H).

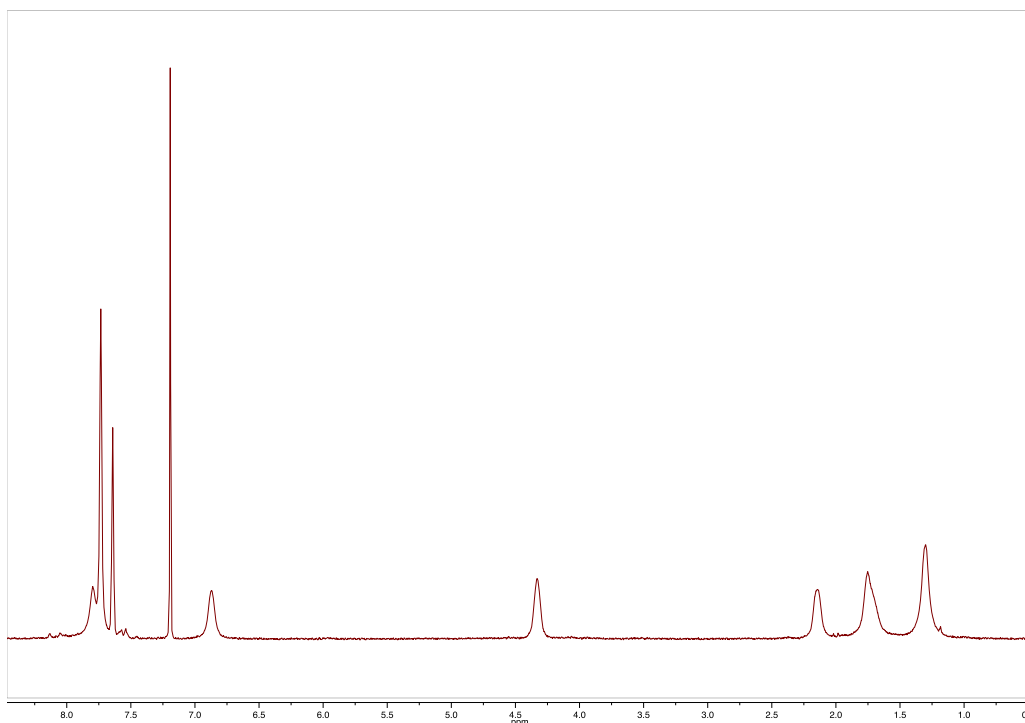
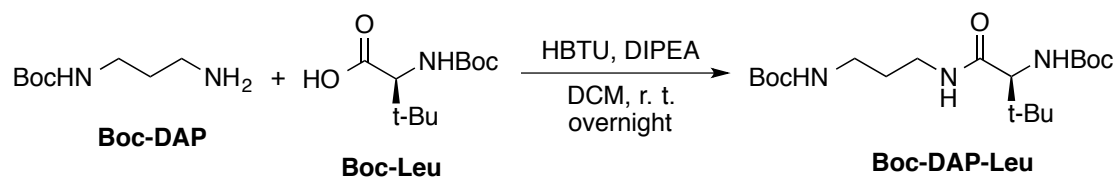


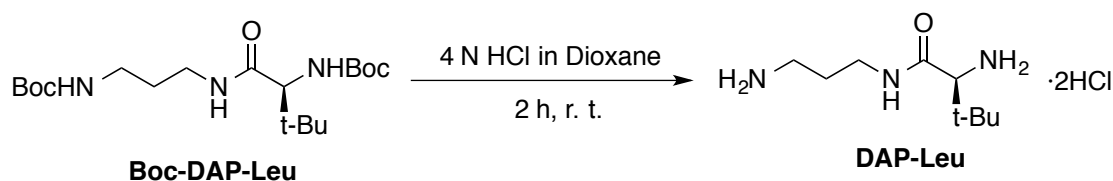
Figure 6.5. ¹H NMR of catalyst **4** (300 MHz, chloroform-*d*).

6.5.5 Preparation of Catalyst **6**



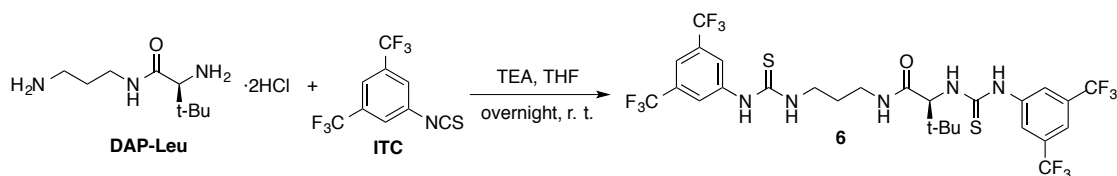
Intermediate product Boc-DAP-Leu was synthesized according to the adapted literature procedure.²⁹ A 25 mL flame-dried Schlenk flask was charged with dry DCM (10 mL). Next, Boc-Leu (100 mg, 0.43 mmol), HBTU (163.1 mg, 0.43 mmol), and DIPEA (0.23 mL, 1.29 mmol) were added to the flask and the reaction was stirred under nitrogen for 15 minutes. After that, Boc-DAP was added (0.082 mL, 0.47 mmol). The reaction mixture was stirred under nitrogen overnight. Afterwards, the reaction mixture was rotvaped, the residue was taken up in DCM, washed sequentially with 1 M aqueous solution of HCl (20 mL), saturated solution of sodium bicarbonate (20 mL), and brine (20 mL). The organic layer was dried with MgSO₄, separated from MgSO₄ via vacuum filtration, and the solvent was removed by rotary evaporation. The residue was purified with column chromatography on silica gel using ethyl acetate / hexanes = 3/1 as an eluant. The product appeared as off-white powder (81%).

¹H NMR (300 MHz, CDCl₃, TMS): δ 6.40 (br s, 1H), 5.28 (br s, 1H), 4.93 (br s, 1H), 3.81 (d, 1H), 3.30 (q, 2H), 3.16 (q, 2H), 1.61 (m, 2H), 1.43 (s, 18H), 0.99 (s, 9H).



Intermediate product DAP-Leu was synthesized according to the adapted literature procedure.²⁹ A 10 mL round bottom flask was charged with 4 N HCl in 1,4-dioxane (19.63 mmol of HCl), then Boc-DAP-Leu (586.9 mg, 1.51 mmol) was added and the reaction mixture was stirred for 2 hours. Next, the volatiles were removed via vacuum transfer. The residue was subjected to high vacuum. The off-white powder was obtained (91%) and used without further purification for subsequent transformations.

^1H NMR (300 MHz, CD_3OD , TMS): δ 3.54 (s, 1H), 3.36 (t, 2H), 3.00 (t, 2H), 1.91 (p, 2H), 1.09 (s, 9H).



A 50 mL flame-dried Schlenk flask was charged with dry THF (25 mL), then DAP-Leu (655.4 mg, 2.52 mmol) was added followed by TEA (2.1 mL, 15.12 mmol). The mixture was stirred under a static blanket of nitrogen for 10 minutes and ITC (0.97 mL, 5.29 mmol) was added dropwise. The reaction mixture was stirred at ambient temperature under nitrogen overnight, the solvent was removed by rotary evaporation, and the residue was purified with column chromatography using EtOAc/Hexanes = 2/3 as an eluant, and the eluted fraction with $R_f = 0.1$ furnished the target catalyst **6** (30%), as a white powder with a pale yellow tint.

^1H NMR (300 MHz, CDCl_3 , TMS): δ 8.71 (br s, 1H), 8.28 (br s, 1H), 7.87 (s, 2H), 7.78 (s, 2H), 7.67 (s, 1H), 7.61 (s, 1H), 7.14 (br s, 1H), 6.54 (br s, 1H), 4.77 (d, 1H), 3.73 (m, 2H), 3.32 (m, 2H), 1.78 (m, 2H), 1.04 (s, 9H).

^{13}C NMR (75 MHz, CDCl_3): δ 181.43, 180.86, 171.92, 139.44, 132.80, 132.35, 124.81, 124.10, 123.43, 121.19, 119.10, 67.09, 42.18, 36.86, 34.65, 32.44, 29.08, 27.12.

HRMS (m/z): calculated 729.1465 (for $\text{C}_{27}\text{H}_{27}\text{F}_{12}\text{N}_5\text{OS}_2$), found 728.1381 (negative ion mode ESI).

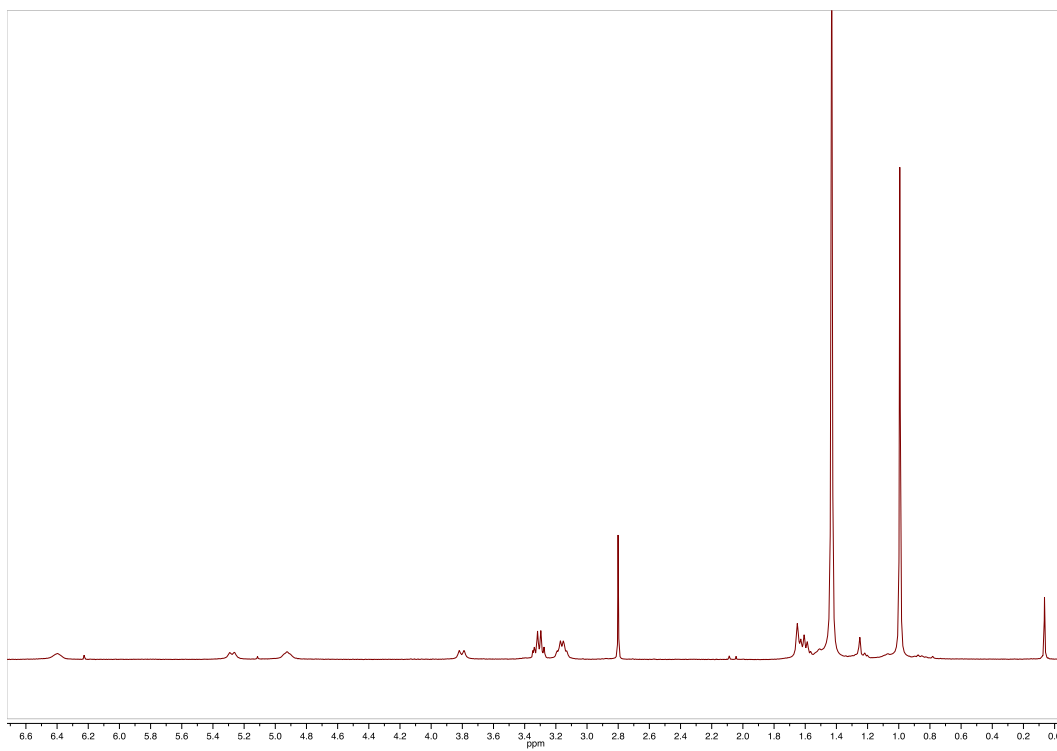


Figure 6.6. ¹H NMR of intermediate product Boc-DAP-Leu (300 MHz, chloroform-*d*).

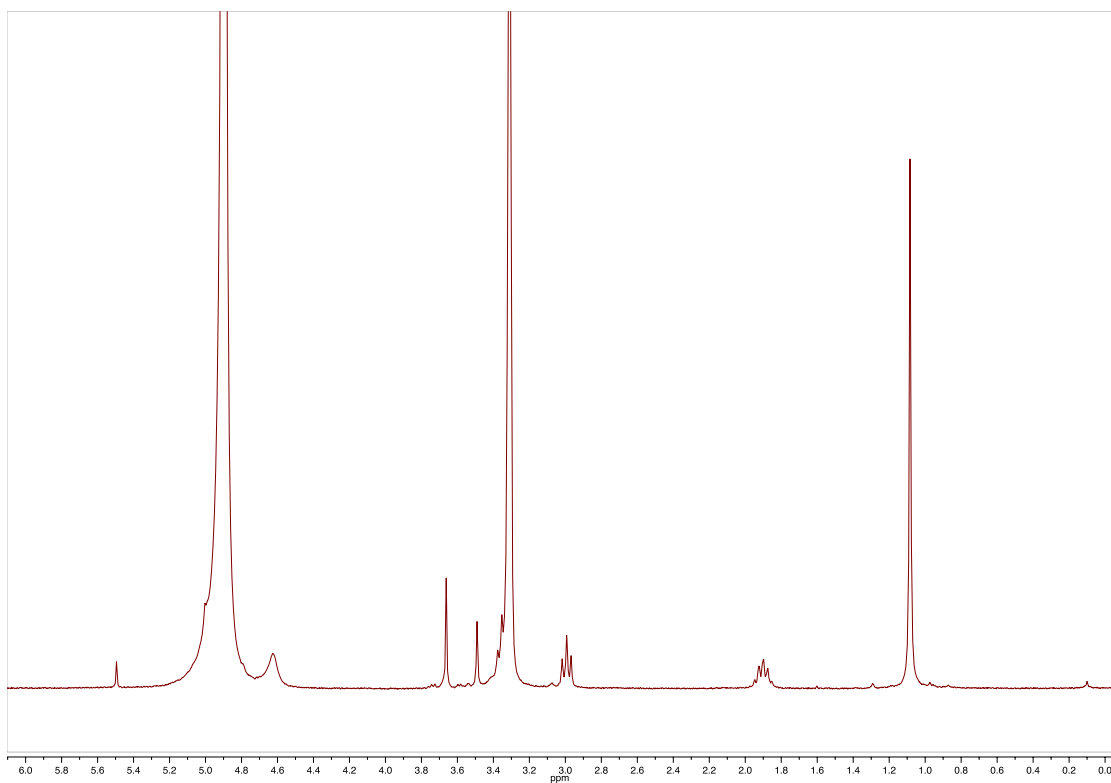


Figure 6.7. ¹H NMR of intermediate product DAP-Leu (300 MHz, methanol-*d*₄).

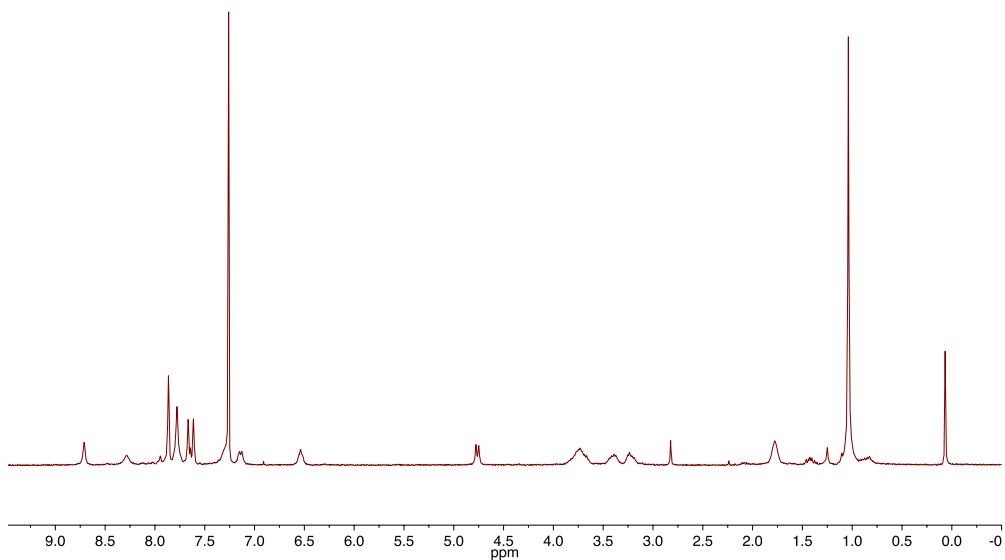


Figure 6.8. ^1H NMR of catalyst **6** (300 MHz, chloroform-*d*).

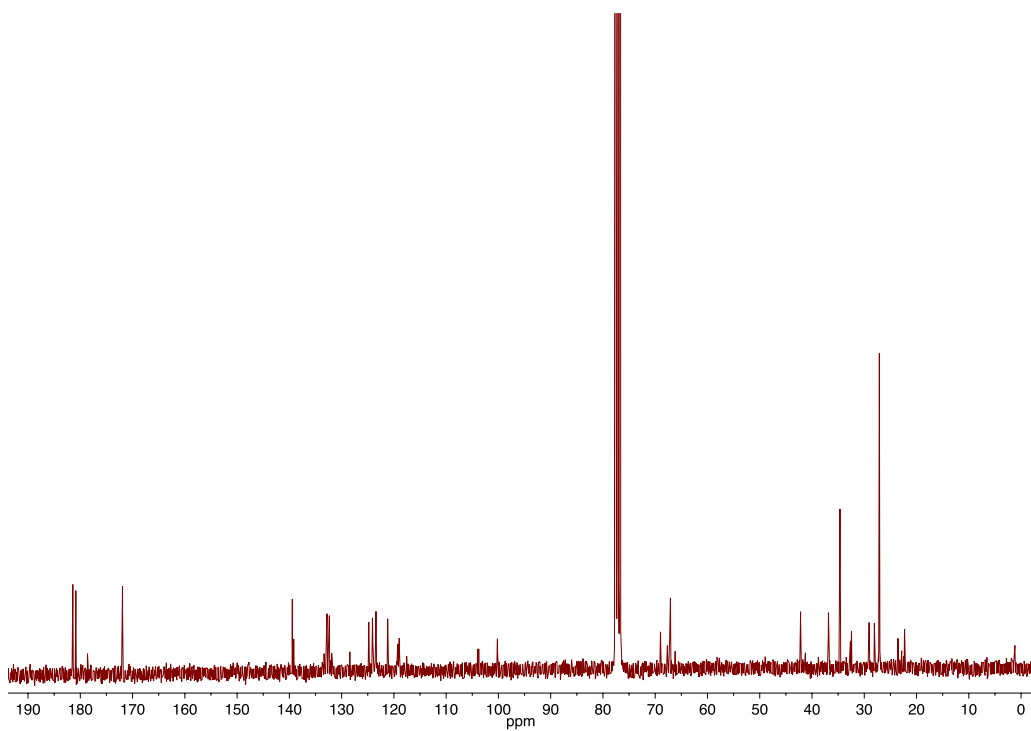


Figure 6.9. ^{13}C NMR of catalyst **6** (75 MHz, chloroform-*d*).

6.5.6 Preparation of catalyst 7

A 50 mL flame-dried Schlenk flask was charged with dry DCM (25 mL), then (1*R*, 2*R*)-*trans*-*N*-Boc-1,2-cyclohexanediamine (776 mg, 3.60 mmol) was added. The mixture was stirred under a static blanket of nitrogen until homogeneous and 3,5-bistrifluoromethylisothiocyanate (0.7 mL, 3.80 mmol) was added dropwise. The reaction mixture was stirred at ambient temperature under nitrogen overnight, the solvent was removed by rotary evaporation, and the residue was purified with column chromatography using EtOAc/Hexanes/TEA = 19/80/1 as an eluant, furnishing the target catalyst **7** (61%) as a white powder. Characterization matched the literature sources.²⁸

¹H NMR (300 MHz, DMSO-*d*₆, TMS): δ 10.16 (br s, 1H), 8.22 (s, 2H), 7.89 (br d, 1H), 7.73 (s, 1H), 6.84 (br d, 1H), 4.09 (br s, 1H), 2.08 (m, 1H), 1.81 (m, 1H), 1.66 (m, 2H), 1.32 (s, 9H), 1.22 (m, 5H).

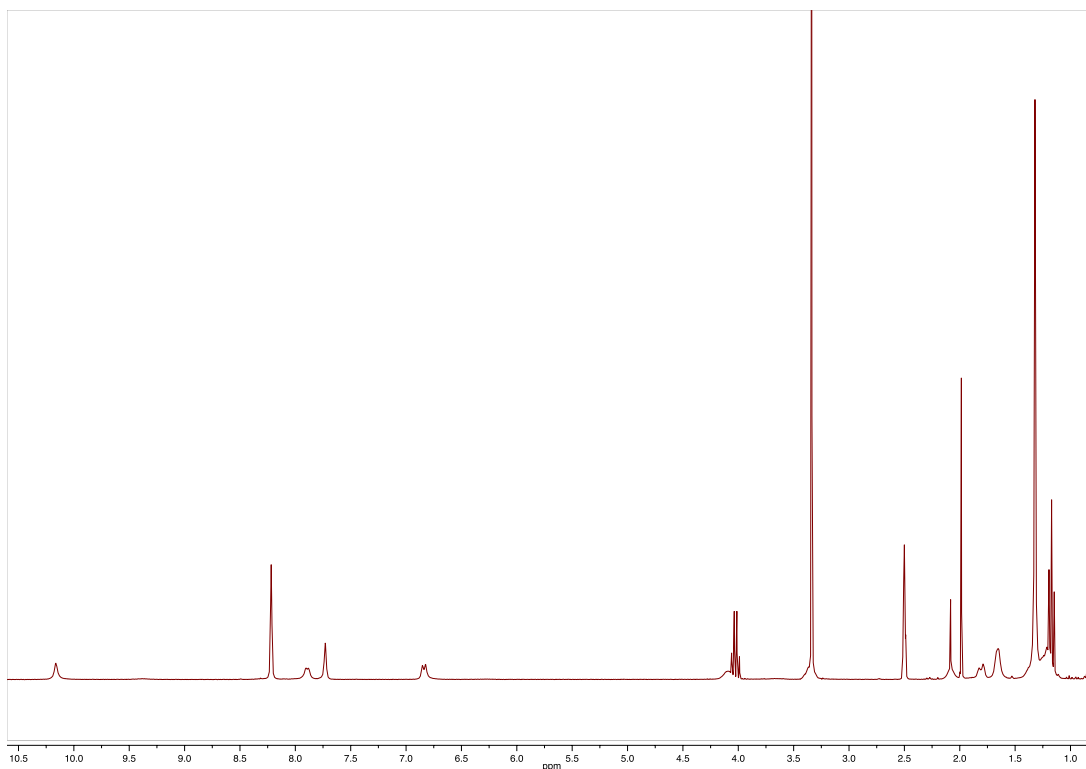


Figure 6.10. ¹H NMR of catalyst **7** (300 MHz, DMSO-*d*₆).

6.5.7 Preparation of catalyst **8**

A 25 mL flame-dried Schlenk flask was charged with dry THF (10 mL), then (*R*)-(+)-1,2,2-triphenylethylamine (253 mg, 0.93 mmol) was added. The mixture was stirred under a static blanket of nitrogen until homogeneous and 3,5-bistrifluoromethylisothiocyanate (0.17 mL, 0.93 mmol) was added dropwise. The reaction mixture was stirred at ambient temperature under nitrogen overnight, the solvent was removed by rotary evaporation, and the residue was purified with column chromatography using EtOAc/Hexanes = 20/80 as an eluant, furnishing the target catalyst **8** as a white powder.

^1H NMR (300 MHz, DMSO- d_6 , TMS): δ 9.84 (br s, 1H), 8.91 (br d, 1H), 8.27 (s, 1H), 7.93 (s, 2H), 7.53 (d, 2H), 7.32 (t, 4H), 7.14 (m, 7H), 6.98 (t, 1H), 6.42 (br t, 1H), 4.65 (br d, 1H).

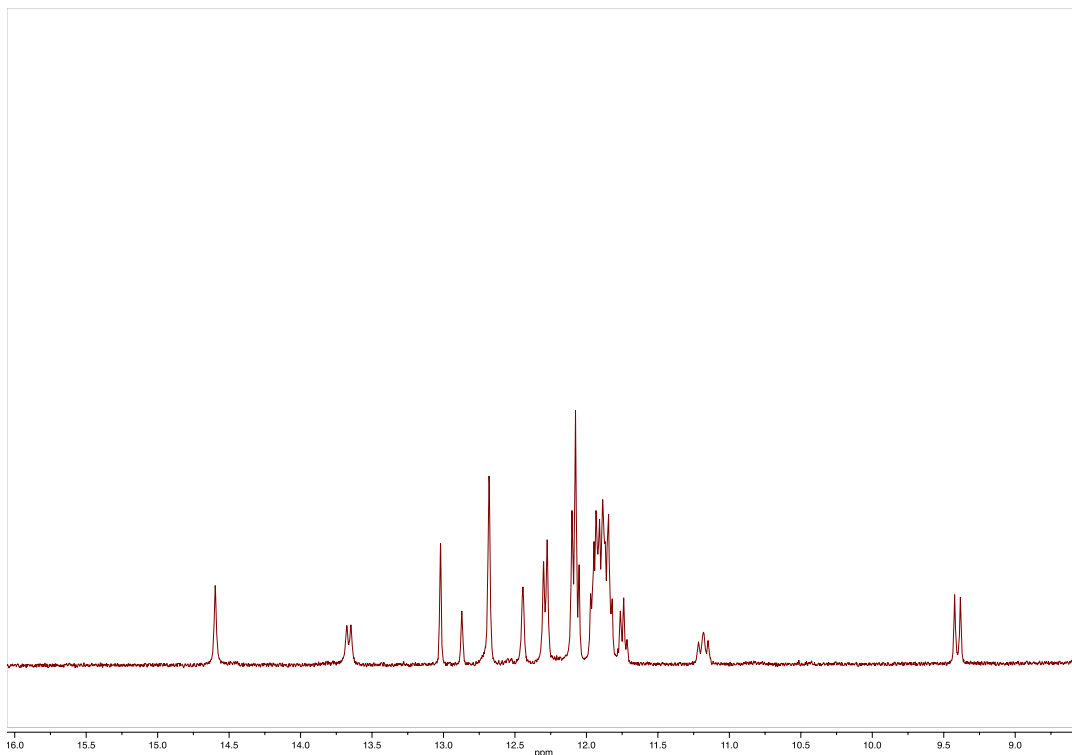


Figure 6.11. ^1H NMR of catalyst **8** (300 MHz, chloroform- d).

Table 6.3. Solvent screen for ROP of *rac*-LA^a catalyzed by **8**.

Entry	Solvent	Conversion, %	Time, h	P _m
1	Chloroform- <i>d</i>	>99	120	0.52
2	DCM	56	70	0.65
3	THF	38	161	0.58
4	<i>o</i> -Dichlorobenzene	98	133	0.53
5	Acetone	96	49	0.53

Notes. I = initiator (benzyl alcohol), C = TU catalyst, B = base (Me₆TREN), M = monomer (*rac*-LA). ^aAll polymerizations were performed at room temperature, [*rac*-LA] = 1.0 M, M/I/C/B, mol. % = 100/1/5/5.

Table 6.4. Base screen for ROP of *rac*-LA^a catalyzed by **8**.

Entry	Base	Conversion, %	Time, h	P _m
1	Me ₆ TREN	>99	120	0.52
2	TACN	97	21	0.58
3	(+)-Sparteine	90	22	0.56
4	PMDTA	>99	206	0.46
5 ^a	DBU	>99	1	0.58

Notes. I = initiator (benzyl alcohol), C = TU catalyst, B = base (Me₆TREN), M = monomer (*rac*-LA). All polymerizations were performed at room temperature in chloroform-*d*, [*rac*-LA] = 1.0 M, M/I/C/B, mol. % = 100/1/5/5. ^aM/I/C/B = 100/1/5/1.

6.6 References

- (1) Kamber, N. E.; Jeong W.; Pratt, R. C.; Lohmeijer, B. G. G; Hedrick J. L.; Waymouth R. M. *Chem. Rev.* **2007**, *107*, 5813–5840.
- (2) Kiesewetter, M. K.; Shin, E. J.; Hedrick, J. L.; Waymouth, R. M. *Macromolecules* **2010**, *43*, 2093–2107.
- (3) Thomas, C.; Bibal, B. *Green Chem.* **2014**, *16*, 1687–1699.
- (4) Bannin, T. J.; Kiesewetter, M. K. *Macromolecules* **2015**, *48*, 5481–5486.
- (5) Datta, P. P.; Kiesewetter, M. K. *Macromolecules* **2016**, *49*, 774–780.
- (6) Spink, S. S.; Kazakov, O. I.; Kiesewetter, E. T.; Kiesewetter, M. K. *Macromolecules* **2015**, *48*, 6127–6131.

- (7) Fastnacht, K. V.; Spink, S. S.; Dharmaratne, N. U.; Pothupitiya, J. U.; Datta, P. P.; Kiesewetter E. T.; Kiesewetter, M. K. *ACS Macro Lett.*, **2016**, *5*, 982–986.
- (8) Stanford, M. J.; Dove, A. P. *Chem. Soc. Rev.* **2010**, *39*, 486–494.
- (9) Thomas, C. M. *Chem. Soc. Rev.* **2010**, *39*, 165–173.
- (10) Dechy-Cabaret, O.; Martin-Vaca, B.; Bourissou, D. *Chem. Rev.* **2004**, *104*, 6147–6176.
- (11) Coates, G. W. *Chem. Rev.* **2000**, *100*, 1223–1252.
- (12) Ovitt, T. M.; Coates, G. W. *J. Am. Chem. Soc.* **1999**, *121*, 4072–4073.
- (13) Tsuji, H. *Macromol. Biosci.* **2005**, *5*, 569–597.
- (14) Drumright, R. E.; Gruber P. R.; Henton, D. E. *Adv. Mater.* **2000**, *12*, 1841–1846.
- (15) Dove, A. P.; Pratt, R. C.; Lohmeijer, B. G. G.; Waymouth R. M.; Hedrick J. L. *J. Am. Chem. Soc.* **2005**, *127*, 13798–13799.
- (16) Berkessel, A.; Mukherjee, S.; Cleemann, F.; Müller, T. N.; Lex, J. *Chem. Commun.* **2005**, *14*, 1898–1900.
- (17) Berkessel, A.; Cleemann, F.; Mukherjee, S.; Müller, T. N.; Lex, J. *Angew. Chem. Int. Ed.* **2005**, *44*, 807–811.
- (18) Dove, A. P.; Li, H.; Pratt, R. C.; Lohmeijer, B. G. G.; Culkin, D. A.; Waymouth, R. M.; Hedrick, J. L. *Chem. Commun.* **2006**, *27*, 2881–2883.
- (19) Zhang, L.; Nederberg, F.; Messman, J. M.; Pratt, R. C.; Hedrick, J. L.; Wade, C. G. *J. Am. Chem. Soc.* **2007**, *129*, 12610–12611.
- (20) Miyake, G. M.; Chen, E. Y.-X. *Macromolecules* **2011**, *44*, 4116–4124.
- (21) Makiguchi, K.; Yamanaka, T.; Kakuchi, T.; Terada, M.; Satoh, T. *Chem. Commun.* **2014**, *50*, 2883–2885.
- (22) Zhu, J.; Chen, E. Y.-X. *J. Am. Chem. Soc.* **2015**, *137*, 12506–12509.
- (23) Sanchez-Sanchez, A.; Rivilla, I.; Agirre, M.; Basterretxea, A.; Etxeberria, A.; Veloso, A.; Sardon, H.; Mecerreyes, D.; Cossío, F. *J. Am. Chem. Soc.* **2017**, *139*, 4805–4814.
- (24) Doyle, A. G.; Jacobsen, E. N. *Chem. Rev.* **2007**, *107*, 5713–5743.

- (25) Okino, T.; Hoashi, Y.; Takemoto, Y. *J. Am. Chem. Soc.* **2003**, *125*, 12672–12673.
- (26) Klausen, R. S.; Jacobsen, E. N. *Org. Lett.* **2009**, *11*, 887–890.
- (27) Sohtome, Y.; Tanatani, A.; Hashimoto, Y.; Nagasawa, K. *Tetrahedron Lett.* **2004**, *45*, 5589–5592.
- (28) Reisman, S. E.; Doyle, A. G.; Jacobsen, E. N. *J. Am. Chem. Soc.* **2008**, *130*, 7198–7199.